5. GEOCHEMICAL FRAMEWORK

5.1 INTRODUCTION

The geochemical system at Yucca Mountain forms part of the natural framework within which the design and performance of a potential repository for high-level radioactive waste must be evaluated. The geochemistry of the rocks and fluids at the site will influence the long-term behavior of components of an engineered barrier system and the ability of any radionuclides that are eventually released to migrate away from the repository. Selection and analysis of design concepts and construction materials need to be made in light of the existing geochemical framework. The geochemistry of the site also provides evidence of how geologic and hydrologic processes have operated during the past. An understanding of these processes is the basis for evaluating the long-term performance of a repository at Yucca Mountain.

This section presents the geochemical framework of the site. First, the rock geochemistry is described, followed by a discussion of the geochemistry of fluids at the site and in its vicinity.

5.1.1 Regulatory Framework

If the Yucca Mountain site is recommended and approved, a description of the geochemical system at Yucca Mountain will be required as part of a license application (proposed 10 CFR 63, Section 63.21(C)(1)(ii) [64 FR 8640]). An understanding of the geochemical framework also contributes to addressing the U.S. Nuclear Regulatory Commission's key technical issues. The applicability of other regulatory documents and standards is assessed in CRWMS M&O (1999).

5.1.2 Key Observations on the Geochemical System

Investigations of the geochemical framework of Yucca Mountain have resulted in the following key observations:

- Most of the tuffs at Yucca Mountain are rhyolites or high-silica rhyolites. Quartz-latitic units are less common and are principally within the upper zones of the Tiva Canyon and Topopah Spring tuffs.

- Feldspars, plus a combination of silica polymorphs, principally characterize the devitrified central mass of the Topopah Spring Tuff, the host rock for the potential repository. Phenocrysts make up from about 2 to 17 volume percent of the rock, with lithic fragments averaging less than 1 percent.

- Below the Calico Hills Formation, nonwelded tuffs are pervasively zeolitized.

- The suite of minerals contained in faults and fractures in the unsaturated zone is highly variable. In the saturated zone, the variability of such minerals is less.

INTENTIONALLY LEFT BLANK

5.2 ROCK GEOCHEMISTRY OF YUCCA MOUNTAIN AND VICINITY

The materials that constitute Yucca Mountain include pyroclastic deposits and rare lava flows, as well as colluvium, alluvium, and soils. The surface materials contain mixed constituents, including pedogenic calcite and opal; as such, they are significant sources of dissolved material introduced into recharge pathways but participate as transport pathways only at a distance from the site. Soils and colluvium are important in their effects on recharge hydrochemistry; since these materials and their effects are discussed in Sections 4.4 and 5.3, the emphasis in the text below is on the pyroclastic units.

The existing chemical variability of the pyroclastic units at Yucca Mountain is the combined result of variable original magmatic compositions, syngenetic alteration, regional hydrothermal alteration, diagenesis, and chemical exchange with groundwater. The role of surficial deposits and pyroclastic lithologies in determining groundwater compositions is covered in Section 5.3. This section provides the lithologic background for the principal rock units in which recharge, flow, and transport occur.

The initial magmatic compositions of the pyroclastic units are reflected in the combined glass fragments, lithic inclusions, and phenocrysts that constituted the original erupted materials. Superimposed on these initial compositions are variations in mineralogy and chemistry introduced by alteration. The chemical and mineralogic features of the rock matrix, fractures, and faults provide information on the record of hydrochemistry and transport at Yucca Mountain.

The data discussed in this section relate to several aspects of site evaluation and prediction of site performance. Evaluation of rock geochemistry provides information on past or ongoing transport of elements that can be related to the transport of radioactive waste. Such information may be explicitly equivalent (e.g., strontium occurs both in nature and in many radioactive wastes) or merely analogous (e.g., cerium, which occurs in nature, can be used as an analog for plutonium, a synthetic element abundant in nuclear waste). Determinations of mineral distributions at the site can be used with mineral-based sorption data to model site performance in three dimensions (Sections 4.8 and 10). Rock geochemistry affects groundwater compositions through rock dissolution and alteration to other minerals, principally in vitric units, and by cation exchange, principally in zeolitic horizons. However, even minor fracture minerals, such as manganese oxides, can operate as oxidation-reduction sites and have a strong effect on trace constituents in solution (Section 5.2.2.2). The mineral distributions at the site are also important in evaluating potential exposures to minerals that are health hazards (Section 4.7.7.2) and in predicting mineral stability and dissolution-precipitation reactions under a repository-induced thermal load (Section 11).

5.2.1 Nature and Origin of Primary Geochemical Variability

In this section, the discussion of primary geochemical variability is used for comparing the effects of alteration, for defining the role that rock compositions play in affecting aqueous geochemistry, and for assessing the geochemical effects that impact radionuclide transport. Both major-element and trace-element data are considered. Stratigraphic aspects of the geochemistry of unaltered tuff units are discussed in Section 4.5.

Compositionally, both the vitric and devitrified tuffs can be classified based on their silica (SiO_2) and alumina (Al_2O_3) content. Figure 5.2-1 compares the abundances of these constituents in unaltered representatives of the major rocks forming Yucca Mountain, normalized to volatile-free compositions (normalized to 100 percent without constituents lost on ignition). These rocks include high-silica rhyolites (greater than 75 percent SiO_2) and rhyolites (72 to 75 percent SiO_2), with some distinctive quartz-latitic rocks (less than 70 percent SiO_2). Alumina and silica are the major crystalline framework constituents that defined the mineralogy formed in devitrification, in vapor-phase alteration, and in the later zeolitization of extensive portions of those rocks that remained vitric after emplacement and initial cooling. Most of the tuffs at Yucca Mountain are rhyolites or high-silica rhyolites. The quartz-latitic units at Yucca Mountain are less common and are principally within the upper zones of the Tiva Canyon and Topopah Spring tuffs (Figure 5.2-1). The Rainier Mesa Tuff also contains an upper quartz-latitic portion. The low-silica rhyolite of the Pah Canyon Tuff (Figure 5.2-1) has chemical affinities to the quartz latites (e.g., high light-lanthanide element contents) despite its rhyolitic major-element composition (Vaniman and Chipera 1996, pp. 4429 to 4431).

Individual pyroclastic eruptive cycles at Yucca Mountain are variably zoned in composition. The best-studied example, the Topopah Spring Tuff, provides a record of progressive evacuation of a single magma chamber that was compositionally zoned downward from phenocryst-poor high-silica rhyolite to phenocryst-rich quartz latite (Schuraytz et al. 1989). Progressive withdrawal of magma during eruption led to upward distortion of the magmatic interface and simultaneous eruption of magma with increasing differences in composition and temperature. The persistence of high-silica rhyolitic pumices throughout the ash flow indicates that none of the pyroclastic rocks represent pure end-member quartz latitic magma and suggests that the eruption was insufficient to exhaust the upper rhyolitic magma layer. Like the Topopah Spring Tuff, the Tiva Canyon Tuff is zoned upward from high-silica rhyolite to rhyolite to quartz latite. The geochemical differences between quartz-latitic and rhyolitic tuffs provide stratigraphic markers of chemical variation, particularly in lanthanide-element composition. Use of these markers is described in Section 5.2.2.1.

The temporal progression of crystallization in devitrified tuff, beginning with high-temperature events over 11 Ma and continuing today, can be illustrated by considering the example of the Topopah Spring Tuff. A detailed discussion of these processes is provided in Sections 5.2.1.1 and 5.2.1.2. Following eruption and emplacement of the Topopah Spring Tuff, the uppermost (quartz latitic) and lowermost (high-silica rhyolite) portions of this compound volcanic series were rapidly cooled below glass quenching and rheomorphic temperatures to preserve thin, nonwelded vitric margins. Glassy portions between the nonwelded vitric margins and the central devitrified mass retained enough heat to compact but not to crystallize and were densely welded to form vitrophyres (the quartz-latitic upper vitrophyre and the high-silica rhyolitic lower vitrophyre). The vast majority (about 90 percent) of the erupted material, between these two vitrophyres, retained enough heat to promote crystallization of all glass. This material is the devitrified core of the Topopah Spring Tuff. Water vapor released from crystallizing glasses in this devitrified core formed a hot fluid from which vapor-phase minerals crystallized along early-formed fractures and within pockets formed by gas expansion (lithophysal cavities). The vapor-phase minerals are dominantly feldspars and silica minerals (especially tridymite) but include a wide variety of other minerals (e.g., amphibole, pseudobrookite, Mn-garnet, andalusite). Crystallization of some of these minerals may have continued as the possibly supercritical fluid

cooled to water vapor and ultimately condensed as liquid water. Much of the tridymite along fractures is now pseudomorphed by quartz that may have formed during this transition. Minerals have continued to form within fractures long after the end of the volcanic cooling cycle; minerals that may still be forming in fractures and cavities of the potential host rock include zeolites, clays, opal, calcite, and manganese oxides.

Phenocrysts are crystalline components of pyroclastic rocks inherited from the parent magmas. Lithic fragments are pieces of preexisting rock entrained in the magma during eruption. The measured phenocryst content of Yucca Mountain tuffs varies from less than 1 volume percent to as much as approximately 25 volume percent, and lithic fragments average a few volume percent (Byers et al. 1976, Figures 5, 9; Broxton et al. 1993, Appendix A). Quartz-latitic units have consistently high phenocryst abundances, but rhyolitic units have variable phenocryst abundances. Among the major rhyolitic units in the vicinity of Yucca Mountain, the bedded tuff at the base of the Calico Hills Formation has the highest phenocryst content (up to about 25 volume percent). The upper part of the Bullfrog Tuff also has phenocryst content as high as 25 volume percent. Lithic inclusions and phenocrysts affect the bulk chemistry of a tuff in proportion to their abundance.

The principal phenocrysts in the tuffs are sanidine, plagioclase, quartz, and biotite. There are many other phenocrysts, such as amphibole, clinopyroxene, orthopyroxene and accessory magnetite, ilmenite, monazite, zircon, apatite, allanite, and perrierite, but these are present in amounts much less than 1 volume percent (Broxton et al. 1993, Appendix A). In general, the K content of sanidine phenocrysts increases with depth among the rocks at Yucca Mountain. Also, the most common of the iron-magnesium-silicate phenocrysts, biotite, provides a measure of Fe/Mg ratios among units; the biotites that occur from the rhyolite of the Topopah Spring Tuff down through the bottom of the Crater Flat Group are more Fe-rich than those that occur above and below.

Although phenocryst compositions have little cumulative effect on aqueous transport, they can provide sites where sorptive alteration phases are concentrated (e.g., manganese oxides concentrated around altered iron-titanium-oxide phenocrysts) (Section 10.3.1.2). In that phenocryst compositions reflect host magma chemistry, these variations represent a subtle overprint on the generally bivariate compositions (rhyolite versus quartz latite) that characterize the major geochemical subdivisions at Yucca Mountain (Broxton et al. 1989, pp. 5965 to 5978). A discussion of the major mineralogic and chemical features above, within, and below the Topopah Spring Tuff, the potential host rock at Yucca Mountain, is provided below.

Above the Potential Host Rock–The Rainier Mesa Tuff of the Timber Mountain Group is the youngest extensive tuff unit exposed at Yucca Mountain, although it is only preserved at lower elevations along the flanks of Yucca Mountain. With this limited distribution, the Rainier Mesa Tuff would be expected to be of little consequence at Yucca Mountain were it not for the fact that the occurrences at Yucca Mountain are vitric. As such, they are local sources for silica and trace minerals released by chemical weathering over the approximate 11-m.y. history of Yucca Mountain. The Rainier Mesa Tuff includes both high-silica rhyolite and quartz latite subunits. This compositional variation, representing the progressive disgorgement of a stratified magma chamber, as described above, is common to the major tuffs of the Paintbrush Group (Tiva Canyon and Topopah Spring) as well.

The Paintbrush Group at Yucca Mountain is dominated by the Tiva Canyon and Topopah Spring tuffs. These tuffs provide most of the surface exposures of Yucca Mountain. Sandwiched between these two tuffs, the Yucca Mountain and Pah Canyon tuffs are volumetrically minor but of potential hydrologic importance because of their contrasting high matrix porosity compared to the Tiva Canyon and Topopah Spring tuffs, which, except for their nonwelded tops and bases, are densely welded and of low matrix porosity. The welded tuffs also have higher fracture abundances and connectivities, providing stratified contrasts in unsaturated hydrologic properties within the Paintbrush Group rocks above the potential repository (Sections 8.3 and 8.7).

The Tiva Canyon Tuff is compositionally zoned from a minor quartz-latitic, vitric-to-devitrified upper portion to a predominantly high-silica rhyolitic, devitrified lower sequence. To reiterate, this compositional zonation is similar to that of the Rainier Mesa and Topopah Spring tuffs. The high-silica rhyolites of the Paintbrush Group have an exceptionally small compositional range (Figure 5.2-1). Across parts of Yucca Mountain, the quartz-latitic upper part of the Tiva Canyon Tuff is vitric or partially vitric; these glasses may be particularly reactive in interactions with recharge waters or with waters that are diverted and flow laterally along slopes and ravines. Phenocryst abundances in the quartz-latitic parts of the Tiva Canyon are high (to more than 20 percent) and consist predominantly of feldspar; the thicker, lower rhyolitic portion contains less than 7 percent phenocrysts. The lowest part of the Tiva Canyon Tuff consists of densely welded to nonwelded high-silica rhyolitic glass. This interval provides another horizon of potential water accumulation in the unsaturated zone, with associated dissolution and mineral alteration (Section 5.3.6). However, water compositions resulting from dissolution and alteration of rhyolitic glass will be distinct from waters that interact with the upper quartz-latitic glass in the same tuff (Vaniman et al. 1996).

The Yucca Mountain Tuff is chemically very similar to the high-silica rhyolites of the Tiva Canyon and Topopah Spring tuffs (Figure 5.2-1). At Yucca Mountain, the Yucca Mountain Tuff is largely vitric, nonwelded, and porous, but may be locally devitrified to silica minerals and feldspar. Although this unit is rhyolitic, it contains both plagioclase and sanidine phenocrysts, whereas the only feldspar phenocrysts in the rhyolitic Tiva Canyon Tuff are of sanidine. This two-feldspar phenocryst composition is also characteristic of the rhyolitic portions of the Topopah Spring Tuff.

The Pah Canyon Tuff is a chemical anomaly within the Paintbrush Group. It is somewhat lower in silica content than the high-silica rhyolites (Figure 5.2-1), and even more different from the other rhyolites in its trace-element chemistry, having a rare-earth-element composition more like quartz latites than rhyolites. The Pah Canyon Tuff is, like the Yucca Mountain Tuff, nonwelded, porous, and largely vitric (but locally devitrified). The high saturation of porous nonwelded units, such as the Yucca Mountain and Pah Canyon units, begins to be more effective in producing alteration where there is an underlying barrier to transmission. Thus, because of the relatively impermeable upper vitrophyre of the underlying Topopah Spring Tuff, the alteration of the immediately overlying Pah Canyon Tuff (principally to smectite) is often more extensive than that of the stratigraphically higher Yucca Mountain Tuff. Therefore, despite its minor volume, the Pah Canyon Tuff has a significant impact on the reactions between unsaturated zone waters and the host tuffs. Phenocryst abundances in the Pah Canyon Tuff are approximately 5 to 14 percent, with a mode of about 7 percent that is intermediate between that of high-silica rhyolites (generally less than 5 percent) and the quartz latites (5 to 18 percent with a mode in the

Topopah Spring Tuff of about 14 percent) (Vaniman et al. 1996, Volume 1, Section 5, pp. 5, 6). The Pah Canyon Tuff is a two-feldspar tuff that has markedly Na-rich plagioclase (Na-rich oligoclase, contrasted with a common range from oligoclase to andesine for most other Paintbrush tuffs).

The Potential Host Rock: The Topopah Spring Tuff–The transition from quartz latite to rhyolite in the Topopah Spring Tuff is marked by progressively decreasing abundances of phenocrysts (from about 17 to 2 percent) and, in particular, by the appearance of quartz phenocrysts and the loss of clinopyroxene phenocrysts. Lithic fragments average less than 1 percent. Within the devitrified central mass of the Topopah Spring Tuff, the remaining bulk of the rock consists of fine-grained devitrification minerals (Byers and Moore 1987, Figures 2 to 5). These devitrification products are principally feldspars plus a variable combination of the silica polymorphs tridymite, cristobalite, and quartz. Quartz phenocryst abundance is a useful stratigraphic marker within the devitrified rhyolitic Topopah Spring Tuff, but quartz phenocrysts are nevertheless much less abundant (less than 0.5 percent) than groundmass quartz (about 20 percent) throughout this interval. The silica polymorph distributions are particularly important because of their thermal stability, dissolution properties, and properties as inhalation hazards (Section 4.7.7). Moreover, although the feldspar abundances in the devitrified rhyolitic Topopah Spring Tuff are essentially constant at approximately 55 percent, the relative proportions of silica polymorphs vary with depth and between lithophysal and nonlithophysal zones.

Other minerals, less common than the silica polymorphs and feldspar, need to be considered in the potential host rock. Although generally devoid of zeolites, except for minor occurrences along some fractures, the devitrified rhyolitic Topopah Spring Tuff contains up to 14 percent of the zeolite mineral stellerite ($CaAl_2Si_7O_{18} \bullet 7H_2O$) in drill hole USW UZ-16 (Figure 5.2-2) (Byers and Moore 1987). Higher stellerite abundances are correlated with lower feldspar abundances, indicating a system relatively closed with respect to alumina and in which the framework-forming constituents in the zeolites were formed at least in part by local alteration at the expense of feldspar. However, the stellerite has effectively accumulated Ca from groundwater; as a result, the stellerite-bearing Topopah Spring Tuff has higher CaO but shows little other difference compared with the unaltered high-silica rhyolite. This rise in CaO is strongly correlated with stellerite content (Figure 5.2-2). The data for unaltered samples in Table 5.2-1 provide a good estimate of "typical" composition of the Topopah Spring Tuff high-silica rhyolite as encountered at depth in the vicinity of the exploration block at Yucca Mountain. This "typical" Topopah Spring Tuff is characteristic of the rock composition in the potential repository horizon. However, it should be remembered that components in the tuff, such as CaO, can still vary with alteration (e.g., calcite accumulation) in the potential repository host rock.

Below the Potential Host Rock–Beneath the Topopah Spring Tuff, the rhyolitic ash flows of the Calico Hills Formation have phenocryst abundances that are generally less than 3 volume percent, although the underlying bedded tuff can have phenocryst abundances of up to 25 percent. Figure 5.2-1 shows that the ash flows of the Calico Hills Formation have exceptionally large variability in composition, with normalized anhydrous SiO_2 values ranging between 76 and 80 percent. These values are based only on unaltered, vitric samples. Where zeolitization has occurred, the silica content is little changed. The typical alteration phases are clinoptilolite [$(Ca, Na, K)_{2-3} Al_3(Al, Si)_2 Si_{13}O_{36} \bullet 12H_2O$] plus minor smectite; mordenite [(Ca,

Na_2, K_2) $Al_2Si_{10}O_{24} \bullet 7H_2O$] becomes as abundant or more abundant than clinoptilolite toward the north at Yucca Mountain. Chabazite ($Ca_2Al_4Si_8O_{24} \bullet 12H_2O$) occurs, in addition to but less abundantly than clinoptilolite, toward the south. Below the Calico Hills Formation, nonwelded tuffs are pervasively zeolitized, and the primary geochemical variability is masked by this alteration, which can greatly alter the abundance of Na, K, Mg, Ca, and Sr. For these units, therefore, the geochemistry of altered rocks is discussed below with the description of primary geochemical variability that is better preserved in the welded, devitrified strata.

Below the Calico Hills Formation lie the rhyolitic ash flows and bedded tuffs of the Crater Flat Group. Phenocryst abundances in the Crater Flat Group have a higher range in the Bullfrog Tuff (up to 25 volume percent) than in the Prow Pass and Tram tuffs (less than 20 volume percent). There is a general similarity of quartz-sanidine-plagioclase-biotite phenocryst populations throughout the Crater Flat Group; within this general similarity is a general increase in the K content of sanidine and in the Ca content of plagioclase with depth, from the Prow Pass to the Tram tuffs. Pyroxene occurs in the upper two tuffs (Prow Pass and Bullfrog) and, despite its minor abundance, may play a role in radionuclide retardation in the Prow Pass Tuff (based on evidence of strong Pu retention by altered orthopyroxenes) (Section 10.3.1). All three of the Crater Flat tuffs have devitrified central portions, with abundant feldspar and quartz and, at least initially, had vitric margins, much of which has been altered to zeolites in the early alteration history of Yucca Mountain. The zeolitization is dominated by clinoptilolite in the south and by clinoptilolite plus mordenite to the north. The nonsorptive zeolite analcime ($NaAlSi_2O_6 \bullet H_2O$) partially displaces these sorptive zeolites up into the lower parts of the Prow Pass Tuff in the northern part of Yucca Mountain, but within and to the south of Drill Hole Wash, analcime does not occur in any significance above the lower alteration zone in the Tram Tuff.

The older volcanic units at Yucca Mountain include the Lithic Ridge Tuff and unnamed older tuffs, designated A, B, and C, plus occurrences of dacitic lavas. These deeper units are far below the water table (about 1.5 to 2.5 km) and are therefore unlikely to be of significance in considering transport from the potential repository. In general, these tuffs and, to the north, associated lavas, are thoroughly altered to analcime and, with increasing depth (grade), to albite, with associated smectite/illite, calcite, and lesser pyrite, barite, and other phases (Bish and Chipera 1989, pp. 27, 36, and 41).

5.2.1.1   Syngenetic Geochemical Processes

Thick pyroclastic deposits like the Topopah Spring and Tiva Canyon tuffs were erupted and emplaced at temperatures from > 650°C to 985°C (Schuraytz et al. 1989, p. 5933, Figure 9) and probably required about 100 to 1,000 yr. to cool (Riehle 1973). Early in the cooling period, the interiors of such tuffs welded by viscous flow and compaction of the glass particles. The process of welding continued to temperatures as low as 475°C in the basal vitrophyre of the Topopah Spring Tuff (Rosenbaum 1986, p. 12,833). After substantial welding had occurred, the tuff in the hottest parts of the interior devitrified, that is, crystallized to an assemblage of alkali feldspar, tridymite, cristobalite, and quartz, plus a variety of accessory minerals. The faster cooling upper and lower margins of the deposits did not weld and experienced little or no devitrification. Some of the moderately to densely welded portions toward the outer margins did not devitrify and have survived in a glassy state (vitrophyres).

In addition to the pervasive devitrification in the interiors of ash flows, localized syngenetic alteration occurred along fractures within and below devitrified tuff at the downward transition from devitrified to vitric tuff in both the Topopah Spring and Tiva Canyon tuffs. The alteration was caused by a combination of water entrained in the ash flow and infiltrating meteoric water that interacted with the rock and occurred during the very late stages of cooling, at near-ambient temperatures (Levy and O'Neil 1989, p. 321). The tuffs were also subject to fracturing, faulting, and brecciation during cooling (Levy 1993, p. 544).

The geochemical significance of devitrification and syngenetic alteration for site characterization lies in two general areas. The original distribution pattern of devitrified and vitric tuffs largely determined the locations of zeolitic and nonzeolitic rocks in those parts of Yucca Mountain where the rocks have been subject to zeolitization. In addition, the field-scale distribution of hydrologic properties reflects the distribution of devitrified and nondevitrified, as well as zeolitic and nonzeolitic, tuffs. Devitrified tuffs have low matrix porosity, so that many rock-water geochemical interactions occur more readily in the fractures.

The bulk of alteration history research into syngenetic alteration pertains to late-stage syngenetic alteration and the interaction of still-hot rock with infiltrating meteoric water. Alteration caused by reheating of tuff by subsequent ashflows can produce minerological changes similar to syngenetic alteration. Alteration of the syngenetic type can serve as a natural analog for hydrothermal alteration in a repository environment. Within the context of in situ thermal tests at Yucca Mountain, characterization of syngenetic alteration allows researchers to identify alteration products of the tests with greater confidence because test products may be mineralogically similar to natural alteration products. Syngenetic alteration studies are also important in mapping the distribution of the carcinogenic zeolite, erionite, because all known occurrences of this mineral at Yucca Mountain are associated with sites of syngenetic alteration.

This research also addresses the detection of recent surface-discharging hydrothermal activity in the Yucca Mountain area and how it might be distinguished from syngenetic alteration that occurred at more than 10 Ma. The natural syngenetic mineral occurrences can be classified according to common aspects of mineralogy, texture, chemical composition, and localization in the host rock. Each category of occurrence exhibits a characteristic zonation or distribution related to the development of thermal gradients and associated fluid-transport mechanisms within an ash flow.

Geochemical Variability Associated with Devitrification–The term devitrification, as applied to the pyroclastic deposits at Yucca Mountain, denotes high-temperature crystallization of volcanic glass to a largely anhydrous mineral assemblage. Little is known about bulk chemical changes associated with devitrification, although short-range chemical transport (up to millimeter-scale) must have occurred during the crystallization of homogeneous glass to an aggregate of microcrystalline discrete mineral phases. The major mineralogic components of the devitrified rocks are alkali feldspar and two or more silica phases. From the top of the Topopah Spring Tuff down through the top of the lower lithophysal zone, the typical secondary-silica phases in the groundmass are cristobalite and tridymite. The characteristic silica phases in the remainder of the devitrified section, including the candidate host rock, are cristobalite and quartz.

Comparisons of the major-element compositions of brown cryptocrystalline devitrified groundmass and vitrophyre glass in the Topopah Spring Tuff indicate general similarities (Byers 1985, pp. 15 to 18), suggesting that little or no bulk-chemical change occurred during devitrification. Devitrified groundmass from the lower Topopah Spring Tuff devitrified-vitric transition zone (the Tptplnc2-Tptpv3 interval of Buesch et al. [1996, p. 8]), with its higher potassium content, diverges in composition from vitrophyre glass and groundmass away from the transition zone. The additional potassium was probably derived from dissolution of vitrophyre glass within the transition zone, a local process that was absent from most of the rock undergoing devitrification.

Geochemical Variability Associated with Syngenetic Alteration–Most syngenetic alteration is located in and near devitrified-vitric transition zones, and the alteration itself represents a transition from devitrification to glass dissolution and secondary-mineral precipitation of mostly zeolites, clay, and silica phases. These transition zones were favored sites for alteration during the late-stage cooling of thick tuff deposits because the reactive glass could be contacted by heated fluids coming from the warmer interior of the deposit. The volume of rock affected by syngenetic alteration is highly variable throughout Yucca Mountain, especially because much of the alteration is concentrated along and adjacent to fractures. In general, the cumulative thickness of affected rock is on the order of tens of meters or less.

The basis for interpreting this alteration as syngenetic is its common textural association with devitrification (Levy 1984a, pp. 961 to 963). Data from a few geochronologic studies of silica have yielded ages a few million years younger than the ages of the ash flows (Paces et al. 1999, pp. S4 to S5; Cowan et al. 1993, p. 1038). The cause of this discrepancy is not known, but could be related to partial recrystallization of the original mineral deposits or deposition of younger material on the older deposits.

Principal stratigraphic locations of syngenetic alteration include the lower Tiva Canyon Tuff (Tpcpln downward into Tpcpv1) and the lower Topopah Spring Tuff (the Tptplnc2-Tptpv3 boundary downward into Tptpv2). In a few places, vitric rock of the upper Topopah Spring Tuff was altered in a manner akin to the vapor-phase crystallization in immediately underlying devitrified tuff. Local alteration in the Tpbt2 bedded tuff immediately above the Topopah Spring Tuff may also be a variant of syngenetic alteration.

Alteration in the Topopah Spring Tuff Tptplnc-Tptpv2 interval is the most widespread and volumetrically abundant example of syngenetic alteration in the unsaturated zone at Yucca Mountain. Common mineral constituents of the altered zone include alkali feldspar, smectite, heulandite, and silica minerals. Minor constituents, not present everywhere, include mordenite, calcite, iron and manganese oxides, and erionite. Table 5.2-2 provides an indication of mineralogic variability in this altered interval.

Depending on the proportions of secondary minerals, this alteration can involve substantial bulk chemical change relative to the original vitric tuff. For example, where smectite and heulandite are abundant, the contents of Al, Mg, and Ca have increased (Levy 1984b, pp. 57, 65 to 66, 74). Another effect of abundant smectite crystallization, in particular, has been a volume increase of alteration products compared to the volume of the original glass (Levy and Valentine 1993,

pp. 147 to 148). The excess product materials, some in colloidal form, migrated through the rock, filling primary and secondary pore spaces.

5.2.1.2 Diagenetic Geochemical Processes

The most extensive post-cooling mineralogic and geochemical change affecting the rocks at Yucca Mountain has been the diagenetic zeolitization of nonwelded glassy tuffs. Diagenetic alteration involved dissolution of glass pyroclasts by groundwater at ambient temperatures and precipitation of clinoptilolite with or without lesser amounts of mordenite, smectite, silica, iron-manganese oxides and hydroxides, and other minor phases. Chemical changes and introduction of chemical variability associated with this alteration are functions of the compositions of the secondary minerals and variability in their relative proportions caused by transport of dissolved or colloidal components into and out of the altered rock. Additional chemical variability has been superimposed on zeolitic rocks by cation exchange between clinoptilolite and percolating groundwater. Zeolitic rocks in the deeper parts of Yucca Mountain have been subjected to differing and additional alteration, with calcite formed in part by Ca released through Na exchange for Ca in analcime or albite formation and an increase in the illite-to-smectite ratio of clays.

The downward transition from vitric to zeolitized tuffs is a gross feature common to all Yucca Mountain drill holes and outcrops. The exact position of the vitric-zeolitic transition has not been precisely fixed throughout the mountain, but the persistence of this feature across the mountain makes it an important part of the evidence relating the timing of zeolitization to pyroclastic depositional events and tectonism. Of particular importance for nuclear waste repository performance, the transition also marks changes in the hydraulic and sorptive properties of nonwelded tuffs.

Researchers studying zeolitization in the Yucca Mountain region have made a variety of inferences about the hydrologic regimes in which zeolitization occurred. The researchers recognized a few probable examples of perched water alteration but tended to favor alteration at or below a static water level (Vaniman et al. 1996, Volume I, pp. 2, 25). The Yucca Mountain glass distribution and zeolite distribution data provide no support for the existence or former existence of a widespread perched water table. Known examples of probable perched water zeolitization are of much smaller vertical and lateral extent than the main mass of zeolitized tuffs. The working hypothesis is that most zeolitization occurred around or below the static water level in place at the time of alteration and that glass in nonwelded tuffs is preserved only where the rocks have not been subjected to prolonged saturation. This concept forms one basis for estimating the highest elevation ever occupied by the static water level (Section 5.2.2.4).

5.2.1.3 Fracture and Matrix Interactions

Faults and associated shear fractures can be either transmissive features or aquitards, depending on the rock types juxtaposed across the faults and the nature of the alteration mineralogy within the faults. Major fracture orientations at Yucca Mountain trend north-northwest and north-northeast; the latter are at a high angle to the minimum compressive stress and therefore may be more open and transmissive (Waddell et al. 1984, p. 27). Although any waste transport is likely to be predominantly through fractures or faults in welded units, diffusion into the tuff matrix will

also be a significant factor in waste-mineral interactions. Therefore, the mineralogies of faults, fractures, and matrix are all important to waste transport retardation.

Fracture Minerals in the Unsaturated Zone: High Variability–Unsaturated zone fractures contain a highly variable suite of minerals, ranging from early syngenetic to late diagenetic phases (Figure 5.2-3a to 5.2-3e). The silica polymorphs quartz, cristobalite, and tridymite are common in fractures in devitrified tuff intervals, and their distribution corresponds to the occurrences of these polymorphs in the adjacent rock matrix (Carlos et al. 1995, p. 7). The zeolite minerals mordenite, heulandite, and stellerite are widespread in fractures in the densely welded, devitrified portions of the Paintbrush Group within the upper unsaturated zone.

The silica mineralogy of devitrified-vitric transition zones includes quartz (often occurring as chalcedony), amorphous opal-A, opal-CT (with short-range cristobalite and tridymite ordering), and rare mogonite, a monoclinic form of crystalline silica. Zeolites are common products of the syngenetic alteration that occurred at the boundaries between the central devitrified portions of ash flows and the overlying or underlying vitric margins, but some occurrences distributed along fractures may be diagenetic. Although the most common fracture coatings in the lower vitrophyre of the Topopah Spring Tuff are smectite, opal-CT, and manganese-oxide dendrites, fractures may also contain heulandite or mordenite as well as other zeolites that are uncommon at Yucca Mountain. Phillipsite coexists with smectite in isolated occurrences in some fractures within this lower vitrophyre. Erionite generally occurs in fractures and the rock matrix in very limited intervals within the vitrophyre and the altered tuff in the overlying transition zone in several drill holes where it comprises less than 1 weight percent of the matrix, but may be as much as 45 weight percent of some fracture coatings. Erionite has also been identified in significant abundances in a 3-m-thick zone in the vitric tuff matrix immediately below the lower vitrophyre in drill hole USW UZ-14.

Clinoptilolite and mordenite both occur in fractures within the zeolitized Calico Hills Formation and in the upper Crater Flat Group, wherever zeolites are common in the adjacent tuff matrix. These occurrences are located in the lower unsaturated zone and into the upper saturated zone. Unlike the matrix alteration, which is commonly dominated by clinoptilolite, mordenite is the principal fracture-lining zeolite.

Smectite is nearly ubiquitous in fractures throughout the volcanic sequence at Yucca Mountain. Kaolinite is much less common but has been identified by X-ray diffraction from fractures in some drill cores where it occurs with smectite or calcite. The chain-structure clay minerals palygorskite and sepiolite occur sporadically in fractures in the Paintbrush Group, either in varying combinations with smectite or separately. Occurrences of chain-structure clays do not extend below the middle of the Topopah Spring Tuff; the sepiolite might have surface origins that provide a marker of downward transport. There is no apparent sequence of clay deposition with depth, except that palygorskite and sepiolite do not occur below about 260-m depth.

Manganese-oxide minerals occur in fractures in the moderately welded to densely welded vitric and devitrified tuffs throughout the pyroclastic sequence at Yucca Mountain, and are less common in zeolitic zones. The layer-structure Mn-oxides lithiophorite (Li-bearing and Al-bearing hydrous Mn-oxide) and rancieite (Ca-bearing hydrous Mn-oxide) are the principal manganese-oxide minerals coating fractures of the unsaturated zone. Pyrolusite is a rarer Mn-

oxide phase in the unsaturated zone, but with rancieite, may be a sink for Ce in groundwaters. Pyrolusite has been texturally associated with calcite precipitation. Data from microautoradiography show that Mn-oxides, such as rancieite, which can oxidize and remove Ce from solution, have a similar capacity for removing Pu from solution (Duff et al. 1999). The iron oxide hematite also occurs as a fracture mineral. Calcite commonly occurs in fractures as well as in lithophysal cavities. It is most common in, but not limited to, the densely welded and devitrified portions of the Tiva Canyon and Topopah Spring tuffs in the unsaturated zone (Whelan et al. 1994, pp. 2738, 2740). Most calcites were deposited incrementally during the past 8 to 10 m.y. (Paces et al. 1997, pp. E-3 to E-4).

Fine-grained fluorite is a widespread and locally prominent fracture and lithophysal cavity coating in the densely welded, devitrified portions of the Topopah Spring Tuff (Carlos et al. 1995, p. 7). Fluorite fracture fillings in bedded tuff above the Topopah Spring Tuff are related to syngenetic alteration associated with late-stage cooling.

Unsaturated Zone Fracture Minerals and Implications for Fracture Flow–Calcite and opal fracture mineral coatings provide a record of past water percolation through the connected fracture network in areas where solutions exceed chemical saturation with respect to various mineral phases. They are typically present in the form of 0.1- to 6-cm-thick coatings in high-angle to low-angle fractures where apertures exceed several millimeters and on floors of lithophysal cavities intersected by fractures. In general, nonwelded tuffs with large matrix permeability and few open fractures or cavities have small abundances compared to values in welded units (CRWMS M&O 2000, Section 6.10). Mineral coatings commonly show a systematic sequence of growth that involves changes in both mineral compositions and textures. Typically, main-stage deposits consisting of calcite follow an early silica phase. Opal is also observed in main-stage deposits (CRWMS M&O 2000, Section 6.10.1).

Dating of fracture minerals by various methods suggests they have accumulated over time. Outer layers generally show younger ages than underlying deposits. For outermost growth surfaces, radiocarbon dates from calcite range from 44 to 16 ka, ^{230}Th/U age for calcite and opal range from greater than 500 to 28 ka, and ^{207}Pb/^{235}U ages range from about 1 Ma to 100 ka. Ages from underlying earlier deposits range from 4 to 10 Ma (CRWMS M&O 2000, Section 6.10.1).

Fracture Minerals in the Saturated Zone: Modest Variability–The silica polymorphs tridymite and, to a large extent, cristobalite are usually absent in fractures of the saturated zone (Figure 5.2-3a to 5.2-3e). These polymorphs are the more soluble of the anhydrous silica polymorphs and are commonly supplanted by opal-CT, which occurs with mordenite and clinoptilolite in the Calico Hills Formation and Crater Flat Group, whether in the saturated zone or unsaturated zone. Instead, quartz is common in fractures in the devitrified intervals of the saturated zone. Lithophysal-type fracture coatings occur in the Bullfrog and Tram tuffs of the Crater Flat Group; although the tridymite morphology has been preserved, the silica mineral is now quartz (Carlos et al. 1995, p. 24). Quartz-lined fractures often contain Mn-oxide minerals and may also contain calcite or mordenite (Carlos et al. 1995, p. 24). Mordenite is generally the only zeolite found in fractures in the devitrified Crater Flat Group, and its distribution varies across the mountain. Fracture-associated mordenite is most common in the southernmost drill holes (Carlos et al. 1995, p. 24). This contrasts with the absence of mordenite in zeolitized

matrix within the Crater Flat Group at this location (Carlos et al. 1995, pp. 5, 8 to 12). Crystals of analcime occur in fractures of the saturated zone at the northern end of Yucca Mountain (Figure 5.2-3), where analcime also occurs in the altered tuff matrix (Carlos et al. 1995, p. 23). Clinoptilolite-heulandite can also occur in fractures at these depths and may coexist in the matrix with analcime. The fracture analcime has a Si-rich, Na end-member composition, similar to the analyses of matrix analcime.

Mn-oxide minerals and iron oxides, with quartz and calcite, are the most common fracture coatings below the water table in the devitrified Crater Flat Group over most of Yucca Mountain. In these devitrified intervals below the static water level, hematite is the dominant iron-oxide mineral. Goethite occurs with hematite in several fractures but is not common. Cryptomelane-hollandite is the most common Mn-oxide mineral throughout the Crater Flat Group below the static water level. Fracture-flow experiments with Np show that the cryptomelane-hollandite minerals in saturated zone fractures provide exceptional retardation of Np migration (Section 10.4.4).

Smectite and mordenite occur together in some fractures in the devitrified intervals in the Crater Flat Group below the water table. Several occurrences of illite have been identified in the deeper tuffs of the saturated zone; green clay (illite) associated with calcite and hematite is the most abundant fracture-filling mineral association in the deepest portions of the Tram Tuff, where clinoptilolite gives way to analcime in the tuff matrix (Carlos et al. 1995, pp. 8 to 12, 23). Illite/smectites with high illite content are likely to be less sorptive than the expandable smectites; for most of the exploration block, however, large illite contents are found only at great depth. Large illite content is generally associated with zones of matrix albite alteration.

Calcite is unevenly distributed but is a locally common fracture filling in the Crater Flat Group. As mentioned above, it is the most common fracture filling in extensively analcime-altered or albite-altered tuffs of the deep saturated zone, but it also occurs over restricted depth intervals in the devitrified tuffs of the shallower saturated zone, usually with Mn-oxide minerals arrayed along transmissive fractures (Carlos et al. 1995, p. 24). In most of these shallower saturated zone occurrences, the calcite is pitted or corroded and shows evidence of alteration to calcium-mordenite (Vaniman and Chipera 1996, p. 4423).

Fault Mineralogy—Fault mineralogy can be a critical component in evaluating flow and transport. Faults can operate as highly transmissive features, particularly if the faults contain no mineralization or if mineralization along the fault is limited to minerals with very low surface area (e.g., sparry calcite). Alternatively, minerals with very high effective surface area such as clays and zeolites can turn a fault into a flow barrier. These distinctions are important, because calcite, smectite, and zeolite have all been observed as fault-filling minerals at Yucca Mountain. Although a simplified consideration suggests that any fault is a discontinuity likely to divert flow, regardless of whether the fault opening is the pathway or the fault barrier is deflecting flow, the very different flow rates and different interactions of minerals such as clays or calcite with radionuclides make the distinction of mineralogy important.

Chlorine-36 studies within the unsaturated Topopah Spring Tuff suggest that the amount of secondary-mineral deposition in major fault zones has been insufficient to significantly decrease the transmissivities of these fault zones. These [36]CI data show that fast paths have transmitted

surface infiltration to the depth of the potential repository host rock during the past 50 yr. The distribution of these results suggests that these fast paths may be associated with fault zones that cut through the Paintbrush nonwelded hydrogeologic unit and that are fed by sufficiently high surface infiltration rates to sustain a component of fracture flow through it. Apparently, the rates of calcite and opal deposition during the past 8 to 10 m.y. have been too low to plug all of the flow paths within the fault zones. Even where secondary mineral deposition may be sufficient to seal a particular fracture within the fault zone, alternate transmissive pathways are still available. In addition, periodic tectonic reactivation can dilate the fault and allow renewed fluid flow. Thus, it is possible that most—if not all—of the fault zones that cut the nonwelded unit above the potential repository host rock have the potential to become fast paths in the future, even at locations where surface infiltration rates feeding these fault zones at the top of the nonwelded unit may presently be too low to sustain fast-path flow through this unit.

In contrast, surface exposures of a fault at Busted Butte provide evidence of mineralization along a fault in the unsaturated zone that juxtaposes vitric nonwelded tuff against welded devitrified tuff. The result here is the most thorough zeolitization (98 percent) of vitric tuff yet observed in any sample from Yucca Mountain, with the zeolitization strictly confined to the fault zone (Broxton et al. 1993, p. 10). This fault mineralization apparently resulted from delivery of water through the fractured, devitrified tuff to the nonwelded vitric tuff at the fault interface. The very restricted penetration of zeolitization into the vitric tuff usefully illustrates limited unsaturated zone transport through this rock type.

Fracture and Matrix Systems Compared–Existing differences in fracture and matrix mineralogy and geochemistry are the result of rock-water interactions during the last 12 m.y. The constituents of fracture coatings and fracture-surface alteration were derived from the rock matrix and from material introduced by percolating waters. The nature and degree of mineralogic differences that develop between fracture and matrix vary with lithology, thermal history, rock hydrologic properties, saturation conditions, and percolation rates. The effects of these factors are discussed below.

Fracture/Matrix Geochemistry in Low-Porosity Tuffs–In low-porosity tuffs, which are exemplified by the densely welded devitrified or vitric units, evidence of short-range fluid and solute transport (decimeter scale) between matrix and fractures is a common attribute of the syngenetic alteration described in Section 5.2.1.1. This transport is thought to have occurred at temperatures slightly above ambient (Levy and O'Neil 1989, Table 1) and over time scales of hundreds to thousands of years.

At present infiltration rates, there is little penetration of fracture-transported fluids into dense rock matrix at ambient temperatures and short time periods. Chlorine-36 isotopic analyses of certain breccia zones and adjacent densely welded, devitrified wall rock 300 m beneath the surface of Yucca Mountain indicate that fluids in the fractured rock and in the intact rock matrix are not in isotopic equilibrium. Because these samples all represent active fast pathways that have apparently received infiltration from the surface within the past 50 yr., and because the isotopic composition of the infiltration they received has changed significantly over this short period due to input of bomb-pulse ^{36}Cl, isotopic disequilibrium within the fluid pathway is readily detectable. Away from the fast-path zones, chloride from fractures and the adjacent

matrix are in isotopic equilibrium. The isotopic values from these sites may indicate fluid residence times on the order of tens of thousands of years (CRWMS M&O 1998, p. 3-1).

Deposits of diagenetic fracture minerals, including clays, manganese oxides, and calcite, do not penetrate as far into the matrix unless syngenetic alteration has resulted in increased porosity. The concentration of diagenetic mineral deposits at fracture surfaces indicates that the dispersed fracture network provides most of the sites for potential radionuclide interactions in the densely welded units.

Fracture/Matrix Geochemistry in Highly Porous Tuffs–In the moderately welded to nonwelded tuffs, syngenetic alteration is largely absent. Wherever exposure to groundwater has been pervasive (below the present-day water table and for about 100 m above the water table), diagenetic zeolites have replaced all of the matrix glass in nonwelded tuffs. No preserved evidence indicates a unique role of fractures in the pervasive diagenetic zeolitization. Textural studies suggest that the pervasive zeolitization occurred early in the diagenetic history of Yucca Mountain (Bryant and Vaniman 1984, pp. 67 to 76). The fracture minerals in these zeolitized horizons are dominated by the same types of zeolites that occur in the matrix (Carlos et al. 1995, p. 28). Evidence discussed in Section 5.2.2.3 indicates that effective matrix interactions of groundwater with zeolites occur in these tuffs.

Correlation of fracture-lining zeolites just above and below the water table with degree and type of zeolitization of the high-porosity host tuff suggests that the fracture coatings may have formed at the same time as the tuff alteration. The similarity of chemical compositions of matrix and fracture-lining clinoptilolite supports this hypothesis. An increase in degree of alteration from clinoptilolite/mordenite to analcime in both fractures and matrix toward the north of Yucca Mountain suggests that this alteration may have been a result of hydrothermal activity related to the Timber Mountain volcanism, constraining the age of the zeolites to >9 Ma or older (Bish and Aronson 1993, pp. 154 to 156). The net evidence from both matrix and fracture minerals in high-porosity tuffs is thus indicative of early pervasive alteration, overprinted at critical boundaries (particularly within the glass-to-zeolite transition in the unsaturated zone) by subsequent cation exchange with existing alteration minerals. Although zeolites might still be forming at Yucca Mountain, the evidence shows that rates of formation are presently very low, and the principal impact of zeolites on site processes is through ion exchange.

Combined Data from Pumping Tests and Mineralogy that Bear on Fracture/Matrix Interactions–Evidence of fracture flow beneath the water table is provided by comparison of mineralogical and geochemical data with the location of transmissive zones determined by pumping of packed-off intervals (Benson et al. 1983, pp. 11, 12, Figures 4, 5, 6, 11). The data indicate that most flow beneath the static water level occurs in the devitrified tuffs between zeolitized layers (Figure 5.2-4). Fractures in these devitrified layers of the saturated zone often have Liesegang banding extended a centimeter or more into the matrix away from the fracture walls (Figure 5.2-5). This is a graphic indication of long-term rock-water interaction in transmissive fractures. The banded alteration is complex and can include hematite, smectite, cryptomelane, todorokite, pyrolusite, calcite, and stellerite. Microautoradiography studies (Section 10.3.1.2) and fracture-flow dynamic transport experiments (Section 10.4.4) have been successful in associating actinide sorption with smectites and manganese oxides that line some of these fractures. Studies conducted of a fracture from the transmissive zone in USW G-4

(Figure 5.2-4) indicate that the Mn-oxide minerals in this sample, principally todorokite, might provide the most significant retardation of Np, a particularly poorly sorbing radionuclide, by any phase at Yucca Mountain.

The distributions of major zeolitic intervals can in general be mapped laterally and predicted with some confidence based on information from boreholes, although there is some latitude in defining the likely effective thicknesses and geometries of these zeolitic intervals (Section 4.8.4.5.1). Within these zeolitic intervals, fracture minerals tend to be zeolites similar to those in the host rock. Between the zeolitic intervals, where tuffs are largely devitrified, cryptomelane-group manganese oxides are typically found in fractures of the more welded portions. Mordenite is also locally abundant in some of the saturated zone fractures. As noted above, heterogeneity of fracture mineralogy occurs in the saturated zone, but it is not as pronounced as in the fractured unsaturated zone.

Figure 5.2-4 shows that most transmissivity in the saturated zone occurs in rocks with few zeolites and clays, except for transmissive zone T5 in the zeolitic, bedded interval at the base of the Bullfrog Tuff in UE-25 b#1 (as shown in Figure 5.2-4). The history of any waste that passes into the saturated zone will thus be determined by the combined processes of transport through transmissive zones, sorption and desorption on fracture-wall minerals within the transmissive zones, and dispersion into tuffs that may interact with waste either predominantly through mineral surface processes in devitrified tuffs or cation exchange in zeolitic tuffs.

The saturated transmissive zones tend to be restricted to discrete intervals less than 20 m thick within the devitrified, nonzeolitic tuffs. Exceptions to this tendency, however, exist. The transmissive zones are at least in part determined by intervals of abundant shear fractures (e.g., the zone at approximately 900 m depth in USW G-4 and the zone at approximately 480 to 500 m depth in UE-25 p#1) (Figure 5.2-4). However, mineralogy may also play a role in delimiting transmissive zones, as in UE-25 b#1 at approximately 810 to 820 m depth, where a transmissive zone is capped by an exceptionally smectite-rich zone in devitrified tuffs. This exclusion of flow from clay-rich intervals illustrates the role of mineralogic aquitards in restricting flow paths within the saturated zone.

Zielinski (1983, p. 14) and Zielinski et al. (1986, pp. 374 to 377) have proposed that abundances of Mn-oxide minerals can be used as a guide to the extent of past rock-water interaction. This conclusion appears to be borne out in the single, prominent transmissive zone in drill hole USW G-4 (Figure 5.2-6). This zone, at a depth of 892 to 902 m, occurs in an interval of intense shear fracturing (878 to 893-m depth) (Spengler and Chornak 1984, pp. 40 to 43). The Mn-oxide minerals cryptomelane and hollandite are also concentrated in this interval. The extent of association between shear fractures, transmissive zones, and manganese-oxide minerals has not been thoroughly demonstrated, but based on what is known, this association appears to be common.

Spengler and Rosenbaum (1991, p. A119) suggested that a 40- to 60-m-thick breccia zone, within the Tram Tuff and dipping 15° northwest, accounts for much of the transmissivity between wells about 2 km southeast of the potential repository. The clasts in this breccia are cemented by quartz, calcite, and hematite. Steeply dipping shear fractures within the breccia zone are hematite-coated. The combined observations of Zielinski (1983), Zielinski et al.

(1986), and Spengler and Rosenbaum (1991) suggest an important role for both manganese oxides and hematite in contributing to the retardation of possible waste movement by surface complexation of heavy metals and indicating present and past transport pathways.

5.2.2   Links between Rock and Fluid Geochemistry

Minerals that have precipitated from or reacted with groundwater provide a record of the chemical species that were carried in solution as well as some evidence related to groundwater composition (e.g., Eh). In general, the most effective mineralogic recorders are those that occur in fractures, particularly in zones where much of the communication between water and rock is related to fracture flow.

Calcites found throughout the thick sequence of unsaturated zone tuffs at Yucca Mountain have surfaces that might be either unaltered or have dissolution textures. Solution pits and etching features can be seen on the surfaces of some calcites in the unsaturated zone. Small rhombic pits of a few micrometers occur in calcites from a variety of unsaturated zone locations; irregular grooving of specific faces is also found. However, growth steps occur on some calcites that have no surface evidence of dissolution. Evidence of both dissolution and precipitation can thus be found among the unsaturated zone calcites, generally without apparent stratigraphic significance (Vaniman and Chipera 1996).

In contrast to the apparently random distribution of dissolution or precipitation textures in the upper unsaturated zone, there is a "barren zone" of few calcite occurrences that extends from approximately 100 to 300 m above to approximately 400 m below the water table; this barren zone thus straddles the boundary between the unsaturated zone and the saturated zone. The barren zone (shown on Figure 5.2-7) contains very deeply etched calcites in the unsaturated zone at the top of the lower vitrophyre of the Topopah Spring Tuff and throughout the saturated zone above the deep carbonate-altered zone, where Mn-rich calcites of different origins are abundant. The origins of these deep Mn-calcites are linked to release of Ca from Ca-bearing zeolites (clinoptilolite and mordenite) in the formation of analcime and albite. The extensively pitted calcites of the barren zone share a common layering of curving, fibrous, Ca-zeolite that drapes the dissolution pits (Figure 5.2-8). The compositions of all of these draping, fibrous zeolites appear to be similar in scanning electron microscope/electron dispersive spectroscopy analysis; they have relatively simple exchangeable-cation compositions (essentially Ca only). X-ray diffraction analysis of the fibrous Ca-zeolite from drill hole G3 at 898 m depth shows that the zeolite is mordenite. The similarity between this and the other calcite-draping, fibrous zeolites suggests that all may be mordenite, which is the only common curved, fibrous zeolite with this morphology at Yucca Mountain.

Very low Sr concentrations can occur in calcites from the barren interval that extends from the base of the Topopah Spring Tuff to the deep carbonate-altered zone (shown on Figure 5.2-7). Calcites from this barren zone may have as little as 1 µg/g Sr. Although these calcites occur in both unsaturated and saturated environments, they share a common association with zeolites and smectites. The calcites from the base of the Topopah Spring Tuff occur in the altered smectite-bearing and zeolite-bearing top of the rhyolitic vitrophyre (v2), just beneath this vitrophyre, or actually within the clinoptilolite-bearing sequence at the very bottom of the Topopah Spring Tuff. Deeper calcites from the saturated portion of the barren zone occur in transmissive

devitrified tuffs that are sandwiched between thick intervals of clinoptilolite-bearing and mordenite-bearing tuff. In all of these cases, there is abundant local zeolite and/or smectite to accumulate Sr, further depleting it in waters that originally precipitated the barren zone calcites.

5.2.2.1 Trace-Element Signatures in Minerals Precipitated from Groundwater

In those areas of Yucca Mountain beneath the potential repository block, densely welded tuffs are largely restricted to the unsaturated zone. Fractures of the unsaturated zone in the densely welded tuffs of the Paintbrush Group contain a generally calcic suite of minerals, including calcite, Ca-zeolites (stellerite, heulandite, and mordenite), Ca-smectite, and rancieite, along with silica polymorphs and lithiophorite. Pore water extracts from parts of the Paintbrush Group above the static water level (Yang 1992) have a chemistry different from that of groundwater from the Paintbrush Group below the static water level (Benson et al. 1983, Table 1 [well J-13]), with increased Ca, Mg, K, and Sr above the static water level. The higher Ca, Mg, and Sr contents of the pore waters, compared with the composition of groundwater below the static water level, are reflected in the fracture-lining mineral assemblages in the Paintbrush Group.

The distribution of lanthanides in Yucca Mountain calcites points strongly to leaching from local quartz latite or rhyolite sources for many of the constituents deposited from waters of the unsaturated zone. The evidence of Ca-rich pore water compositions, discussed above, is in accord with the evidence of common calcite deposition in fractures of the unsaturated zone (Vaniman and Chipera 1996). Lanthanide-element signatures within these calcites provide information on which source rocks have been involved in generating the groundwater chemical compositions. The preponderance of calcite with lanthanide compositions inherited from rhyolitic rather than quartz-latitic sources agrees with the much greater abundance of rhyolitic tuffs at the site. Moreover, the calcites with inherited quartz-latitic lanthanide compositions occur directly beneath the most extensive body of quartz-latitic and quartz-latite-like glass (Topopah Spring Tuff quartz latite and Pah Canyon low-silica rhyolite) at the site. This location is exactly where these calcites should occur if downward-flowing waters in the unsaturated zone are perched on top of the Topopah quartz-latite vitrophyre, react with the quartz-latitic glass, and then resume downward flow.

Figure 5.2-9 illustrates the chemical information deposited in fracture calcites that reflects the local lithologic sources of lanthanide elements in unsaturated zone groundwaters. The key distinctive feature of lanthanide-element compositions in quartz-latitic tuffs, aside from higher light lanthanide (La to Sm) content, is the absence of any significant Eu anomaly in chondrite-normalized plots, in contrast to the characteristic and strong negative Eu anomaly in rhyolitic tuffs (Figure 5.2-9a). When the lanthanide-element compositions of fracture calcites are plotted against their stratigraphic position (Figure 5.2-9b), it can be seen that quartz-latitic source compositions (essentially no Eu anomaly outside the range of quartz latites, signified by Eu measured/calculated between 0.77 and 1.12) are largely restricted to horizons where glassy quartz-latitic rocks occur, within an otherwise rhyolitic series of tuff deposits. This restriction shows that lanthanide elements dissolved from source rocks tend to be deposited locally, with very little down-section transport. If significant transport of lanthanide elements did occur with downward flow in the unsaturated zone, one would expect more quartz-latitic compositions to appear in calcites deposited below the quartz-latitic source rock. It is also notable, however, that many calcites with Eu anomalies intermediate between rhyolites and quartz latites occur in the

quartz-latitic horizon. Some transport of groundwaters with the overwhelmingly predominant rhyolitic signature does occur into the quartz-latitic horizons. Nevertheless, the evidence from Eu anomalies inherited by calcite precipitates points strongly to limited transport of lanthanide elements, which have geochemical affinities with transuranic elements.

5.2.2.2   Mineralogic Record of Groundwater Redox Processes

Lanthanide-element data for the calcites of Yucca Mountain indicate at least two distinct depositional environments: an upper system in which solutions are Ce-depleted through removal of Ce^{3+} oxidized to Ce^{4+}, and a deeper carbonate-altered system in which all of the lanthanide-series elements are Ln^{3+} (Vaniman et al. 1996, Volume 1, Section 4, pp. 33 to 36). Sections 5.3.6 and 5.3.8 of this report provide a discussion of Eh at Yucca Mountain. The deeper carbonate-altered system occurs at depths greater than 400 m below the present water table (Figure 5.2-7) and is of little consequence for transport systems at Yucca Mountain. The shallower carbonate-altered system, with evidence of Ce oxidation and segregation from the other lanthanide elements, is highly relevant. Figure 5.2-10 illustrates the mechanism by which Ce is segregated from the other lanthanide elements (Figure 5.2-10a) and the consequences of this process as recorded in fracture calcites from several different stratigraphic horizons (Figure 5.2-10b). Data collected from mineral separates (Vaniman and Chipera 1996) and surveys for cerium in fracture samples (Carlos et al. 1993, pp. 56, 57, Tables 2, 4) reveal strong correlations of cerium with certain manganese-oxide minerals. These cerium accumulations are most prominent in rancieite and can readily account for the corresponding depletion of cerium in those solutions from which calcite has precipitated (Figure 5.2-10a).

The determination of cerium depletions in calcites, compared against the other lanthanide elements, provides a measure of how effective the cerium accumulation by manganese-oxide minerals has been. Figure 5.2-10b shows that the only calcite samples above the water table with no cerium anomalies are at the very surface, in soil calcretes. All calcite samples at any greater depth (but above the deeper carbonate system, not shown in this figure) have some cerium depletion. However, there is a significant lessening of the cerium anomalies, to measured/calculated values greater than 0.2, in some of the calcites within and just below the glassy tuffs between the crystalline Tiva Canyon and Topopah Spring units. The calcite data summarized in Figure 5.2-10b show some important features. The subsurface environment down to and just below the water table is one in which the cerium abundances in all groundwaters are significantly depleted. Even though surface calcites have no cerium anomalies, and dissolution of tuffs (especially glassy tuffs) provides fresh input of lanthanides without cerium anomaly, the Ce removal mechanism is so effective that these inputs are soon marked by cerium depletion. It should be noted that the input of dissolved fresh glass, from which solutions with essentially no Eu anomaly can be formed (Figure 5.2-9b), nevertheless produces solutions that all have significant cerium anomalies. Moreover, the cerium anomalies remain elevated for modest distances (several tens of meters) below the glass horizon, but do not persist at greater depth. These data point to the very effective operation of the Ce removal system at any transport distances over a few tens of meters, providing a "scale factor" for groundwater interaction with geochemically active fracture minerals.

Characteristic negative cerium anomalies in calcites of the oxidizing system are present in both unsaturated zone and upper saturated zone rocks. Manganese-oxide minerals, particularly

rancieite but possibly others, appear to provide the single most important sink for Ce^{4+} at Yucca Mountain. The virtually universal negative cerium anomalies of oxidizing-zone calcites show that all flow paths in the upper 1 km of Yucca Mountain have some effective contact with manganese oxides. This observation is important in considering the potential impact of manganese oxides and other trace phases on radionuclide transport. Studies specific to Yucca Mountain point to the potentially significant retardation of radioactive wastes by manganese oxides. However, when such minerals are present in only trace amounts, it is uncertain whether fluids can actually interact effectively with such scarce materials. At Yucca Mountain, the universal record of Ce depletions in calcites of the subsurface oxidizing zone, which includes the proximal portions of all transport pathways for radioactive waste, provides a strong indication that fluids do interact with these minerals, despite their low abundance. The calcite data show that even trace minerals, particularly those along fractures, will play an important role in radionuclide interactions.

5.2.2.3   Zeolites and Groundwater Conditioning

Zeolitization of vitric tuff results in an initial mobilization of elements at the time of alteration. However, the zeolites thus formed can also be subsequently modified by cation exchange. White et al. (1980) noted that groundwaters increase in Na and decrease in Ca and Mg after passing through zeolitic tuffs in the unsaturated zone at Rainier Mesa, located 50 km north-northeast of Yucca Mountain. The authors concluded that zeolites (and perhaps clays) selectively removed bivalent cations from the groundwater system. Analyses of vitric and zeolitic tuffs in close proximity and of a single homogeneous depositional unit allow determination of the net effects of both initial chemical alteration and subsequent cation exchange. Generally, the zeolitized samples show gains in Ca, Mg, and Sr with losses in Na, K, and Si in the alteration from glass to zeolites. However, aside from Sr, trace elements are less affected. Broxton et al. (1986, p. 20) showed that, zeolitized tuffs are enriched in Sr, whereas they are depleted in Rb and U relative to source glasses. Since the work by Broxton et al. (1986), data provided in Broxton et al. (1993) have provided the information to also examine variation in lanthanide-element compositions in glasses and adjacent zeolitized rocks. These comparisons are shown in Figure 5.2-11. There is little or no difference in lanthanide-element patterns between vitric sources and zeolitic products.

Data obtained by X-ray fluorescence analysis of samples that had been previously analyzed by quantitative X-ray diffraction show that the strontium increase noted by Broxton et al. (1986, p. 20) is not a general phenomenon but is restricted to the tops of zeolitic horizons at Yucca Mountain. Figure 5.2-12a shows a distinct strontium concentration in the upper approximately 20 m of the major zeolitic horizon of UE-25 UZ#16; there are also distinct strontium concentrations at the top of the horizon with very minor zeolite abundances in SD-12 (Figure 5.2-12b). This occurrence of strontium concentrations at the tops of zeolitic horizons provides evidence that laboratory models of strong strontium selectivity and short-range dispersion through sorption/desorption are indeed supported by natural site data. The data shown in Figure 5.2-12 illustrate the effective action of zeolitized barriers to strontium migration. The occurrence of strontium retention profiles at the tops of zeolitized horizons provides evidence of generally downward flow in the unsaturated zone, although lateral flow along the tops of relatively impermeable zeolitic rocks may also occur. The pronounced concentrations of strontium that occur at the tops of zeolitized zones beneath the potential host rock provide direct

evidence of the effective extraction of strontium from downward-flowing solutions at Yucca Mountain since the time of zeolite formation (Vaniman et al. 1999, p. S5).

5.2.2.4 Past Variation in the Water Table: Mineralogic Evidence

Changes in past elevations in the static water level have implications for possible changes in repository-to-static water level distance under possibly wetter climates in the future. One of the potential mineralogic indicators of past elevations in static water level beneath the exploration block is the distance between the top of the first major zeolitized horizon and the present static water level. Figure 5.2-13, modified from Chipera et al. (1995), summarizes some estimates of this distance from several drill holes. Ideally, a direct correlation between the occurrence of the top of this horizon of abundant zeolitization and an ancient static water level would be seen in all drill holes as a surface occurring at a relatively fixed elevation above the present static water level. However, there are several reasons (Vaniman et al. 1996, Volume I, pp. 2, 25 and 2, 26) for this not to be the case:

- Even if the static water level were to rise, abundant zeolitization would not occur to the height of saturation if appropriate parent material (porous, nonwelded vitric tuff) were not present.

- More than one event of rise in the static water level can result in variable elevations of the zeolitization horizon because of possible tectonic offsets in parts of the exploration block between the timing of ancient and more recent rises in the static water level.

- The present static water level is relatively flat beneath the exploration block but rises sharply to the north and west (Ervin et al. 1993, pp. 1554, 1558, Figure 1). Similar variable elevations may have occurred in an ancient static water level but not necessarily in the same locations as in the present static water level.

- Zeolitization can occur in unsaturated rocks, especially in situations of possible capillary draw, perched water, or lateral transmission from features that may be significant sources of recharge during pluvial episodes.

- Widely spaced sample collections, and, in particular, the need to rely on cuttings or intermittent core/sidewall samples in all H-series and WT-series holes, place large uncertainties on the estimates of the top of the zeolitized horizon (generally at least ± 10 m). The contact between vitric and zeolitic rocks is also gradational (Levy 1991), adding a further uncertainty in the location of the zeolitization front.

Given these caveats, there remains a significant number of drill cores with zeolitization horizons about 106 to 135 m above the present static water level (Figure 5.2-13). Unfortunately, all of these cores are closely clustered in one central area and are thus of uncertain regional significance. The search for ancient static water levels will require the examination of multiple lines of evidence. Combined studies of structural indications of fault displacements of the zeolitization horizon, of glass preservation, and of other mineral distributions (e.g., tridymite) have been interpreted to indicate that past rises in the static water level have been no greater than about 60 m (Levy 1991, p. 477). Studies of Sr isotopes in calcite at Yucca Mountain suggest a possible ancient static water level approximately 85 m above the present static water level

(Marshall et al. 1993). Hydrologic modeling suggests a maximum static water level rise of 130 m (Czarnecki 1984, p. 1). At present, it appears the modeled static water level maximum rise of 130 m may be closest to inferences of past static water level from zeolite occurrences.

Levy (1991, p. 32) pointed out that the localities with almost no drillcore data, in the central and southern part of the exploration block, are critical to this question, for it is here that the vitric-to-zeolitic transition of the Calico Hills Formation occurs. Drill cores USW SD-12 and USW SD-7 provide important data for filling this gap, but the data are sufficiently complex to leave some questions unresolved. The zeolite abundance data from USW SD-12 suggest a maximum past water table rise of 106 m (Figure 5.2-14), but persistence of tridymite at greater depth could be interpreted to limit this rise to less than 45 m. Similarly, the zeolite abundance data from USW SD-7 suggest a maximum past water table rise of 211 m (Figure 5.2-15), yet persistence of tridymite at depth could limit this rise to less than 127 m. Clearly, the mineral occurrences that might be interpreted as indicators of past water table elevations yield conflicting interpretations, and adequate interpretations must explain all of the conflicting data.

It should be remembered that the horizon of concern is that of the vitric-to-zeolitic transition, and a possible surface of past water table rise may be as readily defined based on the deepest preservation of abundant (10 percent or more) nonwelded glass as on the shallowest occurrence of abundant zeolites. Using the depth of abundant glass as a criterion, a different set of "past water table elevations" can be defined, as shown in Figure 5.2-16. Divergences between the zeolite-based (Figure 5.2-13) and glass-based (Figure 5.2-16) model surfaces are in some cases caused by the inadequacies of dealing with widely spaced analyses of cuttings (e.g., ± 34 m in USW H-5), but the more recent data show a real and large overlap of glassy and zeolitic samples across a dispersed vitric-to-zeolitic transition (± 36 m in USW SD-7). In the most extreme example, the vitric-to-zeolitic transition in USW SD-12 is dispersed over a vertical range of 67 m if the slightly to moderately zeolitized samples of the Calico Hills Formation and the Topopah Spring Tuff are considered. (It should be noted that these occurrences of 10 percent or less zeolite were not included when determining the top of the zeolitized horizon in Figure 5.2-13.) This consideration is of more than passing interest, because the abundance at which zeolites become effective in sorption is an important factor to be considered in performance calculations. The Sr data indicate that the 67 m of slightly zeolitized tuff in USW SD-12 can be effective in sorbing those alkaline earth radionuclides for which clinoptilolite is highly selective (Figure 5.2-12b). Although the sorption of complex transuranics by clinoptilolite is minor (Robinson et al. 1995, pp. 18, 20), the potentially greater permeability of partially zeolitized tuffs, in contrast to those that are fully zeolitized, might permit dispersed access of radionuclide-bearing solutions to zeolite surfaces.

INTENTIONALLY LEFT BLANK

5.3 FLUID GEOCHEMISTRY OF YUCCA MOUNTAIN AND VICINITY

5.3.1 Fluid Geochemical and Isotopic Parameters and Their Relevance to Site Characterization and Site Evaluations

The geochemical data and models that are important for site characterization and site performance evaluations are discussed in this section. Geochemical and isotopic data for present-day fluids and for fracture minerals that reflect the site's past water chemistries are reviewed and evaluated for use in developing and testing models to explain variations in water chemistry and of site-scale hydrologic flow models for the unsaturated zone. Such models are required to derive bounds on future variations in the chemical compositions of waters in the Yucca Mountain flow system. These bounds are required to model the transport behavior of radionuclides in the flow system.

In this section:

- Fluid geochemical data that are relevant to site characterization and potential repository evaluations are identified (Section 5.3.2).

- Methods for investigating fluid geochemistry are reviewed (Section 5.3.3).

- Data on geochemical and isotopic compositions of local precipitation (Section 5.3.4) and surface water (Section 5.3.5) are discussed. The compositions of these waters define the starting point for the geochemical evolution of water in the unsaturated zone.

- Data on geochemical and isotopic compositions of unsaturated zone pore waters and perched water (Sections 5.3.6 and 5.3.7), and unsaturated zone gases (Section 5.3.8) are discussed.

- Relevant geochemical data for saturated zone groundwaters (Section 5.3.9) are discussed because the similarity between geochemical compositions of local perched water and saturated zone waters suggests common controls.

- Processes that control fluid compositions and data limitations for each category are described (throughout Section 5.3). See also Section 9.3.7.

- A conceptual model of fluid geochemistry evolution at Yucca Mountain and how these data bear on site characterization and potential repository performance are summarized (Section 5.3.10).

5.3.2 Data Sources

Section 5.3 is a compilation and synthesis of data and other information collected under various activities and reported in publications, Yucca Mountain Site Characterization Project (YMP) reports, the YMP Technical Data Management System, and other databases.

The primary input data used in this section are the geochemical and isotopic analyses of pore waters, perched water, and gases collected from the unsaturated zone at Yucca Mountain and

analytical data for surface waters and groundwaters in the area. The data sources are discussed in greater detail in CRWMS M&O (2000).

5.3.3 Sample Collection and Analytical Methods

This section reviews the sampling or measurement locations and collection methods for the different types of fluid samples analyzed in Yucca Mountain studies, including precipitation, surface waters, pore waters, gases from the unsaturated zone, and perched water. Detailed descriptions can be found in the original publications cited in the discussion below.

5.3.3.1 Sampling Locations

A summary of unsaturated zone geochemical and isotopic data available from Yucca Mountain boreholes is provided in Table 5.3-1. Surface-based boreholes from which water and gas samples were collected are shown in Figure 5.3-1. For subsurface-based boreholes, hydrochemical sampling was conducted in the Busted Butte field test facility; niches, alcoves, and drifts in the Exploratory Studies Facility (ESF); and the east-west Cross Drift (Figures 5.3-1, 5.3-2). The alcoves from which samples were collected include the upper Tiva Canyon alcove (ESF Alcove 1), the Bow Ridge fault alcove (ESF Alcove 2), the upper Paintbrush contact alcove (ESF Alcove 3), the Thermal Test Facility (Alcove 5), and the northern Ghost Dance fault access drift (ESF Alcove 6) (Figure 5.3-2).

5.3.3.2 Gas Samples

Gas samples have been collected from a limited set of surface-based boreholes. Borehole UZ-1 was instrumented for temperature and other probes at 33 levels, which allowed gas composition sampling from 15 distinct intervals (Montazer et al. 1985, p. 439). Additional boreholes were cased from the surface down to some depth and are open below this depth. In some boreholes, packers were installed to isolate specified intervals for gas sampling. In addition, gases were collected from radial and horizontal boreholes drilled from alcoves driven from the ESF Main Drift (LeCain and Patterson 1997, p. 3).

Sulfur hexafluoride, SF_6, was used in each borehole as a gaseous tracer to identify drilling-air contamination of the rock gas (Yang et al. 1996, pp. 9 to 11). Based on 10 yr. of records and the stabilized value in borehole UZ-1, the tracer (SF_6) concentration of less than 0.1 ppmv (parts per million on a volume basis) in the borehole air is used to define uncontaminated rock gas. In some instances, such as boreholes in Alcoves 2 and 3, SF_6 tracer concentrations did not decrease, even after several days of gas pumping (LeCain et al. 1997, p. 38; LeCain and Patterson 1997, p. 3). These residual tracer concentrations are believed to reflect the propensity of SF_6 to adsorb onto clays and zeolites in nonwelded units (Rattray et al. 1995, p. 1).

Two different methods were used to collect CO_2 for isotopic analysis (Yang et al. 1996, pp. 8 to 11). A molecular sieve method was used from 1984 to 1991. Starting in 1991, a whole-gas method was used for batch sampling. The whole-gas method is the preferred technique because the molecular sieve method depletes ^{13}C relative to ^{12}C, such that δ ^{13}C values reported for gas samples collected by this method represent depleted samples and are not representative of in situ

conditions. Consequently, $\delta\ ^{13}C$ data obtained for molecular sieve samples are not included in this section.

Investigations in the ESF alcoves have enabled a better understanding of gas flow in the upper part of the unsaturated zone; provided evidence of gas flow direction, gas flux, and travel time; determined the degree of fracture connectivity in the rocks; and supported conceptual models of fluid flow in the unsaturated zone (LeCain et al. 1997, pp. 18 to 20). In general, stable CO_2 concentrations, at levels significantly higher than atmospheric or alcove (350 ppmv) concentrations, were an indication that the gas being pumped from the borehole was representative of rock gas.

In addition to the analysis of C isotopes in CO_2, other isotopic analyses sometimes included O isotopes in CO_2 (as an indicator of the degree of isotopic exchange with pore water) and H and O isotopes in water vapor.

5.3.3.3   Pore Water Samples

Despite precautions to preserve the integrity of drill core samples for pore water characterization, some geochemical and isotopic characteristics of these fluids may have been perturbed because drilling was conducted using air and the cores were exposed to ambient atmospheric conditions for some time before they were hermetically sealed. Thus, pore water analyses should be used with appropriate caution in subsequent interpretations.

Water samples were extracted from drill core using one of three methods: compression, ultracentrifugation, or vacuum distillation (for analysis of tritium and stable isotopes of H and O). These techniques were applied to core samples recovered from dry-drilled boreholes (LeCain et al. 1997, p. 14; Yang et al. 1988, pp. 29 to 30, 33 to 34; Yang et al. 1990, pp. 250, 258; Yang et al. 1996, p. 12; Yang, Yu et al. 1998, p. 6; Fabryka-Martin, Wolfsberg, Roach et al. 1998, pp. 264 to 265).

Extracted pore waters were filtered through Nucleopore filters (0.45 μm) before chemical analysis (Yang, Yu et al. 1998, p. 7). Cation concentrations were measured using inductively coupled plasma emission spectroscopy, and anion concentrations were measured using ion chromatography. Reported Al values reflect the presence of both dissolved and particulate components less than 0.45 μm.

Pore water data are discussed in Sections 5.3.6.3 and 5.3.7. For densely welded tuff core samples, which generally have moisture contents less than 5 percent by weight, only a few samples produced sufficient pore water by compression or centrifugation to permit a complete chemical analysis. For these samples, vacuum distillation was used to extract water (as vapor) for analyses of tritium and stable isotopes of H and O (Yang et al. 1996, p. 6). This method was applied to core from some surface-based boreholes. In addition, in the Bow Ridge fault alcove, water samples were extracted from cores of boreholes HPF#1 and HPF#2 by vacuum distillation and analyzed for tritium to assess the rate of water infiltration from the land surface (LeCain et al. 1997, p. 40). In the Upper Paintbrush Contact Alcove, water samples were obtained by vacuum distillation from cores of boreholes RBT#1 and RBT#4. These samples were analyzed for tritium to ascertain the spatial distribution of percolation flux near the contact between

Paintbrush Tuff nonwelded (PTn) and underlying Topopah Spring welded (TSw) hydrogeologic units.

5.3.3.4 Perched Water and Groundwater Samples

Samples of perched waters were obtained from deep surface-based boreholes UZ-14, NRG-7a, SD-7, and SD-9 (Yang et al. 1996, pp. 34 to 37) as well as from WT-24. These samples were collected with a bailer or from the surface output of a downhole pump, which makes it difficult to derive reliable values for some parameters of interest, such as pH, Eh, and the major species of redox-sensitive elements, such as ferrous and total Fe. Geochemical and isotopic analyses of perched waters are discussed in Sections 5.3.6.5 and 5.3.7.

Groundwater samples from the saturated zone were generally obtained either with a downhole pump or a bailer (Ogard and Kerrisk 1984, pp. 5, 7; Benson and McKinley 1985, p. 1). Geochemical data for these samples are discussed in Section 5.3.9; isotopic data are discussed in Section 5.3.8.

5.3.3.5 Sample Processing for Isotopic Analyses

Methods of processing samples for isotopic analyses include leaching salts from unsaturated rock cores or cuttings for ^{36}Cl and Sr isotopic analysis, distillation or compression of core to extract water for analysis of tritium or stable isotopes of H and O, compression of core to extract water for C isotopic analysis, and digestion of mineral samples for analyses of Sr isotope ratios or of U-series nuclides. Centrifugation of core has also been used to extract water for some of these isotopic analyses. All uncertainties quoted below are one standard deviation unless stated otherwise.

Tritium–Hydrogen-3 (tritium) was analyzed by liquid scintillation counting, with an uncertainty of $\pm$ 4 tritium units (TU) (one sigma) (Yang, Yu et al. 1998, p. 7). Section 5.3.7.2 provides a statistical evaluation of the tritium data to show that only results above 25 TU can be interpreted unambiguously as containing a component of bomb-pulse tritium. When sufficient water was available, some samples from ESF boreholes were isotopically enriched prior to analysis by liquid scintillation, a method with an uncertainty of $\pm$ 0.7 TU or better (Clark and Fritz 1997, p. 17).

Stable Hydrogen and Oxygen Isotope Ratios–Ratios of ^{2}H to ^{1}H and of ^{18}O to ^{16}O were measured by gas source mass spectrometry. These data are reported as $\delta\,^{2}H$ and $\delta\,^{18}O$, which express the sample's degree of enrichment or depletion of the heavy isotope relative to the Vienna Standard Mean Ocean Water standard (Clark and Fritz 1997, pp. 6 to 8). Uncertainties were $\pm$ 0.2 per mil (‰) for $\delta\,^{18}O$ and $\pm$ 1.0‰ for $\delta\,^{2}H$ (Yang et al. 1996, p. 8).

Stable Carbon Isotope Ratio–The ratio of ^{13}C to ^{12}C was measured by conventional mass spectrometry. It is reported as $\delta\,^{13}C$ with a precision of about 0.2‰ (Yang, Yu et al. 1998, p. 7). Delta carbon-13 is measured relative to the Vienna Pee Dee Belemnite standard ($^{13}C/^{12}C$ equal to 0.011237) (Clark and Fritz 1997, pp. 6, 9).

Carbon-14–Carbon-14 was analyzed either by conventional liquid scintillation or tandem accelerator mass spectrometry (Yang, Yu et al. 1998, p. 7). Both methods have analytical uncertainties on the order of ± 0.7 percent modern carbon (pmc). The advantage of tandem accelerator mass spectrometry, however, is its capability to analyze extremely small samples (less than 5 mg of C), whereas conventional scintillation counting requires between 1 and 3 g of C, depending upon the sample's age (Clark and Fritz 1997, p. 19).

Chlorine-36–Chlorine-36 was analyzed by accelerator mass spectrometry (as $^{36}Cl/Cl$), with typical uncertainties of 5 percent (Sharma et al. 1990, p. 410).

Stable Strontium Isotope Ratio–The ratio of ^{87}Sr to ^{86}Sr was measured using solid-source thermal ionization mass spectrometry. The ratios are commonly expressed as δ ^{87}Sr relative to the ratio of reference seawater Sr ($^{87}Sr/^{86}Sr$ equal to 0.7092) (Paces, Marshall et al. 1997, p. C-1).

Uranium, Thorium, and Lead Isotope Ratios–Solid-source thermal ionization mass spectrometry with isotope dilution was used to obtain $^{234}U/^{238}U$, $^{230}Th/^{238}U$, $^{207}Pb/^{235}U$, and $^{206}Pb/^{238}U$ ratios (Paces, Neymark et al. 1996, p. 16; Paces, Marshall, Whelan, and Neymark 1997, p. E-2).

5.3.4 Chemical Composition of Precipitation

Chloride concentrations in local and regional precipitation, along with associated precipitation quantities, are primary input data that provide the basis for estimating infiltration rates by the chloride mass balance method (Sections 5.3.4.2 and 5.3.10.1). All other precipitation chemistry data are used in a corroborative manner, to characterize local and regional precipitation chemistry in terms of average concentrations and relative ion ratios. These precipitation trend data provide a baseline against which to compare and contrast chemical compositions of the various sources of water at Yucca Mountain, and to illustrate general trends of relative enrichment or depletion of one element when compared to another (Sections 5.3.4.2 and 5.3.4.3).

5.3.4.1 Processes Controlling Precipitation Chemistry

The initial chemical and isotopic composition of Yucca Mountain groundwater is largely established by that of local precipitation and dry fallout. Once the precipitation enters the soil zone, absolute and relative concentrations of the various constituents are shifted to varying degrees by evapotranspiration and by interactions with minerals, organic matter, and the gas phase. The effects of these latter processes are described in subsequent sections. Isotopic data for precipitation are discussed in Section 5.3.7.

Processes and sources that control the initial composition of precipitation or fallout include the following:

- **Salts from marine and terrestrial sources**–For example, ions such as Na and Cl in precipitation are derived predominantly from the ocean, whereas terrestrial sources contribute to Ca and Mg concentrations.

- **Anthropogenic sources**–Acid rain resulting from industrial releases of sulfur is an example of an anthropogenic source that impacts the chemical reactivity of precipitation.

Other examples of anthropogenic sources are freons and fallout of radioactivity from aboveground nuclear tests. Global fallout nuclides (tritium, ^{14}C, and ^{36}Cl) in precipitation are discussed in Sections 5.3.7.2 to 5.3.7.4.

- **Wet and dry deposition processes**–For example, between one-third and two-thirds of the Cl deposition in southern Nevada is from dry deposition of aerosols and particulates, a process also known as dry fallout (Eriksson 1960, p. 82; Dettinger 1989, p. 62).

- **Atmospheric processes**–For example, processes include chemical transformation of molecular species. Different chemical species can be present as inorganic or organic gases or as aerosols, with each species having different average residence times in the atmosphere.

- **Evaporation**–Prior to deposition evaporation will concentrate many solutes, as well as affect the fractionation of H and O isotopes in moisture.

- **Air temperature**–Air temperature affects H and O isotopic fractionation, with the greatest fractionation observed for cold temperatures. Air temperature also controls gas solubilities.

- **Precipitation patterns**–Season, frequency, and cycles of precipitation events also affect precipitation chemistry.

Many problems complicate the collection and analysis of precipitation data. These include evaporation of rain or sublimation of snow in the collector, bacterial modification, and CO_2 uptake or loss. Even major elements may be below instrumental detection limits, and the charge imbalance for these analyses often exceeds 10 percent. Consequently, the use of precipitation chemistry data in this section has been limited to simple illustration of qualitative trends in major ion concentrations and distributions, and no modeling of the solution chemistry is conducted.

5.3.4.2 Present-Day Regional Characteristics

The largest database available for characterizing regional precipitation chemistry is maintained by the National Atmospheric Deposition Program/National Trends Network. The network presently consists of 200 rural stations throughout the United States that monitor wet-only deposition. A limited number of stations also monitor dry deposition, but none of these stations are in Nevada.

Within the YMP, the National Atmospheric Deposition Program/National Trends Network regional database has been used to characterize chloride deposition rates in the southwestern United States. Chloride is the most conservative dissolved chemical species in Yucca Mountain groundwaters, insofar as its origin is strongly dominated by atmospheric sources and the contribution from rock-water interactions generally appears to be negligible. Increases in subsurface concentrations of chloride relative to that in precipitation (including dry fallout of aerosols and particulates) are attributed to evapotranspiration in the soil zone, including sublimation of snow. Because of this characteristic, various pore water constituents are commonly plotted as a function of chloride concentration to assess the direction and magnitude of rock-water interactions in the subsurface (Section 5.3.6.3).

Chloride concentrations in pore water have also been used as a surrogate measure of infiltration rates using the chloride mass-balance method (Scanlon 1991, p. 138), in which total chloride deposition is a key parameter. In general, chloride concentrations in precipitation decrease with increasing distance from the ocean (Eriksson 1960, p. 87). However, dry deposition of chloride is quite variable, showing no clear trend, possibly because dry fallout largely depends upon local sources of chloride in addition to distance from the ocean and wind patterns, which control the regional distribution of aerosol particles and their deposition rates (Winchester and Duce 1967, p. 110; Eriksson 1960, p. 88). Eriksson (1960, p. 82) studied the ratio of chloride concentrations in runoff to those in precipitation and suggested that, as a rule of thumb, precipitation chloride constitutes about one-third of the total chloride deposition, with dry fallout accounting for the remaining two-thirds. In a local study of the Great Basin of Nevada and Utah, Dettinger (1989, p. 62) calculated an average bulk-precipitation concentration of 0.6 mg/L (for eight sites) and an average wet-precipitation concentration of 0.4 mg/L (for 66 sites), implying that dry deposition comprises about 33 percent of the total chloride input in this region. A crude estimate of the contribution of dry fallout to total chloride deposition rates in southern Nevada can also be derived by comparing the average annual chloride concentration in wet fallout at Red Rock Canyon (0.16 mg/L, unweighted average calculated from chloride data) (NADP/NTN 2000) to the average annual Cl concentration in precipitation at 3 Springs Basin, which includes both wet and dry fallout (0.51 mg/L, calculated from data in CRWMS M&O (2000). This comparison indicates that dry fallout comprises about 70 percent of the total fallout in this area.

5.3.4.3 Present-Day Site Characteristics

The isotopic and chemical composition of precipitation at the Yucca Mountain site is largely inferred from measurements made at other local sites (McKinley and Oliver 1994, pp. 1 to 3; 1995, pp. 1 to 3). Major ion chemistries of precipitation for the two precipitation chemistry monitoring stations in 3 Springs Basin (at 3 Springs Creek and Kawich Peak) were used to derive average annual weighted concentrations for major constituents and regression lines for these constituents relative to chloride concentrations (Table 5.3-2). The regression lines are used in Sections 5.3.5 and 5.3.6 to illustrate subsequent changes in water chemistry as it flows through the subsurface.

Chemical data for precipitation are also available for Red Rock Canyon, the desert observation station closest to Yucca Mountain in the National Atmospheric Deposition Program/National Trends Network. This site is about 120 km southeast of Yucca Mountain. The record used for the analysis in this section spans 12 yr., from 1985 to 1997, which includes two El Niño episodes, one in 1986 to 1987, and a long episode from autumn 1989 through summer 1995 (Fabryka-Martin, Turin et al. 1996, Section 4.1.2.2). Neither alkalinity nor carbonate species are reported in this database.

The chemistry of precipitation is important for modeling the composition of waters at Yucca Mountain because precipitation represents the starting point in the evolution of groundwater chemistry. Subsequent changes in the water chemistry as it enters the subsurface are illustrated by three types of diagrams:

1. Trilinear (Piper) diagrams show the relative concentrations of major ionic species. Figure 5.3-3 is a trilinear diagram for the precipitation samples from 3 Springs Basin,

to be compared against other trilinear diagrams for surface waters and subsurface waters in later sections.

2. Frequency distributions (histograms) of major elements are used to contrast the distributions of specific dissolved species in different parts of the hydrologic system.

3. Scatter plots of various major constituents as a function of some conservative species are a common method for evaluating the role of rock-water interactions in changing concentrations along a flow path. Chloride is usually considered to be the most conservative species, and a common assumption is that its concentration in surface and subsurface pore waters reflects increases due solely to evapotranspiration. Figure 5.3-4 presents a set of plots of Na, Ca, sulfate, bicarbonate, and silica as a function of chloride. Only samples with less than 1 mg/L of Cl have been included. The regression lines plotted for each constituent on this figure represent least-squares fits to the precipitation data from the two 3 Springs Basin sites.

Other than the monitoring studies at 3 Springs Basin and Red Rock Canyon, only a few studies of Yucca Mountain precipitation chemistry have been conducted, and the coverage of these studies was limited in time, space, and/or analytical data. Chloride, bromide, and sulfate were measured in a suite of about 100 samples collected from rain gauges at several neutron monitoring boreholes at Yucca Mountain in the spring of 1995. The purpose of these analyses was to provide independent corroboration for estimates of the Cl deposition rate, a parameter used in the chloride mass balance method (Section 5.3.10.1), and to characterize the Cl/Br and SO_4/Cl ratios of precipitation.

5.3.4.4 Representativeness of the Available Data

An important issue to address is the extent to which these data are representative of both past and present precipitation at Yucca Mountain. Monitoring at the site at the present time may not produce valid data because it may not be possible to separate out the effects of site disturbance from natural conditions. Present-day compositions may also not be representative of past (preindustrial) compositions because of the widespread effects of air pollution. The question arises, then, of which of the two available data sets is more representative of natural conditions at Yucca Mountain. The compositions differ in both absolute as well as relative concentrations of major ions (e.g., compare annual average values for Na/Cl, SO_4/Cl, and Ca/Cl in Figure 5.3-4). The Red Rock Canyon data provide a comparatively long (12 yr.) record, with details available for individual storms if desired. However, the proximity of Las Vegas may influence dust loadings and chemical compositions, and the lack of alkalinity analyses is a significant shortcoming that also makes it impossible to calculate a charge balance. In addition, only wet deposition chemistry is measured. The 3 Springs Basin data, although further removed from Yucca Mountain and representing a shorter time period (7 yr.), have reduced urban influence and include both wet and dry deposition data.

These precipitation data are considered adequate for the purposes for which they are used, that is, as input data for simple correlation plots and as corroborative data to support independent estimates of the chloride deposition rate at Yucca Mountain. For the saturated zone, the geochemical evolution of the water is not very sensitive to uncertainties in the precipitation

chemistry. However, for the unsaturated zone, the dominant input function is the composition of precipitation following evapotranspiration and, therefore, predictions of the unsaturated zone pore water compositions based on precipitation inputs can be more sensitive to the precipitation uncertainties because errors may be magnified as the water becomes more concentrated.

5.3.4.5 Scenarios for Future Trends in Precipitation Chemistry

Global climate change could be expected to influence the precipitation chemistry in the future through its effects on carbon-dioxide levels, rainfall patterns, and dust levels and sources. No studies exist or are planned to assess possible future trends or to establish bounds on such factors controlling precipitation chemistry and the possible consequence for the various geochemical parameters.

5.3.5 Chemical Composition of Surface Waters

This section describes the data available on the region's surface water chemistry. Three types of surface water chemistry exist, depending on the water source:

- Relatively dilute waters from runoff during precipitation or snowmelt
- Relatively saline waters from groundwater discharge at springs
- A mixture of the two preceding types.

After an overview of surface water occurrence in the basin, the following discussion focuses on the chemical composition of the first category of surface waters, particularly surface waters from potential recharge areas and along flow paths through the Yucca Mountain area.

5.3.5.1 Overview of Regional and Local Surface Water Bodies and Drainage Areas

Local drainages on Yucca Mountain ultimately enter the Amargosa River. The eastern slope drains via Yucca Wash, Drill Hole Wash, and Dune Wash to Fortymile Wash. Fortymile Wash spreads out into a distributary system in the Amargosa Desert, joining the Amargosa River about 18 km (11.2 mi) north of Death Valley Junction, California. An unnamed ephemeral channel in Crater Flat collects drainage from the western and southern slopes of Yucca Mountain, draining to the Amargosa River near its confluence with Fortymile Wash. In addition, the tributary Carson Slough enters the Amargosa River as it flows southward through the Amargosa Desert. Carson Slough drains spring flow from the Ash Meadows regional groundwater discharge area in the eastern portion of the Franklin Lake Playa (also known as Alkali Flat), a discharge area for Yucca Mountain regional groundwater. However, the Amargosa River and its tributaries are ephemeral streams except for short distances where spring discharges enter the channel system; flow throughout its entire reach occurs rarely (Malmberg and Eakin 1962, p. 7; Walker and Eakin 1963, pp. 14 to 15) because of losses to infiltration and evaporation from the streambed.

Savard (1995, p. F241; 1998, pp. 9, 24) and Grasso (1996, pp. 11 to 13) discussed climatic and weather patterns responsible for Yucca Mountain area streamflow and associated flooding. The winter/spring streamflow occurs during El Niño events when the track of Pacific cyclonic fronts crosses the Yucca Mountain region. Summer streamflow occurs from thunderstorms, often when the summer monsoon in the southwestern United States extends into the region. Occasionally, remnant hurricanes from the Pacific Ocean move in, causing streamflow in the late summer and

fall. These climatic factors influence the initial chemical and isotopic composition of the local precipitation.

Once the water contacts the ground, the chemistry of ephemeral surface waters evolves based upon the geologic materials with which the water comes into contact and the length of contact time between them. Factors that influence the chemistry of ephemeral surface waters include:

- Site topography (e.g., slope, ridgetop, terrace, sideslope, and channel)

- Soil development (e.g., depth of regolith, porosity, soil stratification/profile development, and infiltration rates)

- Soil mineralogy and chemistry

- Biota and vegetative coverage

- Evaporative concentration of solutes during flow.

In addition to ephemeral flows following precipitation events, perennial surface water in the Amargosa River drainage basin is associated with springs (Malmberg and Eakin 1962, p. 8). Flowing water occurs in the Oasis Valley, Ash Meadows, Tecopa, and Bad Water areas after infrequent precipitation and runoff events, as well as during winter months when evapotranspiration is at a minimum. Some areas dry up almost entirely during high evapotranspiration periods during the summer. Perennial surface waters are found at the following locations:

- Numerous permanent or nearly permanent springs discharge along or near the Amargosa River channel in Oasis Valley. Although the flow in the channel is ephemeral through the Amargosa Desert, short reaches of persistent flow occur between the desert and the location at which the channel enters Death Valley. Wet playas occur in the eastern (Peter's Playa) and southernmost (Alkali Flat) parts of Amargosa Desert.

- The Ash Meadows regional groundwater system, which drains the region east of Yucca Mountain, discharges at several perennial springs that sustain small pools at Ash Meadows in the southeastern Amargosa Desert. Crystal Reservoir, a man-made structure, captures discharge from Crystal Spring and several springs in the Point of Rocks area and drains to the Amargosa River by Carson Slough.

- Four small perennial ponds occur in the Amargosa Desert in former clay mining pits.

- Bad Water is a spring discharge pool in the terminal area of the Amargosa River in Death Valley.

5.3.5.2 Relevance of Surface Water Chemistry to Flow and Transport Models

Chemical and isotopic compositions of some of the surface waters described above may be relevant to flow and transport modeling for two major reasons. First, infiltration of surface runoff into the beds of large channels, such as Fortymile Wash, may contribute significantly to

local recharge and may thereby influence the chemistry of saturated zone fluids. Although such fluids do not have the potential to contact waste packages and are furthermore, unlikely to lie along the direct flow path between the potential repository and the accessible environment, characterizing their chemical and isotopic compositions is nonetheless necessary to be able to use these constituents as groundwater tracers for the regional flow system. Second, infiltration from runoff events collected from small channels above the potential repository, at locations where soil cover is negligible, may contribute to seeps that have the potential to directly contact the repository backfill and the waste canisters.

5.3.5.3   Surface Water Chemistry Data

Samples have been collected to document streamflow chemistry during the occasional runoff event as part of Yucca Mountain site characterization studies. Physical characteristics and chemical compositions of these surface runoff sites in the Yucca Mountain area and Fortymile Wash are discussed in this section. Sampling locations are plotted on the map in Figure 5.3-5.

Water quality data are also taken from a compilation of hydrochemical data collected in the Death Valley region from 1910 to 1990, including baseline data from rivers, playas, springs, and wells (Perfect et al. 1995, pp. 1, 3). Although the main objective of the Perfect et al. (1995) report was to document groundwater quality in the Yucca Mountain area, surface water quality was also documented. Chemical analyses in the compilation by Perfect et al. (1995) are taken from four general sources: U.S. Geological Survey unpublished data files, the U.S. Geological Survey National Water Information System database, published reports from federal and state agency investigations, and unpublished data.

The following general observations are made from the chemical data for channel flow and surface runoff (Table 5.3-3). Major ion chemistry for these samples is plotted in the trilinear diagram on Figure 5.3-6. The sampling sites fall into three general categories: channel flow fed by springs and seeps, channel flow from runoff events and surface runoff, and overland runoff mixed with spring discharge.

Nineteen samples were analyzed for major and minor ions between 1984 and 1995 from 15 locations within 15 km (9.3 mi) of Yucca Mountain, along its eastern side. These data were | collected during three series of runoff events:

- Surface water samples collected in Fortymile Wash, Drill Hole Wash, and Busted Butte Wash in August 1984 were the first surface water samples collected during site characterization studies in the Yucca Mountain area (Perfect et al. 1995).

- Emett et al. (1994, p. 550) documented analyses from dip samples of surface water in the Amargosa River drainage basin from six sampling sites during streamflow conditions in January and February 1993. Two of the sites, Stockade Wash at Airport Road and Yucca Wash near its mouth, represent local overland runoff during precipitation.

- During periods of streamflow in 1994 and 1995, surface water quality samples were collected on Yucca Mountain and in Fortymile Canyon during overland runoff and channel flow following precipitation (Savard 1996, p. 28). Some of the overland runoff

from the hillslopes in the drainage basins infiltrated soil and volcanic rock layers and then reemerged as overland runoff. Some of the overland runoff also originated from disturbed areas in the drainage basins such as roads and drill pads where compaction of the surface material reduced infiltration and increased overland runoff. Some surface water quality samples in Fortymile Canyon were taken during overland runoff of precipitation and/or snowmelt, whereas others were taken during the recession period after peak discharge. All samples probably represent a mixing of overland runoff and shallow infiltration waters that discharge along the hillslopes.

Among the dilute runoff samples described above, total dissolved solids range from 45 to 123 mg/L. These waters have similar ionic chemistries when plotted on a trilinear diagram (Figure 5.3-6). The cation field is dominated by Ca, which accounts for 50 to 60 percent of the cation charge, whereas the anion field is dominated by carbonate species, which account for 70 to 90 percent of the total anion charge. The average Cl content of these local runoff waters is 3.5 mg/L.

In addition to surface water samples from the general vicinity of Yucca Mountain, water quality data are also available for 3 Springs Basin and East Stewart Basin, sites that are considered representative of potential recharge areas in central Nevada (McKinley and Oliver 1994, pp. 1 to 3; 1995, pp. 1 to 3). The two basins were studied as analog sites to Yucca Mountain during wetter and cooler periods. Water quality samples were collected from precipitation, springs, and other surface waters from 1986 to 1992. Chemical data for precipitation at the 3 Springs Basin sites were discussed in Section 5.3.4.3. Springs in the basins are probably above the regional groundwater system and do not represent discharge from large groundwater basins, in contrast to springs at Ash Meadows in the Amargosa Desert. The water chemistry of the spring discharges does reflect modification due to water movement through unsaturated volcanic rock layers in the basins. Surface water samples can represent overland runoff from precipitation or snowmelt and also mixing of spring discharge with overland runoff.

Major ion compositions of some of the 3 Springs Basin and East Stewart Basin samples are plotted in the trilinear diagram shown in Figure 5.3-7, and the major constituents are plotted versus chloride concentrations in Figure 5.3-8. These waters are very similar to the Yucca Mountain runoff samples with respect to their relative proportions of the major ions; that is, they are calcium-bicarbonate waters with a significant component of Na. However, the central Nevada samples have slightly higher proportions of Na and Cl, and lower proportions of Ca and carbonate species than the Yucca Mountain waters.

Figure 5.3-8 shows various major constituents plotted against Cl concentrations for channel flow and surface runoff at Yucca Mountain and for surface waters from 3 Springs Basin and Stewart Basin. Also shown on the plots are the regression lines obtained for 3 Springs Basin precipitation chemistry from Table 5.3-2, which are discussed in Section 5.3.4.3. The surface water plots illustrate the direction and magnitude of changes in water chemistry in response to evaporation, dissolution of dry-fall salts accumulated since the last infiltration event, and rock-water interactions. Sulfate in these waters increases to a similar extent as does Cl, as shown by clustering of surface water compositions about the regression line for these two anions on Figure 5.3-8. This observation suggests that sulfate concentrations in these waters are fairly conservative and are mostly a function of evaporative concentration and dissolution of dry-fall

salts. In contrast, both Na and Ca concentrations plot considerably above the precipitation regression lines, suggesting that their concentrations are increased by dissolution of carbonate minerals and weathering reactions of soil minerals. Dissolution of carbonate minerals also leads to a large gain in bicarbonate concentrations, which is also apparent in a comparison of the trilinear plot of Figure 5.3-3 (precipitation) with those in Figures 5.3-6 (Yucca Mountain runoff) and 5.3-7 (surface waters from 3 Springs Basin and Stewart Basin). Finally, the most dramatic constituent increase is observed for silica, which increases by two orders of magnitude over its concentration in precipitation due to fast dissolution of unstable amorphous silica minerals in the soil (Chadwick et al. 1987, p. 977).

Another source of chemical data for surface water samples is compiled from analyses of springs and tunnel seeps from Rainier Mesa (McKinley et al. 1991, pp. 26 to 33). Because of similar geologic settings for Yucca Mountain and Rainier Mesa, these samples expand the database used to develop a conceptual model for the early stages of the geochemical evolution of waters contacting tuff. A trilinear plot of these data is presented in Figure 5.3-9, in which some tunnel seeps (points 8, 9, A) are observed to have similar compositions to those of perched waters at Yucca Mountain (Figure 5.3-10).

These surface water chemical data are also included in the discussion on the geochemical evolution of Yucca Mountain waters (Section 5.3.6.3.2), which present frequency histograms for some of the major ion species (Figures 5.3-11 to 5.3-16).

5.3.5.4   Representativeness of the Data

A key question is the extent to which Yucca Mountain runoff samples are representative of surface water. Under current climatic conditions surface waters at Yucca Mountain are an infrequent occurrence, thereby making it difficult to build a chemical database. Reaeration of surface water as it proceeds down the channel may also affect the chemistry of the collected samples. Some samples were analyzed for bicarbonate in the laboratory instead of on site during collection, so reported bicarbonate concentrations may not represent field conditions.

Some samples may also be affected by site activities because man-made disturbances influence sediment concentrations in surface water. For example, runoff from the ESF pad and tunnel waste piles during light precipitation events travels down the Drill Hole Wash channel. However, none of these concerns affect the conclusions in this section that are based on general geochemical trends. These surface water data are considered adequate as input data for simple correlation plots and histograms to compare against water chemistry in the unsaturated zone. Including the more extensive 3 Springs Basin data is useful to develop and test concepts about geochemical evolution in this environment. The surface geology at the two central Nevada sites is similar to that at Yucca Mountain insofar as both are dominated by silicic volcanic rocks, and the precipitation chemistry is also expected to be similar. The prevailing climatic regime at the central Nevada sites differs from that at Yucca Mountain, leading to differences in soil chemistry, in particular, to less calcic soils. The central Nevada sites also have higher precipitation rates and higher infiltration rates, such that ionic concentrations should be slightly lower for these surface waters than for the Yucca Mountain samples. Nonetheless, general geochemical trends should be the same. These data are used in the following section as

corroborative evidence that the description of geochemical evolution of subsurface waters is consistent with general trends observed in surface waters.

5.3.5.5   Scenarios for Future Variations in Surface Water Chemistry

It is likely that the frequency and distribution of surface waters at Yucca Mountain (e.g., patterns of runoff) could change in the future. Under a wetter climate, local surface waters could be slightly more dilute than present-day waters. However, similarities between the surface water chemistries for the Yucca Mountain area and the 3 Springs Basin samples indicates that the relative ion chemistries of future local surface waters would not be significantly different from those of waters observed under present climatic conditions.

5.3.6   Chemical Composition of Unsaturated Zone Pore Waters and Perched Water

Primary input data for the chemical compositions of unsaturated zone pore water and perched water at Yucca Mountain are listed in Sections 5.3.2.3 (pore water) and 5.3.2.4 (perched water).

5.3.6.1   Processes Controlling the Chemistry of Unsaturated Zone Waters

The major processes that could influence the chemistry of waters in the unsaturated zone, including perched water, include the following:

- **Dry and Wet Deposition (Precipitation)**–This category refers to the compositions of rain, snow, and dust deposited on the surface of Yucca Mountain. These compositions provide the starting point (i.e., input composition) for unsaturated zone water chemistry.

- **Surface Water Chemistry**–Under some conditions, surface waters may be a significant source of recharge to the unsaturated zone in the Yucca Mountain region (see Section 5.3.5). Therefore, the chemistry of surface waters is potentially an important factor in the control of unsaturated zone water compositions.

- **Soil-Zone Processes**–Soil-zone processes of importance to unsaturated zone water chemistry include evapotranspiration, deposition of pedogenic mineral horizons, reaction of infiltrating precipitation waters with soil minerals, and biogenic processes.

- **Infiltration Paths and Rates**–The pathways by which waters infiltrate Yucca Mountain impact water chemistry, not only because they determine the rock/mineral types that the waters contact, but also because they determine the contact times for waters with the various rock and mineral types. These contact times in turn determine the extent of reaction between the waters and the rocks and minerals. Particularly significant to solute transport rates is the distribution of flow between fractures and matrices in each lithologic unit.

- **Rock-Water Interactions**–The extent to which infiltrating waters react with rocks and minerals with which they come into contact will have a major impact on water chemistry. These interactions can include rock and mineral dissolution reactions, ion-exchange reactions, hydrolysis reactions, precipitation reactions, and possibly other alteration reactions.

- **Mineral-Substrate-Water Interactions**–These interactions are a subset of rock and mineral interactions but are separated here because of their potential significance with respect to radionuclide retardation reactions (e.g., sorption).

- **Water-Air Interactions**–The composition of the gas phase in the unsaturated zone is an important factor in the control of unsaturated zone water chemistry. For example, the CO_2 partial pressure influences the carbonic-acid system and the O partial pressure influences the oxidation state of redox-sensitive elements such as C, S, Fe, and Mn.

- **Microbial Influences**–The existence of various microbial populations in the unsaturated zone implies that water chemistry could be altered by microbial activity. For example, microbial metabolic activity could influence pH, the concentrations of redox-sensitive species, and the concentrations of organic acids in unsaturated zone waters.

- **Temperature**–Variations in temperature can influence the composition of unsaturated zone waters by increasing or decreasing the rates of important reactions (e.g., dissolution or precipitation reactions) and by changing the composition of the equilibrium assemblage in the system. Temperature variations beneath Yucca Mountain between depths of about 40 ft (12.2 m) to the top of the water table range from about 18° to 34°C and likely have only small, although measurable, impacts on water chemistry.

- **Pressure**–Pressure variation will have a minor effect on water chemistry through its effect on the dissolution of gases, such as CO_2, in water. More significant, however, is its effect on gas flow patterns, including water vapor transport.

5.3.6.2   Significance and Occurrence of Perched Water

5.3.6.2.1   Significance

Perched water is a zone in which the rocks are locally saturated above the regional water table. The presence of perched water implies that, at some time in the past, the percolation rate through the unsaturated zone has exceeded the saturated hydraulic conductivity of the perching layer. The perched water reservoir may be a remnant of a time when percolation rates were higher or may reflect long-term steady-state conditions. Large perched water reservoirs could indicate the presence of structural or stratigraphic traps that allow infiltrating waters to accumulate. Perched water in proximity to repository waste emplacement tunnels is a potential source of water—in addition to pore water—that may become mobilized as vapor resulting from waste-generated heat, a needed consideration when analyzing the impact of mobilized water on repository performance.

5.3.6.2.2   Water Occurrence

Perched water has been identified below the potential repository horizon in six boreholes in the Yucca Mountain Site area: UZ-1, UZ-14, and NRG-7a in Drill Hole Wash; and SD-7, SD-9, and SD-12 along the ESF Main Drift (Rousseau et al. 1999, pp. 170 to 171; O'Brien 1997, p. 23; Rautman and Engstrom 1996a, p. 8; 1996b, p. 32). The perched water bodies are at elevations significantly below (100 to 200 m) (330 to 660 ft) the potential repository horizon. Although other boreholes in the site area did not detect perched water, this may be because they were not

deep enough to intercept the geologic units where perched water has been identified or because they were drilled with water or foam, which obscured the perched water when it was encountered. In all cases, accumulation of perched water seems to be caused by either the basal vitrophyre of the Topopah Spring Tuff or the vitric-zeolitic boundary in the Calico Hills Formation acting in concert with a lateral structural barrier (Rousseau et al. 1999, pp. 171 to 172). Although not detected in all boreholes, based on field observations and the apparent prerequisite conditions, perched water beneath the site area seems to be a common occurrence and is probably nearly everywhere near the base of the Topopah Spring Tuff in the vicinity of the North Ramp (Rousseau et al. 1999, p. 170).

The following discussion summarizes aspects of perched water occurrence relevant to interpreting their geochemical and isotopic constituents.

Boreholes UZ-1 and UZ-14–These two boreholes penetrated perched water in Drill Hole Wash about 190 m above the water table (Rousseau et al. 1999, pp. 170 to 171). The top of the perched water is within the lower nonlithophysal zone of the Topopah Spring Tuff (Tptpln) about 8 m (26.2 ft) (for UZ-1) and 9 m (29.5 ft) (for UZ-14) above the contact with the crystal-poor vitric zone (Tptpv). Chemical analysis of the water showed that it was contaminated by water used to drill borehole G-1, located about 305 m to the southeast (Whitfield et al. 1990, p. 6).

Borehole NRG-7a–This borehole is located in Drill Hole Wash. Water was first noticed (Rousseau et al. 1999, p. 171) below the contact between the bedded tuff (Tpbt1) and the crystal-poor vitric zone (Tptpv) at the base of the Topopah Spring Tuff. The perched water was encountered near the contact of a series of highly fractured welded tuffs overlying relatively unfractured, nonwelded tuffs, a situation similar to that at boreholes UZ-1 and UZ-14 where perched water may be entrapped in fractures while slowly imbibing into the matrix of the less fractured, underlying rock unit.

Borehole SD-7–This borehole is located on the eastern slope of Yucca Mountain near the ESF Main Drift and near the southern extent of the potential repository area. Water was first observed during coring in the bedded tuffs (Tacbt) at the base of the Calico Hills Tuff (O'Brien 1997, p. 23), about 150 m (492 ft) above the regional water table. The stratigraphically complex bedded tuff zone is a well-sorted volcanic sandstone layer with argillically altered pumice in all layers, predominantly horizontal fractures, and some lamination below 487 m (1,598 ft) (Rautman and Engstrom 1996b, p. 60).

Borehole SD-9–This borehole is located in Drill Hole Wash. Video camera logs revealed that water was seeping through a fracture into borehole SD-9 at a depth 3 m (10 ft) above the contact between the lower nonlithophysal unit (Tptpln) and the crystal-poor vitric unit (Tptpv) of the Topopah Spring Tuff and about 157 m (515 ft) above the predicted regional water table (Ervin et al. 1994, Plate 1). The perched water reservoir is in fractured welded tuff (Tptpv) underlain by less fractured nonwelded and bedded tuffs that comprise the uppermost part of the Calico Hills nonwelded (CHn) unit.

Borehole SD-12–The video camera log of this borehole and in situ pneumatic pressure responses indicates that a perched water zone of limited extent probably is present in the densely welded

vitric unit (Tptpv3) of the Topopah Spring Tuff, extending from the top of this unit down to the base of the moderately welded vitric unit of the CHn unit (Rousseau et al. 1997, p. 21). Fracture densities measured for the core indicate intense fracturing within the lower nonlithophysal unit (Tptpln) and sparse fracturing in the underlying crystal-poor vitric unit (Tptpv) (Rautman and Engstrom 1996a, p. 25).

Borehole WT-24–This borehole is north of the repository block, approximately 1.5 km (0.9 mi) | north of UZ-14. Based on saturation data, water appeared to be perched above either the moderately welded base of the Topopah Spring Tuff (Tptpv2) or the basal vitrophyre of the Topopah Spring Tuff (Tptpv3). The perching layer was difficult to determine because of inadequate core preservation for moisture analysis.

5.3.6.3   Major Constituents in Unsaturated Zone Pore Waters and Perched Waters

This section discusses the data available on the major ion chemistry of pore waters and perched waters in the unsaturated zone. Interpretation of the chemical data in a geochemical framework is based largely on the groundwater chemistry model presented in Triay et al. (1997, Section II).

The compositions of pore waters above the potential repository horizon are significant to transport modeling because they represent the types of waters that could enter the near field of the potential repository. They are also significant because they can be used to constrain models for the rock and mineral-water-gas interactions that occur in the soil zone and the unsaturated zone above the potential repository horizon. Such models can be used to derive estimates of future variations in unsaturated zone water chemistry. Data on major constituents can also be used to evaluate potential flow paths for flow modeling.

Trilinear (Piper) diagrams are used to characterize the relative distributions of major cations and anions in these waters as a function of their stratigraphic depths. Figures 5.3-17 to 5.3-21 present such plots for pore waters from the PTn, TSw, and CHn hydrogeologic units, and from the Prow Pass (Tcp), Bullfrog (Tcb), and Tram (Tct) lithostratigraphic units, respectively. Figure 5.3-10 presents a trilinear plot for the shallow and deep perched water samples. These plots are referenced in the subsequent discussion of the geochemical evolution of pore fluids in the unsaturated zone.

Frequency histograms of chloride concentration data are plotted in Figure 5.3-11 for pore waters from the PTn, CHn, Tiva Canyon welded (TCw), and TSw hydrogeologic units. These concentrations are compared against data for precipitation, surface waters, perched waters, and saturated zone waters to elucidate general trends.

5.3.6.3.1   Major-Ion Chemistry

PTn Unit Pore Water Chemistry–Pore waters extracted from bedded tuff of the PTn unit are calcium-chloride or calcium-sulfate-type waters; that is, samples plot near the top part of the diamond in a trilinear diagram (Figure 5.3-17). This characteristic becomes more pronounced for samples collected deepest within the PTn unit. Pore water samples near the top of the PTn unit have not yet acquired the calcium-chloride or calcium-sulfate signature (e.g., point H from UZ-14 and point Y from UZ#16 on Figure 5.3-17).

TSw Unit Pore Water Chemistry–Data for TSw pore waters are sparse due to the difficulty of extracting sufficient water for analysis from densely welded core. In general, the waters have equal quantities of Na and Ca, with negligible Mg; the dominant anion is bicarbonate, with a much smaller proportion of sulfate than is typical of PTn unit waters (Figure 5.3-18). In terms of relative proportions of anions, the chemical composition of TSw waters is intermediate between those of the PTn and CHn units. The fields occupied by PTn, TSw, and CHn unit pore waters on a trilinear diagram are distinctly different, with only slight overlaps.

CHn Unit Pore-Water Chemistry–Pore waters extracted from the CHn unit are sodium carbonate-bicarbonate-type waters that plot near the lower part of a trilinear diagram (Figures 5.3-19 to 5.3-21). Waters become more strongly sodium carbonate-bicarbonate types with increasing depth within the Calico Hills Formation (compare Figures 5.3-10, 5.3-11, 5.3-19 to 5.3-21).

Total Dissolved Solids–The concentration of constituents in pore waters (Table 5.3-4) is highly variable and is often greater near contacts than in the middle of stratigraphic units (Yang et al. 1996, p. 24). Unsaturated zone pore waters from surface-based boreholes have significantly larger concentrations of total dissolved solids than either perched water (Tables 5.3-5 and 5.3-6) or saturated zone water (Benson and McKinley 1985, p. 5). The larger concentrations suggest either a greater degree of evapotranspiration near the surface (e.g., for PTn unit pore water samples from UZ-14) or a greater degree of rock-water interaction, which could indicate a prolonged contact of percolating water with silicate rocks.

Chloride and Sulfate Concentrations–Chloride and sulfate are generally conservative constituents in oxidizing groundwater and hence are commonly used as indicators of water origins, flow paths, and mixing. The concentrations of chloride and sulfate in many pore water samples from surface-based boreholes are one to two orders of magnitude greater than those of either perched water or saturated zone water. For example, chloride concentrations of deep perched waters lie between 4.1 and 15.5 mg/L (Table 5.3-6) with a mean of 6.8 mg/L, which is similar to that of the saturated zone water from the volcanic rocks beneath Yucca Mountain (9.5 mg/L). In contrast, the chloride concentration of matrix pore water from surface-based boreholes ranges from 10 to 245 mg/L with a mean of about 50 mg/L (calculated from data in Table 5.3-4). If matrix pore water had contributed significantly to the perched water bodies, the chloride concentration of perched water should be similar to that of the pore water. The smaller concentration of chloride in perched water implies that pore waters and perched waters have distinctly different histories of geochemical evolution, undergoing different degrees of evaporation and/or of rock-water interactions.

Figure 5.3-12 shows that sulfate concentrations are similarly elevated in PTn unit pore waters relative to those for the other waters plotted. The higher proportions of chloride and sulfate concentrations in PTn unit pore waters relative to the other waters at the site are also evident by comparing the trilinear plot in Figure 5.3-17 to the trilinear plots in Figure 5.3-19 (upper Calico Hills Formation pore waters), Figure 5.3-20 (lower Calico Hills Formation pore waters), Figure 5.3-21 (Prow Pass Tuff pore waters), and Figure 5.3-10 (perched waters).

Silica Concentrations–The frequency distribution for silica shown in Figure 5.3-13 indicates that silica is low in precipitation but substantially higher in surface waters. By the time

precipitation and surface waters infiltrate into the unsaturated zone, the silica concentrations have reached a limit. This limit is presumably the result of saturation with a silica phase, as discussed further in Section 5.3.6.3.2.

Major Cation Concentrations–The concentrations of Na and Ca are also elevated in pore waters relative to other waters at the site (Figures 5.3-14, 5.3-15). Sodium is elevated in most of the pore water samples, whereas Ca is elevated only in the PTn and TSw unit samples. The trilinear diagram for PTn unit pore waters (Figure 5.3-17) shows that PTn unit pore water compositions extend to higher Ca proportions than observed in either precipitation compositions (Figure 5.3-3) or surface water compositions (Figures 5.3-6, 5.3-7). This enhancement presumably reflects water-soil/rock reactions that release Ca to solution preferentially to the release of Na and Mg. The pore waters in the Calico Hills and Prow Pass units show high proportions of Na (Figures 5.3-19 to 5.3-21). This shift in dominance from divalent to monovalent cations primarily reflects the ion-exchange reactions with zeolites in the CHn unit. The zeolites preferentially take up Ca and Mg while releasing Na to the water.

Vertical Trends in Ion Concentrations–The chemical composition of pore waters within the nonwelded units does not change in a simple or predictable fashion in a given borehole. Chloride and sulfate show large concentration changes within the CHn unit, even by as much as a factor of two for samples separated by less than 0.5 m (e.g., compare two SD-7 samples from $\cong 2,595$ ft (791 m), three UZ-14 samples at $\cong 1,565$ ft (477 m), two WT-24 samples from $\cong 1,745$ ft (532 m), all in Table 5.3-4). Similar large contrasts are noted for Na and total carbonate within the PTn unit. If flow within these units were dominated by vertical percolation of pore water, a monotonic increase in Na and a monotonic decrease in Ca should be noted in the CHn unit because of cation exchange by zeolites (replacement of Na with Ca or Mg on ion-exchange sites). Although pore waters for SD-9 show a continual increase in the Na content with depth, the data set is limited to only four samples. Data for UZ#16 show a decrease in Ca with depth, but changes are fairly erratic and the concentration of Ca rebounds sharply at the top of the Prow Pass Tuff. The data, therefore, suggest at least some component of lateral flow within the nonwelded units.

5.3.6.3.2   Geochemical Evolution

A convenient method for assessing the magnitude and direction of rock/mineral-water interactions experienced by percolating infiltration waters transported through the soil and unsaturated zone is to plot the concentrations of the major constituents in these waters relative to a conservative constituent (i.e., a highly soluble and nonsorbing constituent), such as chloride, in an *x-y* plot. In the absence of other geochemical processes, evaporation or transpiration of a given water sample will result in proportional increases in all constituent concentrations, describing a linear trend in this plot starting at the origin. If processes other than evapotranspiration significantly influence the concentration of a particular constituent, the resulting data point will lie off the evapotranspiration trend. The selection of chloride as the normalizing constituent for such a plot assumes that its concentration is not affected significantly by leakage from fluid inclusions or by geochemical reactions along the flow path.

Calcium and Bicarbonate–Plots showing the concentrations of Ca and bicarbonate versus chloride for various pore water, perched water, and saturated zone samples are presented as

Figures 5.3-22 and 5.3-23, respectively. Included on each plot is a regression line representing a least-squares fit to the weighted annual precipitation data from the 3 Springs Basin monitoring sites (regression lines from data in Table 5.3-2). These plots show that both Ca and bicarbonate concentrations in PTn pore waters generally plot on or below the evapotranspiration lines (Figures 5.3-22a, 5.3-23a). This observation implies that Ca and bicarbonate were lost from these waters relative to chloride. Given the fact that soils on Yucca Mountain contain abundant caliche horizons, this loss likely reflects the precipitation of calcite as the result of evapotranspiration and possibly other reactions in the soil zone.

Pore waters from the Calico Hills and Prow Pass units show even greater depletions of Ca relative to the precipitation trend (Figure 5.3-22b and c). These greater depletions likely reflect ion-exchange processes in which Na in the ion-exchanger phase (e.g., zeolite or clay) was replaced by Ca from the water and vice versa. Unlike the PTn unit pore waters, many Calico Hills Formation and Prow Pass Tuff pore waters are enriched in bicarbonate relative to the precipitation trend (Figure 5.3-23b and c). This fact most likely reflects carbonic acid weathering reactions that start with the dissociation of carbonic acid in the water as follows:

$$H_2CO_3 \Leftrightarrow H^+ + HCO_3^- \qquad \text{(Eq. 5.3-1)}$$

Sodium–In the weathering of aluminosilicate rocks and minerals, weathering reactions include the exchange of the H ions produced in the carbonic acid reaction with Na or other cations on the rock or mineral. This step leads to an increase in Na as well as bicarbonate concentrations in the water. The overall reaction is approximated as follows:

$$>SO\text{--}Na + H_2CO_3 \Leftrightarrow >SO\text{--}H + Na^+ + HCO_3^- \qquad \text{(Eq. 5.3-2)}$$
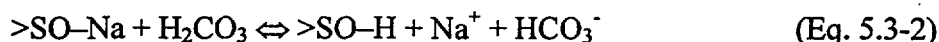
where >SO is a mineral substrate with a surface complexation site at which ions can be exchanged. As shown in Figures 5.3-24b and c, Na concentrations in pore waters from the Calico Hills and Prow Pass units generally plot well above the precipitation trend line. This result is attributed to the Na/H ion-exchange reaction and to ion-exchange reactions involving Ca, Mg, and Na ion exchange on zeolites and clays. Assuming the Na/H ion-exchange reaction is accompanied by the formation of an equimolar amount of bicarbonate, the increase in bicarbonate levels over and above the amount predicted by the precipitation trend line (Figures 5.3-23b and c) would imply a large proportion of the increase in Na concentrations shown in Figure 5.3-24 is due to the Na/H ion reaction.

In contrast to the increase in Na relative to the precipitation trend line for the Calico Hills and Prow Pass units, data for PTn unit pore waters (Figure 5.3-24a) plot below the regression line calculated from the 3 Springs Basin precipitation data. As explained previously, Na is generally leached from minerals and rocks during low-temperature weathering reactions. Such leaching would lead to compositions that plot above the evapotranspiration line, not below it. Furthermore, the PTn unit pore waters also have low values of bicarbonate relative to chloride (Figure 5.3-23a). These trends would seem to preclude reactions similar to those proposed above for the Calico Hills and Prow Pass units to explain the geochemistry of pore waters for the PTn unit. Analytical error is not considered a likely explanation for the Na versus Cl trend because of quality control measures and because nearly all the samples plot below the line, implying they

would all have to be in error, and because the charge balances for the analyses generally agree within ± 10 percent (Table 5.3-4, last column).

Several explanations could account for the observed Na versus Cl trend in the PTn unit pore waters:

- The average Na/Cl ratios in precipitation may have been lower in the past (i.e., closer to the halite line) than present-day ratios measured in 3 Springs Basin. That the weighted-average Na/Cl ratio in precipitation at the Red Rock site near Las Vegas (1.1 molar ratio) is about half of that for the 3 Springs Basin data (2.4 molar ratio) supports this possibility. (The Red Rock Na/Cl ratio is calculated from precipitation-weighted average annual Na and Cl concentrations using data reported in the National Atmospheric Deposition Program/National Trends Network package. The 3 Springs Basin Na/Cl ratio is calculated from precipitation-weighted average annual Na and Cl concentrations using summary data shown in Table 5.3-2).

- Sodium may be taken up by some sort of rock-water interaction not generally considered. However, smectites in the PTn unit are generally low in Na and high in K and Ca. Although present in the PTn unit, zeolites do not appear to be particularly common in this unit, and limited analytical data also show them to be Ca-rich.

- Sodium may have been sequestered in the soil zone as some other Na salt, such as sodium sulfate.

The last hypothesis is the preferred one, insofar as it also accounts for the observed depletion in sulfate relative to chloride for PTn unit pore waters (Figure 5.3-25a).

Sulfate–Like chloride, sulfate is considered to be a generally conservative constituent in dilute oxidizing waters such as the unsaturated zone pore waters in Yucca Mountain. However, as shown in Figures 5.3-25a, b, and c, unsaturated zone pore waters show sulfate-to-chloride ratios consistently lower than the ratios observed in recent precipitation. Because all the unsaturated zone pore water analyses are grossly undersaturated with chloride phases and with gypsum and other possible sulfate phases involving the major cations, it is unlikely that solid chloride or sulfate phases are precipitated in the unsaturated zone (Triay et al. 1997, p. 29). Although anthropogenic sulfate may have elevated the modern-day SO_4/Cl ratio in precipitation, the data used to calculate parameters of the precipitation regression line do not appear to have been significantly influenced by this source because perched waters and saturated zone waters plot near the precipitation regression line (Figure 5.3-25d).

Drever and Smith (1978, p. 1452) presented a model that offers one potential explanation for the low sulfate-to-chloride ratios in the unsaturated zone pore waters (Triay et al. 1997, p. 29). Their model involves drying and wetting cycles in the soil zone. During the drying phase, concentrations of dissolved solutes are increased in soil waters by evapotranspiration to the degree that phases such as calcite, gypsum, silica, and the more soluble salts precipitate. During occasional heavy rains, the phases precipitated during the drying phase are partially redissolved. Because the dissolution rates for highly soluble salts, such as sodium chloride, are higher than the rates for less soluble salts, such as calcite, gypsum, and silica, a portion of the less soluble

salts may remain undissolved after the occasional heavy rains infiltrate through the soil zone. In terms of sulfate and chloride concentrations, this process could lead to soil waters with lower sulfate-to-chloride ratios than those observed in precipitation. The actual concentrations of sulfate and chloride in these waters would depend on the details of the processes involved, including the dissolution kinetics of the sulfate and chloride phases, the residence time of the waters in the soil zone, and the original masses of sulfate and chloride in the soil zone.

An alternative hypothesis to account for the low sulfate-to-chloride ratio is the microbial reduction of sulfate ions in the soil (e.g., initially to hydrogen sulfide, or more likely to a mixture of organic sulfides such as methyl disulfide and dimethyl disulfide). These volatile compounds are commonly produced in soils and are readily lost to the atmosphere. However, decreased SO_4/Cl ratios are not observed in upgradient saturated zone waters. Because upgradient waters recharge in regions with more vegetation and wetter soils, the likelihood of microbial reduction of sulfate is expected to be greater for those waters than for infiltrating waters at Yucca Mountain. Hence, this hypothesis is considered improbable for the Yucca Mountain site.

Although differences in the dissolution kinetics of sulfate and chloride salts may partly explain the low sulfate-to-chloride ratios in unsaturated zone pore waters, these differences are likely augmented, perhaps even dominated, by crystallization sequence effects. For example, it is possible that minerals (e.g., calcite and gypsum) that precipitate from evaporating soil pore waters early in a crystallization sequence are partially or completely sequestered by minerals that precipitate later in the sequence (e.g., being coated by opal-A). Alternatively, early crystallized phases may completely fill smaller pores in the rocks and, therefore, be less accessible to infiltrating waters than minerals crystallized later in the sequence in larger pores (Chadwick et al. 1987, p. 975). During subsequent infiltration events, the latest-formed phases in pores accessible to infiltrating waters would preferentially dissolve, leading to soil solutions enriched in the more soluble salts relative to the less soluble salts.

Silica–A plot of silica versus chloride concentrations in pore waters, perched waters, and saturated zone waters is shown in Figure 5.3-26. Most water samples from the Yucca Mountain area plot above the precipitation trend line. This result suggests that a process other than evapotranspiration is contributing to increased silica concentrations in these waters. According to Gifford and Frugoli (1964, pp. 386 to 388) and Chadwick et al. (1987, p. 977), silica is added to soil waters as a result of dissolution of solid silicic acid (an unstable silica phase) in soil horizons in arid regions. This explanation would be consistent with the presence of amorphous silica (e.g., opal) in Yucca Mountain soils and opal deposits on fracture surfaces exposed in the ESF. It is also consistent with surface waters having much higher silica concentrations than precipitation compositions (Figure 5.3-13).

Perched Water–Perched water compositions are generally distinct from pore waters compositions although they are very similar to saturated zone water compositions (Section 5.3.9). These relationships are readily seen by comparing the trilinear plots of each category of water: perched water (Figure 5.3-10), unsaturated zone pore waters (Figures 5.3-17 to 5.3-21), and groundwater (Figure 5.3-27). The similarity of perched and saturated zone water compositions suggests that these waters are subject to similar rock-water interactions. As discussed in Section 5.3.9, these reactions predominantly involve mineral/rock dissolution and ion exchange.

pH–pH values shift from slightly acidic values for precipitation (pH 6), to increasingly basic values with depth in the unsaturated zone (pH 9 or higher for the deepest pore water samples) (Table 5.3-4) (Figure 5.3-16). Controls on pH in ambient unsaturated zone pore waters and perched waters are dominated by the carbonic acid system and the interaction of H ions with the host rock/mineral. As discussed above, H ions can replace Na ions in the host rock/mineral (e.g., volcanic glass, feldspar) under most conditions. As H ions are used up, carbonic acid dissociation produces additional H ions and bicarbonate ions. If H/Na exchange is inhibited, the pH of a given pore water sample will depend primarily on the partial pressure of CO_2 in the gas phase in contact with the water and on whether the gas phase has equilibrated with the water phase. This process will buffer the pH of the (dilute) pore waters at nearly neutral levels. If calcite is present, it will also act to buffer the pH, in conjunction with gas-phase CO_2. If both the carbonic acid dissociation and H/Na exchange reactions are important, the control of pH becomes a kinetic problem. For example, if the rate at which H ions react with the host rock is fast relative to the rates at which the CO_2 partial pressure changes or the rate at which the CO_2 in the gas phase equilibrates with the water phase, the pH of the water phase could increase above the equilibrium level for the CO_2 partial pressure of interest. Conversely, if the H reaction rate is slow relative to the CO_2 equilibration rate, the pH of the water phase would more directly reflect the CO_2 partial-pressure variations.

Because the Na-versus-chloride concentration data for pore waters from units above the CHn unit (Figure 5.3-24) suggest little or no evidence for the H/Na ion-exchange reaction, the pH of these pore waters likely is controlled in part by the CO_2 partial pressure with which they are in contact. Measured pH values in PTn unit pore waters average 7.2. In contrast, the CHn unit pore waters and perched waters show clear evidence of Na/H ion exchange. The average pH values for these waters are 8.1 for perched water, 8.3 for pore waters from the CHn unit above the Prow Pass Tuff, and 9.0 for pore waters from the Prow Pass Tuff and below. Analytical uncertainties in pH measurements are between 0.2 and 0.3 pH units. Whether the higher pH values for deeper samples reflect the cation/hydrogen-ion exchange rate or simply a lower partial pressure of carbon dioxide in the gas phase has not yet been resolved, although there may be sufficient CO_2 gas data available to do so. However, it is also possible that the pore water pH changes when it is exposed to air during sample collection or that it is affected by the compression of the rock during the pore water extraction process; both processes could vary according to rock type.

Redox State–The oxidation/reduction (redox) state of unsaturated zone waters is likely dominated by the presence of oxygen in the unsaturated zone gas phase. At the two locations where such measurements have been made, the unsaturated zone gas phase has atmospheric levels of oxygen: 21 percent reported for UZ-6S gas in Thorstenson et al. (1990, p. 256) and 18.5 to 21.1 percent reported for UZ-1 gas (Yang et al. 1996, p. 42). These results confirm that unsaturated zone pore waters would generally be oxidizing. Measured Eh would typically be high (400 to 600 mV), even though in low-temperature natural systems this value does not always indicate equilibrium insofar as some redox reactions may not have gone to completion. It is possible that lower redox potentials could be present locally (i.e., in microenvironments) as a result of microbial activity or the presence of a reducing compound (e.g., pyrite).

Microbial Activity–The influence of microbes on the unsaturated zone water chemistry is not well defined. At a minimum, microbes could produce organic acids and locally alter pH and

redox states. Microbial activity could also affect concentrations of sulfate, bromide, and other dissolved species, as well as fractionate isotopes of light elements, such as carbon. According to Kieft et al. (1997, p. 3128), microbial cell counts and microbial biomasses were low at all the locations sampled in the ESF. Kieft et al. (1997, p. 3128) suggest that this result was likely due to low water content and low nutrient availability. However, they note that the potential for microbial activity was high. That is, microbial populations were present but not active. They concluded that if sufficient water and nutrients were added to the system, microbial populations could increase dramatically.

5.3.6.4   Representativeness of Available Data

Pore water and perched water chemistry data are limited in several ways. First, complete pore water analyses are available mainly for those horizons in Yucca Mountain that contain nonwelded tuffs with relatively high porosities. Very few complete pore water analyses are available for well-indurated, low-porosity rocks (e.g., welded tuffs in the repository horizon). Second, pore water and perched water analyses are only available for samples from a limited number of boreholes (Table 5.3-1). Third, the procedure for extraction of water from the pores may have an impact on water chemistry. For example, the release of CO_2 from pore water samples could change the pH of the samples. Similarly, the pH of perched water samples could shift due to degassing as the bailer is brought to the surface or at the pump outlet.

Despite these restrictions, the major ion chemistry of the pore waters is sufficiently consistent and the controls on this chemistry are sufficiently well understood that bounds can be placed on the likely range of variations. An important parameter in estimation of these bounds is the net infiltration rate (i.e., the degree of evapotranspiration) over the period of interest. Bounds on the pH of the pore waters are more difficult to derive because the variations in CO_2 partial pressures within the unsaturated zone gas phase are not well defined at present. However, model calculations assuming saturation with calcite would allow this parameter to be bounded. Lower bounds on the redox state cannot be derived without additional field data.

The compositional variations of pore waters and perched waters in the unsaturated zone at Yucca Mountain reflect a variety of infiltration rates, rock-water interactions, gas-water interactions, and other effects. The range of these processes and effects will likely not change greatly within the potential range of climatic regimes, but their relative importance may change. For example, under climatic regimes involving higher infiltration rates, the ion-exchange processes represented by pore waters from the CHn unit and by the perched waters may become more dominant. This scenario would result in more dilute pore waters with higher proportions of Na ions and possibly higher pH. However, as these types of waters are present in the ambient system, they do not present an unanticipated change in water chemistry.

5.3.6.5   Scenarios for Future Trends in Unsaturated Zone Chemistry

As discussed in the previous section, the range of processes and effects in the unsaturated zone at Yucca Mountain will likely not change greatly within the potential range of climatic regimes likely to affect Yucca Mountain, although their relative importance may change. For example, under climatic regimes involving higher infiltration rates, the processes represented by Calico Hills nonwelded unit pore waters and by perched waters may become more dominant, resulting

in more dilute pore waters with higher proportions of Na ions and possibly higher pH. However, because these types of waters are present in the ambient system, they do not present an unanticipated change in water chemistry.

The potential impacts of the thermal pulse resulting from waste emplacement and components introduced into the repository horizon are discussed in Section 11.

5.3.7 Isotopic Composition of Fluids

This section summarizes available aqueous phase isotopic data for precipitation, surface waters, pore waters, and perched waters recovered from the unsaturated zone and for groundwaters. These data provide constraints for water and solute transport rates and mechanisms. Examples of specific issues addressed by these data include spatial and temporal variability in net fluxes, lateral diversion in specific stratigraphic units, role of faults in controlling flow paths, fracture-matrix interactions, and distribution of water travel times.

The types of isotopic data available for borehole samples from the unsaturated zone are presented in Table 5.3-1. Borehole and tunnel alcove locations are plotted in Figures 5.3-1 and 5.3-2.

5.3.7.1 Overview of Isotopic Methods

Isotopes measured in unsaturated zone fluids as part of YMP activities fall into five general categories as described below, with each method yielding different types of information. This large suite of different approaches has been critical to the development and testing of conceptual models for flow and transport through the unsaturated zone.

Anthropogenic Material–This category of environmental tracers includes radioactive species present in global fallout from nuclear weapons testing and from releases from nuclear fuel reprocessing plants. Tritium, ^{14}C, and ^{36}Cl produced in the atmosphere during aboveground nuclear testing, primarily between 1952 and 1963, have been widely used in hydrologic studies. The presence of these nuclides above background levels in subsurface fluids is generally accepted as a clear indication that some proportion of the water was transported to that depth in less than 50 yr. If the sampled depth is more than a few meters in an arid environment, the presence of global fallout nuclides implies a component of fracture flow. Hence, these isotopic data provide a means for constraining the extent to which solute transport is retarded by diffusion from fractures into the adjacent matrix. Fission products ^{99}Tc and ^{129}I in a subsurface sample (above natural background) would also provide a clear indication of a component of recent water. However, a robust analytical protocol for these species in unsaturated zone fluids has not yet been developed. Other radionuclides in global fallout, such as ^{137}Ce and Pu isotopes, sorb strongly onto most mineral surfaces and hence are largely immobilized in the near-surface soil. Tritium, ^{36}Cl, and ^{14}C data are discussed in Sections 5.3.7.2, 5.3.7.3, and 5.3.7.4, respectively.

Atmospheric Radionuclides–Tritium, ^{36}Cl, and ^{14}C also exist naturally in the atmosphere as the result of the interactions of cosmic rays with atmospheric gases. To the extent that the original concentrations at the surface can be reconstructed, these nuclides are useful indicators of water residence times, with water ages based on the extent of radioactive decay of the atmospheric

component. As part of YMP activities, ^{14}C and ^{36}Cl have been used to constrain water age estimates. Chlorine-36 and ^{14}C data are discussed in Sections 5.3.7.3 and 5.3.7.4, respectively.

Climatic Reconstruction–Stable isotopic compositions of hydrogen and oxygen can be used to infer paleoclimatic conditions. Hydrogen and oxygen isotopic analyses of water samples are summarized in Section 5.3.7.5.

Rock-Water Interactions–Groundwater is commonly out of chemical and isotopic equilibrium with the rocks through which it moves (Davis and Murphy 1987, Section 8). The extent of disequilibrium provides a qualitative method for establishing flow paths and flow chronologies. Furthermore, if the kinetics of chemical or isotopic exchange between the water and minerals along its flow path are well known, then semiquantitative estimates of water travel times may be possible. Sections 5.3.7.6 and 5.3.7.7 address the hydrologic implications of trends observed in isotopic ratios for Sr and U in pore waters.

5.3.7.2 Tritium

Primary input data used to characterize the distribution of tritium in the unsaturated zone at Yucca Mountain, which provide a basis for water travel time estimates, are listed in Section 5.3.2.5.

5.3.7.2.1 Background

Natural tritium (^{3}H, or T) is produced in the upper atmosphere by the bombardment of N by the flux of neutrons in cosmic radiation (Clark and Fritz 1997, p. 174):

$$^{14}_{7}N + ^{1}_{0}n \Rightarrow ^{12}_{6}C + ^{3}_{1}H$$

(Eq. 5.3-3)

where n is a neutron. Once produced, tritium (T) oxidizes rapidly to tritiated water (HTO). Transfer of tritium to the troposphere occurs during spring in midlatitude zones. Tritiated water has a short residence time in the troposphere (less than 1 yr.) and is eventually removed from the atmosphere in precipitation or through isotopic exchange. Historical concentrations in rain water in the middle latitudes are estimated to be on the order of 10 tritium units (TU). Tritium values in precipitation prior to the 1950s were between 2 and 25 TU (Yang et al. 1996, p. 51). Because of the relatively short half-life of tritium (12.3 yr.) (Parrington et al. 1996, p. 18), groundwater infiltrating prior to 1952 with an initial tritium content of 10 TU would have a present-day content of 0.7 TU or less.

Aboveground testing of nuclear devices in the northern hemisphere between 1952 and 1963 produced significant amounts of tritium in the earth's atmosphere. Bomb-pulse tritium overwhelmed natural background levels by as much as several orders of magnitude (Figure 5.3-28). Peak concentrations in precipitation, expressed as annual precipitation-weighted averages, were reached in 1963 when the annual average measured values at Albuquerque, New Mexico, and Salt Lake City, Utah—the two stations probably most representative of fallout at Yucca Mountain—were about 1,900 and 3,600 TU, respectively (IAEA 1981, pp. 134, 154). Seasonal variations in post-bomb tritium concentrations in precipitation are quite significant (Davis and Murphy 1987, pp. 36 to 37; Clark and Fritz 1997, pp. 177 to 178). These variations

are caused by changes in atmospheric circulation between the troposphere and the stratosphere, which is a major reservoir of tritium. During the early 1960s in the northern hemisphere, early summer maxima at many monitoring locations were 10 times as large as the winter minima. Even in the early 1980s, 20 yr. after the cessation of atmospheric nuclear tests, summer maxima were still more than twice winter minima at many stations. Consequently, the seasonal timing of precipitation is a critical determinant of the magnitude of the tritium signal introduced into the subsurface.

As a result of the nuclear test ban treaty of 1963, tritium concentrations have gradually decreased to about 10 to 40 TU measured in precipitation at the Nevada Test Site from November 1983 to June 1985. Precipitation samples from 3 Springs Basin in central Nevada, slightly north of the Nevada Test Site, showed slightly lower tritium concentrations in samples collected between 1985 and 1991, ranging from 6 to 22 TU (McKinley and Oliver 1994, pp. 27, 74). Annual mean values and monthly maximum values for monitoring stations in states surrounding Nevada likewise were in this range (i.e., still elevated above pre-1952 background levels) from 1988 to 1993 (Yang et al. 1996, p. 51). In January and February 1993, the tritium content of surface runoff collected from several sites in the vicinity of Yucca Mountain ranged from 3 to 10 TU (Emett et al. 1994, p. 550; Savard 1996, p. 28); tritium values during the winter are typically the lowest of the year.

It is possible that venting of tritium from subsurface nuclear detonations on the Nevada Test Site may also have contributed to tritium in precipitation at Yucca Mountain. For example, the Project Plowshare Schooner event on December 8, 1968, was a shallow cratering experiment conducted in Area 20 (Pahute Mesa) of the Nevada Test Site, about 40 km due north of Yucca Mountain, and was known to have vented tritium to the atmosphere (EPA 1971, pp. i, ii, 34, 42). Immediately following the event, concentrations of 1,630 to 3,135 TU were reported for snow samples from three sites in Nevada. However, trajectories for this particular event were mostly northerly and northeasterly, such that Yucca Mountain precipitation was unlikely to have been influenced by it.

The extent to which detectable quantities of tritium enter the subsurface depends on spatial and temporal variations in precipitation. If precipitation is insufficient to lead to net infiltration following a storm event, then the tritium is lost back to the atmosphere by evapotranspiration. Consequently, because Yucca Mountain experienced below average levels of precipitation from 1958 to 1964 (Precipitation Station 4JA) (French 1985, pp. 52 to 56), it is entirely possible that much of the peak tritium concentrations were never transported into the bedrock at Yucca Mountain. In this regard, the behavior of tritium as a tracer of modern water differs substantially from that of ^{36}Cl. In the latter case, all global fallout ^{36}Cl eventually is carried into the subsurface.

5.3.7.2.2 Overview of Yucca Mountain Site Characterization Project Tritium Results

As part of YMP activities, tritium has been analyzed in more than 800 pore water fluids extracted from unconsolidated material in shallow surface-based boreholes, from drill core from deep surface-based boreholes, and from ESF drill holes. Analyses are also available for water samples bailed and pumped from perched water bodies (Table 5.3-7) and from the saturated zone. Detectable levels of tritium have been observed in the Bow Ridge fault zone in ESF

Alcove 2 and in pore waters extracted from core samples from surface-based boreholes. These detections occur within the TCw, PTn, and TSw units, and also in some samples from the CHn unit, as deep as the Prow Pass member of the Crater Flat Tuff.

Because of the implications of the tritium data for the presence of fast transport paths and large fluxes, it is important to define the threshold at which a given signal can be considered as being above background. Although the analytical uncertainty is 4 TU (for 1 sigma) based on counting statistics, other factors contribute to a larger uncertainty in the measured value. For this analysis report, Chauvenet's criterion for identifying outliers was the basis of the statistical test used to establish the minimum tritium activity that would indicate the presence of bomb-pulse water in a sample (Bevington and Robinson 1992, p. 58). The standard deviations are plotted in Figure 5.3-29, in which they are compared against Chauvenet's criterion (solid line) as a function of ranking. The plot varies smoothly within the region of background. All values above 25 TU are considered to lie outside the range of the population of background samples. The limitation of this approach is that, in this case, background includes post-bomb waters that have returned to pre-bomb tritium levels. A more appropriate statistical analysis would compare the sample data against the results obtained for analytical blanks since the objective is to identify the presence of any tritium with nonzero concentrations as indicative of any component of water less than 50 years old, post-bomb as well as bomb-pulse.

Following this simple statistical analysis, Table 5.3-8 summarizes the distribution of pore water samples in each borehole, according to the total number of samples analyzed for each hydrogeologic unit and the number that exceeded the threshold of 25 TU. Of the 718 samples included in this summary table, 51 had contents above 25 TU. These individual samples are listed in Table 5.3-9.

5.3.7.2.3   Tritium Associated with Faults

The largest published concentrations of tritium within the unsaturated zone at Yucca Mountain are those associated with the Bow Ridge fault. Samples were collected from drill hole HPF#1, which was drilled into the fault from the ESF Bow Ridge Fault Alcove. A concentration of 155 TU was measured for pore water 3.4 m west of the fault within the pre-Rainier Mesa Tuff (LeCain et al. 1997, p. 40). Values of 118 and 128 TU were found in pore waters within the fault breccia. The high values indicate minimal mixing of the percolating fluids with older fluids and may be a consequence of the width of the fault zone at the surface, the lack of alluvium upslope from the fault, and the shallow depth of the fault where sampled (approximately 20 to 30 m).

No other samples from the ESF had tritium contents above 25 TU, including seven samples extracted from core from a drill hole transecting the Ghost Dance fault in the northern Ghost Dance fault access drift (Alcove 6) (LeCain and Patterson 1997, pp. 16 to 17), despite the fact that elevated levels of ^{36}Cl were measured in Alcove 6 (Section 6.6.3).

5.3.7.2.4   Tritium in Surface-Based Boreholes

Tritium data for the unsaturated zone boreholes show several inversions (larger tritium concentrations located below smaller tritium concentrations in a vertical profile) (Yang et al. 1996, p. 31). These inversions suggest that vertical water percolation through the rock matrix

may not be the predominant flow mechanism in the unsaturated zone for all stratigraphic units at Yucca Mountain. Post-bomb tritium concentrations were observed down to bedded tuff or Pah Canyon Tuff in many surface-based boreholes. The occurrence of detectable tritium in waters below nontritium-bearing water (i.e., older water) in a vertical profile is strong evidence of fracture and lateral flow occurring at Yucca Mountain. An alternative hypothesis would be that the inversion results from piston flow of the atmospheric input signal, with the 1960s peak remaining higher than the 1980s input.

The following is a summary of occurrences of tritium above 25 TU in surface-based boreholes:

- **Borehole UZ#16 (Table 5.3-9)**—The maximum concentration (148.5 TU) occurs at a depth of 48 m, just above the bedded tuff unit in the PTn unit. Several tritium peaks are observed in the Topopah Spring Tuff at depths of 80 and 204 m and the interval of 317 to 357 m. Other peaks occur in the Calico Hills Formation at depths of 426 m (44 TU) and 437 m (103 TU).

- **Borehole UZ-14 (Table 5.3-9)**—Tritium concentrations between 21 and 32 TU were observed in intervals between 35 to 45 m in the Pah Canyon Tuff and a value of 23 TU was measured for one sample at a depth of 385 m in the Topopah Spring Tuff.

- **Boreholes NRG-6 and NRG-7a (Table 5.3-9)**—Because of limited coring, only small intervals of these two boreholes have been analyzed for tritium. A broad peak of high tritium concentrations between 30 and 140 TU was observed in NRG-6, from 53 to 75 m in the Pah Canyon Tuff and near the top of the Topopah Spring Tuff. A single large tritium concentration of 47 TU was observed at a depth of 109 m (top of the TSw unit) in NRG-7a.

- **Boreholes SD-6, SD-7, SD-9, and SD-12 (Table 5.3-9)**—SD-6, which is located in the bottom of a small wash, had clusters of elevated tritium values in the TSw unit at about 1,440 ft (27 to 30 TU) and in the Prow Pass portion of the CHn unit at about 1,752 ft (30 to 43 TU). None of the samples from the TCw or PTn units contained tritium above 25 TU. One sample from the Prow Pass in SD-12 contained 39 TU (Table 5.3-9). All tritium analyses from SD-7 and SD-9 were less than 25 TU.

- **Boreholes UZ#4 and UZ#5 (Table 5.3-10, Corroborative Data)**—A cluster of four samples with levels of 38 to 45 TU occurred in the interval of 44.8 to 49.5 m in UZ#4, within and below the Yucca Mountain unit. In UZ#5, a zone of samples with an average level of 44 TU occurred in the interval of 28.3 to 36.7 m, at the base of the Tiva Canyon unit, with a peak of 75 TU.

- **ESF Boreholes (Corroborative Data)**—Forty-four tritium analyses of pore water extracted from ESF cores were all well below 25 TU (ESF Alcove 3, Alcove 4, Alcove 6, Alcove 7, South Ramp holes 1 and 2, and North Ramp 13). Another 17 samples from ESF boreholes analyzed following isotope enrichment had analytical uncertainties of ± 0.2 TU or less. Of this set, the highest tritium activity was 1 TU in ESF-SR-MOISTSTDY#7 (ESF Alcove 6, ESF-NDR-MF#1, and South Ramp holes 1, 2, 5, 6, and 7, and North Ramp holes 4, 13, and 16). Because of concerns about isotopic

exchange with tunnel air, this result is not considered to indicate the presence of young water.

5.3.7.2.5   Tritium in Perched Water

Isotopic compositions have been measured in perched water from four Yucca Mountain boreholes (Table 5.3-7). None of the tritium analyses were above the 25 TU threshold indicating the presence of bomb-pulse tritium.

5.3.7.3   Chlorine-36

Primary input data used to characterize the distribution of ^{36}Cl at Yucca Mountain, which provide a basis for water travel time estimates, are listed in Section 5.3.2.6.

5.3.7.3.1   Background

Measurements of chloride (Cl) concentrations and ^{36}Cl/Cl for salts extracted from water, soil, and rocks have been used to provide information on characteristics of water movement and solute transport through the unsaturated zone at Yucca Mountain (Fabryka-Martin, Wolfsberg et al. 1997, pp. 75, 77 to 79; Fabryka-Martin, Wolfsberg, Levy, Roach et al. 1998, p. 93; Fabryka-Martin, Wolfsberg, Roach et al. 1998, p. 264; Wolfsberg et al. 1998, p. 81). Chlorine-36 is a radioactive isotope of Cl, with a half-life of 3.01×10^5 yr. (Parrington et al. 1996, p. 22), and in nature, it occurs primarily as the chloride anion. As such, it is relatively inert in the subsurface environment and behaves conservatively. This radionuclide is present in infiltrating waters as a natural tracer produced mainly in the upper atmosphere by the bombardment of Ar gas by cosmic radiation (Clark and Fritz 1997, p. 232):

$$^{40}Ar + p \Rightarrow \, ^{36}Cl + n + \alpha$$
$$^{36}Ar + n \Rightarrow \, ^{36}Cl + p$$

(Eq. 5.3-4)

where n is a neutron, p is a proton, and α is an alpha particle. Common Cl in the atmosphere is also irradiated by the atmospheric neutron flux to produce Cl and gamma radiation:

$$^{35}Cl + n \Rightarrow \, ^{36}Cl + \gamma$$

(Eq. 5.3-5)

The relatively long half-life of ^{36}Cl theoretically permits the detection of travel times up to several hundred thousand years. To normalize the data for the variable effects of evapotranspiration, the ^{36}Cl concentration is generally reported relative to that of stable Cl$^-$. Expressed in this manner, the present-day background level of ^{36}Cl/Cl is 502 ($\pm$ 53) $\times$ 10^{-15} (Table 5.3-11, discussed in Section 5.3.10.2.3).

Global fallout from thermonuclear tests conducted primarily in the Pacific Proving Grounds resulted in a ^{36}Cl bomb-pulse with maximum meteoric ratios in excess of 200,000 $\times$ 10^{-15} (Figure 5.3-28). These extremely high values were diluted by mixing processes in the soil zone and subsurface and are not observable today. Nevertheless, high ^{36}Cl/Cl ratios (those greater than about 1,250 $\times$ 10^{-15}) indicate some bomb-pulse component, and their appearance in an environmental sample signals the presence of at least a small component of bomb-pulse ^{36}Cl.

Present-day ^{36}Cl/Cl ratios in Yucca Mountain surface soils generally range from $1,500 \times 10^{-15}$ to $3,000 \times 10^{-15}$ (CRWMS M&O 1998, pp. 3 to 5). In subsurface water, similar high ratios suggest travel times from the ground surface of 50 yr. or less.

Although the existence of bomb-pulse ^{36}Cl enables the study of solute transport with travel times of 50 yr. or less, the natural cosmogenic background permits analysis of much longer term transport processes. However, the use of ^{36}Cl/Cl for dating older waters is not as straightforward as the case for bomb-pulse signals due to the time-varying input signal. Both theoretical considerations as well as measurements of soil profiles and fossil urine from ancient pack-rat middens support the hypothesis that the present-day background ratio has remained relatively constant during the Holocene (the last 10 k.y.) (Plummer et al. 1997, Figure 3B, p. 539). Expected lower rates of stable Cl deposition during the Pleistocene (2 Ma to 10 ka), in combination with higher rates of cosmogenic ^{36}Cl deposition as a result of southern shifts in the jet stream, would have led to higher local meteoric ^{36}Cl/Cl values relative to those that were present throughout the Holocene (Plummer et al. 1997, p. 540). Superimposed on this effect are varying atmospheric ^{36}Cl production rates caused by variations in the earth's geomagnetic field. Based on these two factors, the meteoric ^{36}Cl/Cl at Yucca Mountain has been reconstructed for the last 1.8 m.y. (Fabryka-Martin, Wolfsberg et al. 1997, pp. 4 to 5). Analyses of ^{36}Cl/Cl in ^{14}C-dated pack-rat midden samples are generally consistent with the reconstruction, although these data can only cover the last 40 k.y. due to the comparatively short half-life of ^{14}C (Figure 5.3-30).

Chlorine-36 is also produced in rocks due to a low but ubiquitous neutron flux resulting from the decay of U and Th isotopes and their daughters, but these background levels are low relative to those measured in Yucca Mountain water samples (Fabryka-Martin, Wolfsberg et al. 1997, pp. 8, 13). Although U concentrations reach several hundred parts per million in some silica deposits lining fractures in the unsaturated zone, such concentrations do not elevate the local neutron flux (or ^{36}Cl production rates) because the flux is determined by U and Th concentrations averaged on a much larger scale (e.g., 10^4 cm^3).

Together, the bomb-pulse record and the long-term reconstruction allow ^{36}Cl/Cl observations in subsurface fluids at Yucca Mountain to be divided into four classes:

- Ratios over $1,250 \times 10^{-15}$ provide clear evidence of bomb-pulse influence, and indicate the presence of some rapid transport pathways (Fabryka-Martin, Wolfsberg et al. 1997, p. 18).

- Ratios near the present-day value of 500×10^{-15} suggest Holocene precipitation of pre-nuclear-age (from 1950, extending back to about 10 ka) (Figure 5.3-30a). A value of 500×10^{-15} is very unlikely to indicate extremely young (post-1980) precipitation because bomb-pulse ^{36}Cl is still widely prevalent in surface soils at Yucca Mountain, based on analyses of surface soils and surface runoff.

- Ratios that are elevated above present-day background but less than $1,250 \times 10^{-15}$ cannot be interpreted unambiguously in terms of water travel time, in the absence of additional geochemical or isotopic information. These may be attributed to Pleistocene water that is not so old as to unequivocally demonstrate radioactive decay (note elevated ratios at

the end of the Pleistocene [Fabryka-Martin, Wolfsberg et al. 1997, pp. 4 to 5, Figure 31b]). Alternatively, these ratios may reflect the presence of a small component of bomb-pulse ^{36}Cl, possibly as low as 1 percent of the total flow.

- Ratios significantly less than 350×10^{-15} clearly show the effects of radioactive decay of ^{36}Cl. Actual estimates of water age depend on the past meteoric ratios, which must be considered highly speculative for the period before the earliest pack-rat data (40 k.y.). However, based on the current reconstruction, these ratios imply ages in excess of 200 k.y.

Unfortunately, only interpretation of the highest ratios (indicating bomb-pulse water) and the lowest ratios (indicating radioactively decayed ancient water) may usually be considered relatively unequivocal. Intermediate ratios may represent Holocene or Pleistocene input with corresponding travel times or may represent mixtures of waters of different ages. Nonetheless, the intermediate ratios shed light on the interpretation of water ages when considered in conjunction with other independent evidence, such as other isotopic measurements and infiltration studies and results of flow and transport simulations of alternative conceptual models.

More than 900 ^{36}Cl measurements have been conducted thus far for the YMP. Analyzed samples include surface soils and soil profiles; rock samples collected from surface-based boreholes, the ESF, and the Cross Drift; water samples, including surface runoff, unsaturated zone pore water, perched water, and saturated zone water; and fossilized urine from pack-rat middens. Observations from these sample analyses are summarized in Table 5.3-12 and discussed below.

5.3.7.3.2   Chlorine-36 in Shallow Samples

Analyses of bomb-pulse ^{36}Cl and Cl profiles in soil and alluvial profiles show that thick alluvium is generally effective at reducing net infiltration to levels less than 1 mm/yr. (Fabryka-Martin, Turin et al. 1996, Section 5.1.2). An exception to this generalization may be in channels and at the base of sideslopes, as illustrated by the penetration of bomb-pulse ^{36}Cl into the soil exposed at the NRG#5 drill pad and in samples as deep as 3.3 m in the soil-test pit NRSF-TP-19 at the North Portal.

Similarly, borehole samples collected from the PTn unit where this rock unit is overlain by thick alluvium do not show any evidence for the presence of bomb-pulse ^{36}Cl.

In contrast, where alluvial cover is thin (i.e., less than a few meters thick) or missing, water is able to readily enter bedrock fractures, as shown by the detection of bomb-pulse ^{36}Cl measurements in some samples. For example, fast transport through the TCw unit is indicated by bomb-pulse $^{36}Cl/Cl$ ratios measured in several boreholes that intersect the PTn unit, which lies below the TCw unit. Bomb-pulse levels of ^{36}Cl were also observed in drillcore samples from the top of the Calico Hills unit in the shallow Busted Butte Field Transport Facility.

5.3.7.3.3   Bomb-Pulse Chlorine-36 in the Exploratory Studies Facility and Cross Drift

Evidence for fast pathways that persist into the TSw unit is provided by bomb-pulse $^{36}Cl/Cl$ ratios measured at locations in the Cross Drift (Figure 5.3-31, Table 5.3-13). More than 250 samples have been analyzed from the ESF tunnel. Of these, more than 40 had ^{36}Cl levels

sufficiently elevated as to be interpreted as unambiguous evidence for the presence of bomb-pulse ^{36}Cl. For example, bomb-pulse ^{36}Cl was detected in the Drill Hole Wash fault zone, in the vicinity of the Sundance fault zone in the Main Drift and ESF Niche #1, and near the Sundance fault zone and the Ghost Dance fault zone where they were intersected by the northern Ghost Dance fault access drift (Alcove 6). Similar to the ESF results, 5 out of 15 Cross Drift samples had ratios above $1,250 \times 10^{-15}$, and nine were above $1,000 \times 10^{-15}$ (data not yet qualified).

The correlation of the elevated ^{36}Cl measurements with the surface expression of faulting indicates that the pathway and travel time may involve locally modified PTn unit fracture properties (Fabryka-Martin, Wolfsberg et al. 1997, p. 78; Fabryka-Martin, Flint et al. 1997, pp. 6-22, 8-18). These data support the hypothesis that faulting or other disturbances increase PTn unit fracture permeability, thereby generating a local environment in the PTn unit that supports fracture flow and hence rapid transport of solutes. Once through the PTn unit, flux distributions favor fracture flow in the TSw unit, thereby providing a continuous pathway to the sampled depths.

A validation study of ^{36}Cl data is underway. The study was initiated to further examine multiple bomb-pulse tracers (e.g., ^{36}Cl) from qualified samples taken within the ESF. Samples were collected at regular intervals throughout the study zone. As of May 1, 2000, these validation measurements had detected no evidence of bomb-pulse ^{36}Cl and do not indicate evidence for increased ^{36}Cl production rates during the Pleistocene. Based on recent data alone, the chlorine in ESF appears old, in contrast to results of work reported above. Furthermore, the tritium measurements from the Sundance fault in the ESF show no indication of bomb-pulse tritium. Testing is continuing to understand why these results differ from previous results.

As a first step in trying to resolve the issue between the two data sets, a homogeneous tuff sample will be prepared from which representative splits will be distributed to two different laboratories for leaching experiments. This reference sample will serve two purposes. The first is that it will be a "standard reference material" whose ^{36}Cl concentration, for any specific procedure, is accepted. To validate the rock as a standard reference material, it will be necessary to demonstrate that splits of the crushed rock all have the same ^{36}Cl concentration. Once this is demonstrated, it will serve as a source of reference material to use in tests. The second goal is to investigate the effect of chlorine extraction techniques on the measured ^{36}Cl concentrations. It is anticipated that such experiments will involve systematic studies of dependencies on leaching techniques, leaching times, further crushing of the samples, and other possible variables. The significance of these studies is immediately relevant to the differences seen in the validation study. These data may also provide important constraints on the nature of those processes affecting the exchange of recharge water with pre-existing pore water in the rock.

5.3.7.3.4 Non-Bomb-Pulse Chlorine-36 in the Exploratory Studies Facility

Most of the ESF sample analyses had ratios less than the threshold for indicating bomb-pulse ^{36}Cl (Figure 5.3-31). In the southern part of the ESF, beyond Station 45+00, most samples had ^{36}Cl/Cl ratios typical of Holocene water, which could suggest travel times of less than 10 k.y. to this depth. (Averages of water with greater and lesser values provide a less likely explanation because the mixing proportions would have to be the same for the large number of samples.) A number of samples from this part of the system also had ^{36}Cl signals that were significantly

below the present-day background value, suggesting the possible presence of zones of relatively stagnant water.

Many samples from the northern part of the ESF, up to Station 45+00, had ^{36}Cl/Cl ratios variably above the present-day background, providing a striking contrast to the nearly constant ratios measured in its southern part (Figure 5.3-31). The largest signals—those above a ratio of 1,250 × 10^{-15}—are attributed to global fallout ^{36}Cl. Fabryka-Martin, Wolfsberg et al. (1997, pp. 19, 21) discuss alternative hypotheses to account for these highly elevated signals and rule out sample contamination as well as in situ production of ^{36}Cl either at the surface or deeper in the profile. The favored hypothesis is that fast hydrologic paths capable of conducting bomb-pulse ^{36}Cl to the level of the ESF are more prevalent in the northern part of the ESF than in the southern part, due to a greater number of faults in the north that cut through the comparatively unfractured PTn unit where it overlies the ESF. With regard to those intermediate samples with ratios greater than present-day background but less than 1,250 × 10^{-15}, it is not presently possible to assess whether these intermediate signals indicate the presence of a very small component of bomb-pulse ^{36}Cl or whether the elevated signals reflect travel times exceeding 10 k.y., the most recent time when the signal in infiltrating water would have been high enough to provide the ^{36}Cl/Cl signatures found in water from this area.

5.3.7.3.5   Chlorine-36 in Deep Boreholes

Measured ^{36}Cl/Cl ratios for samples of moderately to densely welded tuff from boreholes are systematically lower than the values for ESF samples. This apparent discrepancy is probably attributable to differences in sample collection techniques (Fabryka-Martin, Turin et al. 1996, Section 6.2). Borehole samples are obtained from ream cuttings. Rock Cl is released to the cuttings during drilling and is subsequently leached together with the pore water Cl during sample preparation for ^{36}Cl analysis. This source of Cl has a ^{36}Cl/Cl ratio on the order of 40 × 10^{-15}. The extent to which rock Cl contributes to the total amount of Cl leached from the rock can be estimated from its Br/Cl ratio (Fabryka-Martin, Wolfsberg et al. 1997, pp. 30 to 32; Fabryka-Martin, Turin et al. 1996, Section 6.2.1). Because of the low ^{36}Cl/Cl of the rock Cl, the ^{36}Cl/Cl calculated for the meteoric component of Cl in the borehole samples is always equal to or higher than the measured ratio. Samples collected from tunnel walls are not as greatly affected by rock Cl as are borehole samples because the manual collection method used in the tunnel does not pulverize the rock as does the ream bit. Borehole samples from nonwelded units (PTn, CHn, and Prow Pass) also do not appear to be greatly affected by the release of rock Cl, probably because the concentration of leachable rock Cl in these particular units is negligibly small relative to that in the pore water fluids. Differences between uncorrected ^{36}Cl/Cl ratios for borehole samples from welded units and those from the ESF demonstrate the importance of recognizing the magnitude of the influence of rock Cl to the ^{36}Cl/Cl values measured for borehole samples. After correcting for this effect, the two sets of analyses are consistent (Fabryka-Martin, Wolfsberg et al. 1997, p. 33). None of the few ^{36}Cl/Cl measurements available for samples collected below the potential repository horizon are sufficiently high to indicate the unambiguous presence of bomb-pulse ^{36}Cl (Table 5.3-12, observations for TSw and CHn samples). The maximum ratio measured for a surface-based borehole sample in or below the Tptpul unit was 843 × 10^{-15} for SD-12 (1,940 to 1,941 ft (abut 600 m), Tcp2 unit).

5.3.7.3.6 Chlorine-36 in Perched Water

The variation of input signal for $^{36}Cl/Cl$ over time enables $^{36}Cl/Cl$ measurements in perched water (Table 5.3-7) to be interpreted in support of ^{14}C ages. Figure 5.3-30(b) shows that covariation of ^{14}C and $^{36}Cl/Cl$ is irregular but can be smoothed as a "meteoric water curve" (Figure 5.3-32). This covariation can be used as corroborative data to support interpreted ^{14}C ages as being less than or greater than about 10 k.y. For example, ^{14}C activity is plotted against $^{36}Cl/Cl$ for perched water samples on the same curve (Figure 5.3-32). The data match the meteoric water curve well and the ages of the perched water can be estimated by interpolation along the meteoric water curve. Chlorine-36 and other isotopic analyses of perched water provide a consistent estimate of the age of the perched water bodies. Ages of the perched water can be estimated by interpolation along a characteristic curve based on a predicted correlation between reconstructed ^{14}C and ^{36}Cl input functions for the past 25 k.y. By this approach, the ^{36}Cl analyses indicate ages ranging from 2 to 12 k.y. for the different perched water bodies sampled, which is in general agreement with ^{14}C based ages. However, there is substantial uncertainty in attributing $^{36}Cl/Cl$ data to particular ages above 10 k.y., as well as uncertainty in the quantitative interpretation of ages from ^{14}C data.

5.3.7.3.7 Consistency of Data with Site-Scale Flow and Transport Models

A flow and transport model using the FEHM code was used to simulate transport of ^{36}Cl into the ESF tunnel (Fabryka-Martin, Wolfsberg et al. 1997, pp. 78 to 79). Modeling results show that observed ^{36}Cl signals are consistent with the above site-scale conceptual model and with reasonable parameter estimates. The overall picture from these studies is that:

- Infiltration is spatially variable and, on the average, exceeds 1 mm/yr. over the potential repository block.

- Fracture transport can be critical, permitting rapid transport through otherwise low-conductivity materials.

- Isolated fast paths associated with faults and fractures may penetrate deep into the mountain.

These modeling studies showed that the arrival of even small (1 percent of the input flux) amounts of bomb-pulse ^{36}Cl at the ESF and Cross Drift horizon in under 50 yr. generally required percolation fluxes of at least 1 to 10 mm/yr., depending on the characteristics of the secondary permeability assumed for the model layers corresponding to the PTn unit (Fabryka-Martin, Wolfsberg et al. 1997, Tables 8-4 to 8-6). This modeling study considered the stratigraphy at two locations within the ESF, one where the thickness of the PTn unit was large (ESF Station 35+00) and one where the PTn unit was relatively thin (ESF Station 59+00). Conclusions drawn from the one-dimensional modeling study included the following (Fabryka-Martin, Flint et al. 1997, Section 8.3):

- Generally, fracture flow through the PTn unit could be sustained more readily with increases in percolation flux and secondary permeability and when fractures contributing to the secondary permeability were assumed to be sparse (thereby minimizing fracture-matrix interactions) and to have large apertures.

- Increases to the assumed water retention capacity of the fractures by adjusting poorly constrained parameters that described the fracture's capillary properties also resulted in more sustained fracture or fault flow through the PTn unit at lower fluxes.

- Fluxes insufficient to sustain fracture flow in the densely welded Tiva Canyon and Topopah Spring tuffs resulted in water samples at the ESF that were very old, with predicted ^{36}Cl/Cl ratios that indicated significant decay (approximately 300×10^{-15} to 600×10^{-15}) and that were generally too small relative to those obtained for what were considered to be non-bomb-pulse samples (500×10^{-15} to $1,500 \times 10^{-15}$).

- The predicted ratios for non-bomb-pulse samples were generally consistent with those predicted using assumed percolation fluxes of 1 to 10 mm/yr. Just as fluxes on the order of 0.1 mm/yr. led to ^{36}Cl/Cl ratios at the ESF horizon that displayed considerable decay of the meteoric signal, fluxes greater than 10 mm/yr. resulted in short travel times that led to introduction of Holocene water with ^{36}Cl/Cl ratios lower (500×10^{-15}) than observed for the non-bomb-pulse samples.

5.3.7.4 Carbon Isotopes

5.3.7.4.1 Background

The best developed isotopic method for dating groundwater is that using ^{14}C, which is produced naturally in the upper atmosphere by bombardment of N by the secondary neutron flux (Clark and Fritz 1997, p. 202):

$$^{14}_{7}N + ^{1}_{0}n \Rightarrow ^{14}_{6}C + ^{1}_{1}p$$

(Eq. 5.3-6)

The modern atmospheric activity of ^{14}C is set by convention to 13.56 decays per minute per gram of C in 1950 and is considered to have an activity of 100 percent modern C (Clark and Fritz 1997, p. 18). Based on a half-life of 5,715 yr. (Parrington et al. 1996, p. 19), this specific activity corresponds to a ^{14}C/C ratio of about 1.2×10^{-12}. The effect of aboveground testing of nuclear devices was to temporarily increase the ^{14}C content by as much as a factor of two (Figure 5.3-28). The decrease since 1964 is due to the exchange of ^{14}C for nonradioactive C from the biosphere and hydrosphere, predominantly the ocean. Other secondary influences on the atmospheric ^{14}C inventory are releases of ^{14}C from nuclear fuel reprocessing plants and dilution by releases of nonradioactive C from the burning of fossil fuels.

Despite its extensive use in hydrologic studies, numerous processes related to C geochemical reactions complicate the interpretation of ^{14}C analyses in water. These processes involve the isotopic exchange between carbonate species dissolved in pore water, and carbonates in soil and fracture minerals along the flow path, as well as with CO_2 in the gas phase. Hence, the successful use of ^{14}C to date groundwater depends on a thorough understanding of geochemical reactions involving C species in the hydrologic system. This stipulation is even more important for unsaturated zone fluids. Stable C isotope ratios (δ^{13}C values) are invaluable for evaluating the likelihood and magnitude of subsurface reactions involving C. Delta ^{18}O has been measured in CO_2 gases in YMP studies for a similar reason.

As part of YMP activities, ^{14}C and stable C isotopes have been analyzed in perched waters, unsaturated zone gases, and pore waters extracted from drill core from surface-based boreholes and from four alcoves in the ESF (Table 5.3-1) (Yang et al. 1996, pp. 27 to 34, 37, 38, 40, 42, 44 to 48; Yang, Yu et al. 1998, pp. 16 to 23; LeCain and Patterson 1997, pp. 3, 4, 11, 14; LeCain et al. 1997, pp. 18 to 20, 37 to 39).

5.3.7.4.2 Carbon-14 in Pore Water Samples

As is the case for tritium, post-bomb levels of ^{14}C have been observed in a few samples collected above and within the PTn hydrogeologic unit. None of the pore water samples from surface-based boreholes have shown post-bomb levels of ^{14}C, that is, activities above 100-percent modern carbon (Table 5.3-14; corroborative data in Table 5.3-15). However, it is possible that the presence of a relatively small volume of post-bomb water could be obscured by mixing with a large volume of old water, such that the resulting mixture would have an activity less than 100 percent modern carbon. A histogram of the data shown in Table 5.3-14 from the PTn and CHn units (Figure 5.3-33) shows that the PTn unit values cluster tightly about the range of 80 to 90 percent modern carbon, whereas the CHn unit values spread more evenly across the range, presumably reflecting a larger spread in groundwater travel times to this depth, as would be expected if fracture flow were mixing to variable extents with slower matrix flow. Stable carbon isotope ratios for these same pore waters show a wide range in both hydrogeologic units (Figure 5.3-33), which may be a consequence of a variety of processes but which is also consistent with spatially and temporally variable infiltration rates and mixing between fast fracture flow and slow matrix flow. The extent of contamination with drilling air for some samples has not yet been resolved.

The ^{14}C pore water data do not show any trend with stratigraphic depth, with larger ^{14}C activities interspersed among smaller ^{14}C activities in a vertical profile (Table 5.3-14). These irregular profiles are consistent with a conceptual model in which fracture flow and perhaps lateral flow occur in some of the stratigraphic units at Yucca Mountain (Yang et al. 1996, p. 32; Yang, Yu et al. 1998, p. 23). In general, ^{14}C activities in PTn and CHn unit pore waters suggest apparent ages that are less than 6 k.y. Apparent ages are based on the assumption that the initial ^{14}C activity is 100 percent modern carbon and that the Carbon isotopic composition of the sample has not been significantly altered by any geochemical processes, such that changes relative to the initial atmospheric activity are solely the result of radioactive decay. This assumption is supported by the high ^{14}C activities measured in the annulus of shallow boreholes (Table 5.3-16).

Detailed evaluations of the various processes that could affect ^{14}C activities and stable carbon isotope ratios in Yucca Mountain pore waters are presented in Yang et al. (1996, pp. 31 to 34) and in Yang, Yu et al. (1998, pp. 21, 23). These processes include:

- Atmospheric contamination of pore-water samples during drilling possibly shifting ^{14}C activities to higher values

- $^{14}CO_2$ in the gaseous phase possibly exchanging with bicarbonate species in the groundwater

- Seasonal variations in $\delta^{13}C$ in soil gas as a function of the stage of vegetative growth possibly affecting the isotopic signature in infiltrating waters

- Dissolution of caliche and calcites in fractures, with their wide variations in ^{14}C ages, possibly diluting the initial ^{14}C activity of infiltrating pore water and shifting its $\delta^{13}C$ value.

To some extent, the significance of these processes can be evaluated by examining the $\delta^{13}C$ and ^{14}C data for trends as a function of borehole, depth, and stratigraphic unit and by comparing pore water data to those for the gas phase, perched water, and groundwaters for which some of the above processes can be assumed to be negligible. Figure 5.3-34 plots $\delta^{13}C$ versus ^{14}C for these different categories. This plot suggests the idea that some of the high ^{14}C percent modern carbon values and young apparent ages may be the result of contamination from $^{14}CO_2$ in the drilling air (about 120 percent modern carbon, $\delta^{13}C$ about –8‰). Although the total mass of carbon in pore water is orders of magnitude higher than that in subsurface air, it is possible that the injection of large volumes of drilling air may alter the carbon isotopic composition of pore waters under some conditions.

5.3.7.4.3   Carbon-14 in Gas Samples

Gas samples were collected from open surface-based boreholes following overnight pumping to remove atmospheric air from the well bore (Tables 5.3-17, 5.3-18). Gas samples have also been collected from two instrumented surface-based boreholes, with records available from 1984 to 1995 for UZ-1, and for 1996 for SD-12 (Table 5.3-19). Finally, gas samples from ESF drill holes were collected after CO_2 and SF_6 concentrations had stabilized (Table 5.3-20) (Section 5.3.3.2).

The carbon isotope data for gas samples are discussed in greater detail in Section 5.3.8.2. The observed distribution can be summarized as follows:

Gas Samples in Open Surface-Based Boreholes–See Tables 5.3-17 and 5.3-18. Uncorrected radiocarbon ages range from modern to 2.6 k.y. in the TCw unit, modern to 3,100 yr. in the PTn unit, 650 yr. to 7.2 k.y. in the Tptpul and Tptpmn, and modern to 11.2 k.y. in the CHn unit. Radiocarbon profiles generally do not show any clear trend, with apparently younger gas often underlying older gas. However, for gas collected from open boreholes, it is often difficult to discern a clear trend with respect to the spatial distribution of ^{14}C activities in unsaturated zone gases. The downhole packer system did not completely seal against the borehole wall for all of these samples. Thus, trends are obscured by including data that probably show the effects of atmospheric contamination. Although $\delta^{13}C$ and CO_2 concentrations can often be used to identify such contamination, there is no simple rule by which to identify which ^{14}C activities represent in situ conditions because $\delta^{13}C$ and CO_2 also vary in the subsurface as a function of surface conditions (e.g., soil thickness and vegetative activity). Nor are ^{14}C activities in nearby pore waters a good guide. If the CO_2 in the gas phase were in isotopic equilibrium with CO_2 in the aqueous phase of the pore water, then the ^{14}C activities in the two phases should be comparable; however, the pore waters themselves may have been contaminated by drilling air. Because of these various unresolved issues, Yang et al. (1996, p. 32) conclude "it would be difficult to make a good age correction. However, a possible range of ages with some uncertainty can be assigned

in the future when more data become available. At present, apparent ages will be used to make preliminary interpretation."

Gas Samples in Instrumented Surface-Based Boreholes–See Table 5.3-19. Carbon-14 data from samples from the two instrumented boreholes are the most reliable indicators of in situ conditions. Uncorrected radiocarbon ages for UZ-1 are modern at the probe near the top of the PTn unit, about 3.6 k.y. at the probe closest to the base of the PTn unit, about 7 k.y. in the Tptpmn, and about 7.8 k.y. and 16 k.y. at the bottom two probes, in the Tptpll. Uncorrected ages for SD-12 are of similar magnitude although the profile is not as smooth. The gas age is about 1 k.y. at the top of the PTn unit and about 2.1 k.y. at its base. The age increases to nearly 8 k.y. in the Tptpul and to about 11 k.y. at probe B near the top of the CHn unit.

Gas Samples from Instrumented Boreholes in ESF Alcoves–See Table 5.3-20. Carbon-14 isotope results are available for gases from boreholes in ESF Alcoves 1 and 6. Samples from three boreholes in Alcove 1, all tapping intervals within the TCw unit, contained 93, 101, and 107 percent modern C. Ten samples from the Alcove 6 borehole, which penetrated the Ghost Dance fault zone in the TSw unit, ranged from 75.1 to 58.1 percent modern C, corresponding to uncorrected ^{14}C ages of 2.4 to 4.5 k.y., somewhat younger than those obtained for similar stratigraphic depths in UZ-1 and SD-12.

5.3.7.4.4 Carbon-14 and Delta Carbon-13 in Perched Waters

Carbon-14 activities and δ^{13}C values of perched waters are shown in Table 5.3-7. The ^{14}C values range from 67 to 27 percent modern C, corresponding to apparent ^{14}C residence times of about 3.3 to 11 k.y. (Yang et al. 1996, p. 34). Water ^{14}C ages can be affected by the dissolution of older C in the carbonate minerals, which would result in anomalously old apparent ages. Reaction with or incorporation of gas-phase CO_2 from deep in the unsaturated zone can also result in an anomalous apparent age. Recent input of post-bomb ^{14}C is expected to be minor because all perched water samples contain background tritium concentrations. If post-bomb water is present in the perched bodies, the component is too small to be detectable.

The δ^{13}C values measured for perched water are quite variable, ranging from −9.2 to −16.6‰ (Table 5.3-7). A weak correlation is observed between these values and the surface material in which the drill hole is located. Perched water in SD-7, a borehole that is essentially started in bedrock, has heavy values of about −9.5‰, only slightly lighter than atmospheric CO_2. In contrast, perched water from NRG-7a, which was drilled through soil, has the lightest value of −16.6‰, presumably reflective of the isotopic composition of soil CO_2 gas. This observation is similar to that made for Sr isotopic data, which show a less radiogenic input for bedrock and fracture coatings where there is no soil and for pore waters from a drill hole that was started in bedrock (Section 5.3.7.6). In summary, δ^{13}C data show that most of the bicarbonate in unsaturated zone matrix pore fluids originated in the soil zone. In contrast, most of the perched water bodies and groundwater in the Yucca Mountain area have heavier (less negative) δ^{13}C values that do not show the same degree of soil influence as do the unsaturated zone pore waters (Figure 5.3-34).

5.3.7.5   Stable Hydrogen and Oxygen Isotopes

5.3.7.5.1   Background

Large differences in H and O isotopic ratios (δ^2H and δ^{18}O) in water arise from phase changes that do not go to completion, that is, partial evaporation, condensation, crystallization, or melting (Davis and Murphy 1987, p. 119). Such incomplete processes are typical of rainfall, snowfall, evapotranspiration, and sublimation of snow and ice. As a consequence, regional differences arise in surface waters as a function of elevation, distance from water sources (i.e., the ocean), orographic (rain shadow) effects, degree of evaporation, and air temperature during precipitation. If the first four of these factors stay relatively constant for a given location, then variations in δ^2H and δ^{18}O in infiltrating water may be related to temperature variations during precipitation events. Factors that might complicate simple interpretations of such data at Yucca Mountain include shifts in δ^{18}O in pore waters due to alteration, dissolution, or precipitation of minerals containing O; isotopic exchange; and sorption of water by clays and zeolites (Yang, Yu et al. 1998, p. 24).

5.3.7.5.2   Stable Isotope Characteristics of Precipitation, Surface Water, Perched Water, and Groundwater

The standard method for presenting stable isotope data is by plotting δ^2H versus δ^{18}O, as has been done on Figure 5.3-25 for precipitation, surface water, perched water, and regional groundwater. The following observations are made from this figure:

- Precipitation data from 3 Springs Basin and Stewart Basin (Figure 5.3-35a) illustrate how fractionation of oxygen and hydrogen isotopes in atmospheric moisture results in a well-defined correlation line, called the "meteoric water line." Interpretations of isotopic data for other waters are all based upon the extent to which their compositions shift along or away from this line. Based on its lower elevation and warmer temperatures, modern precipitation at Yucca Mountain is generally expected to fall along the upper end of the range shown, with heavier (less negative) compositions, as demonstrated by four local precipitation samples plotted on Figure 5.3-35.

- Surface water data from 3 Springs Basin and Stewart Basin (Figure 5.3-35b) illustrate how stable isotopes reflect average climatic conditions prevailing during infiltration events. The cooler climate at Stewart Basin results in lighter (more negative) isotopic compositions. The isotopic data plot on the meteoric line indicates that these surface waters have not undergone much evaporation . Such a conclusion is supported by the dilute chemical compositions of these waters (Section 5.3.5.3). Data for two Yucca Mountain surface runoff samples, both collected in February 1993, also show negligible evaporation. Their heavy isotopic signatures overlap with those of the four precipitation samples collected at Yucca Mountain in 1984 (Figure 5.3-35a).

- Stable isotopic data of the perched water samples also lie close to the meteoric water line, indicating little evaporation occurred before infiltration (Figure 5.3-35c).

- Groundwaters beneath Fortymile Wash (Figure 5.3-35d) have stable isotope values similar to those for perched water beneath Yucca Mountain. Both data sets are consistent with recharge during the Holocene (i.e., post-glacial climate), as suggested by the ^{14}C data for these waters (Section 5.3.7.4) (Figure 5.3-34c and d).

- Among the groundwaters in the Yucca Mountain area, the lightest waters are from wells in the southwesternmost portion of the site (e.g., VH-1, WT#10, H-3). Local groundwaters with the heaviest isotopic values overlap with the values measured for perched waters and for wells in Fortymile Wash.

- Groundwaters from Pahute Mesa have lighter isotopic values than do the perched waters and groundwaters from Fortymile Wash. This difference is more consistent with recharge of the Pahute Mesa waters under colder climatic conditions than those that prevailed for the perched waters and samples from Fortymile Wash and with subsequent modification of the Pahute Mesa waters by rock-water interactions that shift $\delta^{18}O$ to heavier values. Although isotopic shifts due to evaporative loss cannot be altogether ruled out, this process seems unlikely to be significant for the Pahute Mesa recharge waters.

5.3.7.5.3 Stable Isotope Characteristics of Pore Waters

Extraction of Pore Waters for Isotopic Analysis–In contrast with the types of samples discussed in Section 5.3.7.5.2, hydrogen and oxygen isotope data for unsaturated zone pore waters are more difficult to interpret, presumably due to complications related to fluid extraction methods. Vacuum distillation and compression extraction (squeezing) were the two methods of pore water extraction for stable isotope analysis of δ^2H and $\delta^{18}O$ used in the site characterization investigation (Yang, Yu et al. 1998, pp. 25 to 27). For both extraction methods, stable isotope ratios are determined by mass spectrometry.

The two methods yielded comparable results for samples from the PTn unit. However, isotopic compositions of water obtained by vacuum distillation are more depleted in δ^2H and $\delta^{18}O$ than water obtained by the compression method for cores containing clay or zeolite minerals, particularly for samples from the CHn unit, Prow Pass Tuff, and Bullfrog Tuff (Yang, Yu et al. 1998, Figures 15, 16). Subsequent tests (Yang, Yu et al. 1998, p. 44) have shown that the compression-extraction process only extracts pore water, whereas the vacuum distillation process extracts both pore water and water held by zeolites or clays.

Interpretation of Isotopic Characteristics of Pore Waters–The oxygen and hydrogen isotopic compositions of pore waters can yield information about infiltrating waters, provided that sampling has not disturbed the original compositions. Significant amounts of drilling air were injected into the formation during borehole drilling, which could have caused drying of the core samples. The potential magnitude of this effect can be examined by plotting the stable isotope compositions of the pore water on the δ^2H versus $\delta^{18}O$ diagram, as has been done for UZ-14 on Figure 5.3-36. Data for unsaturated zone pore water samples obtained by squeezing the core plot on or slightly below the meteoric precipitation line, indicating minor evaporative loss (Figure 5.3-36b). This evaporation may have occurred either prior to recharge or during drilling.

Alternatively, the shift away from the meteoric water line may reflect oxygen isotopic exchange with the host rock.

In contrast, the composition of the CHn unit pore waters extracted by distillation is significantly lighter than that of the PTn unit pore waters (Figure 5.3-36a). The lighter values for CHn unit pore waters do not result from incomplete recovery by the distillation method because more than 96 percent of the water was recovered by vacuum distillation in laboratory tests in which tap water of known mass and isotopic composition was imbibed into an oven-dried core (Yang, Yu et al. 1998, Table 13). On the basis of these experiments, Yang, Yu et al. (1998, pp. 41 to 43) concluded that these extremely light oxygen isotopic signatures are not representative of in situ pore waters but rather are caused by isotopic fractionation induced by the distillation technique.

Comparison of isotopic compositions of unsaturated zone pore waters (Figure 5.3-36b) with those of the saturated zone groundwaters (Figure 5.3-35d) beneath Yucca Mountain show that the CHn unit pore waters are similar to the heaviest (least negative isotopic values) groundwaters in the Yucca Mountain area, whereas the PTn unit pore waters are significantly heavier (less negative) than either data set. Again, this difference is consistent with recharge of the CHn unit pore waters and Yucca Mountain groundwaters occurring under colder climatic conditions than recharge for the PTn unit pore waters. In the TSw unit basal vitrophyre, δ^2H values in pore water from three boreholes (SD-7, SD-9, and SD-12) are consistently shifted to more negative values, implying that waters were infiltrated during the colder climate of the last ice age (Yang, Rattray et al. 1998, p. 27, Figure 2). The δ^2H values in pore waters from the underlying CHn unit are heavier than those for pore waters from the basal vitrophyre and similar to those for waters above the basal vitrophyre zone, indicating post-ice-age water.

5.3.7.5.4   Stable Isotope Characteristics of Perched Waters

Stable isotopic data of the perched water are generally between –12.8 and –13.8‰ for $\delta^{18}O$ and –94‰ and –99.8‰ for δ^2H (Table 5.3-7). These values are slightly greater than those for the saturated zone values and similar to values for pore waters. They are generally close to the Yucca Mountain precipitation line, indicating little evaporation before infiltration (Figure 5.3-35c). All stable isotopic values are similar to modern precipitation and are therefore consistent with recharge during the Holocene, as suggested by the ^{14}C data for the perched waters and consistent with the [36]Cl data for these samples.

5.3.7.6   Strontium Isotopes

Calcite is ubiquitous at Yucca Mountain, occurring in soils and as fracture and cavity coatings within volcanic tuff. Strontium is a trace element in calcite, with concentrations generally tens to hundreds of parts per million. Decay of [87]Rb is the source of stable [87]Sr. Because calcite contains very little rubidium and the half-life of the [87]Rb parent is 4.9×10^{10} yr. (Parrington et al. 1996, p. 29), [87]Sr/[86]Sr ratios of calcite record the ratio in the water from which the calcite precipitated. (In a closed system, dissolution and reprecipitation do not alter strontium isotopic compositions.) Thus, in the absence of other sources of strontium, the strontium ratios along a flow path are expected to preserve variations inherited from strontium in the soil zone (Marshall, Futa et al. 1998, pp. 55 to 56).

Strontium isotope compositions of calcites from various settings in the Yucca Mountain region have contributed to understanding the unsaturated zone, especially in distinguishing unsaturated zone calcite from saturated zone calcite. Different populations of calcite have been compared, either to group them together or distinguish them from each other in terms of their strontium isotope compositions. Groundwater and perched water have also been analyzed. This section focuses on strontium isotope data obtained from pore water.

Although pore water can be squeezed from the nonwelded tuffs at Yucca Mountain, the volumes recovered from reasonable lengths of drill core are small (Marshall, Futa et al. 1998, pp. 55 to 56). Dry-drilled core samples that have dried during storage were used as repositories of pore water salts that can be carefully leached with deionized water for analysis of strontium isotope ratios. Crushed core is sieved to obtain a coarse sand (30 to 60 mesh) fraction that is then leached for less than 1 hr. with deionized water to redissolve the pore water salts. This water sample is then centrifuged and filtered; strontium is separated by standard techniques for analysis by thermal ionization mass spectrometry. Strontium isotope ratios are reported as differences from modern seawater in parts per thousand using

$$\delta^{87}Sr = (^{87}Sr/^{86}Sr \div 0.7092 - 1) \times 1000 \qquad \text{(Eq. 5.3-7)}$$

A single comparison between $\delta^{87}Sr$ from water-leached pore water salts and from that of water squeezed from adjacent core from UZ-14 suggests that the extraction method is valid, at least for nonwelded samples. Strontium isotope compositions in the host volcanic rocks differ significantly from those of the pore waters, indicating that pore water has not reached equilibrium with the tuffs. Pore water strontium data obtained from SD-7 core (Figure 5.3-37) are remarkable in their systematic variation with depth and their distinction from whole rock compositions. At the top of the core, the $\delta^{87}Sr$ value in the pore water is 3.6, matching the $\delta^{87}Sr$ values found in surface coatings of calcite at the drill pad. The $\delta^{87}Sr$ values increase with depth; this increase is especially evident within the PTn unit and is only slightly discernible in the underlying TSw unit.

Although the data preclude local equilibrium between pore water and rock, the rock data can predict the strontium isotope composition of the pore water if recalculated as a downhole cumulative value weighted according to strontium content of the rock samples and the associated depth interval. An additional weighting factor that takes into account the higher reactivity of the PTn unit provides a close match to observed pore water strontium values throughout most of the TSw unit. Pore water $\delta^{87}Sr$ values are likely to deviate from the predicted values are likely due to the presence of clays or zeolites, which may contain a long-lived record of pore water strontium compositions and could have been partially leached in the laboratory.

A working model assumes that strontium is added to infiltrating water by dissolution of calcite in the soil zone (Marshall, Futa et al. 1998, pp. 55 to 56). During times of increased surface vegetation, soil waters are more acidic and volcanic detritus in the soil zone can contribute radiogenic strontium into infiltrating water, thus increasing the $^{87}Sr/^{86}Sr$ ratio in the thick calcretes formed during these times. There are two separate populations of soil carbonate that can contribute strontium to infiltrating water; one is dominated by eolian carbonate with a $\delta^{87}Sr$ value of 3.6 and the other is dominated by calcretes in thick alluvial soils with a $\delta^{87}Sr$ value of 4.5 (Marshall and Mahan 1994, Figure 7). Although the eolian signal, represented by soil A/B

horizons and calcite coatings on bedrock surfaces, exists throughout the Yucca Mountain region, the strontium signal from calcretes may dominate over the eolian component of the strontium when both sources are present.

Water infiltrating into welded tuff (Tiva Canyon Tuff or Topopah Spring Tuff) tends to retain the strontium isotope composition of the overlying soil. However, the pore water data indicate that water infiltrating into or percolating through nonwelded tuff (e.g., the PTn unit) reacts readily and acquires a strontium isotope signature reflecting interaction with this unit. The strontium isotope composition of the volcanic rocks changes systematically over millions of years due to the decay of ^{87}Rb. As a result, pore waters interacting with these rocks would have δ^{87}Sr values that decrease linearly with age. Delta ^{87}Sr values of pore waters in the TSw unit are predicted to change from a modern value of 4.9 to about 0.4 at the time of TSw unit emplacement (12.7 Ma). The observation that δ ^{87}Sr values vary with microstratigraphic position within thick calcite coatings that occur in the TSw unit and the match between these ratios and the predicted values strongly suggests that the calcite coatings derive their strontium from the same source as the pore water. In other words, both pore water and the fracture water leading to calcite deposition within the TSw unit derive strontium from rock-water interaction in the overlying section, dominantly in the nonwelded units. This model indicates that pore waters in the PTn unit are redistributed between pore and fracture water that subsequently percolates through the TSw unit.

5.3.7.7 Uranium Isotopes

Uranium isotopic ratios have been used to address the question of local recharge to the water table through the unsaturated zone at Yucca Mountain and the prevalence and frequency of fracture flow. The presence of calcite and opal lining fractures and cavities in the lowest units of the TSw unit exposed in the east-west Cross Drift and in core from underlying unsaturated zone units suggests that water moving through fractures has reached these depths. Flow through the matrix also accounts for some portion of the total infiltration. However, the fraction of the shallow groundwater beneath Yucca Mountain that is locally versus regionally derived and the ratio of fracture flow versus matrix flow contributing to local recharge are poorly known. Uranium isotopic compositions of unsaturated zone fracture minerals, pore water, perched water, and shallow groundwater contribute to the conceptualization of these issues (Paces, Ludwig et al. 1998, pp. 187 to 188; Paces and Peterman 1999, pp. 134 to 138), which is summarized in this section.

Unlike oxygen, carbon, and strontium isotope signatures, which are largely inherited during infiltration through soils, uranium isotopic compositions of percolating water are significantly modified from values observed in soil water and surface water, which usually have ^{234}U/^{238}U activity ratios from 1.4 to 1.8 (Muhs et al. 1990, Table 24, Figure 3; Paces et al. 1994, p. 2400; Paces et al. 1995, Figures 9, 10, 13, 16, 17, 20, 21, 25, 26, 27, 32, 36, 39, 42, 45, 46, and 53), to ^{234}U/^{238}U activity ratios as large as 9 at the potential repository horizon (Paces, Neymark et al. 1996, Figure 3.7; Paces, Marshall et al. 1997, Figure D3). As a consequence of radioactive decay, ^{234}U is preferentially enriched relative to ^{238}U in migrating groundwater (Osmond and Cowart 1992, Figure 9.1). The primary causes for this enrichment are the greater solubility of ^{234}U due to radiation damage of crystal lattice sites containing ^{234}U atoms (Szilard-Chalmers effect) and the greater probability that these ^{234}U atoms have been converted to the more soluble uranyl ion due to the effects of radiation-induced ionization (Gascoyne 1992, Section 2.5.1).

In addition, decay of ^{238}U can cause the displacement of the intermediate ^{234}Th daughter (which rapidly decays to ^{234}U) off crystal surfaces into the adjacent water by alpha-recoil processes. The amount of excess ^{234}U relative to ^{238}U is controlled by ^{234}U decay, water/rock ratios, flow path length, and the amount of bulk rock dissolution in the aquifer.

Meteoric water that interacts with readily soluble soil components results in infiltration containing relatively large amounts of both ^{234}U and ^{238}U (Table 5.3-21) derived by bulk dissolution. As infiltrating water descends through the fracture network, small amounts of ^{234}U that have become available from radioactive decay will be incorporated into these solutions. If water fluxes are large relative to the amount of ^{234}U produced along fracture surfaces, then the $^{234}U/^{238}U$ ratio will remain relatively unchanged from its initial infiltration value. If water fluxes are small and only occur infrequently, ^{234}U can build up in sufficient amounts along the fracture surface between infiltration events such that the $^{234}U/^{238}U$ activity ratio in the water becomes elevated. The large $^{234}U/^{238}U$ ratios in unsaturated zone flow at Yucca Mountain imply that percolation volumes are small relative to shallow environments that receive larger amounts of percolation.

Data supporting this conceptual model of $^{234}U/^{238}U$ evolution were obtained from water samples collected during the Single Heater Test conducted in the Thermal Test Facility (ESF Alcove 5) (Figure 5.3-38). Water derived from the welded tuffs proximal to the heater was mobilized and flowed through a connected fracture network for several months into a nearby borehole. Uranium concentrations decreased from about 0.1 to 0.03 ppb between late November 1996 and late May 1997. In the same samples, $^{234}U/^{238}U$ activity ratios dropped from a value of 8.03 in the first water collected, to values of 4.56 and 4.13 in the two subsequent collections. These data are interpreted as evidence that the fracture pathways used by mobilized water during the test had not experienced recent natural flow and had built up substantial amounts of ^{234}U on their surfaces. Fracture water mobilized during the early stages of the test incorporated the more labile ^{234}U en route to the collection site. Once the most reactive components were dissolved, later water flowing along the same flow paths incorporated less total uranium as well as less ^{234}U, resulting in smaller uranium concentrations and $^{234}U/^{238}U$ activity ratios with time. A longer duration test would presumably have resulted in water with $^{234}U/^{238}U$ activity ratios approaching either secular equilibrium ($^{234}U/^{238}U$ activity ratio of 1.0) or values that are characteristic of readily exchangeable pore water ($^{234}U/^{238}U$ activity ratio between 1 and 4). Although large $^{234}U/^{238}U$ activity ratios were not observed in early water from the much larger and more complex Drift Scale Heater Test, a similar pattern of decreasing values with time is present in water mobilized from volumes of rock much larger than the Single Heater Test (Figure 5.3-39). This pattern illustrates, in a qualitative sense, the likelihood that frequent flushing of fracture surfaces may not allow sufficient accumulation of ^{234}U on fracture surfaces to substantially alter the $^{234}U/^{238}U$ ratios in fracture water.

Uranium isotope data from other areas of the Nevada Test Site that receive recharge sufficient to support small-volume spring discharge can also be interpreted to indicate that small fluxes and infrequent flux events are required to attain the large $^{234}U/^{238}U$ ratios observed at Yucca Mountain. Springs and seeps discharging from perched water zones on the Nevada Test Site have $^{234}U/^{238}U$ activity ratios ranging between 1.9 and 3.8 (Figure 5.3-40). These values are larger than those associated with surface water and pedogenic minerals (Paces et al. 1995) but are lower than $^{234}U/^{238}U$ ratios in most of the perched water at Yucca Mountain (Table 5.3-7) as

well as the initial $^{234}U/^{238}U$ ratios in young calcite and opal in the deep unsaturated zone (Paces, Neymark et al. 1996). Waters discharging from Nevada Test Site springs have relatively large volume-to-path-length ratios and either continuous or frequent flow that does not permit accumulation of substantial excess ^{234}U on solid surfaces along flow paths. As a result, uranium in water from these systems has isotopic compositions that are only slightly greater than values observed in the infiltrating water. In contrast, waters perched within the welded TSw unit at Yucca Mountain (boreholes WT-24, UZ-14, NRG-7a) have larger $^{234}U/^{238}U$ activity ratios (Table 5.3-7). These values (5.2 to 8.4) are in the range of initial $^{234}U/^{238}U$ activity ratios observed for young calcite and opal from the potential repository horizon in the ESF.

Groundwater from the saturated zone beneath Yucca Mountain also has elevated $^{234}U/^{238}U$ ratios compared to well water in adjacent areas (compare Figures 5.3-41 and 5.3-42) (Ludwig et al. 1993, Figure 2; Paces, Ludwig et al. 1998, p. 185). Regional saturated zone groundwater in carbonate rock, alluvial, and Precambrian rock aquifers from Oasis Valley, Amargosa Valley, Spring Mountains, and the easternmost Nevada Test Site have $^{234}U/^{238}U$ activity ratios between 1.5 and 4. Groundwater $^{234}U/^{238}U$ activity ratios from volcanic rock aquifers in the region are commonly between 4 and 6; however, shallow saturated zone groundwater beneath Yucca Mountain has anomalously large $^{234}U/^{238}U$ activity ratios between 6 and 8.5. Groundwater obtained from Paleozoic carbonate rocks at depth beneath Yucca Mountain (UE-25 p#1) has a much smaller $^{234}U/^{238}U$ ratio of 2.32, typical of the regional carbonate aquifer and indicative of the stratification of shallow and deep aquifers at the site. Upgradient regions, including Timber Mountain, Pahute Mesa, and Rainier Mesa, are at higher topographic elevations and receive greater amounts of recharge. Although the number of analyzed wells in these areas is relatively small, observed $^{234}U/^{238}U$ activity ratios are equal to or less than about 5. Smaller $^{234}U/^{238}U$ ratios (activity ratios less than 6) are also characteristic of groundwater in the volcanic rock aquifer in the Fortymile Wash and Crater Flat areas east and west of Yucca Mountain and in downgradient water wells along Highway 95 and in the Amargosa Valley. Uranium concentrations in groundwaters from most of these areas range from about 0.5 to 3 ppb.

The anomalous uranium isotopic compositions of shallow saturated zone water beneath Yucca Mountain are similar to the elevated initial $^{234}U/^{238}U$ compositions measured for deep unsaturated zone minerals and perched water bodies within the welded TSw unit. The similarity of the unsaturated zone and saturated zone uranium reservoirs at Yucca Mountain is interpreted as an indication of a genetic linkage between the two. Therefore, some component of recharge through the thick unsaturated zone at Yucca Mountain is required. If this recharge made up only a small proportion of the saturated zone groundwater beneath Yucca Mountain, a $^{234}U/^{238}U$ value that is only slightly larger than the presumed upgradient signature would be expected. Instead, the observed value is near the upper end of the range observed in the unsaturated zone materials, implying that the local recharge has not been highly diluted by through-flow from the north. Likewise, groundwater downgradient from Yucca Mountain should have a relatively large $^{234}U/^{238}U$ signature if the local recharge contributed significantly to the U budget. Groundwater containing elevated $^{234}U/^{238}U$ ratios is not observed in either Fortymile Wash (with the exception of J-13, the main supply well for activities in Nevada Test Site Area 25) or along the southern margin of Yucca Mountain at Highway 95. More or less uniform uranium concentrations in waters throughout this area indicate that the different groundwaters should have roughly equal weighting when mixed on a volume basis. Because of this similarity, small volumes of groundwater in adjacent areas should not rapidly mask the uranium isotopic contributions of

Yucca Mountain saturated zone groundwater. Therefore, local recharge is considered an important component to the saturated zone immediately below Yucca Mountain; however, this component does not contribute significantly to the regional water budget in the Fortymile Wash or Crater Flat hydrologic flow systems. These conclusions are consistent with major ion data, as well as δ^2H, $\delta^{18}O$, and $\delta^{87}Sr$ data from the shallow groundwaters at Yucca Mountain that are interpreted to indicate kilometer-scale heterogeneities over the same areas (Peterman and Patterson 1998, pp. 277 to 278; Paces and Peterman 1999, p. 137).

Preliminary U isotopic data from pore water extracted by centrifugation may indicate that most of the local recharge flows through fracture pathways rather than through the matrix. Several samples of pore water (1.5 to 3.0 mL) have been extracted from the upper lithophysal unit of the welded Tpt. Pore water has U concentrations of about 1 ppb and $^{234}U/^{238}U$ activity ratios of 2.5 to 3.0. These ratios are slightly larger than most pore water squeezed from nonwelded tuff near the top of the PTn unit ($^{234}U/^{238}U$ activity ratios of 1.5 to 2.5) but are smaller than water collected from boreholes associated with in situ heater tests ($^{234}U/^{238}U$ activity ratios of 2.5 to 5.6). Larger values approaching those that are indicative of fracture water (initial $^{234}U/^{238}U$ in fracture minerals as well as water perched within the Tpt) or characteristic of shallow saturated zone groundwater have not been observed. Substantial differences in $^{234}U/^{238}U$ compositions between pore water and fracture water indicate a general lack of equilibration between the two unsaturated zone water sources and implies minimal liquid exchange. These differences also indicate that fracture water is likely the most dominant contributor to recharge of the shallow saturated zone beneath Yucca Mountain.

5.3.8 Chemical and Isotopic Composition of Gases

5.3.8.1 Processes Controlling Gas Chemistry

The major processes that control the chemistry of the gas phase include the following:

- **Atmospheric Gas Chemistry**–The composition of air is the primary control on unsaturated zone gas chemistry.

- **Soil-Zone Processes**–Soil-zone processes, such as plant respiration, can alter the chemistry of gases that diffuse into the unsaturated zone. Carbon-dioxide partial pressures are particularly susceptible to modification by these processes.

- **Water-Air Interactions**–Once gases diffuse from the soil zone into the unsaturated zone, the gas-phase composition will tend to equilibrate with the waters present in the unsaturated zone. For example, CO_2 will tend to dissolve or exsolve from the waters depending on the partial pressures of CO_2 in the soil zone versus the upper unsaturated zone.

- **Upward Gas Flow**–Gases can migrate upward through the unsaturated zone along various gradients, including concentration, temperature, and pressure gradients. The gases migrating along these gradients may have a nonatmospheric composition. Therefore, as they mix with the indigenous gases in the unsaturated zone, they alter the overall gas composition.

- **Matrix, Fracture, and Fault Structures**–Because gas permeabilities of matrices, fractures, and faults are very different, the composition of the gas phase in a certain part of Yucca Mountain at a given time may deviate from the average composition.

- **Microbial Influences**–Microbial metabolic activity may locally influence the composition of the gas phase in the unsaturated zone.

- **Temperature**–Temperature can influence the composition of the gas phase in the unsaturated zone primarily through its influence on the kinetics of the various reactions that control the composition of the gas phase. In addition, temperature controls the equilibrium fractionation of light stable isotopes, particularly oxygen. A summary of temperature data available for the unsaturated zone at Yucca Mountain is presented in Section 5.3.6.1.

- **Pressure**–Variations in total gas pressure can influence the composition of unsaturated zone waters through their effect on the partial pressures of separate gases in the gas phase. For example, the partial pressure of carbon dioxide in the gas phase varies directly with total gas pressure. Such variations in the CO_2 partial pressure directly affect the concentration of CO_2 in water, which in turn affects the dissociation of carbonic acid and, thereby, the pH. More significant, however, is its effect on gas flow patterns, including water vapor transport.

5.3.8.2   Gas Compositions

Data exist on the abundances of the major atmospheric gases in the unsaturated zone gas phase at Yucca Mountain, including data obtained from the instrumented borehole UZ-1 (Yang et al. 1996, Table 8) as well as several other boreholes. To a depth of 368 m (1,207 ft) in UZ-1, the concentrations of oxygen, nitrogen, and argon are within analytical error of atmospheric compositions. According to Thorstenson et al. (1990, p. 260), all gas samples from UZ-6S, UZ-6, and the neutron boreholes collected to date also show concentrations of O_2, N_2, and Ar that are identical to the concentrations of these gases in atmospheric air to the limits of analytical precision. The authors report that all soil gases sampled on and near Yucca Mountain showed methane concentrations that were depleted relative to the atmospheric value of about 1.7 ppm by volume (ppmv), but still greater than 0.5 ppmv (Thorstenson et al. 1990, p. 267). In contrast, neutron hole and UZ-6S gases generally showed methane concentrations near zero, ranging up to a maximum value of 0.5 (± 0.1) ppmv, suggesting that methane consumption occurs in the subsurface, even below the soil zone (Thorstenson et al. 1990, Figure 4).

Carbon-dioxide concentrations are generally larger in the rock gas (about 0.1 percent) than in air (0.034 percent). Carbon-dioxide gas concentrations in boreholes ranged from 0.01 to 1.3 percent by volume (Thorstenson et al. 1990, Figure 4; Yang et al. 1996, Table 8) compared to an atmospheric value of approximately 0.035 percent by volume. The CO_2 concentration profiles as a function of time in UZ-1 show that relatively low CO_2 concentrations were measured in 1983 shortly after completion of the borehole and that, except for Probe 13, concentrations steadily increased until 1987 (Yang et al. 1996, Table 8, Figure 18). Thus, the early CO_2 samples were probably diluted by drilling air (Yang et al. 1996, p. 40). As the semiannual gas sampling process proceeded, most of the drilling air was removed from the hole. Halfway down the hole

in the 1994 data set, carbon dioxide dropped to 0.08 percent by volume, but increased with increasing depth to 0.36 percent by volume at the lowest sampling point in the hole (367.9 m). The more recent samples probably represent uncontaminated rock gas. This conclusion is supported by data collected from 1986 through 1994, which show that CO_2 concentration from 100 to 360 m changed very little (Yang et al. 1996, Figure 18).

The CO_2 concentrations on the upper portions of UZ-1 are elevated due to their proximity to the soil zone where biologic activity increases CO_2 concentrations (Yang et al. 1996, p. 40). The increased CO_2 concentrations at the bottom of the borehole probably represent breakdown of organic polymers from drilling fluids. The consistently low values for CO_2 concentrations at Probe 13 cannot be explained by currently available data. If Probe 13 were sensing a fracture connected to the atmosphere, the concentrations would indeed be anomalously low, but the $\delta^{13}C$ composition would also be anomalously heavy, which is not the case (Yang et al. 1996, Figure 19).

Yang et al. (1996, Table 9) published several analyses for the partial pressure of CO_2 in NRG-6 and NRG-7a in which CO_2 concentrations ranged from 0.05 to 0.19 percent by volume. Some of these data are also listed in Table 5.3-17. Note that essentially all the data indicate that the partial pressure of CO_2 in the unsaturated zone gas phase is higher by factors of three or more than that in the atmosphere.

5.3.8.3 Carbon Isotopes in Gases

Carbon isotopes were monitored at the different sampling depths in UZ-1 starting in 1984 (Yang et al. 1996, Figures 19, 20). Early data show the effects of contamination by drilling air, as evidenced by shifts in the radiocarbon profile from one sampling period to the next. The ^{14}C activities have stabilized since 1989 (top part of Figure 5.3-43) and these more recent data sets are more representative of in situ conditions, although some of the $\delta^{13}C$ values show fluctuations at a given sampling depth that lie outside the range of analytical uncertainty (e.g., Probe 11 in the bottom part of Figure 5.3-43). Most values for $\delta^{13}C$ lie within the range of -16 to $-22‰$ (Table 5.3-19 and Figure 5.3-43). SD-12 gases are lighter, with values ranging from -20 to $-25‰$ (two samples with values of -16 and $-17‰$ are believed to have been contaminated with atmospheric air, based on their ^{14}C activities) (Table 5.3-19). Slightly heavier $\delta^{13}C$ values, ranging from -13.5 to $-16.5‰$, were obtained for gas samples from boreholes in ESF Alcoves 1 and 6 (Table 5.3-20). There is little overlap between the $\delta^{13}C$ values for UZ-1 and SD-12 gases and those obtained for the gases from the ESF boreholes. However, the slightly heavier $\delta^{13}C$ values observed in the ESF alcoves are likely to be due to contamination by atmospheric CO_2 as a result of ESF ventilation through highly fractured TSw unit tuff. Hence, the UZ-1 $\delta^{13}C$ values that were obtained before the excavation of the ESF are considered to be more representative of in situ rock gas $\delta^{13}C$ values.

The ^{14}C data for UZ-1 have been very consistent for the last 7 yr. of monitoring, with a gradual decrease in ^{14}C activity with depth to about 23 percent modern C at 368 m (Figure 5.3-43). The ^{14}C profile shows an abrupt change in the slope within the Pah Canyon interval of the PTn unit. The gas transport velocity (^{14}C concentration gradient over distance) within the PTn unit is smaller than the transport velocity in the TSw unit (Yang et al. 1993, p. 404). The smaller transport velocity may be due to a greater degree of water saturation in this unit. An estimate of

the minimum travel time of gas in the TSw unit based on the apparent ^{14}C ages and depths in the borehole yields gas movement of 3.26 cm/yr. This rate, as well as results of gas transport modeling (Yang et al. 1996, pp. 47, 49), is consistent with downward movement of atmospheric CO_2 by simple Fickian diffusion. The fact that the ^{14}C values of rock gas in the closed (i.e., instrumented) borehole decrease steadily with depth indicates that inhalation and exhalation of gases in response to changes in atmospheric pressure, as observed in open boreholes, is not a significant process under undisturbed conditions. If such a topographic effect were to be significant, then ^{14}C values would not decrease steadily as seen in UZ-6 and UZ-6s. Although diffusion may not be the only mechanism for gas movement in the TSw unit at UZ-1, it seems to be the dominant mechanism and can account for the observed distribution of gaseous ^{14}C with depth.

The extent to which rock gas is in isotopic equilibrium with the pore waters is not clear. The isotopic composition of pore waters is highly variable, with δ^{13}C ranging from –9 to –27‰ (Table 5.3-14, Figure 5.3-33). Unsaturated zone gases show a nearly identical range, with δ^{13}C ranging from –8 to –26‰ (Tables 5.3-17 to 5.3-20). At equilibrium, C in bicarbonate in water should be about 8.5‰ heavier than C in CO_2 in the gas phase at 25°C (Clark and Fritz 1997, Figure 5-4, p. 120, Table 5.3, p. 521). For the example shown in this reference, δ^{13}C would be – 15.1‰ for aqueous-phase HCO_3 in equilibrium with gas-phase CO_2 with δ^{13}C of –23‰. Although no data exist for gas and pore water extracted from the same sample, Table 5.3-22 compares samples that were collected from the same general depth ranges in Yucca Mountain boreholes. For these, the differences for δ^{13}C in gas and pore water are much less than 8.5‰ for all but a couple of samples from the CHn unit in UZ-14. It is inconceivable that CO_2 gas in the pore spaces would not be in isotopic equilibrium with the pore water after coexisting for hundreds, or even thousands, of years. The apparent disequilibrium between the two phases is probably a consequence of the drilling or sampling technique. For example, in a fractured rock the pore water may have been contaminated by drilling air or the sampled gas may not be derived from the immediate vicinity of the packed-off interval, such that the sampled gas may consist mostly of fracture gas not in equilibrium with the pore gas.

Although the data sets are less extensive, data for NRG-6 and NRG-7a (Table 5.3-14) yield different results from those for UZ-1 and SD-12 (Table 5.3-19). In these drill holes, ^{14}C activity does not appear to decrease with depth and, in fact, all three gas analyses from NRG-7a show post-bomb C. However, leakage of air through poor sealing of the packer system against the borehole wall could account for these large ^{14}C activities.

The ^{14}C activity of gas in borehole SD-12 is similar to that of UZ-1 in that there is a decrease from surface to depth, but with some irregularly large deviations from the trend (Table 5.3-19). Another difference is the markedly lighter C in SD-12 and the strong correlation between δ^{13}C and ^{14}C activities. Rousseau et al. (1997, p. 64) noted that the pneumatic pressures in the two deepest stations of SD-12 (both within the CHn unit) were lower than predicted by extrapolation of the static pressure profile developed across the overlying TSw unit. This gas pressure deficiency could be due to the presence of hydrocarbons, perhaps breakdown organic products from the drilling operation. The oxidation of hydrocarbons, such as methane, could account for the anomalously light C in the drill hole. Assuming that the methane is older than 50 k.y., this source would also account for the low ^{14}C activity of the sample at 407 m (1,335 ft). Because

the postulated methane would be affecting both C isotopes, the two isotopic compositions would tend to be correlated.

The smooth ^{14}C trends observed in the SD-12 data are consistent with the UZ-1 data, supporting the concept of gas transport by a diffusion mechanism as previously concluded. However, the large fluctuations toward greater percentages of modern C at a couple of the SD-12 stations probably represent a fracture-flow component. Alternatively, the component in the bottom of the hole could be modern atmospheric C, given the sharp increase in both δ ^{13}C and [14]C (Table 5.3-19). Tests conducted on SD-12 instrument stations in January 1997 revealed a leak between one monitoring station (Station C at a depth of 385.6 m (1,265.1 ft) in the Tptplnc unit) | and the open fiberglass support pipe (Rousseau et al. 1997, p. 21), which probably allowed gas samples from this station to be contaminated with atmospheric air (Yang, Rattray et al. 1998, p. 21). Monitoring data suggest that atmospheric contamination of the lowest station (A) may have occurred prior to instrumentation and sealing of the borehole.(Yang, Rattray et al. 1998, p. 21).

5.3.8.4 Representativeness of Available Gas Chemical and Isotopic Data

Gas chemical and isotopic data reported for boreholes UZ-1 and SD-12 are considered to be representative of in situ conditions at specific depths. Borehole UZ-1 data obtained in annual sampling events for gas compositions over a decade have established that variability in gas compositions (i.e., CO_2 partial pressure and isotopic compositions) tends to decrease with time in instrumented boreholes. This fact suggests that reported gas compositions reflect distinct zones in the borehole and that the compositions reflect in situ (i.e., natural) compositions.

Data for samples collected from open boreholes are less useful because the gas samples are subject to contamination from atmospheric gas as a result of drilling and because most gas samples were integral samples in that they were obtained from open boreholes. This approach makes it difficult to associate a given gas analysis with pore water from a specific depth interval.

The number of boreholes for which gas data are available is limited in terms of both areal coverage and depth. This fact makes it difficult to evaluate the $\delta^{13}C$ variations in gas compositions in the unsaturated zone of Yucca Mountain.

5.3.8.5 Scenarios for Future Variations in Gas-Phase Chemistry

It is most likely that, in the future, the composition of the gas phase in the unsaturated zone will remain very near atmospheric except possibly for CO_2 and methane, which are controlled by vegetation and soil-zone processes. Without a better model of the causes for the variations in CO_2 partial pressures in UZ-1, it is difficult to predict future variations in these parameters or to estimate past variations.

5.3.9 Chemical and Isotopic Composition of Saturated Zone Groundwater

5.3.9.1 Processes that Control Saturated Zone Water Chemistry

The chemistry of saturated zone waters is determined by a series of processes that are linked in space and time. In this section, the primary focus will be on processes that control the chemistry of groundwaters along flow paths from recharge areas north of Yucca Mountain, through Yucca

Mountain, and downgradient from Yucca Mountain to the accessible environment. The similarities in compositions between groundwater and perched water suggest that similar geochemical processes control their compositions and that these processes differ from those controlling the geochemistry of unsaturated zone pore waters. The chemistries of local saturated zone waters and perched waters are compared in Section 5.3.9.3.

The main processes that determine groundwater chemistry along its flow paths are:

- Precipitation quantities and compositions (Section 5.3.4)

- Surface water quantities and compositions at recharge areas and along flow paths between recharge areas and the accessible environment (Section 5.3.5)

- Soil-zone processes at recharge areas and along flow paths between recharge areas and the accessible environment, including the effects of evapotranspiration

- Rock-water-gas interactions in the unsaturated zone at recharge areas

- Rock-water-gas interactions in the unsaturated zone at Yucca Mountain (Section 5.3.8)

- Rock-water interactions in the saturated zone along flow paths between the recharge areas and the accessible environment

- Temperature and pressure along flow paths between recharge areas and the accessible environment

- Mixing of groundwaters from different flow systems.

The recharge areas for saturated zone waters in Yucca Mountain are located to the northeast of Yucca Mountain in the direction of Buckboard Mesa, Rainier Mesa, and the easternmost portion of Pahute Mesa. The rock types dominating the recharge areas are silicic and basaltic volcanic units (Byers et al. 1976, pp. 6, 7, 19). Although Paleozoic limestones and other sedimentary units are present at great depth, they do not appear to influence the compositions of waters that occur in the volcanic units in the saturated zone beneath Yucca Mountain.

Climatic conditions in the recharge areas are somewhat different from those that prevail at Yucca Mountain. Specifically, they receive more precipitation and are cooler on average than the Yucca Mountain area and support a greater abundance of vegetation. Accordingly, infiltration rates on Pahute Mesa are also expected to be higher on average than infiltration rates on Yucca Mountain. Higher infiltration rates imply that dissolved salts and other constituents that may accumulate in the soil zone as a result of evapotranspiration of infiltrating waters (i.e., precipitation) have shorter residence times in this zone. This process is likely the reason that soils on Pahute Mesa and adjacent areas contain much less pedogenic calcite and/or silica than soils on Yucca Mountain. The higher infiltration rates also imply that waters infiltrating into the saturated zone will have lower salt and silica concentrations than waters at Yucca Mountain. This dilute composition makes these waters more reactive with respect to the rock units through which they may subsequently migrate.

As discussed in Section 5.3.6, rock-water reactions that recharging waters encounter in the soil zone or the unsaturated zone include dissolution reactions, mineral precipitation reactions, alteration reactions, and ion-exchange reactions. Because the waters percolating downward from the soil zones in recharge areas are likely to be more reactive than soil waters percolating into the unsaturated zone in Yucca Mountain, dissolution reactions are likely to be more important in the unsaturated zones of the recharge areas. The dominant changes to the water compositions that result from these reactions are major increases in silica, sodium, and bicarbonate (White et al. 1980, pp. Q15 to Q17).

Once the water has undergone the initial dissolution reactions, the rate of change in water composition would likely decrease. This decrease occurs because the rate of dissolution is a function of the degree to which the water has approached thermodynamic equilibrium with the rock units it contacts. The closer the water is to thermodynamic equilibrium with the host rock, the slower the reaction rate.

Actual calculation of the degree to which the reaction approaches thermodynamic equilibrium is difficult because the reactions involved are commonly incongruent. For example, in the case of feldspar equilibration with a given water composition, the feldspar crystals do not simply dissolve into the solution. It appears that the cation/H ion-exchange reaction discussed previously (Section 5.3.6.3.2) causes the feldspar surface layers to be converted (i.e., hydrolyzed) into a poorly structured hydrogen aluminosilicate solid phase. Sodium, K, and Ca are the major cations that participate in this exchange. The solubility of this solid phase would then control the rate of disappearance of the feldspar crystal (Brantley and Stellings 1996, p. 101). Unfortunately, the thermodynamic properties of this solid phase are not well defined. The same situation occurs with the hydrolysis of volcanic glass at ambient temperatures.

The dominant rock-water reactions that impact the water chemistry after the initial dissolution reactions are silica precipitation reactions and ion-exchange reactions involving minerals such as zeolites and clays. The cation/H ion-exchange reaction will also continue to be of significance. The ion-exchange reactions will tend to lead to increased Na concentrations and decreased Ca, Mg, and K concentrations in the waters. However, changes in the concentrations of these ions will occur only if zeolites and/or clays are present in adequate quantities in rock units through which the waters migrate. The Na/H ion-exchange reaction will continue to increase the Na content of the waters until thermodynamic equilibrium is achieved with the host rock (although the formation of metastable phases may cause the approach to equilibrium to be very slow).

The degree to which alteration reactions involving silicates and aluminosilicates in the host rock control water compositions is unclear. For example, volcanic glass is thermodynamically unstable in contact with water at ambient conditions, and given enough time, it will alter to secondary minerals such as clays, zeolites, silica polymorphs, and other minerals. However, glass is still present in great abundance in the volcanic units that make up Pahute Mesa and Rainier Mesa (Byers et al. 1976, pp. 6, 7, 19). Although glass alteration reactions are taking place, the rate at which this happens appears to be much slower than the rate of the initial dissolution reactions and ion-exchange reactions. For purposes of predicting water compositions, restricting the discussion to the latter reaction is probably adequate, given the current state of knowledge.

Controls on the pH of groundwaters in the saturated zone are similar to those discussed in Section 5.3.6.3.2. In brief, the primary controls on pH are the partial pressure of CO_2 and the rate at which H ions are consumed by the rock/mineral matrix. In the saturated zone, access to the CO_2 reservoir in the gas phase of the unsaturated zone becomes progressively more difficult with depth. Therefore, unless a secondary source of carbonic acid or another source of acidity (i.e., sulfide minerals) exist in the saturated zone, the reaction of H ions with the rock/mineral matrix will eventually consume the available acidity, leading to increased pH. The high pH value observed in H-3 (pH 9.4) (Ogard and Kerrisk 1984, p. 9) likely reflects this process.

Controls on redox states in the saturated zone are more difficult to define. Potential redox reactions in the saturated zone include various redox couples such as O/water, ferrous/ferric Fe, sulfide/sulfate, nitrite/nitrate, and other couples. The methane/CO_2 couple is not likely to be of significance where methane abundances are very low because this redox couple only becomes active at low temperatures if it is microbially mediated. If dissolved O is higher than approximately 0.1 mg/L, it could produce a relatively high redox potential (Eh greater than 600 mV). The redox state of saturated zone waters as calculated from the concentrations or activities for respective couples may or may not be at equilibrium. Lindberg and Runnels (1984, p. 925) argued that ground and surface waters are rarely in equilibrium in terms of redox couples and that different couples may give different redox potentials (i.e., Eh). However, this conclusion is based primarily on measurements of young groundwaters. Deep groundwaters such as those in the saturated zone at Yucca Mountain have had longer residence times during which to reach equilibrium.

In summary, the dominant processes that are likely to control water compositions along the flow paths from recharge areas to the saturated zone beneath Yucca Mountain are dissolution reactions, silica and calcite precipitation reactions, and ion-exchange reactions. The pH of these waters will be controlled primarily by the partial pressure of CO_2 and the rate at which the rocks consume H ions. Controls on the redox state in the saturated zone are poorly defined at the present time.

5.3.9.2 Present-Day Regional Characteristics

This section summarizes the available data for groundwater chemistry in volcanic aquifers and tuffaceous valley fill in the saturated zone in the Yucca Mountain region extending from recharge areas north of Yucca Mountain along flow paths through Yucca Mountain and to the accessible environment boundary south of Yucca Mountain.

Figure 5.3-44 shows the locations of several wells on Pahute Mesa from which water samples have been obtained. All of these wells were completed in Tertiary volcanic rocks (McKinley et al. 1991, Table 5). Full identifiers for these wells are shown on Figure 5.3-45. Based on regional flow models, only those wells in the eastern part of Pahute Mesa are likely to lie along flow paths that pass through the Yucca Mountain area. Those wells located in the western part of Pahute Mesa apparently lie along flow paths that pass through Oasis Valley. Water samples from springs located in the area of Rainier Mesa may reflect the compositions of waters recharging the saturated zone in the Pahute Mesa area.

The available data on saturated zone waters from the recharge areas consist primarily of analyses of the major constituents, although a limited number of isotopic analyses have been reported. A trilinear plot of relative major-ion abundances in saturated zone waters from eastern Pahute Mesa and southern Rainier Mesa is shown on Figure 5.3-45. The data indicate that the waters are dominated by sodium bicarbonate. These waters have pH values ranging from 7.4 to 8.2 and total dissolved solids ranging from 169 to 578 mg/L. Claassen (1985, p. F13) noted that these waters are chemically relatively evolved. By this, Claassen was apparently referring to the fact that the ratio of Na to other major cations was high. Because these waters occur in the recharge area (i.e., they are the youngest waters in the flow system), this is an important observation.

The locations of wells in the vicinity of Yucca Mountain from which groundwater samples were taken to obtain geochemical data are shown on Figure 5.3-46. Physical data for these wells are listed in Table 5.3-23. The relative abundances of major ionic constituents in saturated zone waters from wells in the vicinity of Yucca Mountain are plotted in Figure 5.3-27. Comparison of Figures 5.3-45 and 5.3-27 shows saturated zone waters from volcanic aquifers to be very similar in both areas. Data for downgradient waters were not plotted in the cations/anions versus chloride plots (Figures 5.3-22 to 5.3-26) because they directly overlap data points for Yucca Mountain area saturated zone waters. The downgradient waters show a pH range from 7.5 to 8.2 and a range in total dissolved solids from 217 to 233 mg/L, depending on where the southern boundary is placed (Oliver and Root 1997, Excel file yucca.xls). The fact that the downgradient waters are even farther from the recharge areas than those in the Yucca Mountain area again suggests these waters are close to equilibrium with their host rocks.

5.3.9.3 Present-Day Characteristics of Groundwaters in the Yucca Mountain Area

As pointed out in the last section, saturated zone waters from volcanic aquifers in the recharge area are compositionally similar to saturated zone waters from the Yucca Mountain area (Figures 5.3-45, 5.3-27). Analyses of groundwater from drill holes that penetrate the host rock and other volcanic units in the area of the exploration block indicate that they are principally sodium-bicarbonate waters (Figure 5.3-27) with low contents of total dissolved solids (200 to 400 mg/L) (Oliver and Root 1997). Compared to waters in the recharge areas, the Yucca Mountain area waters show a greater range in pH values from 6.6 to 9.2, and total dissolved solids range from 181 to 887 mg/L (Oliver and Root 1997).

Plots of the major cations versus chloride show that saturated zone waters (as well as perched waters, based on data from Sections 5.3.6.3 and 5.3.7.5) are generally distinct from unsaturated zone pore waters in the Yucca Mountain area in several ways:

- Saturated zone waters and perched waters have much lower chloride concentrations than the pore waters (Figure 5.3-11). This result suggests the saturated zone and perched waters were subject to less evapotranspiration than the pore waters. An alternative explanation, loss of chloride from solution by reactions with glass or hydroxyl phases in tuff, is improbable for unsaturated zone pore waters at Yucca Mountain.

- Saturated zone waters are either on or above the precipitation trend line in a sulfate versus chloride plot, suggesting that they gained sulfate, perhaps by dissolving some sulfate mineral(s) such as gypsum (Figure 5.3-25). Among the unsaturated zone pore

waters, only some samples from the PTn unit show a similarly high SO_4/Cl ratio. The vast majority of pore waters plot well below the trend line.

• Unlike unsaturated zone waters, all of the perched waters and a significant proportion of the saturated zone waters plot above the precipitation trend line in a Ca versus Cl⁻ plot (Figure 5.3-22). This result suggests some of these waters gained Ca, while others lost Ca. The fact that nearly all of these waters gained bicarbonate (Figure 5.3-23) suggests the Ca gained may have come from the dissolution of calcite. The loss of Ca likely reflects ion-exchange reactions on clays and zeolites. This possibility is supported by the fact that these waters have all gained Na (Figure 5.3-24).

• Silica concentrations in these waters are slightly lower than those measured in most pore waters. However, nearly all waters are oversaturated with alpha-cristobalite (Figure 5.3-26), suggesting that a different silica phase may control their concentrations.

On trilinear diagrams, local groundwater and perched waters show distributions of major ions that are quite similar to one another (Figures 5.3-10 and 5.3-27) and considerably different from those of unsaturated zone pore waters. The relative abundances of cations in saturated zone waters show considerable variation from east to west across Yucca Mountain, with perched water being most like groundwater from wells in Fortymile Wash (e.g., J-13). Wells on Yucca Mountain and just to the west (USW H-3, USW H-5, and USW H-6) plot nearest the Na apex of Figure 5.3-27. Wells on the eastern slopes and washes (USW H-1, USW H-4, USW G-4, J-13, and UE-25 b#1) show increasing levels of Ca. The Na+K/Ca+Mg molar ratio increases from 3.8 in J-12 to 263 in H-3. This result most likely reflects ion-exchange reactions involving the zeolites and clays in the saturated zone units beneath Yucca Mountain and the Na/H ion-exchange reaction. The fact that bicarbonate concentrations also increase from east to west suggests a significant contribution from the latter reaction.

The anionic constituents of the Yucca Mountain groundwaters show a relatively uniform distribution in all the wells, with about 80 percent bicarbonate and the remainder as sulfate and chloride (usually present in nearly equal molar concentrations) and fluoride (in varying concentrations). Perched waters have a slightly higher molar proportion of bicarbonate (about 85 percent of total anions) and more than twice the proportion of sulfate relative to chloride (Figure 5.3-10).

5.3.9.4 Representativeness of Available Data

Because the analyses of major constituents in saturated zone groundwaters from volcanic aquifers in the Yucca Mountain region show only limited variability (Figures 5.3-45, 5.3-27), the available data are sufficiently representative for characterization and modeling purposes. For pH, bounds can be placed on the likely variability to be expected, based on observations and hydrochemical models.

5.3.9.5 Scenarios for Future Variations in Saturated Zone Chemistry

The consistency in saturated zone water chemistry discussed previously suggests that climatic influences on saturated zone water chemistry are damped in the flow system. Future climatic change could involve higher infiltration rates in the recharge areas but would not likely involve

lower rates. Higher rates would result in more dilute water compositions (e.g., lower chloride). Such changes to water compositions would not lead to greater transport of waste radionuclides compared to transport rates that would occur under current conditions.

The effect of variations in climatic regimes on redox states and microbial populations is uncertain, given the present database. However, it is unlikely that higher infiltration rates would negatively affect these parameters in terms of transport behavior of important radionuclides.

5.3.10 Fluid Geochemical Indicators of Flow and Transport Processes

5.3.10.1 Chloride as a Hydrologic Tracer

Chloride pore water concentrations obtained from unsaturated core samples serve several purposes within the Yucca Mountain investigation:

- **Infiltration Estimates**–Chlorine concentrations provide independent corroboration of surface infiltration rates estimated by modeling. The chloride mass balance method estimates infiltration as a proportion of precipitation based on the enrichment of Cl in pore water relative to its concentration in precipitation.

- **Perched Water Origin**–The origin and age of perched water bodies underlying Yucca Mountain have been problematic because their Cl concentrations (4 to 10 mg/L) are generally considerably lower than those of pore waters from the unsaturated zone above the bodies. Expanding the spatial coverage of the pore water data helps constrain the various hypotheses on the derivation of the perched water.

- **Mixing of Waters**–Chlorine, Br, and SO_4 pore water concentrations indicate the extent to which water geochemistry is homogenized as it percolates through the nonwelded Paintbrush unit. Fracture-dominated flow in the overlying low-permeability, highly fractured TCw unit is expected to transition to matrix-dominated flow in the high-permeability, comparatively unfractured PTn unit (Wolfsberg et al. 1998, p. 82). The transition process from fracture to matrix flow in the PTn unit, as well as the transition from low to high matrix storage capacity, could damp out most seasonal, decadal, and secular variability in surface infiltration. This process could also result in the homogenization of the variable geochemical and isotopic characteristics of pore water entering the top of the PTn unit. In contrast, fault zones that provide continuous fracture pathways through the PTn unit may damp climatic and geochemical variability only slightly and may provide fast paths from the surface to the sampled depths, whether within the PTn unit or in underlying welded tuffs (Wolfsberg et al. 1998, p. 82, Figure 2). If this concept can be validated, it would suggest that potential repository design and performance assessment can be based on fluxes that are uniform in time, except near fault zones.

- **Lateral Diversion**–Variability in Cl, Br, and SO_4 pore water concentrations can be used to assess the extent to which water may be laterally diverted due to contrasting hydrologic properties of the various stratigraphic units above the potential repository horizon (although it is recognized that this aspect may be obscured by climatic variability in the geochemistry of infiltrating fluids).

- **Model Calibration**–To the extent that the Cl pore water database can be extended to a wide spatial and stratigraphic coverage, it is an increasingly valuable data set for site-scale modelers to use in calibrating flow and transport models of Yucca Mountain.

5.3.10.2   Infiltration Estimates Using the Chloride Mass-Balance Method

5.3.10.2.1   Chloride Mass-Balance Method

The chloride mass balance approach is based on the premise that the flux of Cl deposited at the surface equals the flux of Cl carried beneath the root zone by infiltrating water. With increasing depth, as water is extracted by evapotranspiration, Cl concentrations in pore waters increase and apparent infiltration rates decrease. Net infiltration is the flux of water moving below the zone of evapotranspiration, at which depth Cl concentrations remain relatively constant (Figure 5.3-47a). Infiltration rates can thus be estimated from measured Cl concentrations using the relationship:

$$I = (P\ C_0)/C_p \qquad\qquad \text{(Eq. 5.3-8)}$$

where I is average net infiltration (mm/yr.); P is average annual precipitation (mm/yr.); C_0 is the effective average Cl concentration in precipitation (mg/L) including the contribution from dry fallout; and C_p is the measured Cl concentration in pore water (mg/L). This approach has been widely used to estimate water transport rates in alluvial profiles through the unsaturated zone and basin-wide recharge (Dettinger 1989, pp. 57 to 61; Herczeg and Edmunds 2000, pp. 49 to 50; Phillips 1994, pp. 19 to 21; Scanlon et al. 1997, pp. 470 to 472).

5.3.10.2.2   Method Assumptions

The chloride mass balance method is based on the following simplifying assumptions:

- The average annual Cl deposition rate (the product of precipitation and Cl concentration in precipitation) is known and constant throughout the time period of interest.

- Chlorine deposition is uniform across the site.

- Run-on or runoff is negligible.

- Lateral subsurface flow, such as along the bedrock/alluvial contact, is negligible.

- Precipitation (dry and wet fallout) is the only source of Cl.

- There is no sink for Cl.

- Transport of Cl in soil can be approximated as piston flow (i.e., uniform downward movement of water without dispersion).

- Preferential flow that allows a portion of dilute infiltrating water to bypass the root zone (e.g., via root channels or fractures) is negligible.

- Extracted pore water is representative of in situ infiltrating water.

Applicability of the chloride mass-balance method to the specific conditions at Yucca Mountain (e.g., shallow soil cover over fractured rock) is an assumption to be verified. It is possible, that relatively dilute water that has infiltrated rapidly through fracture pathways may be inadequately represented by matrix pore water because of incomplete mixing. If this is the case, matrix pore water samples might be biased toward the slower moving, more concentrated matrix component of flow, and percolation estimates based on these samples would constitute lower bounds on the actual percolation rates. In the PTn unit, some component of the flux can bypass the matrix as fracture or fault flow, as evidenced by the presence of bomb-pulse tracers in the ESF. However, based on the discussion of these assumptions, the method appears to be valid for a first approximation of infiltration at Yucca Mountain (Fabryka-Martin, Flint et al. 1997, Section 6.3.1).

5.3.10.2.3   Method Parameter Values

Two approaches can be used to estimate the deposition rate of meteoric Cl onto the land surface at Yucca Mountain: (1) measuring Cl concentrations in precipitation and dry fallout, and (2) dividing the natural ^{36}Cl fallout at the site, which varies with latitude, by the pre-bomb ^{36}Cl/Cl ratio (Phillips 1994, pp. 22 to 23). Both approaches have been taken for Yucca Mountain. Deposition is highly variable on short time scales; thus long-term monitoring records are needed that cover all seasons for several years or more. Section 5.3.4.2 summarizes the available precipitation records for the area:

- In the study of desert basins in Nevada, Dettinger (1989, p. 62) calculated an average bulk precipitation concentration of 0.6 mg/L (using data from eight sites). For the study of recharge in the Las Vegas Valley, this author used an average concentration of 0.4 mg/L (for 74 sites) but noted that 66 of the sites had only wet fallout data (Dettinger 1989, pp. 63, 66).

- At 3 Springs Basin, north of Yucca Mountain, the average annual Cl concentration was 0.51 mg/L, with an average annual precipitation rate of 335 mm (calculated from data published in McKinley and Oliver [1994, pp. 23 to 27, 66 to 74], and McKinley and Oliver [1995, pp. 17, 18, 29, 30]).

- Chlorine data for the Red Rock Canyon site, outside of Las Vegas, average 0.16 mg/L for an average annual precipitation of 162 mm, but include only wet fallout.

- The concentration of Cl in 111 samples collected from Yucca Mountain for the present study during the spring of 1995 ranged from 0.3 to 1.8 mg/L, averaging 0.5 mg/L.

A longer term record is provided by the second approach, in which the Cl deposition rate (D_{Cl}) is estimated from:

$$D_{Cl} = D_{36}/(^{36}Cl/Cl)_0 \qquad \text{(Eq. 5.3-9)}$$

where D_{36} is the deposition rate of pre-bomb ^{36}Cl, and $(^{36}Cl/Cl)_0$ is the pre-bomb ^{36}Cl/Cl ratio (i.e., 502×10^{-15}), based on analyses of 41 samples of soil, alluvium, and fossil pack-rat urine (Table 5.3-11). The data for radiocarbon-dated pack-rat samples indicate that this ratio has been fairly constant throughout the Holocene. For the latitude at which Yucca Mountain is located,

Phillips (2000, Figure 10.2, p. 308) presented an empirical equation for estimating ^{36}Cl deposition rate as a function of precipitation:

$$D_{36} = 0.047\,P + 8.09 \qquad \text{(Eq. 5.3-10)}$$

where D_{36} has units of atoms/m^2/s, and P is average annual precipitation in millimeters. The average annual precipitation over Yucca Mountain is 172 mm and ranges from 128 mm at the lower elevations (3,000 ft) (about 900 m) to more than 231 mm at higher elevations (6,000 ft) (about 1,800 m) (Hevesi et al. 1992, p. 677, Equation 5, p. 685). Using these precipitation bounds, estimates for D_{36} range from 14 atoms/m^2/s (for an average annual precipitation of 128 mm), to 19 atoms/m^2/s (for 231 mm), averaging 16 atoms/m^2/s for Yucca Mountain itself (172 mm). Estimates for D_{Cl} thus range from 52 to 70 mg/m^2/yr. (for precipitation of 128 and 231 mm/yr., respectively), corresponding to effective Cl concentrations of 0.40 and 0.31 mg/L for these two precipitation rates. In general, however, the spatial distribution of precipitation directly over the potential repository site is fairly uniform, with high rates over the crest (184 mm/yr. at U2-6), decreasing to 160 or 150 mm/yr. in the lower washes (Hevesi et al. 1992, Table 3). The average Cl deposition rate for Yucca Mountain is 60 mg/m^2/yr. with an effective concentration of 0.35 mg/L, assuming 170 mm/yr. precipitation.

From this discussion, the following is concluded:

- The rate of Cl deposition is proportional to the precipitation rate and is probably fairly constant on the time scales of interest for estimating infiltration at Yucca Mountain (i.e., hundreds or thousands of years).

- Estimates of average annual Cl concentrations in precipitation at Yucca Mountain range from 0.3 to 0.6 mg/L, with 0.35 mg/L being the best estimate for a long-term average.

The relationship between measured pore water concentration and inferred infiltration rate is plotted in Figure 5.3-47(b) for this range of concentrations and a precipitation rate of 170 mm/yr.

5.3.10.2.4 Infiltration Rates at Yucca Mountain

Values of net infiltration estimated at Yucca Mountain using the chloride mass balance technique range from less than 0.1 mm/yr. to nearly 20 mm/yr. (Tables 5.3-24 and 5.3-25). Table 5.3-24 lists Cl pore water concentrations for boreholes in the ESF, Cross Drift, and Busted Butte, together with the associated apparent infiltration rates. Average concentrations for the Yucca Mountain samples are tabulated in Table 5.3-25. Average Cl concentrations for the North Ramp (23 mg/L) and Main Drift (20 mg/L) are similar to that for the Cross Drift (22 mg/L) and about a third of the average value for the South Ramp (64 mg/L). Assuming precipitation of 170 mm/yr. with an average Cl concentration of 0.35 mg/L, these pore water concentrations correspond to infiltration rates of 5 to 14 mm/yr. above the North Ramp, Main Drift, and Cross Drift, and 1 to 2 mm/yr. above the South Ramp. Thus, this difference implies that the infiltration rates above the ESF North Ramp samples are somewhat higher than those above the South Ramp samples. Despite the variable Cl concentrations in the easternmost South Ramp samples, the corresponding infiltration rates calculated for individual samples cover a narrow range, 0.4 to 4 mm/yr. (Table 5.3-24), because of the insensitivity of the chloride mass balance method to concentrations above about 20 mg/L (Figure 5.3-47b).

Table 5.3-25 lists average Cl pore water concentrations for surface-based boreholes, together with the associated apparent infiltration rates. In the north part of the study area, Cl concentrations are higher—and associated infiltration rates lower—for pore waters from these boreholes compared to pore waters from tunnel boreholes. This difference is probably due to the location of the surface-based boreholes in washes with thick alluvial cover. On the basis of chloride concentration data from alluvium and from the PTn unit, along with supporting information from neutron moisture logging and ^{36}Cl analyses, the alluvium is, in most cases, a significant barrier to water movement, and infiltration is indeed higher where alluvium is thin or absent. Some channel boreholes, as well as some soil samples collected from sideslopes, displayed chloride profiles that suggested recent flushing of chloride from the soil profile (as evidenced by low concentrations in the surficial soil). Based on Cl concentrations, infiltration through the alluvium is less than 0.05 mm/yr. at UZ#16 and UZ-N54, which are located on alluvial terraces, and 0.4 to 0.8 mm/yr. at UZ-N37, which is located in a channel. Pore water chloride concentrations from the PTn unit at UZ#16 resulted in an estimated percolation flux of 2 to 3 mm/yr. Pore water chloride concentrations from the top of the PTn unit at UZ-14 resulted in an estimated percolation flux of 0.2 to 0.4 mm/yr. Estimates of percolation flux in the PTn unit using the chloride mass balance equation were 0.6 to 1.0 mm/yr. at UZ#4 and 1.4 to 2.4 mm/yr. at UZ#5.

5.3.10.3 Origin, Age, and Continuity of Perched Water Bodies

The origin of the perched water bodies is uncertain at the present time. However, hydrochemical and isotopic data are useful in the evaluation of alternative hypotheses for their origin. Possible alternative hypotheses include the following:

- They represent a transient rise in the water level in the saturated zone.

- They represent a remnant from a time during which percolation rates were higher and locally exceeded the hydraulic conductivity of the rock units in the unsaturated zone.

- They reflect long-term steady-state conditions.

Although analyses of major chemical constituents in perched water and saturated zone waters suggest a close similarity (Section 5.3.9.2), isotopic data generally do not. The $\delta\ ^{13}$C values, $\delta\ ^{87}$Sr values, and ^{234}U/^{238}U activity ratios for perched waters are generally distinct from those obtained for saturated zone waters (Section 5.3.7). Further, there are consistent trends in $\delta\ ^{13}$C values, $\delta\ ^{87}$Sr values, and ^{234}U/^{238}U activity ratios in water and secondary mineral samples from the soil zone down through the unsaturated zone and into the uppermost saturated zone (Section 5.3.7). These observations strongly suggest that the waters in the perched zones originated at the surface of Yucca Mountain and do not represent upwelling from the saturated zone.

Assuming the water in the perched water bodies originated at the surface of Yucca Mountain, the next important question is how the water accumulated in the perched water bodies. Did it accumulate in a steady-state process that may be ongoing, or did it accumulate during a transient period of increased infiltration at some time in the past? Analyses of major chemical constituents in perched water samples and pore waters squeezed from core samples indicate that

these two water types are generally different in composition. The pore waters have much higher concentrations of most constituents compared to the perched water samples (Tables 5.3-4 and 5.3-6) (Figures 5.3-11 to 5.3-13). This observation suggests that these two water types represent different infiltration mechanisms. The higher ionic strength of the pore waters can be explained by higher rates of evapotranspiration at the infiltration points for these waters as compared to the locations at which perched waters infiltrate the subsurface. Thus, perched waters appear, on average, to have spent less time in the near-surface zones than did unsaturated zone pore waters.

The mechanism proposed to explain the chemical differences in pore waters and perched waters is one in which pore waters flow primarily through the rock matrix, whereas perched waters accumulate from flow that occurred primarily through the fractures in the host rock. For perched waters, isotopic data suggest that the flux of water through fractures is likely episodic and of small volume compared to the hydraulic conductivity of the fracture. For example, $^{234}U/^{238}U$ activity ratios measured in perched water samples are much higher than the ratios in pore waters (Section 5.3.7.7). The high activity ratios in perched waters would be most readily produced when there are episodic fluxes through many small fractures. Under these conditions of rare episodic fracture flow, ^{234}U that has accumulated on the fracture surfaces between fracture flow events is preferentially leached into the water relative to ^{238}U. If the original concentration of U in the water is small, or if the flux of water is small, a high $^{234}U/^{238}U$ activity ratio can be produced in the percolating water. Clearly, the higher the fracture surface area to water volume ratio, the higher the resulting $^{234}U/^{238}U$ activity ratio, assuming all other factors remain constant.

The identification of bomb-pulse constituents at depth within Yucca Mountain (Sections 5.3.7.2, 5.3.7.3, and 5.3.7.4 for tritium, ^{36}Cl, and ^{14}C, respectively) suggests that flow along fractures can be rapid. However, the absence of a clear bomb-pulse signal for any of these radionuclides in perched water samples (Table 5.3-7) (Section 5.3.7.3) indicates that the flux of water from the surface downward through fractures to perched water bodies must be small.

In summary, the hydrochemical evidence suggests that pore waters and perched waters in the unsaturated zone at Yucca Mountain originated at the surface of the mountain. Perched waters appear to form as a result of episodic fracture flow involving small volumes of water. The travel time of waters percolating from the surface to the depth of the perched water bodies can be short (i.e., less than 40 yr.). The matrix pore waters apparently represent a more continuous percolation of water infiltrated at the surface and moving slowly downward after enough residence time in the soil zone to gain the major-ion constituent concentrations observed in the pore waters.

Data bearing on the age of perched water were discussed in Section 5.3.7.4.4. The ^{14}C values range from 67 to 27 percent modern carbon, corresponding to residence times of 3.5 to 11 k.y. These residence times have not been corrected for dead carbon that may have been gained by the waters due to the dissolution of carbonate minerals along flow paths from the surface.

5.3.10.4 Ion Exchange in the Calico Hills Tuff

Data on major-ion concentrations in unsaturated zone waters beneath the potential repository horizon are of great significance as corroborative data for radionuclide transport calculations.

For example, the fact that pore waters in the lower portions of the zeolitized Calico Hills Tuff have negligibly low Ca and Mg concentrations compared to pore waters in the overlying units indicates that ion-exchange processes operate on the pore waters that percolate through the zeolitic tuffs. These processes tend to remove Ca and Mg from the percolating waters, replacing them with equimolar concentrations of Na. When combined with ^{14}C age data suggesting relatively young ages (up to 100 percent modern carbon) for CHn unit pore waters, these data indicate that ion-exchange processes operate on vertically migrating young pore waters in the CHn unit. This suggests ion-exchange processes would also operate on radionuclides released from the potential repository into aqueous solutions that migrate vertically into the zeolitic CHn unit.

5.3.11 Conclusions and Conceptual Models for the Geochemical and Isotopic Evolution of Fluids

An extensive database of geochemical and isotopic characteristics has been established for pore waters and gases from the unsaturated zone, perched water, and saturated zone waters in the Yucca Mountain area. The analytical work has been driven by diverse needs of the YMP, process modeling, and performance assessment communities. Water and gas chemistries influence the sorption behavior of radionuclides and the solubilities of the radionuclide compounds that form. The chemistry of waters that may infiltrate the potential repository will be determined in part by that of water present in the unsaturated zone above the potential repository horizon, whereas pore water compositions beneath the potential repository horizon will influence the sorption behavior of the radionuclides transported toward the water table. However, more relevant to the discussion in this section, development and testing of conceptual flow and transport models for the Yucca Mountain hydrologic system are strengthened through the incorporation of natural environmental tracer data into the process. Chemical and isotopic data are used to establish bounds on key hydrologic parameters and to provide corroborative evidence for model assumptions and predictions. Examples of specific issues addressed by these data include spatial and temporal variability in net fluxes, lateral diversion in specific stratigraphic units, the role of faults in controlling flow paths, fracture-matrix interactions, the age and origin of perched water, and the distribution of water travel times. This section summarizes the types of data available and their implications for key hydrologic processes at Yucca Mountain.

5.3.11.1 Chemical Composition

Total Dissolved Solids and Chloride–Pore water samples were extracted by triaxial compression and by centrifugation from unsaturated core samples recovered from dry-drilled boreholes. Only nonwelded to poorly welded tuffs generally yield sufficient water for analysis, and complete chemical analyses of pore water from densely welded units are scarce. In general, unsaturated zone pore waters have higher total dissolved solid concentrations than perched or saturated zone waters, reflecting the low surface infiltration rates. The variability in the dissolved solids content of the shallowmost nonwelded unit (the PTn unit) directly reflects the spatial variability of surface infiltration rates. Concentrations in this unit are highest beneath the terraces of large washes and are lower elsewhere. This inverse relationship between infiltration rates and pore water chloride concentrations is reflected in the fact that infiltration rates calculated on the basis of the chloride mass balance method are generally consistent with rates calculated on the basis of physical methods.

Geochemical Evolution of Major Ion Chemistry–The relative distributions of ions in pore water samples also impart information about percolation processes. Most of the major chemical characteristics of the pore waters appear to be established by soil-zone processes—predominantly evapotranspiration and dissolution or precipitation of pedogenic calcite and amorphous silica—such that pore waters entering the bedrock are nearly always saturated with respect to these two phases. The infiltrating water compositions will range from calcium-sodium bicarbonate types to calcium-sodium sulfate-chloride types, depending on the residence time of the water in the soil zone. During large rainfall events that lead to percolation of soil waters directly into the unsaturated zone, the waters may be predominantly of the calcium-sodium bicarbonate type. During smaller rainfall or snowfall events, waters that percolate into the unsaturated zone may be closer to the calcium-sodium chloride-sulfate type.

Major-ion compositions of deeper pore waters indicate that rock-water reactions are very restricted during percolation through the unsaturated zone. Relative abundances of cations are altered through ion-exchange reactions with clays and zeolites along the flow paths. As a result of these reactions, pore waters extracted from the CHn unit are sodium (carbonate+bicarbonate) type waters, again a characteristic that becomes stronger with increasing depth. In contrast to the PTn unit pore waters, chemical compositions in the CHn unit are generally similar within a given stratigraphic unit and markedly different between different host lithologies in any given borehole, implying significant lateral movement of water within the CHn unit.

Samples that deviate from this general geochemical evolution provide insight into the role that may be played by other factors that can influence water chemistry, such as faults as pathways.

5.3.11.2   Isotopic Composition

If the sampled depth is more than a few meters, the presence of global fallout nuclides implies a component of fracture flow. Hence, these isotopic data provide a means for constraining the extent to which solute transport is retarded by diffusion from fractures into the adjacent matrix. The available isotopic data support the following observations.

Tritium–Several hundred tritium analyses exist for pore water fluids extracted from unconsolidated material in shallow surface-based boreholes, from drill core of deep surface-based boreholes and from ESF drill holes. Analyses are also available for water samples bailed and pumped from perched water bodies and from the saturated zone. Detectable levels of tritium have been observed along major structural features in ESF drill holes and in pore waters extracted from core samples from surface-based boreholes. These detections occur predominantly within the PTn unit, but also in some of the samples from the Topopah Spring Tuff and Calico Hills unit and as deep as the Prow Pass member of the Crater Flat Tuff.

Bomb-pulse tritium concentrations are present in the PTn unit at several locations: in some fault zones, in the lower part of the TSw unit, and in the CHn unit in one hole. Among perched water samples, post-bomb tritium was detected only in that from drill hole NRG-7a. Tritium was below detection in all groundwater samples.

Chlorine-36–Chlorine-36 analyses exist for several hundred rock samples from surface-based boreholes and the ESF. Bomb-pulse concentrations are present in the PTn unit at several

locations and in the vicinity of some fault zones in the ESF. Bomb-pulse ^{36}Cl does not appear to be present in perched water or groundwater from the site.

Carbon-14–Uncorrected ^{14}C ages of unsaturated zone pore waters and perched waters are 5 to 12 k.y. Questions regarding corrections to these ages remain to be resolved, and the corrected ages could be younger if the dissolved inorganic carbonate has been diluted by dead C through isotopic exchange with old calcite along its flow path. Elevated ^{14}C levels indicating a bomb-pulse component are present in the TSw or CHn units in four of the six surface-based boreholes sampled to this depth. Carbon-14 ages of the gas phase increase with depth in UZ-1 and SD-12, and the measured profiles are consistent with gas transport modeling of downward movement of atmospheric CO_2 by simple Fickian diffusion. In other boreholes, the trends are less clear. Rock gas does not appear to be in isotopic equilibrium with the pore waters with respect to carbon | isotopes.

Carbon-13–Relative to stable carbon isotope ratios in the atmosphere, most pore water samples | are isotopically light. This signature suggests that these pore waters have been influenced by biogenic processes, probably in the soil zone.

Deuterium and Oxygen-18–Stable isotopic compositions of hydrogen and oxygen reflect | climatic conditions at time of recharge. Spatial differences in Yucca Mountain samples are not large, but the general trend is that groundwaters to the south of the site tend to be isotopically lighter than those farther to the north or east, suggesting that recharge occurred under cooler climatic conditions. Similarly, for unsaturated zone waters, lighter values for CHn unit pore waters suggest that much of the water at this depth originated either during winter precipitation or during a time of colder climate, as compared to the origin of pore water in the PTn unit. This may also explain the more dilute nature of the CHn unit pore waters, because waters are subject to less evapotranspiration during winter precipitation or during a colder climate.

5.3.11.3 Flow Paths

Geochemical and isotopic data in waters from the unsaturated zone and saturated zone at Yucca Mountain are consistent with a flow model in which all unsaturated zone waters, including perched waters, originate at the surface of the mountain. Although flow paths appear to be predominantly vertical, there is evidence that suggests lateral flow in some units. For example, the observation that samples from the PTn unit with tritium values well above background are found beneath samples with tritium at background values is difficult to explain without calling upon some type of lateral flow mechanism. The isotopic data further provide evidence of water that has flowed rapidly to at least the depth of the ESF. This water presumably flowed along pathways that included fractures and/or faults. To account for the data, there must also be fractures and/or faults through the PTn unit. How much of the total percolation flux is due to this fracture flow is difficult to quantify. The available hydrochemical data suggest that the proportion is small. This implies that the bulk of the water in the unsaturated zone moves through the matrix. However, the fact that CHn unit pore waters are considerably more dilute than pore waters in the overlying tuffs suggests that the fracture flow component can dominate the chemistry of the deeper unsaturated zone waters. Alternatively, the more dilute nature of the CHn unit fluids could reflect infiltration under cooler climates than the present climate at Yucca Mountain.

5.3.11.4 Infiltration Rates

Apparent infiltration rates were estimated by the chloride mass balance method, using chloride concentrations for pore water samples from 11 surface-based boreholes, 53 ESF drill holes, and 24 Cross Drift drill holes. Alluvium deeper than 5 m on terraces flanking wide washes had apparent infiltration rates less than 0.05 mm/yr. (UZ-14, UZ#16). Slightly higher rates were calculated for deep alluvium in a smaller wash or in the channel itself (UZ-N37, UZ-N54). Apparent infiltration rates in the PTn unit were generally higher than the rates estimated for alluvium, even for samples from the same boreholes, presumably due to lateral flow and mixing within this unit. Nonetheless, the rates appear to be roughly correlated with surface topography. PTn unit samples beneath deep alluvium had infiltration rates between 0.6 and 3.3 mm/yr. PTn and TSw unit pore waters beneath sideslopes and ridgetops, which have thin alluvial cover, had average infiltration rates between 5 and 14 mm/yr. in the northern half of the study area (e.g., Cross Drift, North Ramp, Main Drift up to Station 45+00), but only about 1 mm/yr. in the southern half (e.g., ESF South Ramp). The overall average infiltration rate for pore water samples collected along the Main Drift and Cross Drift (30 samples) is about 6 mm/yr.

5.3.11.5 Perched Water

The existence of perched water bodies beneath Yucca Mountain is of interest because of potential implications for flow and transport in the unsaturated zone. With respect to flow issues, the existence of the perched water bodies could reflect an earlier period of increased infiltration rates, or it could reflect a steady-state phenomenon. The fact that perched water samples appear to be up to 11 k.y. old, based on ^{14}C and ^{36}Cl ages, favors the former explanation. Major-ion concentrations and U isotope data suggest that these bodies were formed by water flowing through fractures in the unsaturated zone rather than through the matrix. The fact that these waters do not appear to have equilibrated with water in the matrix of units in which the perched water bodies are found also supports a distinct origin (e.g., fracture flow) for these waters and very slow exchange between fracture and matrix reservoirs.

5.3.11.6 Implications for Potential Repository Performance

The chemistry of water is a potentially important factor in radionuclide transport because it influences the solubilities of radionuclide compounds that form and because it influences the sorption behavior of the radionuclides. In addition, the chemistry of waters that may infiltrate the potential repository will be determined in part by the chemistry of water present in the unsaturated zone above the potential repository horizon.

Variations expected in water compositions that intersect the near-field environment will be strongly dependent on the climatic regime and on flow paths. Because most flow paths that would produce water in the potential repository horizon will likely represent fracture flow paths, the water compositions may be more dilute than those of matrix pore waters extracted from welded and nonwelded tuffs. If infiltration rates increased in the site area as a result of a climatic shift, these compositions would likely become even more dilute, presumably more like the perched water compositions.

Data on major-ion concentrations in unsaturated zone waters beneath the potential repository horizon are of great significance to radionuclide transport. For example, the fact that pore waters in the lower portions of the zeolitized Calico Hills Tuff have very low Ca and Mg concentrations compared to pore waters in the overlying units indicates that ion-exchange processes operate on the pore waters that percolate through the zeolitic tuffs. These processes tend to remove Ca and Mg from the percolating waters, replacing them with equivalent concentrations of Na. When combined with ^{14}C age data suggesting relatively young ages (up 100 percent modern C) for CHn unit pore waters, these data indicate ion-exchange processes operate on vertically migrating young pore waters in the CHn unit. This suggests ion-exchange processes would also operate on radionuclides released from the potential repository into aqueous solutions that subsequently migrated vertically into the zeolitic CHn unit.

INTENTIONALLY LEFT BLANK

5.4 SUMMARY

5.4.1 Rock Geochemistry

The geochemistries of both surficial deposits (Section 4.4) and of pyroclastic units (Section 5.2) play roles in defining groundwater compositions at Yucca Mountain. The pyroclastic units provide the framework in which a repository may be developed and the barriers that will mitigate radionuclide migration should the engineered barrier systems be bypassed. The pyroclastic units at Yucca Mountain consist principally of rhyolites and high-silica rhyolites, with lesser volumes of quartz-latitic rocks above the potential repository horizon. These rock types are locally represented by glassy units that are particularly important in rock dissolution processes affecting groundwater compositions. At distances of about 100 m above the present water table, the glassy units have been altered to zeolites that play an important role in modifying groundwater compositions through cation exchange, providing cation-exchange barriers for some waste elements and providing units of low permeability. Zeolites and other alteration minerals at Yucca Mountain have been produced by a combination of syngenetic and diagenetic processes that can be used to help predict the extent of future alteration under repository thermal conditions. Geochemical studies provide evidence for the effective barrier characteristics, not only of major zeolitic horizons, but also of fracture-related minor minerals, such as manganese oxides.

5.4.2 Fluid Geochemistry

5.4.2.1 Chemical Composition

In general, unsaturated zone pore waters have higher total dissolved solid concentrations than perched or saturated zone waters, reflecting the low surface infiltration rates. The variability in the dissolved solids content of the shallowest nonwelded unit, the Paintbrush Tuff nonwelded (PTn) unit, directly reflects the spatial variability of surface infiltration rates in that there is an inverse relationship between infiltration rates and pore water chloride concentrations.

Most major chemical characteristics of the pore waters appear to be established by soil-zone processes—predominantly evapotranspiration and dissolution or precipitation of pedogenic calcite and amorphous silica—such that pore waters entering the bedrock are nearly always saturated with respect to these two phases. Major-ion compositions of deeper pore waters indicate that rock-water reactions are very restricted during percolation through the unsaturated zone. In contrast to the PTn unit pore waters, chemical compositions in the Calico Hills nonwelded (CHn) unit are generally similar within a given stratigraphic unit and markedly different between different host lithologies in any given borehole, implying significant lateral movement of water within the CHn unit.

5.4.2.2 Isotopic Composition

Detectable levels of tritium have been observed along major structural features in the Exploratory Studies Facility (ESF) drill holes and in pore waters extracted from core samples from surface-based boreholes. These detections occur predominantly within the PTn unit, but also in some samples from the Topopah Spring Tuff and Calico Hills unit, and as deep as the Prow Pass member of the Crater Flat Tuff. Among perched water samples, post-bomb tritium

was detected only in that from drill hole NRG-7a. Tritium was below detection in all groundwater samples.

Bomb-pulse concentrations of ^{36}Cl are present in the PTn unit at several locations and in the vicinity of some fault zones in the ESF. Bomb-pulse ^{36}Cl does not appear to be present in perched water or groundwater from the site.

Uncorrected ^{14}C ages of unsaturated zone pore waters and perched waters are 5 to 12 k.y. Carbon-14 ages of the gas phase increase with depth in UZ-1 and SD-12, and the measured profiles are consistent with gas transport modeling of downward movement of atmospheric CO_2 by simple Fickian diffusion. Rock gas does not appear to be in isotopic equilibrium with the pore waters with respect to C isotopes.

Carbon-13 data suggest that most pore waters have been influenced by biogenic processes, probably in the soil zone.

The isotopic compositions of hydrogen and oxygen of groundwaters suggest that recharge south of the site occurred under cooler climatic conditions than for groundwaters located farther to the north or east. Similarly, for unsaturated zone waters, much of the CHn unit pore waters may have originated either during winter precipitation or during a time of colder climate as compared to pore water in the PTn unit.

5.4.2.3 Flow Paths and Infiltration Rates

Geochemical and isotopic data in waters from the unsaturated zone and saturated zone at Yucca Mountain are consistent with a flow model in which all unsaturated zone waters, including perched waters, originate at the surface of the mountain. Although flow paths appear to be predominantly vertical, there is evidence that suggests lateral flow in some units. The isotopic data further provide evidence of water that has flowed rapidly to at least the depth of the ESF. This water presumably flowed along pathways that included fractures and/or faults.

Alluvium deeper than 5 m on terraces flanking wide washes had apparent infiltration rates of less than 0.05 mm/yr. Slightly higher rates were calculated for deep alluvium in a smaller wash or in the channel itself. Apparent infiltration rates in the PTn unit appear to be roughly correlated with surface topography. Rates beneath deep alluvium were between 0.6 and 3.3 mm/yr., whereas beneath thin alluvium they were between 5 and 8 mm/yr. in the northern half of the study area and only about 1 mm/yr. in the southern half. The overall average infiltration rate for pore water samples collected along the Main Drift and Cross Drift is about 6 mm/yr.

5.4.2.4 Perched Water

The fact that perched water samples appear to be up to 11 ka based on ^{14}C and ^{36}Cl ages implies earlier period(s) of increased infiltration. Major-ion concentrations and uranium isotope data suggest that these bodies were formed by water flowing through fractures in the unsaturated zone rather than through the matrix. The fact that these waters do not appear to have equilibrated with water in the matrix of units in which the perched water bodies are found also supports a distinct origin, via fracture flow for these waters and very slow exchange between fracture and matrix reservoirs.

5.4.2.5   Implications for Repository Performance

Variations expected in water compositions that intersect the near-field environment will strongly depend on the climatic regime and on flow paths. Because most flow paths that would produce water in the potential repository horizon will likely represent fracture flow paths, the water compositions may be more dilute than those of matrix pore waters extracted from welded and nonwelded tuffs. If infiltration rates increased in the site area as a result of a climatic shift, these compositions would likely become even more dilute, presumably more like the perched water compositions.

The fact that pore waters in the lower portions of the zeolitized Calico Hills Tuff have very low Ca and Mg concentrations compared to pore waters in the overlying units indicates that ion-exchange processes operate on the pore waters that percolate through the zeolitic tuffs. These data, combined with ^{14}C age data, suggesting relatively young ages for CHn unit pore waters, indicate ion exchange processes operate on vertically migrating young pore waters in the CHn unit. Thus, ion exchange processes should also operate on radionuclides released from the potential repository into aqueous solutions that subsequently migrated vertically into the zeolitic CHn unit.

INTENTIONALLY LEFT BLANK

5.5 REFERENCES

5.5.1 Documents Cited

Benson, L.V. and McKinley, P.W. 1985. *Chemical Composition of Ground Water in the Yucca Mountain Area, Nevada, 1971-84.* Open-File Report 85-484. Denver, Colorado: U.S. Geological Survey. ACC: NNA.19900207.0281.

Benson, L.V.; Robison, J.H.; Blankennagel, R.K.; and Ogard, A.E. 1983. *Chemical Composition of Ground Water and the Locations of Permeable Zones in the Yucca Mountain Area, Nevada.* Open-File Report 83-854. Denver, Colorado: U.S. Geological Survey. ACC: NNA.19870610.0028.

Bevington, P.R. and Robinson, D.K. 1992. *Data Reduction and Error Analysis for the Physical Sciences.* 2nd Edition. New York, New York: McGraw-Hill. TIC: 243514.

Bish, D.L. and Aronson, J.L. 1993. "Paleogeothermal and Paleohydrologic Conditions in Silicic Tuff from Yucca Mountain, Nevada." *Clays and Clay Minerals, 41,* (2), 148-161. Long Island City, New York: Pergamon Press. TIC: 224613.

Bish, D.L.; Carey, W.J.; Levy, S.S.; and Chipera, S.J. 1996. "Mineralogy-Petrology Observations Regarding the Near-Field Environment." Chapter 3, Section 3.4.3 of *Near-Field and Altered-Zone Environment Report.* Wilder, D.G., ed. UCRL-LR-124998. Volume II. Livermore, California: Lawrence Livermore National Laboratory. ACC: MOL.19961212.0122.

Bish, D.L. and Chipera, S.J. 1989. *Revised Mineralogic Summary of Yucca Mountain, Nevada.* LA-11497-MS. Los Alamos, New Mexico: Los Alamos National Laboratory. ACC: NNA.19891019.0029.

Bish, D.L. and Chipera, S.J. 1991. "Detection of Trace Amounts of Erionite Using X-Ray Powder Diffraction: Erionite in Tuffs of Yucca Mountain, Nevada, and Central Turkey." *Clays and Clay Minerals, 39,* (4), 437-445. [Long Island City, New York]: Pergamon Press. TIC: 203789.

Brantley, S.L. and Stillings, L. 1996. "Feldspar Dissolution at 25°C and Low pH." *American Journal of Science, 296,* (2), 101-127. New Haven, Connecticut: Yale University, Kline Geology Laboratory. TIC: 239822.

Broxton, D.E.; Chipera, S.J.; Byers, F.M., Jr.; and Rautman, C.A. 1993. *Geologic Evaluation of Six Nonwelded Tuff Sites in the Vicinity of Yucca Mountain, Nevada for a Surface-Based Test Facility for the Yucca Mountain Project.* LA-12542-MS. Los Alamos, New Mexico: Los Alamos National Laboratory. ACC: NNA.19940224.0128.

Broxton, D.E.; Warren, R.G.; Byers, F.M.; and Scott, R.B. 1989. "Chemical and Mineralogic Trends Within the Timber Mountain-Oasis Valley Caldera Complex, Nevada: Evidence for Multiple Cycles of Chemical Evolution in a Long-Lived Silicic Magma System." *Journal of*

Geophysical Research, 94, (B5), 5961-5985. Washington, D.C.: American Geophysical Union. TIC: 225928.

Broxton, D.E.; Warren, R.G.; Hagan, R.C.; and Luedemann, G. 1986. *Chemistry of Diagenetically Altered Tuffs at a Potential Nuclear Waste Repository, Yucca Mountain, Nye County, Nevada.* LA-10802-MS. Los Alamos, New Mexico: Los Alamos National Laboratory. ACC: MOL.19980527.0202.

Bryant, E.A. and Vaniman, D.T., eds. 1984. *Petrofabric Constraints of the Age of Zeolitization at Yucca Mountain.* Chapter VIII. C. of *Research and Development Related to the Nevada Nuclear Waste Storage Investigations, July 1—September 30, 1983.* LA-10006-PR. Los Alamos, New Mexico: Los Alamos National Laboratory. ACC: HQS.19880517.1962.

Buesch, D.C.; Spengler, R.W.; Moyer, T.C.; and Geslin, J.K. 1996. *Proposed Stratigraphic Nomenclature and Macroscopic Identification of Lithostratigraphic Units of the Paintbrush Group Exposed at Yucca Mountain, Nevada.* Open-File Report 94-469. Denver, Colorado: U.S. Geological Survey. ACC: MOL.19970205.0061.

Byers, F.M., Jr. 1985. *Petrochemical Variation of Topopah Spring Tuff Matrix with Depth (Stratigraphic Level), Drill Hole USW G-4, Yucca Mountain, Nevada.* LA-10561-MS. Los Alamos, New Mexico: Los Alamos National Laboratory. ACC: HQS.19880517.1103.

Byers, F.M., Jr.; Carr, W.J.; Orkild, P.P.; Quinlivan, W.D.; and Sargent, K.A. 1976. *Volcanic Suites and Related Cauldrons of Timber Mountain-Oasis Valley Caldera Complex, Southern Nevada.* Professional Paper 919. Washington, D.C.: U.S. Geological Survey. TIC: 201146.

Byers, F.M., Jr. and Moore, L.M. 1987. *Petrographic Variation of the Topopah Spring Tuff Matrix Within and Between Cored Drill Holes, Yucca Mountain, Nevada.* LA-10901-MS. Los Alamos, New Mexico: Los Alamos National Laboratory. ACC: NNA.19900510.0144.

Carlos, B.A. 1987. *Minerals in Fractures of the Saturated Zone from Drill Core USW G-4, Yucca Mountain, Nye County, Nevada.* LA-10927-MS. Los Alamos, New Mexico: Los Alamos National Laboratory. ACC: NNA.19900222.0149.

Carlos, B.A.; Chipera, S.J.; and Bish, D.L. 1995. *Distribution and Chemistry of Fracture-Lining Minerals at Yucca Mountain, Nevada.* LA-12977-MS. Los Alamos, New Mexico: Los Alamos National Laboratory. ACC: MOL.19960306.0564.

Carlos, B.A.; Chipera, S.J.; Bish, D.L.; and Craven, S.J. 1993. "Fracture-Lining Manganese Oxide Minerals in Silicic Tuff, Yucca Mountain, Nevada, U.S.A." *Chemical Geology, 107,* 47-69. Amsterdam, The Netherlands: Elsevier Science Publishers B.V. TIC: 208629.

Chadwick, O.A.; Hendricks, D.M.; and Nettleton, W.D. 1987. "Division S-5—Soil Genesis, Morphology, and Classification, Silica in Duric Soils: I. A Depositional Model." *Soil Science Society of America Journal, 51,* 975-982. Madison, Wisconsin: Soil Science Society of America. TIC: 236964.

Chipera, S.J.; Vaniman, D.T.; Carlos, B.A.; and Bish, D.L. 1995. *Mineralogic Variation in Drill Core UE-25 UZ#16, Yucca Mountain, Nevada.* LA-12810-MS. Los Alamos, New Mexico: Los Alamos National Laboratory. ACC: NNA.19940427.0099.

Claassen, H.C. 1985. *Sources and Mechanisms of Recharge for Ground Water in the West-Central Amargosa Desert, Nevada — A Geochemical Interpretation.* Professional Paper 712-F. [Reston, Virginia]: U.S. Geological Survey. TIC: 204574.

Clark, I.D. and Fritz, P. 1997. *Environmental Isotopes in Hydrogeology.* Boca Raton, Florida: Lewis Publishers. TIC: 233503.

Cowan, D.L.; Priest, V.; and Levy, S.S. 1993. "ESR Dating of Quartz from Exile Hill, Nevada." *Applied Radiation and Isotopes, 44,* (7), 1035-1039. [New York, New York]: Pergamon Press. TIC: 224595.

Craig, R.W. and Johnson, K.A. 1984. *Geohydrologic Data for Test Well UE-25p#1, Yucca Mountain Area, Nye County, Nevada.* Open-File Report 84-450. Denver, Colorado: U.S. Geological Survey. ACC: NNA.19870406.0256.

Craig, R.W. and Robison, J.H. 1984. *Geohydrology of Rocks Penetrated by Test Well UE-25p#1, Yucca Mountain Area, Nye County, Nevada.* Water-Resources Investigations Report 84-4248. Denver, Colorado: U.S. Geological Survey. ACC: NNA.19890905.0209.

CRWMS M&O 1998. *Evaluation of Flow and Transport Models of Yucca Mountain, Based on Chlorine-36 and Chloride Studies for FY98.* BA0000000-01717-5700-00007 REV 00. Las Vegas, Nevada: CRWMS M&O. ACC: MOL.19981208.0119.

CRWMS M&O 1999. *MGR Compliance Program Guidance Package for Geochemical System.* BA0000000-01717-5600-00011 REV 00. Las Vegas, Nevada: CRWMS M&O. ACC: MOL.19990419.0375.

CRWMS M&O 2000. *Analysis of Geochemical Data for the Unsaturated Zone.* ANL-NBS-HS-000017 REV 00. Las Vegas, Nevada: CRWMS M&O. ACC: MOL.20000725.0453.

Czarnecki, J.B. 1984. *Simulated Effects of Increased Recharge on the Ground-Water Flow System of Yucca Mountain and Vicinity, Nevada-California.* Water-Resources Investigations Report 84-4344. Denver, Colorado: U.S. Geological Survey. ACC: HQS.19880517.1750.

Davis, S.N. and Murphy, E. 1987. *Dating Ground Water and the Evaluation of Repositories for Radioactive Waste.* NUREG/CR-4912. Washington, D.C.: U.S. Nuclear Regulatory Commission. ACC: NNA.19900522.0260.

Day, W.C.; Potter, C.J.; Sweetkind, D.S.; Dickerson, R.P.; and San Juan, C.A. 1998. *Bedrock Geologic Map of the Central Block Area, Yucca Mountain, Nye County, Nevada.* Miscellaneous Investigations Series Map I-2601. [Washington, D.C.]: U.S. Geological Survey. TIC: 237019.

Dettinger, M.D. 1989. "Reconnaissance Estimates of Natural Recharge to Desert Basins in Nevada, U.S.A., by Using Chloride-Balance Calculations." *Journal of Hydrology, 106,* 55-78. Amsterdam, The Netherlands: Elsevier Science. TIC: 236967.

Drever, J.I. and Smith, C.L. 1978. "Cyclic Wetting and Drying of the Soil Zone as an Influence on the Chemistry of Ground Water in Arid Terrains." *American Journal of Science, 278,* 1448-1454. New Haven, Connecticut: Yale University, Kline Geology Laboratory. TIC: 237357.

Duff, M.C.; Newville, M.; Hunter, D.B.; Bertsch, P.M.; Sutton, S.R.; Triay, I.R.; Vaniman, D.T.; Eng, P.; and Rivers, M.L. 1999. "Micro-XAS Studies with Sorbed Plutonium on Tuff." *Journal of Synchrotron Radiation, 6, [(3)],* 350-352. [Copenhagen, Denmark: Munksgaard International Booksellers and Publishers]. TIC: 248072.

Eckhardt, R.C. 2000. "Site Description, Sec. 5 & 10, Selected Tables and Figures." Letter from R.C. Eckhardt (LANL) to A. Simmons (LBNL), EES-13-06-00-176, June 27, 2000, with enclosures. ACC: MOL.20000808.0058.

Emett, D.C.; Hutchinson, D.D.; Jonson, N.A.; and O'Hair, K.L. 1994. *Water Resources Data, Nevada, Water Year 1993.* Water-Data Report NV-93-1. Carson City, Nevada: U.S. Geological Survey. TIC: 236836.

EPA (Environmental Protection Agency) 1971. *Final Report of Off-Site Surveillance for Project Schooner, December 8, 1968.* PNE-524. Las Vegas, Nevada: Environmental Protection Agency. TIC: 246092.

Eriksson, E. 1960. "The Yearly Circulation of Chloride and Sulfur in Nature: Meteorological, Geochemical, and Pedalogical Implications. Part II." *Tellus, 12,* (1), 63-109. Stockholm, Sweden: Swedish Geophysical Society. TIC: 236893.

Ervin, E.M.; Luckey, R.R.; and Burkhardt, D.J. 1993. "Summary of Revised Potentiometric-Surface Map for Yucca Mountain and Vicinity, Nevada." *High Level Radioactive Waste Management, Proceedings of the Fourth Annual International Conference, Las Vegas, Nevada, April 26-30, 1993. 2,* 1554-1558. La Grange Park, Illinois: American Nuclear Society. TIC: 208542.

Ervin, E.M.; Luckey, R.R.; and Burkhardt, D.J. 1994. *Revised Potentiometric-Surface Map, Yucca Mountain and Vicinity, Nevada.* Water-Resources Investigations Report 93-4000. Denver, Colorado: U.S. Geological Survey. ACC: NNA.19930212.0018.

Fabryka-Martin, J.T.; Flint, A.L.; Sweetkind, D.S.; Wolfsberg, A.V.; Levy, S.S.; Roemer, G.J.C.; Roach, J.L.; Wolfsberg, L.E.; and Duff, M.C. 1997. *Evaluation of Flow and Transport Models of Yucca Mountain, Based on Chlorine-36 Studies for FY97.* LA-CST-TIP-97-010. Los Alamos, New Mexico: Los Alamos National Laboratory. ACC: MOL.19980204.0916.

Fabryka-Martin, J.T.; Turin, H.J.; Wolfsberg, A.V.; Brenner, D.; Dixon, P.R.; and Musgrave, J.A. 1996. *Summary Report of Chlorine-36 Studies.* LA-CST-TIP-96-003. Draft. Los Alamos, New Mexico: Los Alamos National Laboratory. ACC: MOL.19970103.0037.

Fabryka-Martin, J.T.; Wolfsberg, A.V.; Dixon, P.R.; Levy, S.S.; Musgrave, J.A.; and Turin, H.J. 1997. *Summary Report of Chlorine-36 Studies: Sampling, Analysis, and Simulation of Chlorine-36 in the Exploratory Studies Facility.* LA-13352-MS. Los Alamos, New Mexico: Los Alamos National Laboratory. ACC: MOL.19980812.0254.

Fabryka-Martin, J.T.; Wolfsberg, A.V.; Levy, S.S.; Roach, J.L.; Winters, S.T.; Wolfsberg, L.E.; Elmore, D.; and Sharma, P. 1998. "Distribution of Fast Hydrologic Paths in the Unsaturated Zone at Yucca Mountain." *High-Level Radioactive Waste Management, Proceedings of the Eighth International Conference, Las Vegas, Nevada, May 11-14, 1998.* Pages 93-96. La Grange Park, Illinois: American Nuclear Society. TIC: 237082.

Fabryka-Martin, J.T.; Wolfsberg, A.V.; Roach, J.L.; Winters, S.T.; and Wolfsberg, L.E. 1998. "Using Chloride to Trace Water Movement in the Unsaturated Zone at Yucca Mountain." *High-Level Radioactive Waste Management, Proceedings of the Eighth International Conference, Las Vegas, Nevada, May 11-14, 1998.* Pages 264-268. La Grange Park, Illinois: American Nuclear Society. TIC: 237082.

Flint, L.E. and Flint, A.L. 1995. *Shallow Infiltration Processes at Yucca Mountain, Nevada— Neutron Logging Data 1984-93.* Water-Resources Investigations Report 95-4035. Denver, Colorado: U.S. Geological Survey. ACC: MOL.19960924.0577.

French, R.H. 1985. *Daily, Seasonal, and Annual Precipitation at the Nevada Test Site, Nevada.* DOE/NV/10384-01. Las Vegas, Nevada: Desert Research Institute, Water Resources Center. TIC: 206773.

Gascoyne, M. 1992. "Geochemistry of the Actinides and Their Daughters." Chapter 2 of *Uranium-Series Disequilibrium: Applications to Earth, Marine, and Environmental Sciences.* Ivanovich, M. and Harmon, R.S., eds. 2nd Edition. New York, New York: Oxford University Press. TIC: 234680.

Gifford, R.O. and Frugoli, D.M. 1964. "Silica Source in Soil Solutions." *Science, 145,* 386-388. Washington, D.C.: American Association for the Advancement of Science. TIC: 239118.

Grasso, D.N. 1996. *Hydrology of Modern and Late Holocene Lakes, Death Valley, California.* Water-Resources Investigations Report 95-4237. Denver, Colorado: U.S. Geological Survey. ACC: MOL.19970204.0218.

Herczeg, A.L. and Edmunds, W.M. 2000. "Inorganic Ions as Tracers." Chapter 2 of *Environmental Tracers in Subsurface Hydrology.* Cook, P.G. and Herczeg, A.L., eds. Boston, Massachusetts: Kluwer Academic Publishers. TIC: 247093.

Hevesi, J.A.; Flint, A.L.; and Istok, J.D. 1992. "Precipitation Estimation in Mountainous Terrain Using Multivariate Geostatistics. Part II: Isohyetal Maps." *Journal of Applied Meteorology, 31,* (7), 677-688. Boston, Massachusetts: American Meteorological Society. TIC: 225248.

IAEA (International Atomic Energy Agency) 1981. *Statistical Treatment of Environmental Isotope Data in Precipitation.* Technical Reports Series No. 206. Pages XI-XX,2-3,135-

137,154-155,245-247,249-251,253-255. Vienna, Austria: International Atomic Energy Agency. TIC: 246103.

Kieft, T.L.; Kovacik, W.P., Jr.; Ringelberg, D.B.; White, D.C.; Haldeman, D.L.; Amy, P.S.; and Hersman, L.E. 1997. "Factors Limiting Microbial Growth and Activity at a Proposed High-Level Nuclear Repository, Yucca Mountain, Nevada." *Applied and Environmental Microbiology, 63*, (8), 3128-3133. [Washington, D.C.]: American Society for Microbiology. TIC: 236444.

LeCain, G.D. and Patterson, G.L. 1997. "Milestones — Submittal of Milestone SPH35EM4." Memorandum from G.D. LeCain and G.L. Patterson (USGS) to R. Craig (USGS-TPO), March 11, 1997, with attachment. ACC: MOL.19980224.0146.

LeCain, G.D.; Patterson, G.L.; and Severson, G.R. 1997. *Results from Pneumatic Monitoring, Hydrochemistry Sampling, Air-Injection, and Tracer Testing in the Upper Tiva Canyon, and Bow Ridge Fault Alcoves, Yucca Mountain, Nevada, November, 1994 to July, 1996.* Milestone 3GUS619M-1996. Denver, Colorado: U.S. Geological Survey. ACC: MOL.19970415.0387.

Levy, S.S. 1984a. "Studies of Altered Vitrophyre for the Prediction of Nuclear Waste Repository-Induced Thermal Alteration at Yucca Mountain, Nevada." *Scientific Basis for Nuclear Waste Management VII, Symposium held November 1983, Boston, Massachusetts.* McVay, G.L., ed. *26,* 959-966. New York, New York: Elsevier Science. TIC: 204393.

Levy, S.S. 1984b. *Petrology of Samples from Drill Holes USW H-3, H-4, and H-5, Yucca Mountain, Nevada.* LA-9706-MS. Los Alamos, New Mexico: Los Alamos National Laboratory. ACC: MOL.19970729.0322.

Levy, S.S. 1991. "Mineralogic Alteration History and Paleohydrology at Yucca Mountain, Nevada." *High Level Radioactive Waste Management, Proceedings of the Second Annual International Conference, Las Vegas, Nevada, April 28-May 3, 1991. 1,* 477-485. La Grange Park, Illinois: American Nuclear Society. TIC: 204272.

Levy, S.S. 1993. "Surface-Discharging Hydrothermal Systems at Yucca Mountain - Examining the Evidence." *Scientific Basis for Nuclear Waste Management XVI, Symposium held November 30-December 4, 1992, Boston, Massachusetts.* Interrante, C.G. and Pabalan, R.T., eds. *294,* 543-548. Pittsburgh, Pennsylvania: Materials Research Society. TIC: 208880.

Levy, S.S. and O'Neil, J.R. 1989. "Moderate-Temperature Zeolitic Alteration in a Cooling Pyroclastic Deposit." *Chemical Geology, 76,* (3/4), 321-326. Amsterdam, The Netherlands: Elsevier Science. TIC: 237819.

Levy, S. and Valentine, G. 1993. "Natural Alteration in the Cooling Topopah Spring Tuff, Yucca Mountain, Nevada, As an Analog to a Waste-Repository Hydrothermal Regime." *Proceedings of the Topical Meeting on Site Characterization and Model Validation, FOCUS '93, September 26-29, 1993, Las Vegas, Nevada.* Pages 145-149. La Grange Park, Illinois: American Nuclear Society. TIC: 102245.

Lindberg, R.D. and Runnells, D.D. 1984. "Ground Water Redox Reactions: An Analysis of Equilibrium State Applied to Eh Measurements and Geochemical Modeling." *Science, 225*, 925-927. Washington, D.C.: American Association for the Advancement of Science. TIC: 224111.

Lobmeyer, D.H. 1986. *Geohydrology of Rocks Penetrated by Test Well USW G-4, Yucca Mountain, Nye County, Nevada*. Water-Resources Investigations Report 86-4015. Lakewood, Colorado: U.S. Geological Survey. ACC: NNA.19890918.0510.

Lobmeyer, D.H.; Whitfield, M.S., Jr.; Lahoud, R.G.; and Bruckheimer, L. 1983. *Geohydrologic Data for Test Well UE-25b#1, Nevada Test Site, Nye County, Nevada*. Open-File Report 83-855. Denver, Colorado: U.S. Geological Survey. ACC: NNA.19890922.0285.

Ludwig, K.R.; Peterman, Z.E.; Simmons, K.R.; and Gutentag, E.D. 1993. "$^{234}U/^{238}U$ as a Ground-Water Tracer, SW Nevada-SE California." *High Level Radioactive Waste Management, Proceedings of the Fourth Annual International Conference, Las Vegas, Nevada, April 26-30, 1993. 2*, 1567-1572. La Grange Park, Illinois: American Nuclear Society. TIC: 208542.

Malmberg, G.T. and Eakin, T.E. 1962. *Ground-Water Appraisal of Sarcobatus Flat and Oasis Valley, Nye and Esmeralda Counties, Nevada*. Ground-Water Resources – Reconnaissance Series Report 10. Carson City, Nevada: State of Nevada, Department of Conservation and Natural Resources. TIC: 208666.

Marshall, B.D.; Futa, K.; and Peterman, Z.E. 1998. "Hydrologic Inferences from Strontium Isotopes in Port [Pore] Water from the Unsaturated Zone at Yucca Mountain, Nevada." *Proceedings of FTAM: Field Testing and Associated Modeling of Potential High-Level Nuclear Waste Geologic Disposal Sites, Lawrence Berkeley National Laboratory, December 15-16, 1997*. Bodvarsson, G.S., ed. LBNL-42520. Pages 55-56. Berkeley, California: Lawrence Berkeley National Laboratory. TIC: 243019.

Marshall, B.D. and Mahan, S.A. 1994. "Strontium Isotope Geochemistry of Soil and Playa Deposits Near Yucca Mountain, Nevada." *High Level Radioactive Waste Management, Proceedings of the Fifth Annual International Conference, Las Vegas, Nevada, May 22-26, 1994. 4*, 2685-2691. La Grange Park, Illinois: American Nuclear Society. TIC: 210984.

Marshall, B.D.; Peterman, Z.E.; and Stuckless, J.S. 1993. "Strontium Isotopic Evidence for a Higher Water Table at Yucca Mountain." *High Level Radioactive Waste Management, Proceedings of the Fourth Annual International Conference, Las Vegas, Nevada, April 26-30, 1993. 2*, 1948-1952. La Grange Park, Illinois: American Nuclear Society. TIC: 208542.

McKinley, P.W.; Long, M.P.; and Benson, L.V. 1991. *Chemical Analyses of Water from Selected Wells and Springs in the Yucca Mountain Area, Nevada and Southeastern California*. Open-File Report 90-355. Denver, Colorado: U.S. Geological Survey. ACC: NNA.19901031.0004.

McKinley, P.W. and Oliver, T.A. 1994. *Meteorological, Stream-Discharge, and Water-Quality Data for 1986 through 1991 from Two Small Basins in Central Nevada*. Open-File Report 93-651. Denver, Colorado: U.S. Geological Survey. ACC: NNA.19940114.0099.

McKinley, P.W. and Oliver, T.A. 1995. *Meteorological, Stream-Discharge, and Water-Quality Data for Water Year 1992 from Two Basins in Central Nevada.* Open-File Report 94-456. Denver, Colorado: U.S. Geological Survey. ACC: MOL.19950124.0284.

Montazer, P.; Weeks, E.P.; Thamir, F.; Yard, S.N.; and Hofrichter, P.B. 1985. "Monitoring the Vadose Zone in Fractured Tuff, Yucca Mountain, Nevada." *Proceedings of the NWWA Conference on Characterization and Monitoring of the Vadose (Unsaturated) Zone, November 19-21, 1985, Denver, Colorado.* Pages 439-469. Dublin, Ohio: National Water Well Association. TIC: 201366.

Muhs, D.R.; Whitney, J.W.; Shroba, R.R.; Taylor, E.M.; and Bush, C.A. 1990. "Uranium-Series Dating of Secondary Carbonates Near Yucca Mountain, Nevada: Application to Tectonic, Paleoclimatic, and Paleohydrologic Problems." *High Level Radioactive Waste Management, Proceedings of the International Topical Meeting, Las Vegas, Nevada, April 8-12, 1990.* 2, 924-929. La Grange Park, Illinois: American Nuclear Society. TIC: 202058.

NADP/NTN (National Atmospheric Deposition Program/National Trends Network) 2000. "NADP/NTN Monitoring Location NV00." Champaign, Illinois: Illinois State Water Survey. Accessed July 6, 2000. TIC: 248288. http://nadp.sws.uiuc.edu/nadpdata/siteinfo.asp?id=NV00&net=NADP?

O'Brien, G.M. 1997. *Analysis of Aquifer Tests Conducted in Boreholes USW WT-10, UE-25 WT#12, and USW SD-7, 1995-96, Yucca Mountain, Nevada.* Water-Resources Investigations Report 96-4293. Denver, Colorado: U.S. Geological Survey. ACC: MOL.19980219.0822.

Ogard, A.E. and Kerrisk, J.F. 1984. *Groundwater Chemistry Along Flow Paths Between a Proposed Repository Site and the Accessible Environment.* LA-10188-MS. Los Alamos, New Mexico: Los Alamos National Laboratory. ACC: HQS.19880517.2031.

Oliver, T. and Root, T. 1997. *Hydrochemical Database for the Yucca Mountain Area, Nye County, Nevada.* Denver, Colorado: U.S. Geological Survey. ACC: MOL.19980302.0367.

Osmond, J.K. and Cowart, J.B. 1992. "Ground Water." Chapter 9 of *Uranium-Series Disequilibrium: Applications to Earth, Marine, and Environmental Sciences.* Invanovich, M. and Harmon, R.S., eds. 2nd Edition. New York, New York: Oxford University Press. TIC: 234680.

Paces, J.B.; Ludwig, K.R.; Peterman, Z.E.; Neymark, L.A.; and Kenneally, J.M. 1998. "Anomalous Ground-Water $^{234}U/^{238}U$ Beneath Yucca Mountain: Evidence of Local Recharge?." *High-Level Radioactive Waste Management, Proceedings of the Eighth International Conference, Las Vegas, Nevada, May 11-14, 1998.* Pages 185-188. La Grange Park, Illinois: American Nuclear Society. TIC: 237082.

Paces, J.B.; Mahan, S.A.; Ludwig, K.R.; Kwak, L.M.; Neymark, L.A.; Simmons, K.R.; Nealey, L.D.; Marshall, B.D.; and Walker, A. 1995. *Progress Report on Dating Quaternary Surficial Deposits.* Milestone 3GCH510M. Final Draft. Denver, Colorado: U.S. Geological Survey. ACC: MOL.19960611.0220.

Paces, J.B.; Marshall, B.D.; Whelan, J.F.; and Neymark, L.A. 1997. "Submission of Milestone: SPC23FM4, Due March 14, 1997." Memorandum from J.B. Paces, B.D. Marshall, J.F. Whelan, and L.A. Neymark (USGS) to R.W. Craig, March 14, 1997, with attachment, "Progress Report on Unsaturated Zone Stable and Radiogenic Isotope Studies." ACC: MOL.19980224.0119.

Paces, J.B.; Menges, C.M.; Widmann, B.; Wesling, J.R.; Bush, C.A.; Futa, K.; Millard, H.T.; Maat, P.B.; and Whitney, J.W. 1994. "Preliminary U-Series Disequilibrium and Thermoluminescence Ages of Surficial Deposits and Paleosols Associated with Quaternary Faults, Eastern Yucca Mountain." *High Level Radioactive Waste Management, Proceedings of the Fifth Annual International Conference, Las Vegas, Nevada, May 22-26, 1994. 4,* 2391-2401. La Grange Park, Illinois: American Nuclear Society. TIC: 210984.

Paces, J.B.; Neymark, L.A.; Marshall, B.D.; Whelan, J.F.; and Peterman, Z.E. 1996. *Letter Report: Ages and Origins of Subsurface Secondary Minerals in the Exploratory Studies Facility (ESF).* Milestone 3GQH450M, Results of Sampling and Age Determination. Las Vegas, Nevada: U.S. Geological Survey. ACC: MOL.19970324.0052.

Paces, J.B.; Neymark, L.A.; Whelan, J.F.; Peterman, Z.E.; Marshall, B.D.; and Amelin, Y.V. 1999. "Characteristics of Unsaturated-Zone Fracture Flow Interpreted from Calcite and Opal Deposits at Yucca Mountain, Nevada." *Eos, Transactions (Supplement), 80,* (17), S4. Washington, D.C.: American Geophysical Union. TIC: 246468.

Paces, J.B. and Peterman, Z.E. 1999. "Isotope Hydrology of Ground-Water Flow Systems, Southern Nevada." *Proceedings of the International Symposium on Dynamics of Fluids in Fractured Rocks Concepts and Recent Advances, February 10-12, 1999.* Faybishenko, B., ed. LBNL-42718. Pages 134-138. Berkeley, California: Lawrence Berkeley National Laboratory. TIC: 246681.

Parrington, J.R.; Knox, H.D.; Breneman, S.L.; Baum, E.M.; and Feiner, F. 1996. *Nuclides and Isotopes, Chart of the Nuclides.* 15th Edition. San Jose, California: General Electric Company and KAPL, Inc. TIC: 233705.

Perfect, D.L.; Faunt, C.C.; Steinkampf, W.C.; and Turner, A.K. 1995. *Hydrochemical Data Base for the Death Valley Region, California and Nevada.* Open-File Report 94-305. Denver, Colorado: U.S. Geological Survey. ACC: MOL.19940718.0001.

Peterman, Z.E. and Patterson, G. 1998. "Isotopes Aid in Understanding the Yucca Mountain Flow System." *High-Level Radioactive Waste Management, Proceedings of the Eighth International Conference, Las Vegas, Nevada, May 11-14, 1998.* Pages 182-184. La Grange Park, Illinois: American Nuclear Society. TIC: 237082.

Phillips, F.M. 1994. "Environmental Tracers for Water Movement in Desert Soils of the American Southwest." *Soil Science Society of America Journal, 58,* 15-24. Madison, Wisconsin: Soil Science Society of America. TIC: 240651.

Phillips, F.M. 2000. "Chlorine-36." Chapter 10 of *Environmental Tracers in Subsurface Hydrology.* Cook, P.G. and Herczeg, A.L., eds. Boston, Massachusetts: Kluwer Academic Publishers. TIC: 247021.

Plummer, M.A.; Phillips, F.M.; Fabryka-Martin, J.; Turin, H.J.; Wigand, P.E.; and Sharma, P. 1997. "Chlorine-36 in Fossil Rat Urine: An Archive of Cosmogenic Nuclide Deposition During the Past 40,000 Years." *Science, 277,* 538-541. Washington, D.C.: American Association for the Advancement of Science. TIC: 237425.

Rattray, G.W.; Striegl, R.G.; and Yang, I.C. 1995. *Adsorption of Sulfur Hexafluoride onto Crushed Tuffs from the Yucca Mountain Area, Nye County, Nevada.* Water-Resources Investigations Report 95-4057. Denver, Colorado: U.S. Geological Survey. ACC: MOL.19970331.0042.

Rautman, C.A. and Engstrom, D.A. 1996a. *Geology of the USW SD-7 Drill Hole Yucca Mountain, Nevada.* SAND96-1474. Albuquerque, New Mexico: Sandia National Laboratories. ACC: MOL.19971218.0442.

Rautman, C.A. and Engstrom, D.A. 1996b. *Geology of the USW SD-12 Drill Hole Yucca Mountain, Nevada.* SAND96-1368. Albuquerque, New Mexico: Sandia National Laboratories. ACC: MOL.19970613.0101.

Riehle, J.R. 1973. "Calculated Compaction Profiles of Rhyolitic Ash-Flow Tuffs." *Geological Society of America Bulletin, 84,* 2193-2216. [Boulder, Colorado: Geological Society of America]. TIC: 224792.

Robinson, B.A.; Wolfsberg, A.V.; Zyvoloski, G.A.; and Gable, C.W. 1995. *An Unsaturated Zone Flow and Transport Model of Yucca Mountain.* Milestone 3468. Draft. Los Alamos, New Mexico: Los Alamos National Laboratory. ACC: MOL.19960415.0218.

Rosenbaum, J.G. 1986. "Paleomagnetic Directional Dispersion Produced by Plastic Deformation in a Thick Miocene Welded Tuff, Southern Nevada: Implications for Welding Temperatures." *Journal of Geophysical Research, 91,* (B12), 12,817-12,834. Washington, D.C.: American Geophysical Union. TIC: 233555.

Rousseau, J.P.; Kwicklis, E.M.; and Gillies, D.C., eds. 1999. *Hydrogeology of the Unsaturated Zone, North Ramp Area of the Exploratory Studies Facility, Yucca Mountain, Nevada.* Water-Resources Investigations Report 98-4050. Denver, Colorado: U.S. Geological Survey. ACC: MOL.19990419.0335.

Rousseau, J.P.; Loskot, C.L.; Thamir, F.; and Lu, N. 1997. *Results of Borehole Monitoring in the Unsaturated Zone Within the Main Drift Area of the Exploratory Studies Facility, Yucca Mountain, Nevada.* Milestone SPH22M3. Denver, Colorado: U.S. Geological Survey. ACC: MOL.19970626.0351.

Savard, C.S. 1995. "Ground-Water Recharge from Small to Large Streamflow Events During El Niño Periods Under Fortymile Wash near Yucca Mountain, Nevada." *Eos, Transactions (Supplement).* Page F241. Washington, D.C.: American Geophysical Union. TIC: 237433.

Savard, C.S. 1996. *Selected Hydrologic Data from Fortymile Wash in the Yucca Mountain Area, Nevada, Water Years 1993-94.* Open-File Report 95-709. Denver, Colorado: U.S. Geological Survey. ACC: MOL.19980226.0548.

Savard, C.S. 1998. *Estimated Ground-Water Recharge from Streamflow in Fortymile Wash Near Yucca Mountain, Nevada.* Water-Resources Investigations Report 97-4273. Denver, Colorado: U.S. Geological Survey. TIC: 236848.

Scanlon, B.R. 1991. "Evaluation of Moisture Flux from Chloride Data in Desert Soils." *Journal of Hydrology, 128,* 137-156. Amsterdam, The Netherlands: Elsevier Science. TIC: 224126.

Scanlon, B.R.; Tyler, S.W.; and Wierenga, P.J. 1997. "Hydrologic Issues in Arid, Unsaturated Systems and Implications for Contaminant Transport." *Reviews of Geophysics, 35,* (4), 461-490. [Washington, D.C.]: American Geophysical Union. TIC: 246881.

Schuraytz, B.C.; Vogel, T.A.; and Younker, L.W. 1989. "Evidence for Dynamic Withdrawal from a Layered Magma Body: The Topopah Spring Tuff, Southwestern Nevada." *Journal of Geophysical Research, 94,* (B5), 5925-5942. Washington, D.C.: American Geophysical Union. TIC: 225936.

Sharma, P.; Kubik, P.W.; Fehn, U.; Gove, H.E.; Nishiizumi, K.; and Elmore, D. 1990. "Development of ^{36}Cl Standards for AMS." *Nuclear Instruments and Methods in Physics Research, B52,* 410-415. Amsterdam, The Netherlands: Elsevier Science Publishers. TIC: 224755.

Spengler, R.W. and Chornack, M.P. 1984. *Stratigraphic and Structural Characteristics of Volcanic Rocks in Core Hole USW G-4, Yucca Mountain, Nye County, Nevada with a Section on Geophysical Logs by D.C. Muller and J.E. Kibler.* Open-File Report 84-789. Denver, Colorado: U.S. Geological Survey. ACC: NNA.19890804.0012.

Spengler, R.W. and Rosenbaum, J.G. 1991. "A Low-Angle Breccia Zone of Hydrologic Significance at Yucca Mountain, Nevada." *Abstracts with Programs - Geological Society of America, 23,* (5), A119. Boulder, Colorado: Geological Society of America. TIC: 247113.

Thorstenson, D.C.; Weeks, E.P.; Hass, H.; and Woodward, J.C. 1990. "Physical and Chemical Characteristics of Topographically Affected Airflow in an Open Borehole at Yucca Mountain, Nevada." *Proceedings of the Topical Meeting on Nuclear Waste Isolation in the Unsaturated Zone, FOCUS '89, Las Vegas, Nevada, September 17-21, 1989.* Pages 256-270. La Grange Park, Illinois: American Nuclear Society. TIC: 212738.

Triay, I.R.; Meijer, A.; Conca, J.L.; Kung, K.S.; Rundberg, R.S.; Strietelmeier, B.A.; and Tait, C.D. 1997. *Summary and Synthesis Report on Radionuclide Retardation for the Yucca Mountain Site Characterization Project.* Eckhardt, R.C., ed. LA-13262-MS. Los Alamos, New Mexico: Los Alamos National Laboratory. ACC: MOL.19971210.0177.

Vaniman, D.T.; Bish, D.L.; Chipera, S.J.; Carlos, B.A.; and Guthrie, G.D., Jr. 1996. *Chemistry and Mineralogy of the Transport Environment at Yucca Mountain.* Volume I of *Summary and Synthesis Report on Mineralogy and Petrology Studies for the Yucca Mountain Site Characterization Project.* Milestone 3665. Los Alamos, New Mexico: Los Alamos National Laboratory. ACC: MOL.19961230.0037.

Vaniman, D.T.; Carey, J.W.; Bish, D.L.; and Chipera, S.J. 1999. "Cation Profiles Generated by Downward Transport Into Unsaturated Zeolitic Strata at Yucca Mountain, Nevada." *Eos, Transactions (Supplement), 80,* (17), [S5]. Washington, D.C.: American Geophysical Union. TIC: 246464.

Vaniman, D.T. and Chipera, S.J. 1996. "Paleotransport of Lanthanides and Strontium Recorded in Calcite Compositions from Tuffs at Yucca Mountain, Nevada, USA." *Geochimica et Cosmochimica Acta, 60,* (22), 4417-4433. New York, New York: Pergamon Press. TIC: 231351.

Waddell, R.K.; Robison, J.H.; and Blankennagel, R.K. 1984. *Hydrology of Yucca Mountain and Vicinity, Nevada-California--Investigative Results Through Mid-1983.* Water-Resources Investigations Report 84-4267. Denver, Colorado: U.S. Geological Survey. ACC: NNA.19870406.0343.

Walker, G.E. and Eakin, T.E. 1963. *Geology and Ground Water of Amargosa Desert, Nevada-California.* Ground-Water Resources – Reconnaissance Series Report 14. Carson City, Nevada: State of Nevada, Department of Conservation and Natural Resources. TIC: 208665.

Whelan, J.F.; Vaniman, D.T.; Stuckless, J.S.; and Moscati, R.J. 1994. "Paleoclimatic and Paleohydrologic Records from Secondary Calcite: Yucca Mountain, Nevada." *High Level Radioactive Waste Management, Proceedings of the Fifth Annual International Conference, Las Vegas, Nevada, May 22-26, 1994. 4,* 2738-2745. La Grange Park, Illinois: American Nuclear Society. TIC: 210984.

White, A.F.; Claassen, H.C.; and Benson, L.V. 1980. *The Effect of Dissolution of Volcanic Glass on the Water Chemistry in a Tuffaceous Aquifer, Rainier Mesa, Nevada.* Geochemistry of Water. Geological Survey Water-Supply Paper 1535-Q, Washington, D.C.: U.S. Government Printing Office. TIC: 221391.

Whitfield, M.S.; Thordarson, W.; Hammermeister, D.P.; and Warner, J.B. 1990. *Drilling and Geohydrologic Data for Test Hole USW UZ-1, Yucca Mountain, Nye County, Nevada.* Open-File Report 90-354. Denver, Colorado: U.S. Geological Survey. ACC: NNA.19900622.0450.

Winchester, J.W. and Duce, R.A. 1967. "The Global Distribution of Iodine, Bromine, and Chlorine in Marine Aerosols." *Naturwissenschaften, [54],* ([5]), 110-113. [New York, New York: Springer-Verlag]. TIC: 226930.

Wolfsberg, A.V.; Fabryka-Martin, J.T.; Roemer, G.J.C.; and Robinson, B.A. 1998. "Modeling Flow and Transport Pathways to the Potential Repository Horizon at Yucca Mountain." *High-Level Radioactive Waste Management, Proceedings of the Eighth International Conference, Las Vegas, Nevada, May 11-14, 1998.* Pages 81-84. La Grange Park, Illinois: American Nuclear Society. TIC: 237082.

Yang, I.C. 1992. "Flow and Transport Through Unsaturated Rock – Data from Two Test Holes, Yucca Mountain, Nevada." *High Level Radioactive Waste Management, Proceedings of the Third International Conference, Las Vegas, Nevada, April 12-16, 1992. 1,* 732-737. La Grange Park, Illinois: American Nuclear Society. TIC: 204231.

Yang, I.C.; Davis, G.S.; and Sayre, T.M. 1990. "Comparison of Pore-Water Extraction by Triaxial Compression and High-Speed Centrifugation Methods." *Minimizing Risk to the Hydrologic Environment, Conference held in Las Vegas, Nevada, March 13-15, 1990.* Zaporozec, A., ed. Pages 250-259. Dubuque, Iowa: American Institute of Hydrology. TIC: 224435.

Yang, I.C.; Peters, C.A.; and Thorstenson, D.C. 1993. "Carbon Isotopic Data from Test Hole USW UZ-1 Yucca Mountain, Nevada." *High Level Radioactive Waste Management, Proceedings of the Fourth Annual International Conference, Las Vegas, Nevada, April 26-30, 1993. 1,* 401-406. La Grange Park, Illinois: American Nuclear Society. TIC: 208542.

Yang, I.C.; Rattray, G.W.; and Scofield, K.M. 1998. "Carbon and Hydrogen Isotopic Compositions for Pore Water Extracted from Cores at Yucca Mountain, Nevada." *High-Level Radioactive Waste Management, Proceedings of the Eighth International Conference, Las Vegas, Nevada, May 11-14, 1998.* Pages 27-32. La Grange Park, Illinois: American Nuclear Society. TIC: 237082.

Yang, I.C.; Rattray, G.W.; and Yu, P. 1996. *Interpretation of Chemical and Isotopic Data from Boreholes in the Unsaturated Zone at Yucca Mountain, Nevada.* Water-Resources Investigations Report 96-4058. Denver, Colorado: U.S. Geological Survey. ACC: MOL.19980528.0216.

Yang, I.C.; Turner, A.K.; Sayre, T.M.; and Montazer, P. 1988. *Triaxial-Compression Extraction of Pore Water from Unsaturated Tuff, Yucca Mountain, Nevada.* Water-Resources Investigations Report 88-4189. Denver, Colorado: U.S. Geological Survey. ACC: NNA.19890309.0161.

Yang, I.C.; Yu, P.; Rattray, G.W.; Ferarese, J.S.; and Ryan, J.N. 1998. *Hydrochemical Investigations in Characterizing the Unsaturated Zone at Yucca Mountain, Nevada.* Water-Resources Investigations Report 98-4132. Denver, Colorado: U.S. Geological Survey. ACC: MOL.19981012.0790.

Zielinski, R.A. 1983. *Evaluation of Ash-Flow Tuffs as Hosts for Radioactive Waste: Criteria Based on Selective Leaching of Manganese Oxides.* Open-File Report 83-480. Denver, Colorado: U.S. Geological Survey. ACC: HQS.19880517.1582.

Zielinski, R.A.; Bush, C.A.; Spengler, R.W.; and Szabo, B.J. 1986. "Rock-Water Interaction in Ash-Flow Tuffs (Yucca Mountain, Nevada, U.S.A.) – The Record from Uranium Studies." *Uranium, 2,* 361-386. Amsterdam, The Netherlands: Elsevier Science Publishers B.V. TIC: 222472.

5.5.2   Codes, Standards, Regulations, and Procedures

64 FR 8640. Disposal of High-Level Radioactive Wastes in a Proposed Geologic Repository at Yucca Mountain, Nevada. Proposed rule 10 CFR 63.   Readily available.

5.5.3 Source Data, Listed by Data Tracking Number

LA0002JF831222.001. Apparent Infiltration Rates in Alluvium from USW UZ-N37, USW UZ-N54, USW UZ-14 and UE-25 UZ#16, Calculated by Chloride Mass Balance Method. Submittal date: 02/25/2000.

LA0002JF831222.002. Apparent Infiltration Rates in PTN Units from USW UZ-7A, USW UZ-N55, USW UZ-14, UE-25 UZ#16, USW NRG-6, USW NRG-7A, and USW SD-6, SD-7, SD-9 and SD-12 Calculated by the Chloride Mass Balance Method. Submittal date: 02/25/2000.

$$SiO_2 = -2.25(Al_2O_3)+105.03$$

Calico Hills Formation
Paintbrush Group
Older Tuff A
Crater Flat Group
Pah Canyon Tuff
Lithic Ridge Tuff
high silica
rhyolites
low silica
quartz latites

Legend:
- ○ Rainier Mesa
- ● Tiva Canyon
- □ Yucca Mtn.
- ■ Pah Canyon
- △ Topopah Spg.
- ▲ Calico Hills
- ◇ Prow Pass
- ◆ Bullfrog
- ▽ Tram
- ▼ Lithic Ridge
- × Older Tuffs

weight % SiO₂ (y-axis)
weight % Al₂O₃ (x-axis)

52-01.CDR.SITEDESC-R01
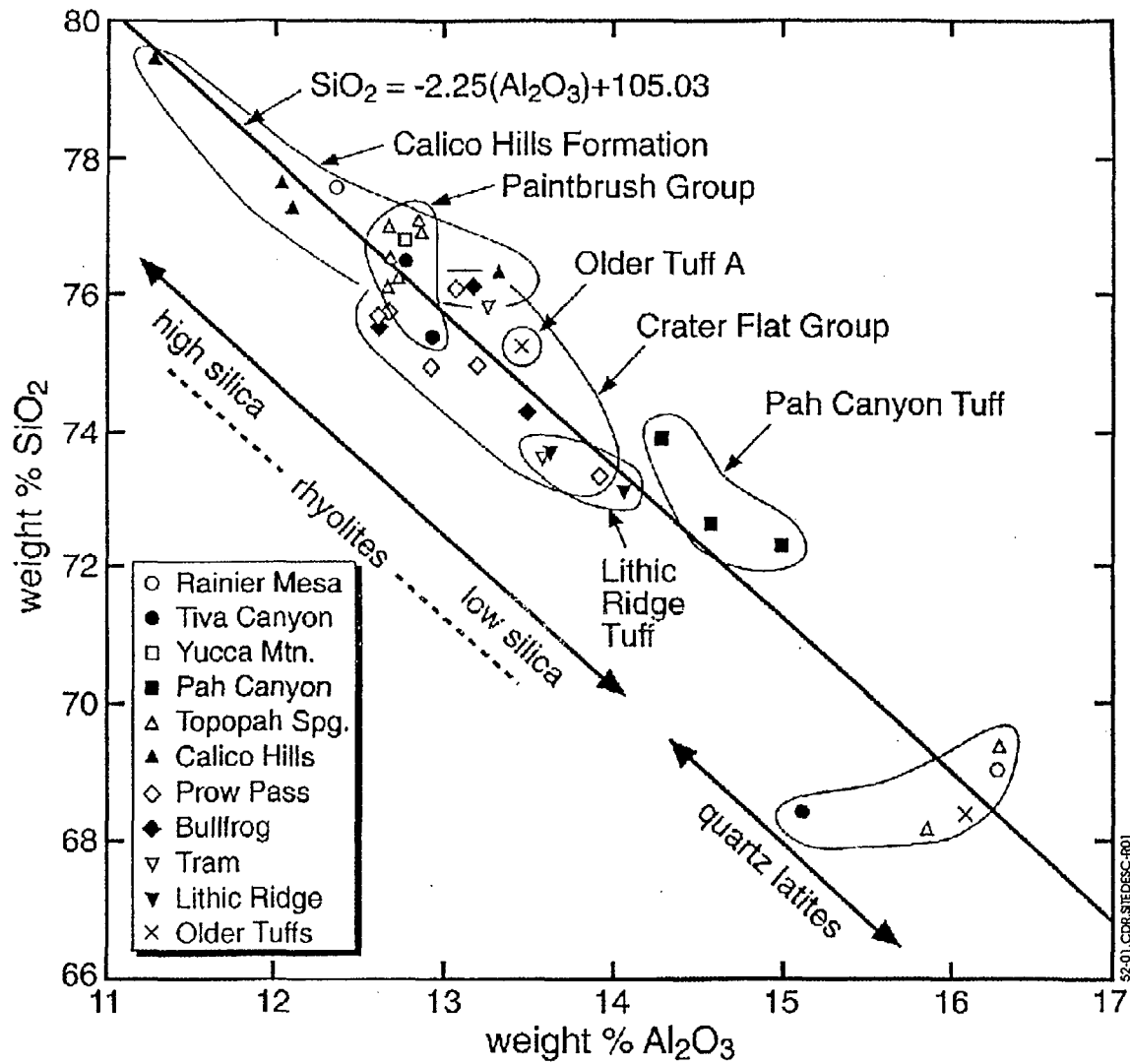
Source: Vaniman et al. (1996, Figure 1.3)

Figure 5.2-1. Geochemical Variation in Pyroclastic Units at Yucca Mountain, Based on Alumina and Silica Content Adjusted to Water-Free Compositions
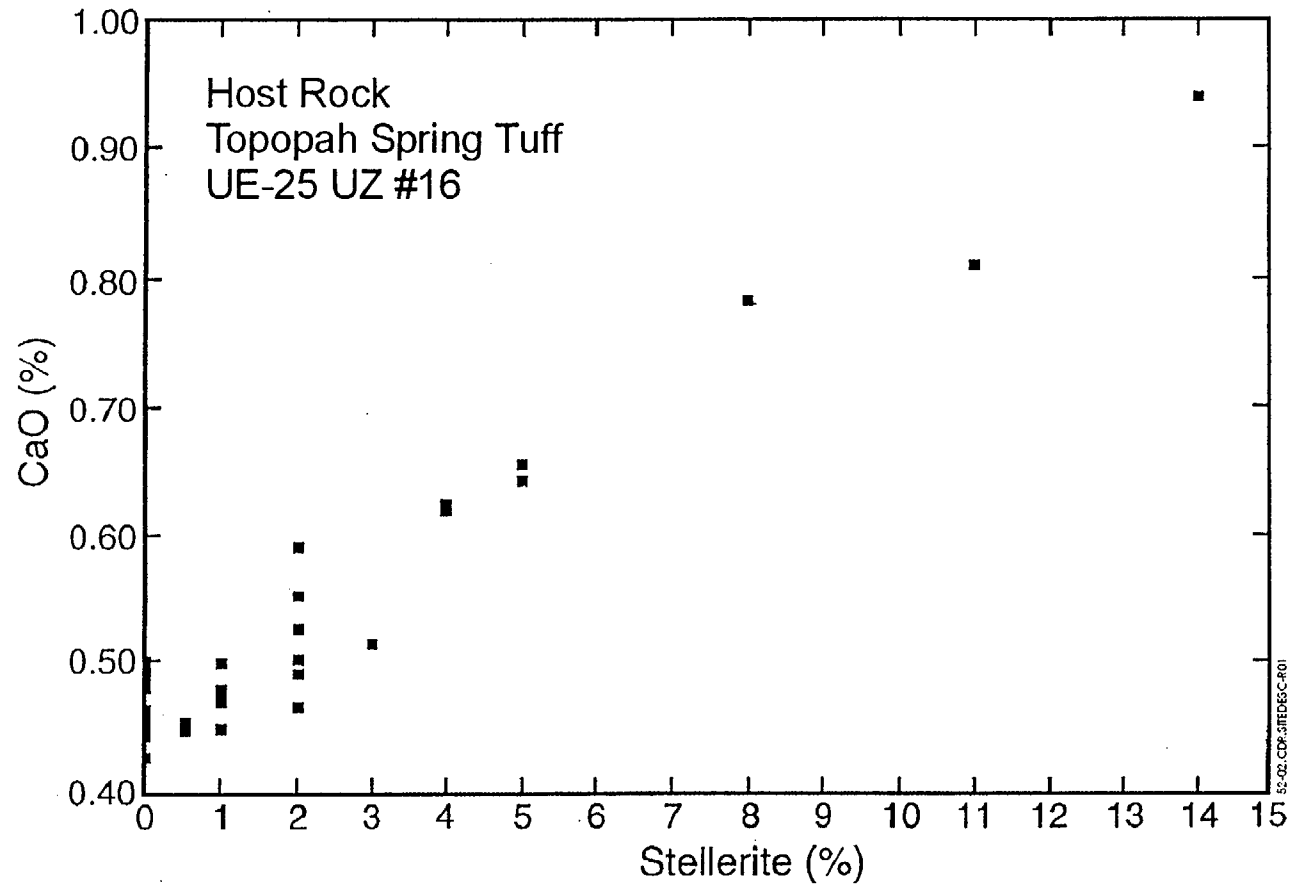
Source: Vaniman et al. (1996, Figure 3.14)

Figure 5.2-2. Plot of Weight Percent Stellerite versus Weight Percent CaO in the Devitrified Rhyolitic Topopah Spring Tuff, Drill Core UE-25 UZ#16

Source: Carlos et al. (1995)

Figure 5.2-3a. Distribution of Fracture-Lining Minerals in Drill Cores UE-25 a#1 and UE-25 b#1

Figure 5.2-3b. Distribution of Fracture-Lining Minerals in Drill Core USW G-1

Smectite
Mordenite
Clinoptilolite
Stellerite
Tridymite
Cristobalite
Opal-CT
Calcite
Mn-Oxides
Hematite
Fluorite
Other Minerals
Sample Locations

Depth (m)

0

(No Drill Core)

100

200

Topopah Spring Tuff

300

400

Calico Hills Formation

500

(Few Coated Fractures)

SWL

600

Prow Pass Tuff

700

Bullfrog Tuff

800

900

Tram Tuff

(No Coated Fractures)

1000

52-03b.TIF.SITEDESC-R01

Source: Carlos et al. (1995)

Figure 5.2-3b. Distribution of Fracture-Lining Minerals in Drill Core USW G-1

Source: Carlos et al. (1995)

Figure 5.2-3c. Distribution of Fracture-Lining Minerals in Drill Core USW G-2
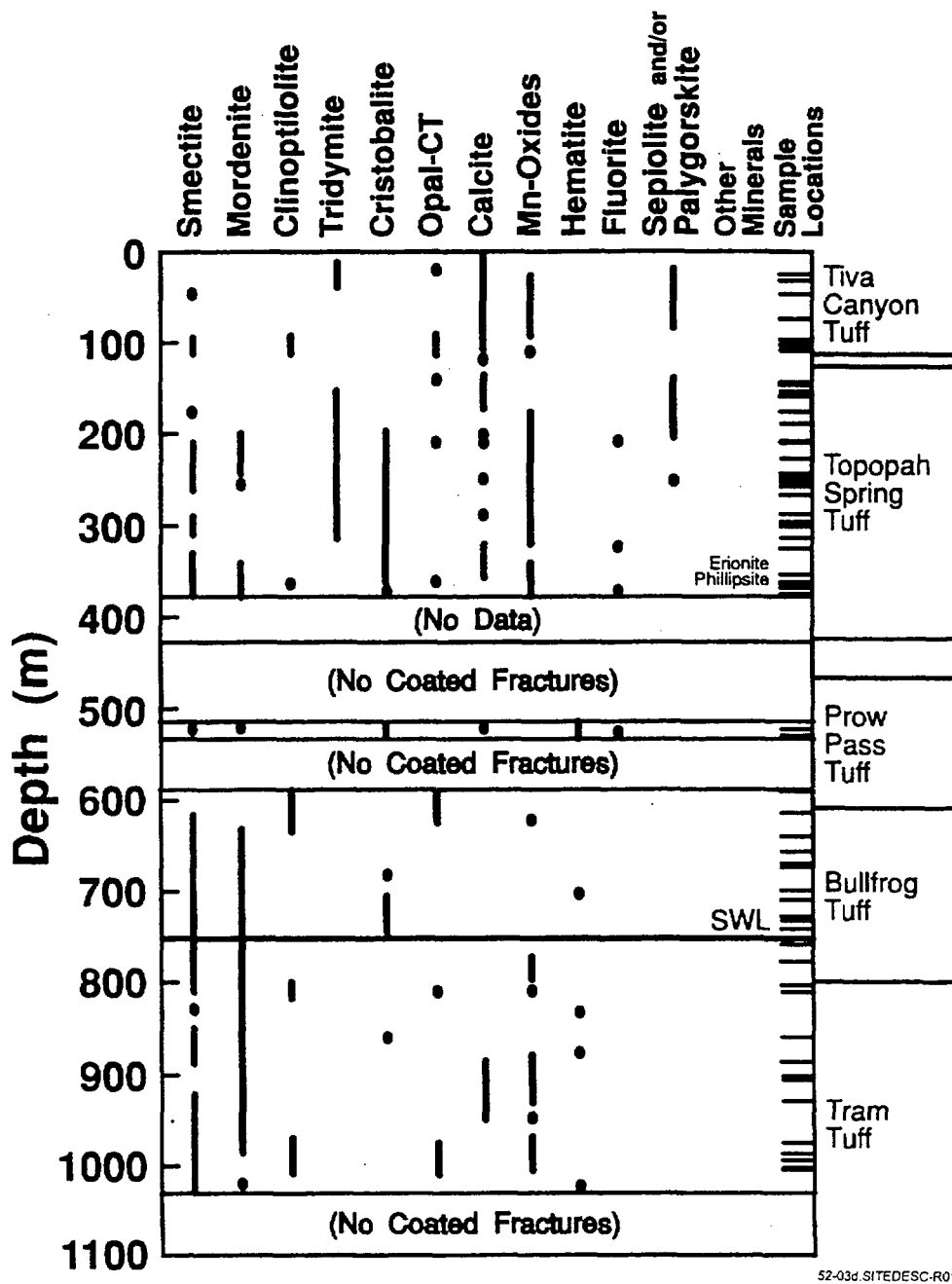
Source: Carlos et al. (1995)

Figure 5.2-3d. Distribution of Fracture-Lining Minerals in Drill Cores USW GU-3 and USW G-3
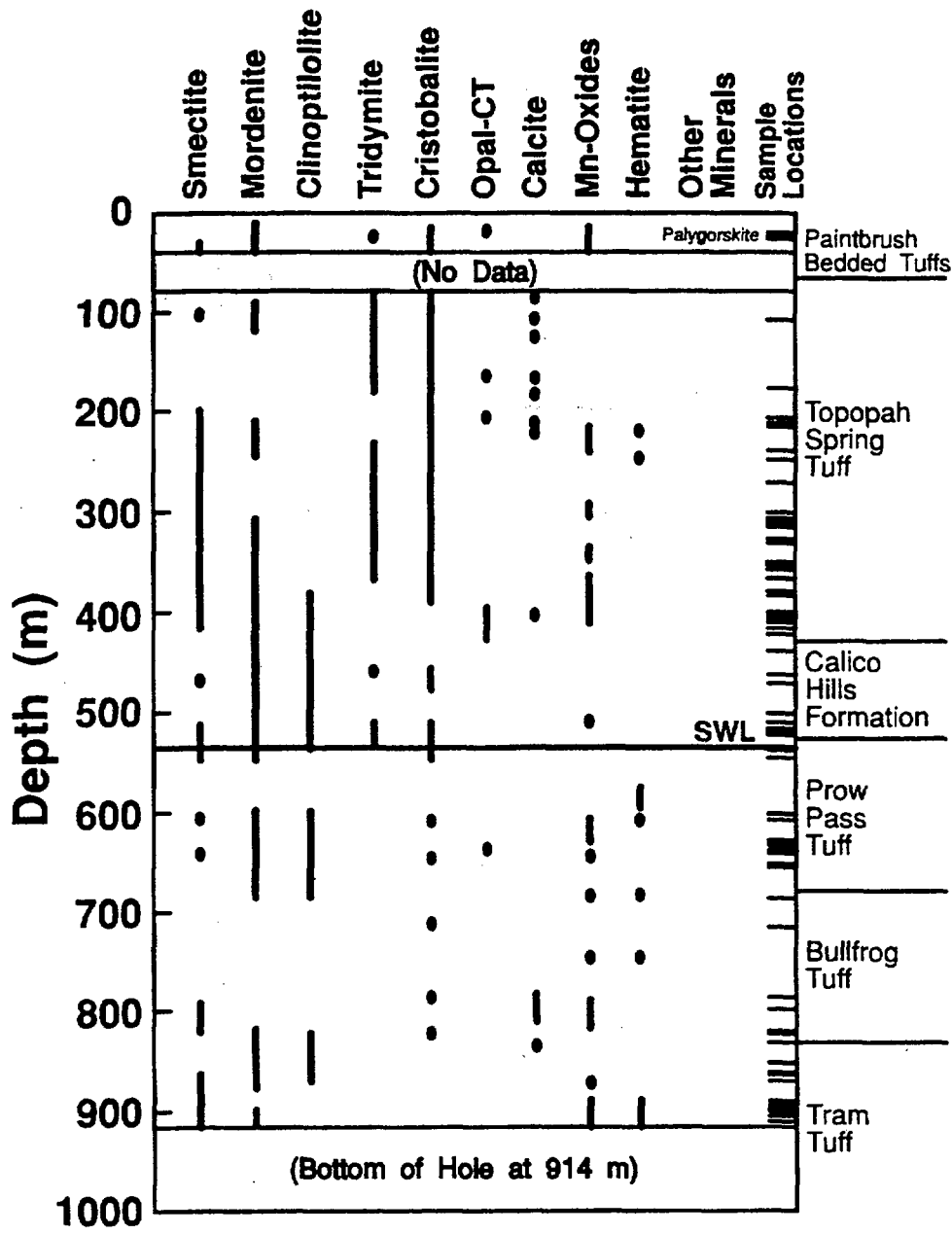
Source: Carlos et al. (1995)

Figure 5.2-3e. Distribution of Fracture-Lining Minerals in Drill Core USW G-4
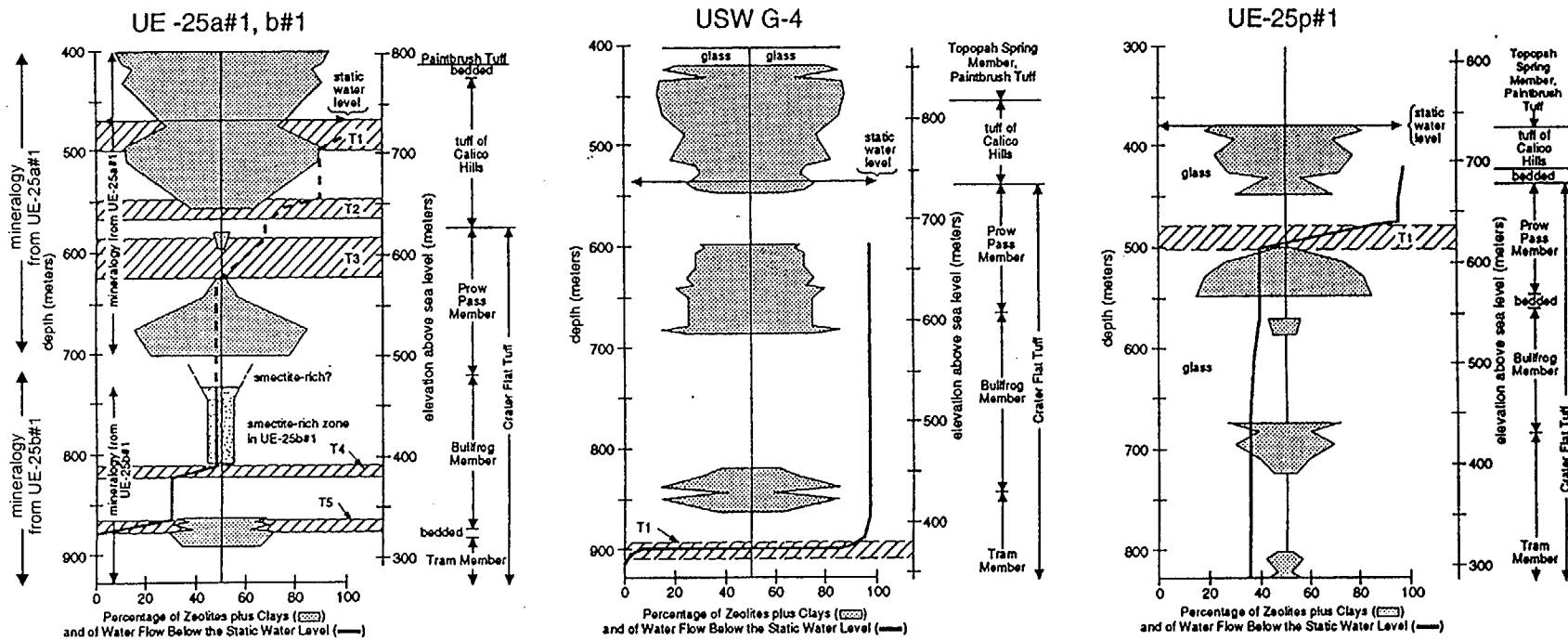
52-04.CDR.SITEDESC-R01

Sources: Bish and Chipera (1989); Craig and Johnson (1984); Craig and Robison (1984); Lobmeyer (1986); Lobmeyer et al. (1983, Figure 8, p. 25)

NOTE: Intervals of abundant shear fractures are shown by fractured pattern. Stippled patterns show zones with abundant zeolite (close stipples in all three plots) or abundant smectite (widely-spaced stipples in UE-25 b#1). Solid lines show percent of total flow in numbered transmissive zones (e.g., T1, T2). Horizontal scale applies to both mineral abundances (measured across the width of the stippled patterns) and cumulative percentage of total flow.

Figure 5.2-4. Transmissive Zones below the Water Table in Three Drill Holes at Yucca Mountain

52-05.CDRSITEDESC-R01

Source: Vaniman et al. (1996, Figure 3.36)

NOTE: Sample is from transmissive zone T3 shown for UE-25 a#1, b#1 in Figure 5.2-4.

Figure 5.2-5. Fracture with Liesegang Banding from UE-25 b#1h at 2025.2 to 2026.2 Feet Depth
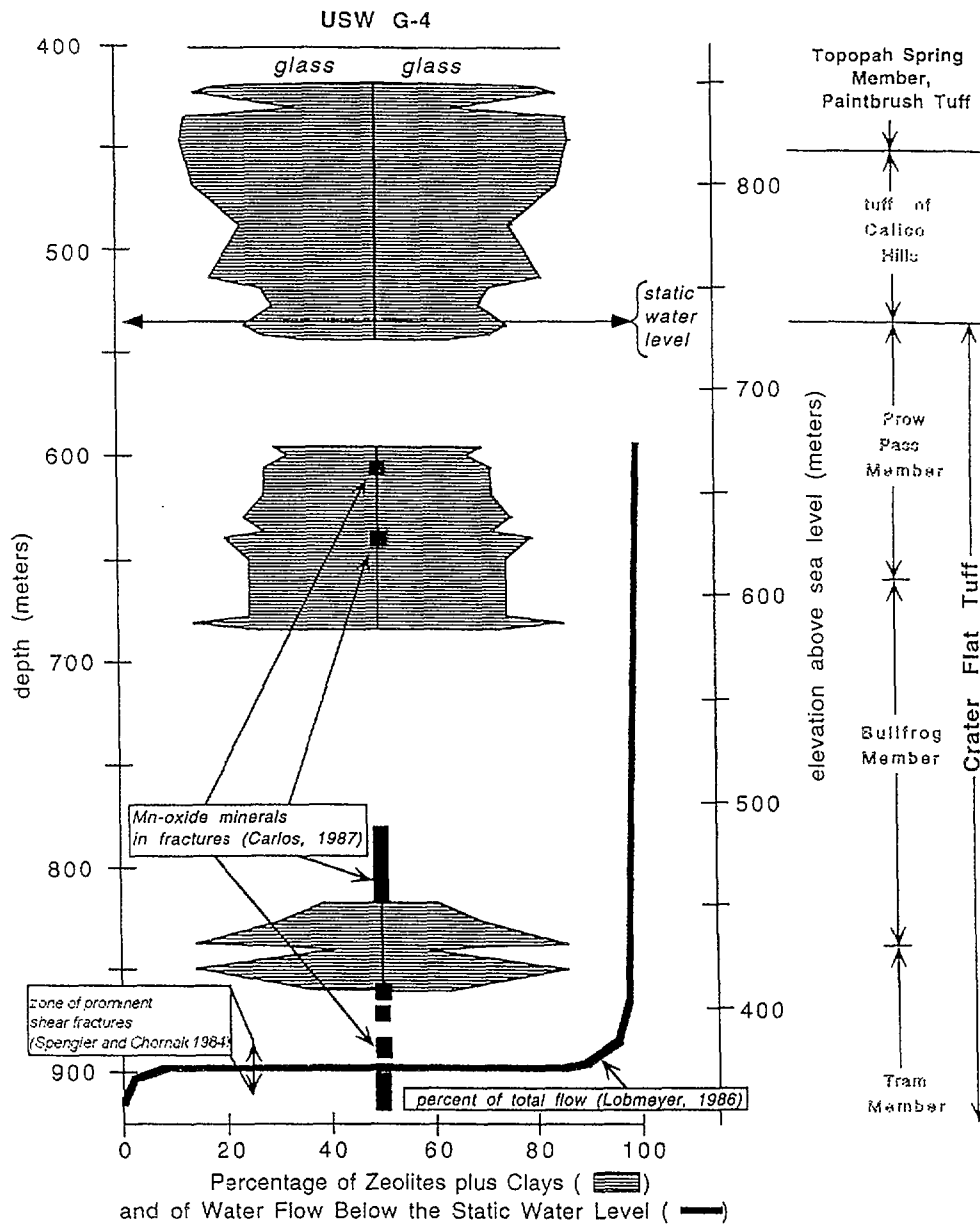
C 01

Sources: Bish and Chipera (1989); Craig and Johnson (1984); Craig and Robison (1984); Lobmeyer (1986);
Lobmeyer et al. (1983, Figure 8, p. 25)

NOTE: This figure is based on Figure 5.2-4.

Figure 5.2-6.   Detailed Representation of the Dominant Transmissive Zone at 900-Meter Depth in
USW G-4

Elevation Relative to Sea Level (m)

1600

1400

1200

1000

800

600

400

200

0

-200

-400

-600

G-2

G-1

G-3

NRG-6

A-7

G-4

UZ-16

Tiva Canyon Tuff

nonwelded Paintbrush tuffs

Topopah Spring Tuff

older tuffs

water table

barren zone

carbonate-altered zone

calcite + analcime

calcite + albite (fossil hydrothermal system)

473
476
477
314
131
204 v1
1179
1640
1756
1655

142
156
193
203
325

141
186
230
259

107
115
180
265
401
361

137
150
353
810

14
46
73
12 97
17
30 34
32
169 358
195
289
301
500

295
313

898
917

1464

v2

52-07.CDRSITEDESC-R01

Source: Vaniman and Chipera (1996)

NOTE: The two vitrophyres of the Topopah Spring Tuff are shown, the upper quartz-latite vitrophyre (v1) and the lower rhyolitic vitrophyre (v2). The nonwelded Paintbrush tuffs above v1 include the upper Yucca Mountain Tuff (vertical-line pattern) and the lower Pah Canyon Tuff (no pattern); the Pah Canyon is a low-silica rhyolite with lanthanide composition more similar to the quartz latites than to the high-silica rhyolites (see Figure 5.2-9a). The "barren zone" extending from v2 to the carbonate-altered zone is exceptionally calcite-poor. Numbers along drill holes indicate depth in drill hole.

Figure 5.2-7. Cross Section Showing Depths of Calcite Samples Analyzed from Seven Drill Holes (Variable Horizontal Scale)
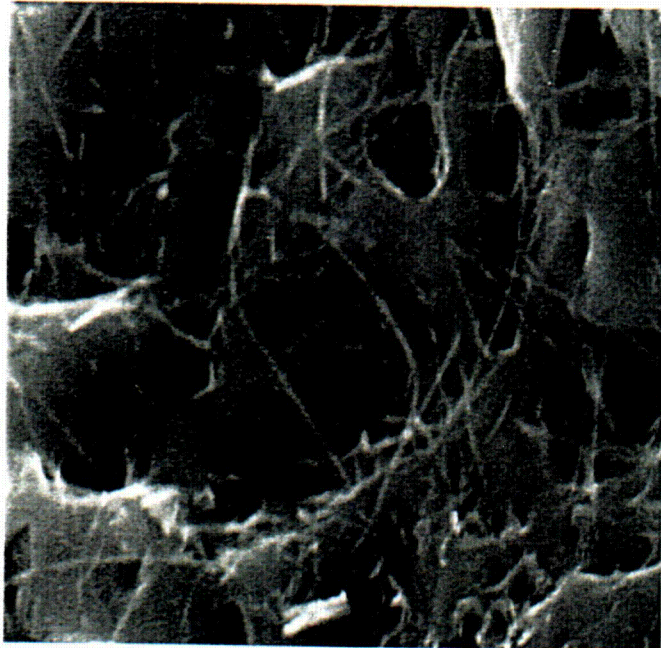
52-08.CDR.SITEDESC-R01

Source: Vaniman and Chipera (1996)

Figure 5.2-8. Scanning Electron Microscope Micrograph of Mordenite Fibers on the Etched Surface of a
Calcite Sample from 500 Meter Depth in UE-25 UZ#16 (Just below the Water Table)

(a)

(b)
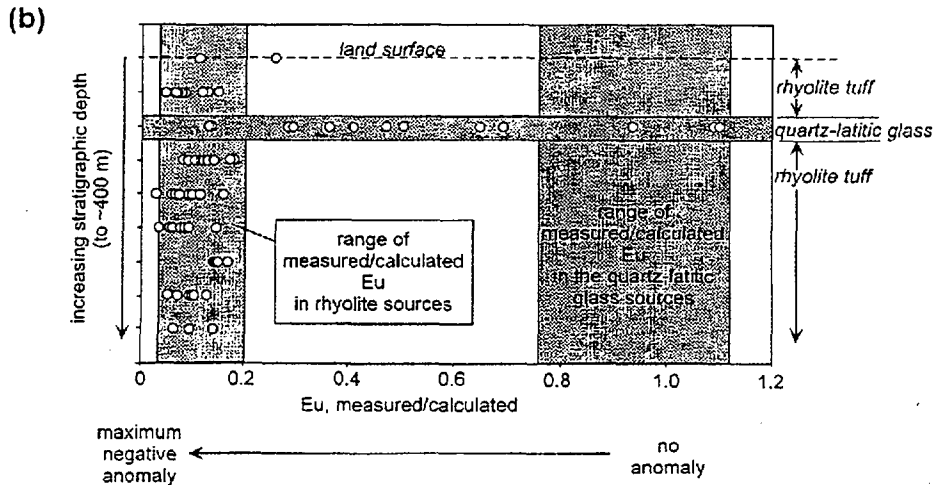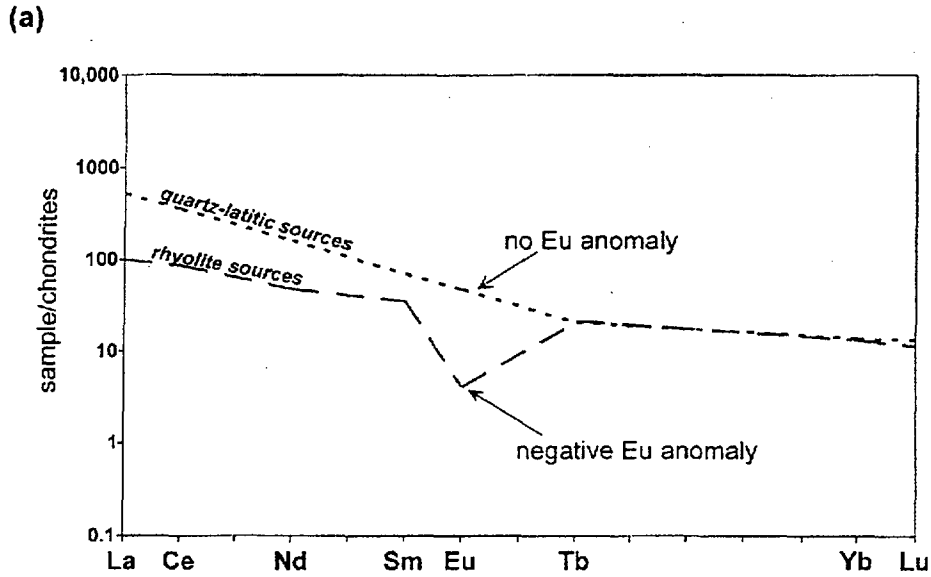
Source: Eckhardt (2000)

NOTE: Part (a) shows the notable presence of a negative europium anomaly in rhyolite sources and an absence of such an anomaly in quartz-latitic sources. Part (b) shows the corresponding record of europium anomalies in calcites from the land surface (calcretes) and deposited at eight stratigraphic horizons of the unsaturated zone, with acquisition of a diminished europium anomaly only where glassy quartz-latitic rocks with similar lanthanum character occur (a dissolution-driven process).

Figure 5.2-9. Primary Differences in Chondrite-Normalized Lanthanide-Element Patterns for Rhyolite and Quartz-Latitic Source Rocks

(a)

Ce enrichment in sorptive fracture-lining minerals

rancieite

glass sources

calcites

Ce depletion in passive fracture-lining minerals

sample/chondrites

10,000
1000
100
10
1
0.1

La Ce   Nd   Sm Eu   Tb   Yb Lu

(b)

Increasing stratigraphic depth (to ~400 m)

land surface

crystalline tuff

fresh glass

crystalline tuff

range of measured/calculated Ce in source soils and rocks

52-10.CDR.SITE DESC-R01

0   0.2   0.4   0.6   0.8   1.0   1.2

Ce, measured/calculated

maximum negative anomaly ← ———————————— no anomaly

Source: Eckhardt (2000)

NOTE: Part (a): With only very rare exceptions at the north end of Yucca Mountain (Figure 5.2-11), glass sources lack any cerium anomaly, but such anomalies are generated through fracture transport and accumulation of cerium in manganese oxides (example rancieite), leaving calcite-depositing solutions cerium-depleted. Part (b) illustrates the loss of cerium and development of negative cerium anomalies in fracture calcites of stratigraphic horizons immediately below the glassy layer where dissolution and fresh input of lanthanide elements without cerium anomaly occurs (a process driven by interaction with fracture minerals).

Figure 5.2-10. Development of Cerium Anomalies in Fracture-Lining Manganese Oxides and Calcites

(a)

Basal Topopah Spring Tuff
Busted Butte

sample 206
95% glass, no clay or zeolite

sample 432
no glass, 98% clinoptilolite

samples/chondrites

La Ce   Nd   Sm Eu   Tb Dy   Yb Lu

(b)

Basal Topopah Spring Tuff
NW Yucca Mtn.

sample 189
no glass,
71% clinoptilolite

sample 191
89% glass,
no clinoptilolite

sample 190
54% glass,
17% clinoptilolite

samples/chondrites

La Ce   Nd   Sm Eu   Tb Dy   Yb Lu
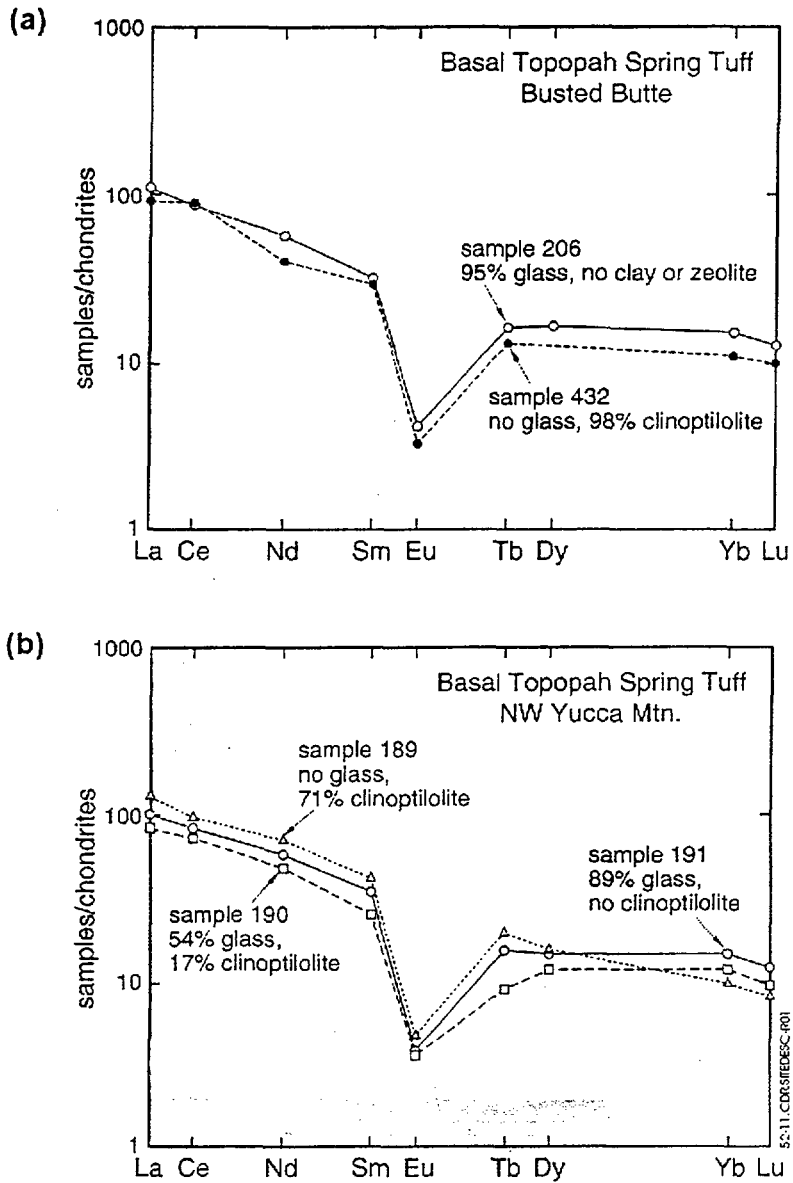
Source: Broxton et al. (1993)

NOTE: (a) The sample in this panel is from the basal Topopah Spring Tuff at Busted Butte, south of the potential repository site. (b) The sample in this panel is from the north end of Yucca Mountain, north of the potential repository site. Differences in chondrite-normalized lanthanide patterns for vitric and zeolitic representatives at both sites are negligible.

Figure 5.2-11.   Two Examples of Zeolitized and Adjacent Vitric Samples from within the Same Geochemical Unit
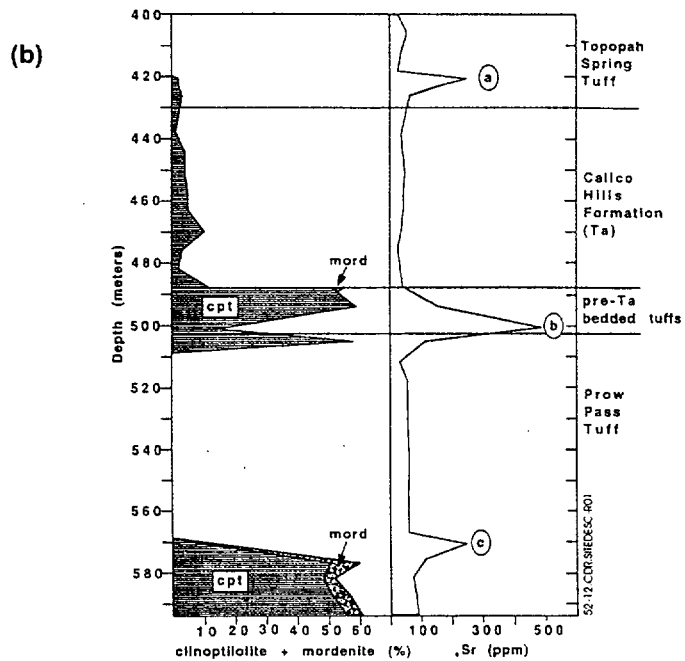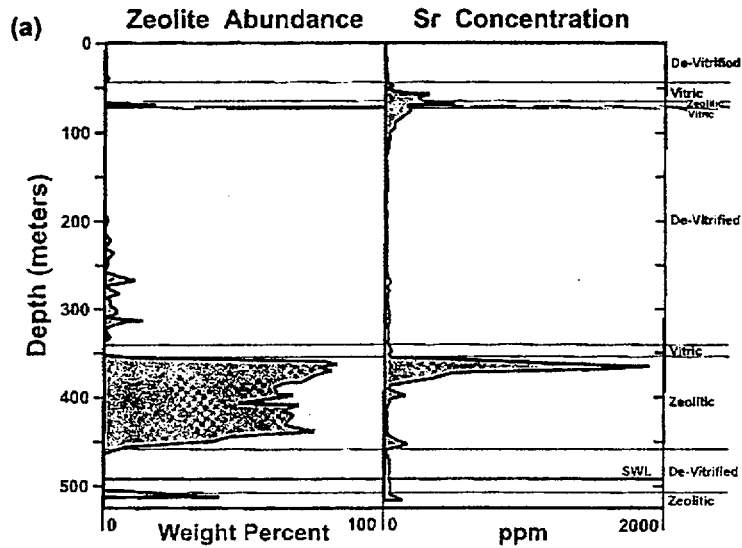
Source: Eckhardt (2000)

NOTE: Part (a) shows abundances in UE-25 UZ#16. Part (b) shows abundances in USW SD-12. Strontium concentrations are particularly high at the top of the major zeolitized horizon in UZ#16. Lesser strontium accumulations are evident at positions (a) and (c) in SD-12, at the tops of the two zeolitized horizons that occur above the water table. Note that the strontium spike at position (b) in the lower panel reflects a depositional accumulation of strontium-rich feldspar, rather than later accumulation of strontium in zeolites by cation exchange.

Figure 5.2-12. Profiles of Zeolite and Strontium Abundance
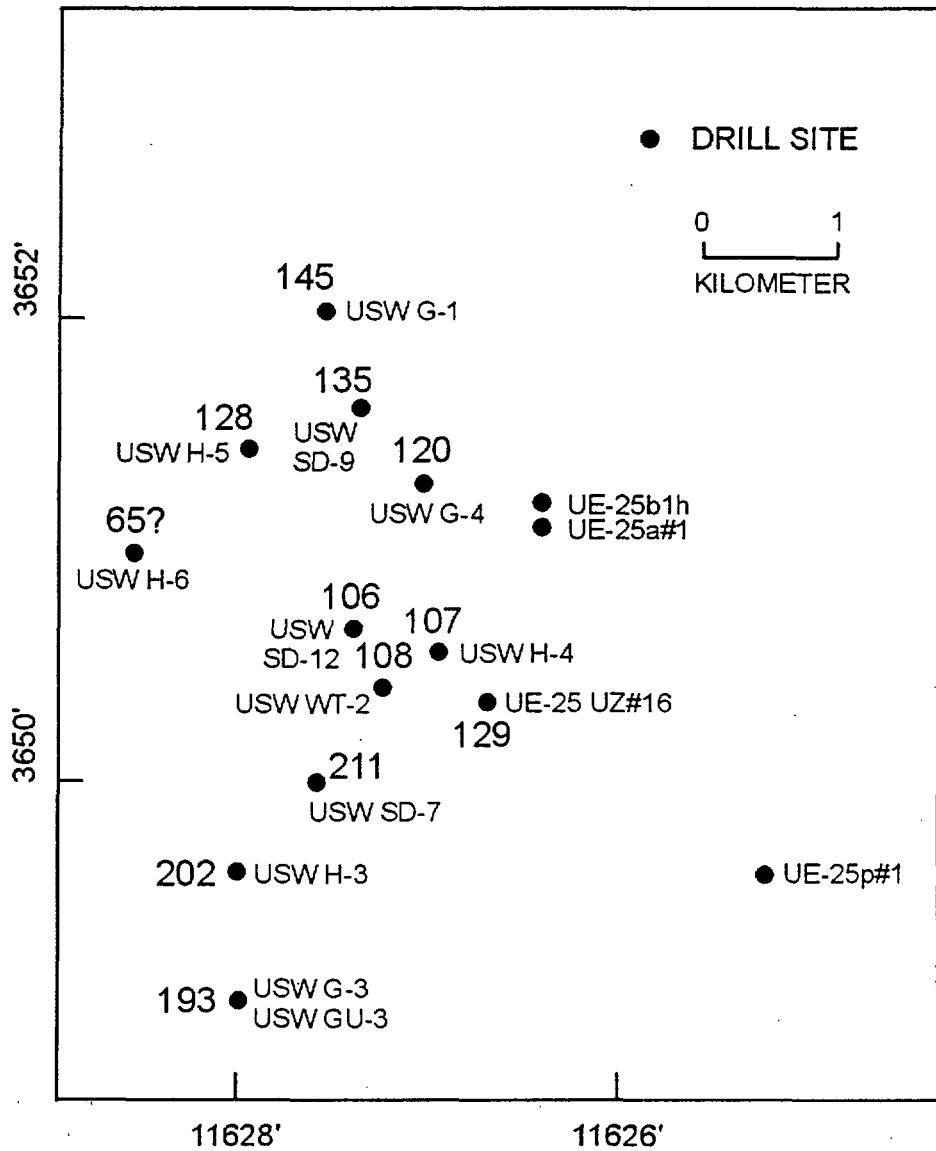
Source: Chipera et al. (1995, Figure 6)

NOTE: Bold numbers denote elevation in meters. See Figure 1.3-1 for perimeter of preclosure controlled area.

Figure 5.2-13. Elevations (Meters) above Present Water Table of the Top of the Most Abundantly Zeolitized Horizon in Drill Holes at Yucca Mountain
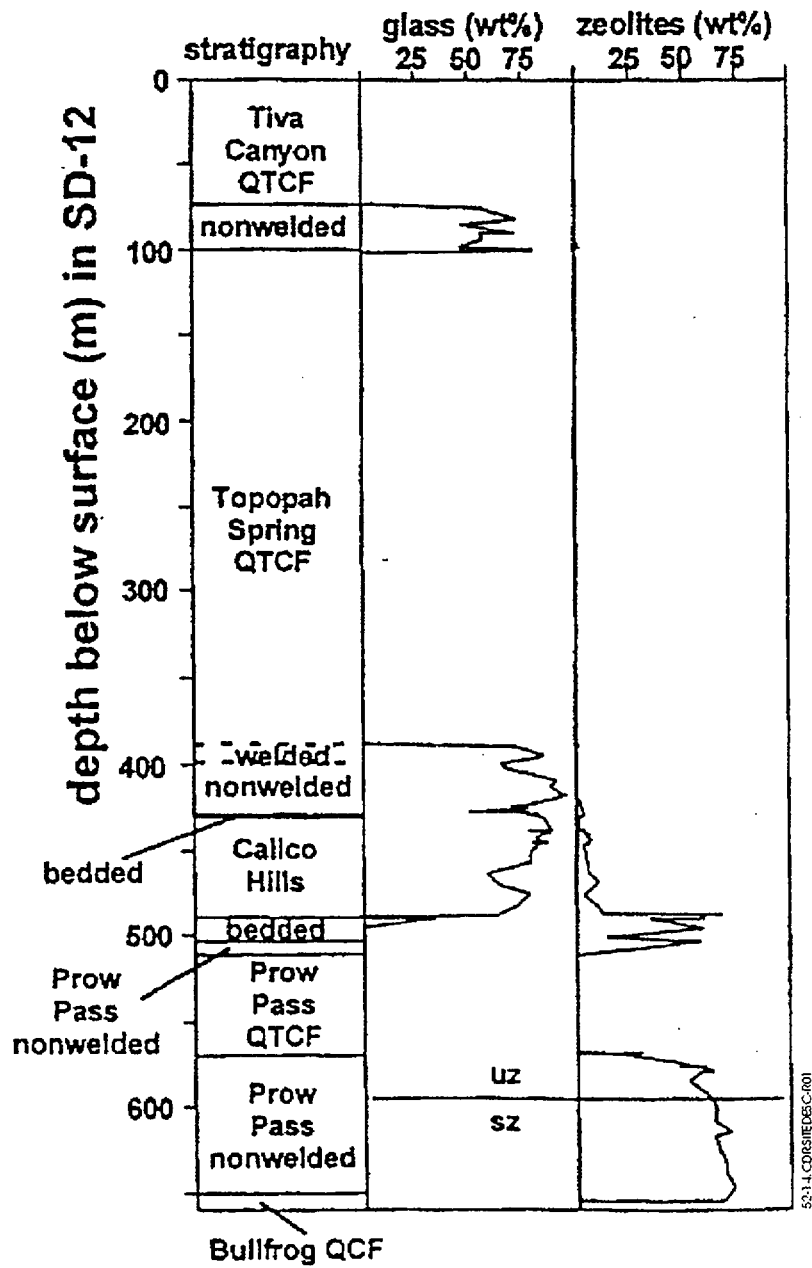
Source: Eckhardt (2000)

Figure 5.2-14. Zeolite Abundance as a Function of Depth and Stratigraphy for Borehole USW SD-12
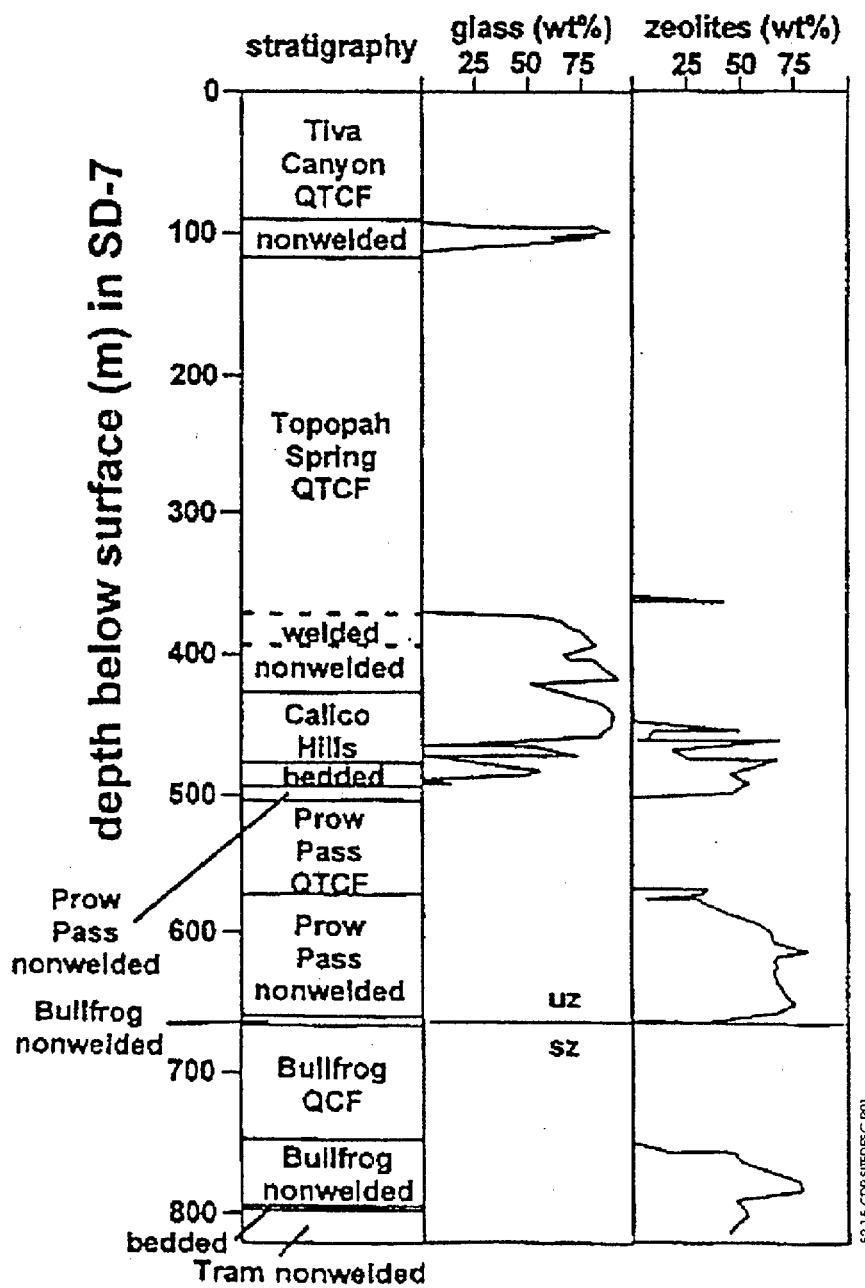
Source: Eckhardt (2000)

Figure 5.2-15. Zeolite Abundance as a Function of Depth and Stratigraphy for Borehole USW SD-7
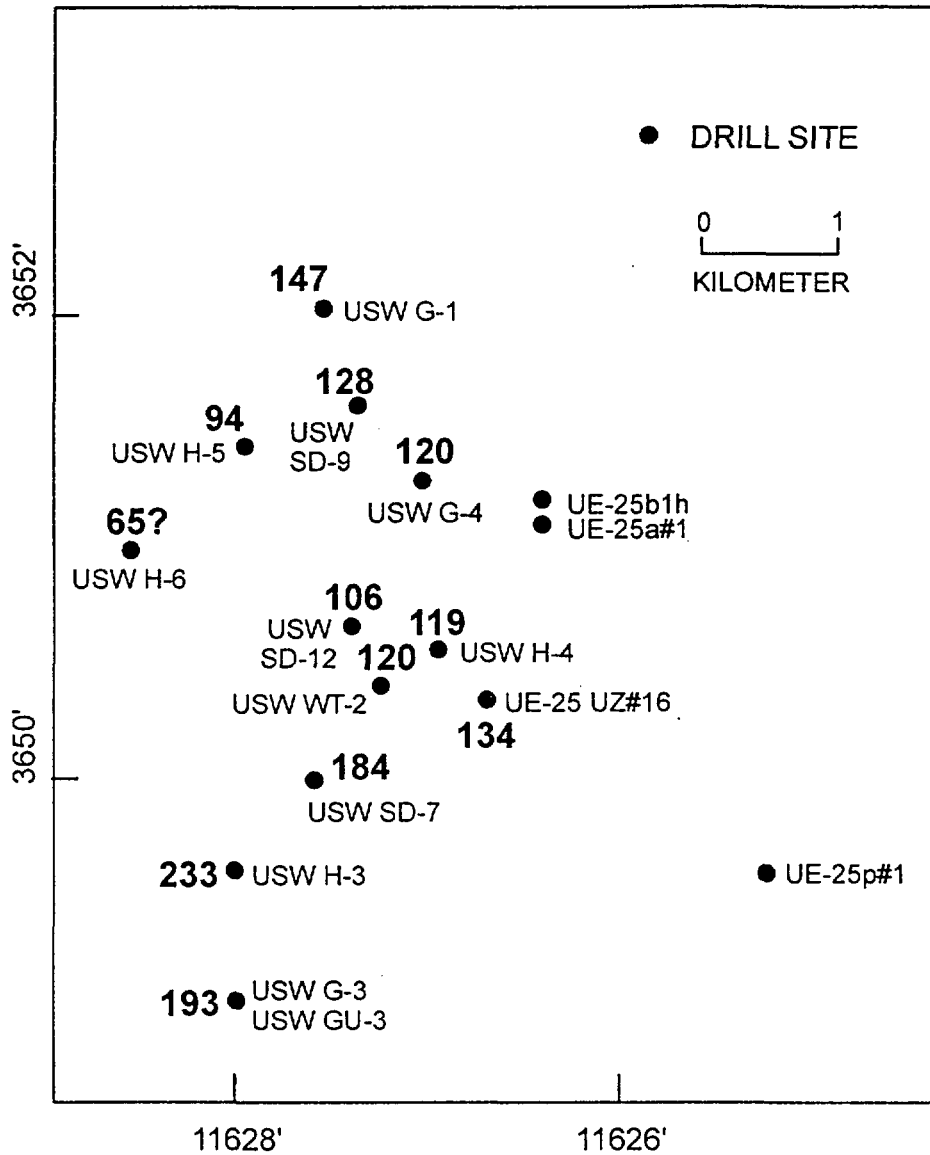
Source: Chipera et al. (1995)

NOTE: Bold numbers denote elevation in meters. See Figure 1.3-1 for perimeter of preclosure controlled area.

Figure 5.2-16. Elevations (Meters) above Present Water Table of the Bottom of the Deepest Abundant Nonwelded Glass in the Unsaturated Zone for Drill Holes at Yucca Mountain

YUCCA MOUNTAIN
SITE LOCATION

NEVADA

	Trace of Exploratory Studies Facility (ESF), and ESF station number	o	Borehole location and name
20+00			Quaternary deposits
			Tertiary volcanic rocks
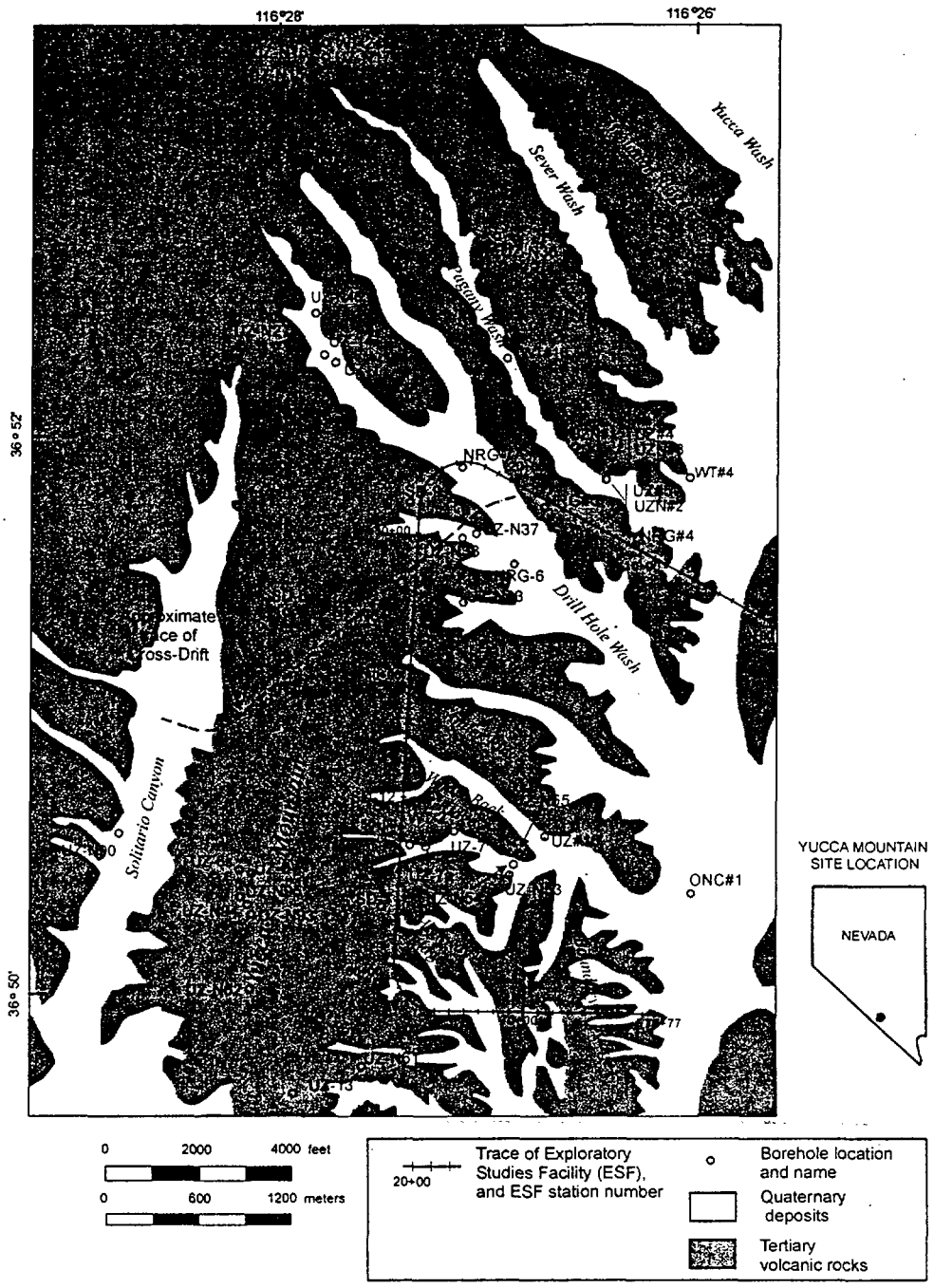
53-01.DOC.SITEDESC-R01

Source: CRWMS M&O (2000, Figure 3)

NOTE: This map shows the locations of surface-based boreholes for which isotopic and geochemical data are available for water and gas samples (Table 5.3-1). Boreholes that are not shown because they are outside the map area are UZ-N11, UZN#39, and UZN#91.

Figure 5.3-1. Yucca Mountain Site Characterization Project Boreholes

116°28'   116°26'

36°52'

20+00

Alcove #5
TTF

30+00

Alcove #4
LPCA

Alcove #3
UPCA

Approximate
trace of
Cross-Drift

10+00

Alcove #2
BRFA   Alcove #1
UTCA

Ghost Dance
Fault

Alcove #6
NGDFA

0+00

Solitario Canyon Fault

40+00

Ghost Dance
Fault

50+00

Bow Ridge Fault

YUCCA MOUNTAIN
SITE LOCATION

Alcove #7
SGDFA

NEVADA

36°50'

60+00

70+00   78+77

0   2000   4000 feet

0   600   1200 meters

20+00 Trace of Exploratory
Studies Facility (ESF),
and ESF station number

UTCA   Upper Tiva Canyon (0+70)
BRFA   Bow Ridge Fault (1+68)
UPCA   Upper Paintbrush (nonwelded) Contact (7+54)
LPCA   Lower Paintbrush (nonwelded) Contact (10+28)
TTF   Thermal Test Facility (28+30)
NGDFA   Northern Ghost Dance Fault (37+37)
SGDFA   Southern Ghost Dance Fault (50+64)

53-02.DOC.SITEDESC-R01

Source: CRWMS M&O (2000, Figure 4)

NOTE: Alcove locations are shown relative to faults mapped at the surface by Day et al. (1998, Plate 1). Not all faults
on that map are shown here.

Figure 5.3-2. Locations of Exploratory Studies Facility Test Alcoves

CATIONS   % OF TOTAL MEQ/L   ANIONS
19 SAMPLES
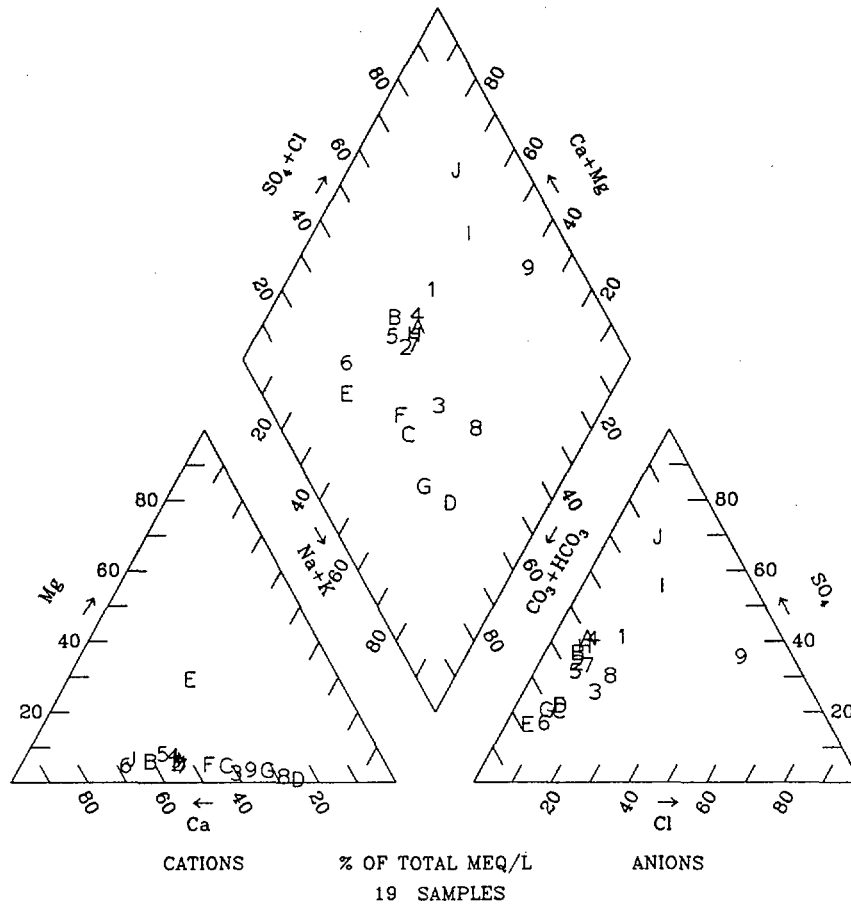
Legend	
Points	**Sample Location**
1-9, A-B	3 Springs Creek
C-J	Kawich Peak

53-03.DOC.SITEDESC-R01

Source: CRWMS M&O (2000, Figure 5)

NOTE: The intent of this plot is to show the extent to which different water samples are similar or dissimilar in composition. For those waters that are very similar (i.e., data symbols plot over each other), it is not important to be able to discern individual points.

Figure 5.3-3. Trilinear Diagram for Precipitation from the Kawich Range, Nevada

3 Springs Basin
☐ Individual samples
■ Annual weighted average
─── Regression line

Red Rock Canyon
○ Quarterly weighted average
✕ Annual weighted average
─ ─ Halite line

53-04a.AI.SITEDESC-R01
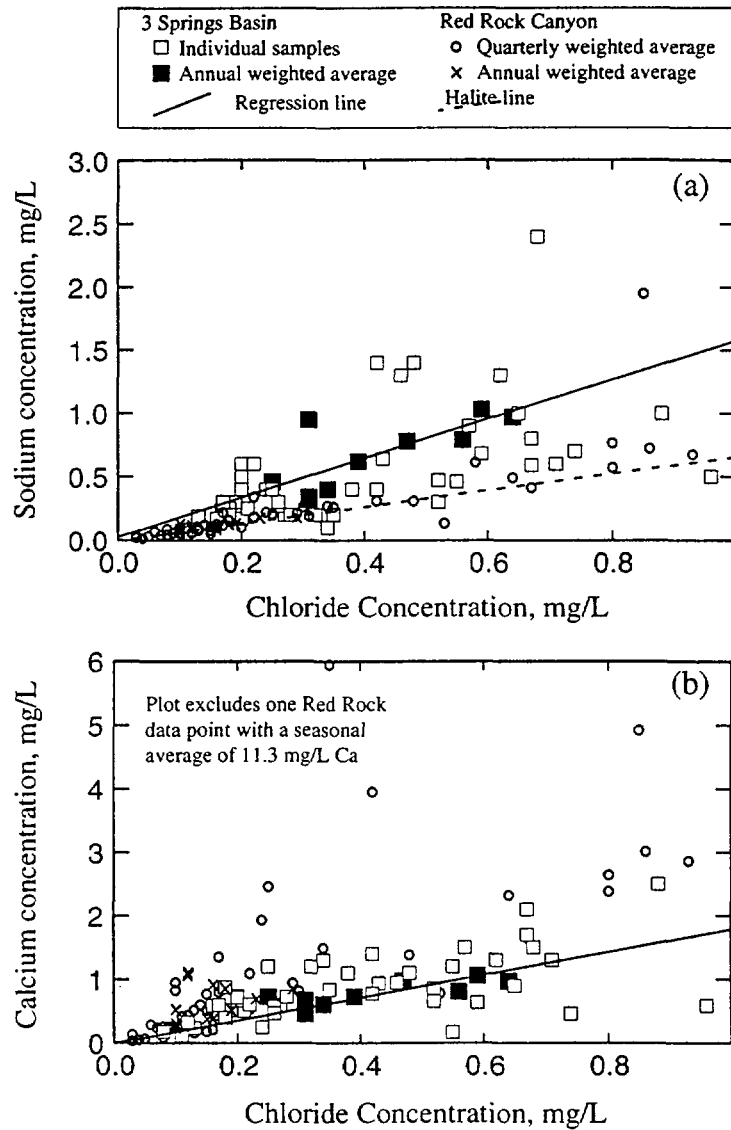
Source: CRWMS M&O (2000, Figure 6)

NOTE: Samples are from 3 Springs Basin and Red Rock Canyon, Nevada. Plots show chloride versus: (a) sodium, (b) calcium, (c) sulfate, (d) bicarbonate, and (e) silica. Only data with chlorine concentrations less than 1 mg/L have been included in this figure. Regression lines for 3 Springs Basin data are from Table 5.3-2. The halite line on plot (a) is based on a 1:1 molar ratio of sodium to chloride in order to show the trend for halite dissolution.

Figure 5.3-4. Constituents Plotted versus Chloride for Precipitation Samples

Plot excludes one data point with a seasonal average of 1.5 mg/L SiO2
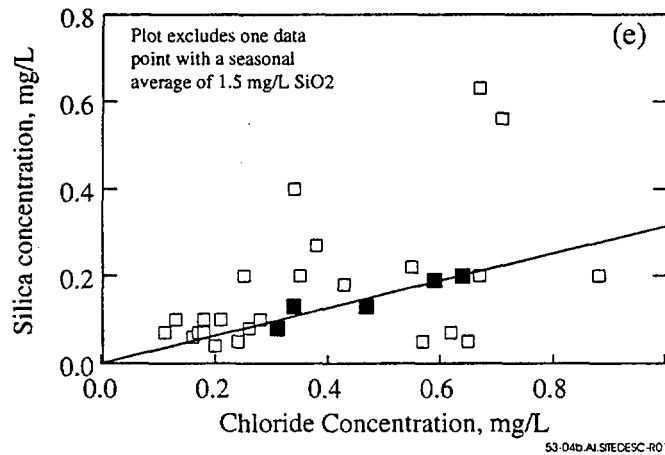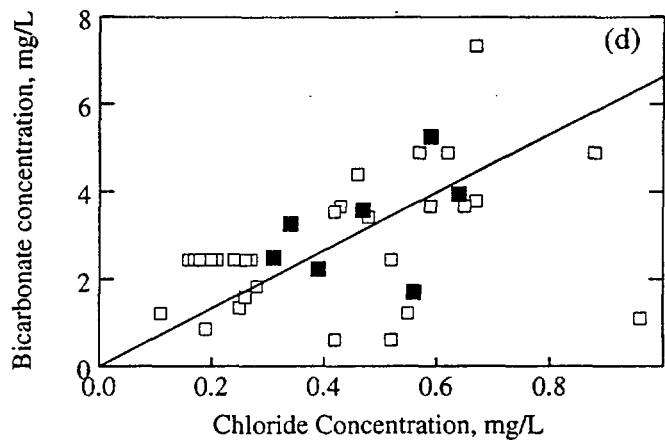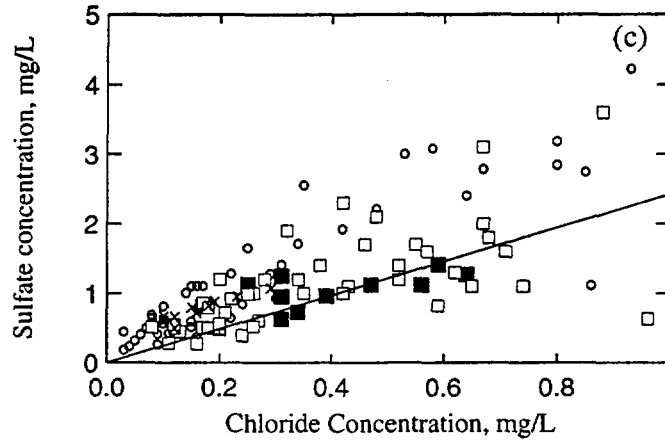
53-04b.AI.SITEDESC-R01

Source: CRWMS M&O (2000, Figure 6)

Figure 5.3-4. Constituents Plotted versus Chloride for Precipitation Samples (Continued)

Figure caption / map labels:

E500000m   E550000m   E600000m

N4150000m
N4100000m
N4050000m
N4000000m

Potential
repository
site

22 ▲
▲23

53 52

Beatty

31 56
    26
33 57, 58, 59

61 60

374
373
190
95
180

Death Valley

N

0   30 miles
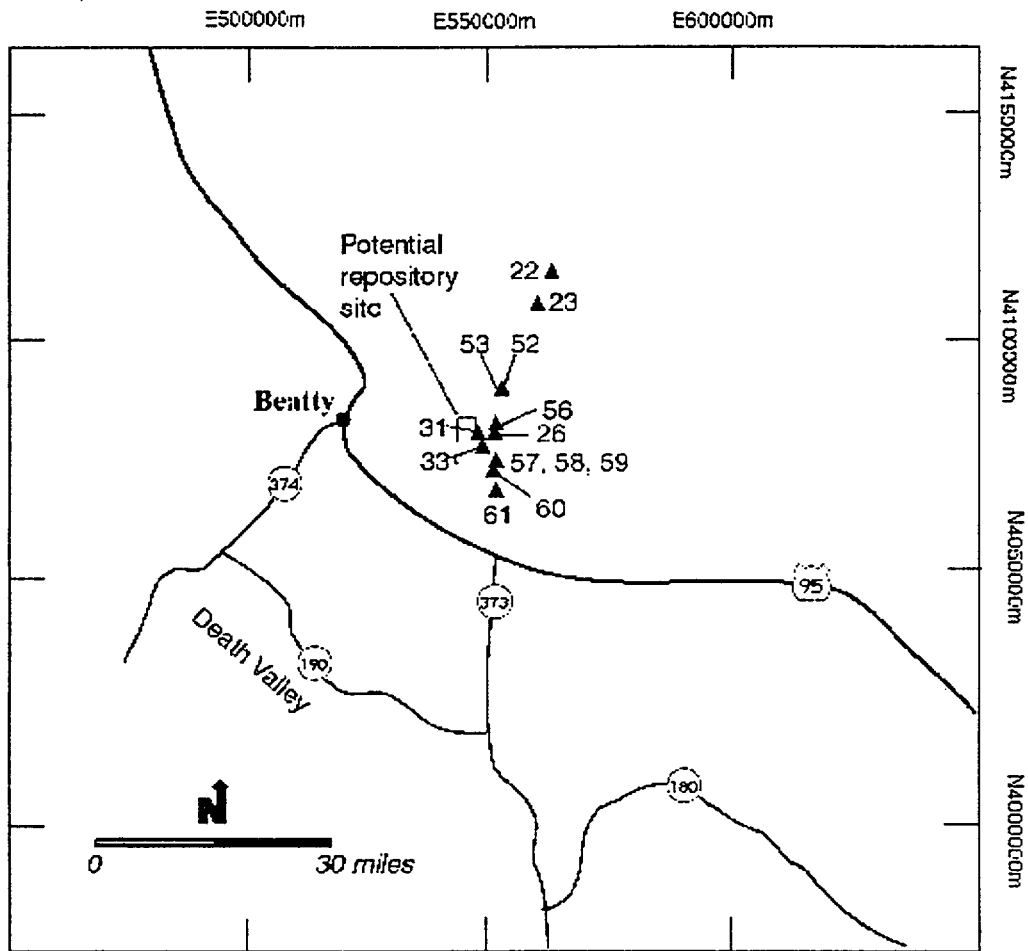
53-05.DOC SITEDESC-R01

NOTE: Surface water quality data collection sites in the vicinity of Yucca Mountain, Nevada. Site numbers are identified (in parentheses) on the legend of Figure 5.3-6.

Figure 5.3-5. Surface Water Collection Sites

CATIONS   % OF TOTAL MEQ/L   ANIONS
                      16 SAMPLES
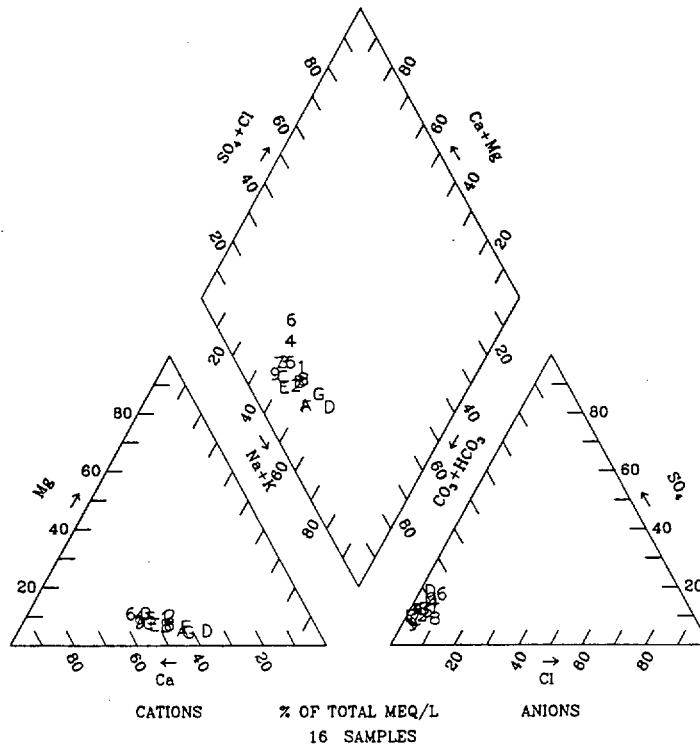
Legend		
List of Plotted Points, Sample Locations, and Site Numbers		
1-2	Tributary to Stockade Wash (22)	B Wren Wash (31)
3	Stockade Wash (23)	C Split Wash (33)
4-5	Pah Canyon (52)	D Drillhole Wash (58)
6	Overland flow near Pah Canyon (53)	E Fortymile Wash at H-Road (59)
7	Overland flow in Fortymile Canyon (56)	F Busted Butte Wash (60)
8-9	Yucca Wash (26)	G Fortymile Wash at J-12 (61)
A	Fortymile Wash above Drillhole Wash (57)	

53-06.DOC.SITEDESC-R01

Source: CRWMS M&O (2000, Figure 8)

NOTE: Sampling locations are shown on Figure 5.3-5. The intent of this plot is to show the extent to which different water samples are similar or dissimilar in composition. For those waters that are very similar (i.e., data symbols plot over each other), it is not important to be able to discern individual points.

Figure 5.3-6. Trilinear Diagram for Surface Runoff from the Yucca Mountain Area

CATIONS   % OF TOTAL MEQ/L   ANIONS

14 SAMPLES
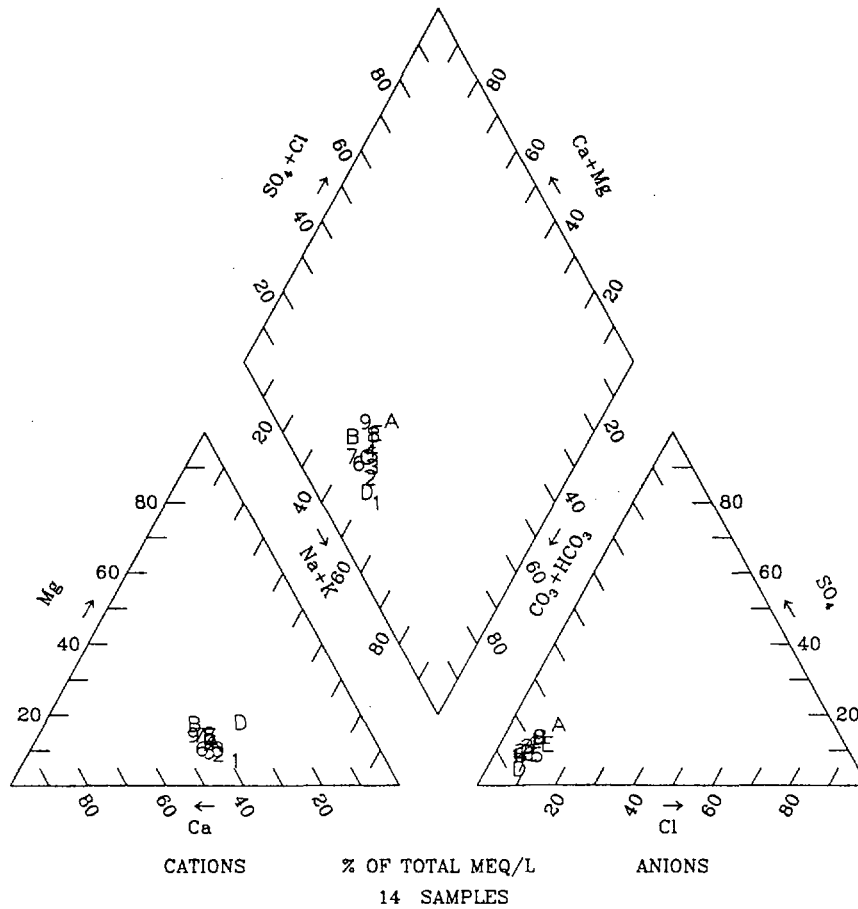
Legend	
List of Plotted Points and Sample Locations	
Stewart Basin, Toiyabe Range	*3 Springs Basin, Kawich Range*
1-2 Veg Spring	7-8 3 Springs Creek near 3 Spring #3
3-4 East Stewart Creek	9, A 3 Springs Creek near Warm Springs
5-6 Hellebore Spring	B-C 3 Springs Creek near 3 Spring #2
	D-E 3 Springs Creek near Ledge Spring

53-07.DOC.SITEDESC-R01

Source: CRWMS M&O (2000, Figure 9)

NOTE: Because of the relative constancy of the chemical compositions, only two data points are plotted for each location. The intent of this plot is to show the extent to which different water samples are similar or dissimilar in composition. For those waters that are very similar (i.e., data symbols plot over each other), it is not important to be able to discern individual points.

Figure 5.3-7. Trilinear Diagram for Surface Waters from 3 Springs Basin and Stewart Basin, Nevada
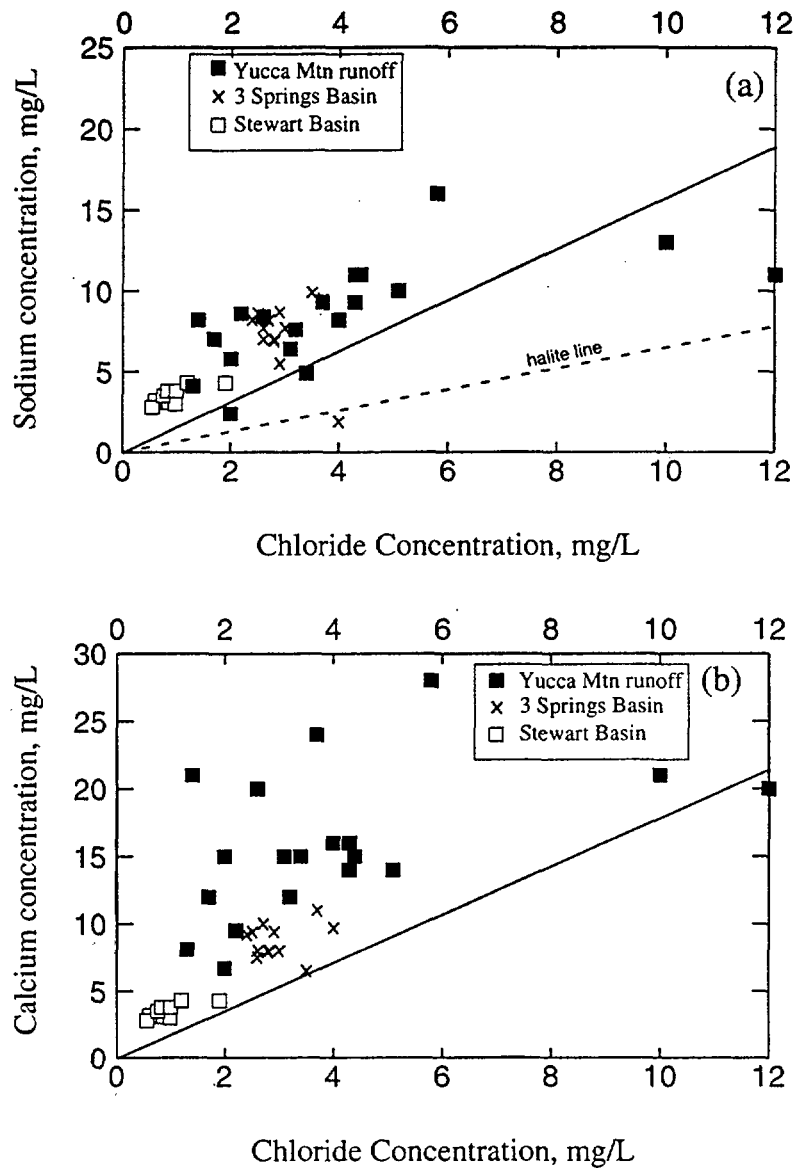
Source: CRWMS M&O (2000, Figure 10)

NOTE: Surface-water and runoff samples are from Yucca Mountain, 3 Springs Basin, and Stewart Basin, Nevada. Plots show chloride versus: (a) sodium, (b) calcium, (c) sulfate, (d) bicarbonate, and (e) silica as SiO_2. Because of the constancy of their composition, only three data points are shown for each surface-water sampling location in 3 Springs Basin and Stewart Basin. Also shown are lines of best-fit to the 3 Springs Basin precipitation data, from Table 5.3-2. The halite line on plot (a) is based on a 1:1 molar ratio of sodium to chloride to show the trend for halite dissolution.

Figure 5.3-8. Constituents Plotted versus Chloride for Surface-Water and Runoff Samples
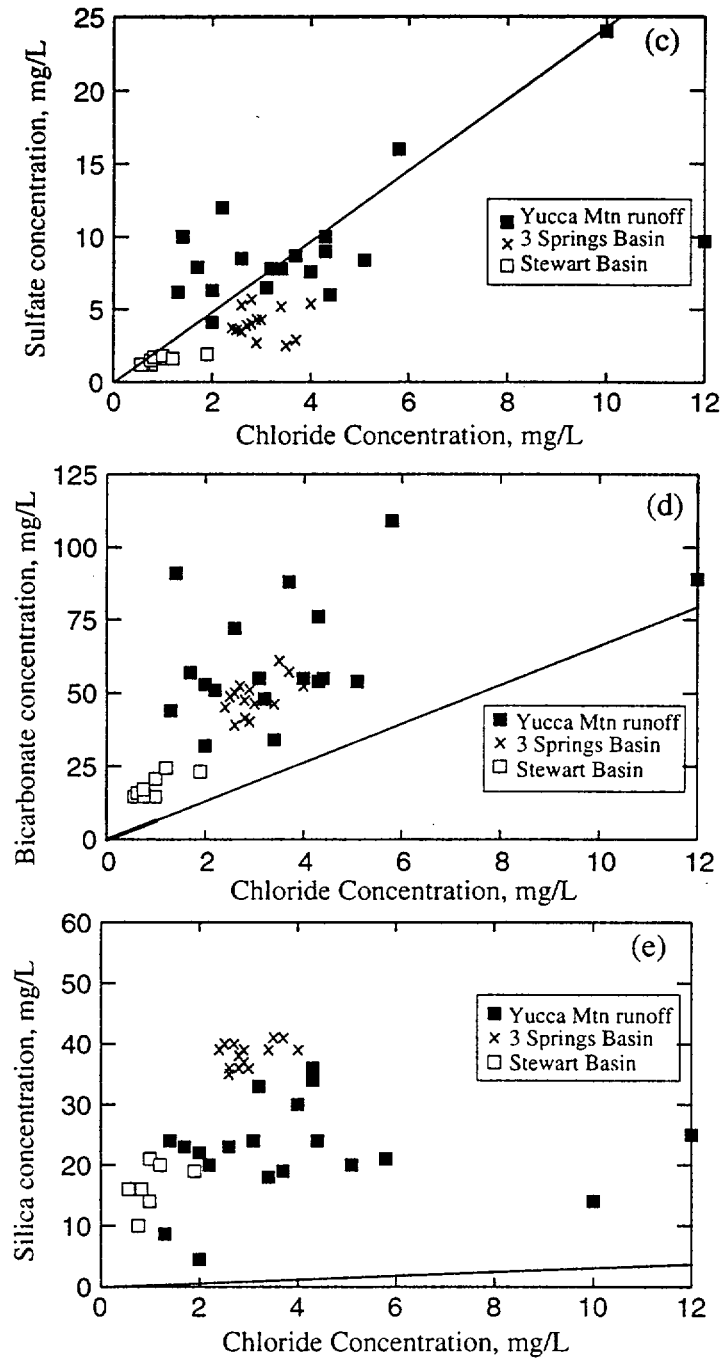
Figure 5.3-8. Constituents Plotted versus Chloride for Surface-Water and Runoff Samples (Continued)

Source: CRWMS M&O (2000, Figure 10)

CATIONS   % OF TOTAL MEQ/L   ANIONS
                      11 SAMPLES
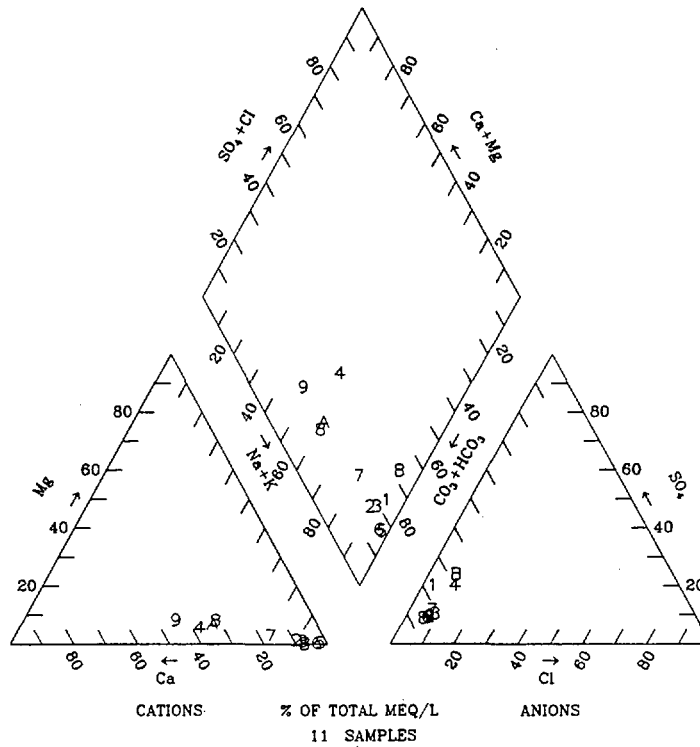
Legend						
List of Plotted Points, Sample Identifiers, and Sample Site Names						
1	131	Captain Jack Spring		7	147	Tunnel Seep, U-12t.03
2	137	Rainier Spring		8	148	Tunnel Seep, U-12t.03
3	143	Tunnel Seep, U-12e.06		9	149	Tunnel Seep, U-12t.03
4	144	Tunnel Seep, U-12n		A	150	Tunnel Seep, U-12t.04
5	145	Tunnel Seep, U-12n.03		B	206	Whiterock Spring
6	146	Tunnel Seep, U-12t				

Source: CRWMS M&O (2000, Figure 11)

NOTE: Locations of sampling sites are shown on Figure 5.3-44. The intent of this plot is to show the extent to which different water samples are similar or dissimilar in composition. For those waters that are very similar (i.e., data symbols plot over each other), it is not important to be able to discern individual points.

Figure 5.3-9. Trilinear Diagram for Springs and Seeps, Rainier Mesa, Nevada

CATIONS   % OF TOTAL MEQ/L   ANIONS

15 SAMPLES
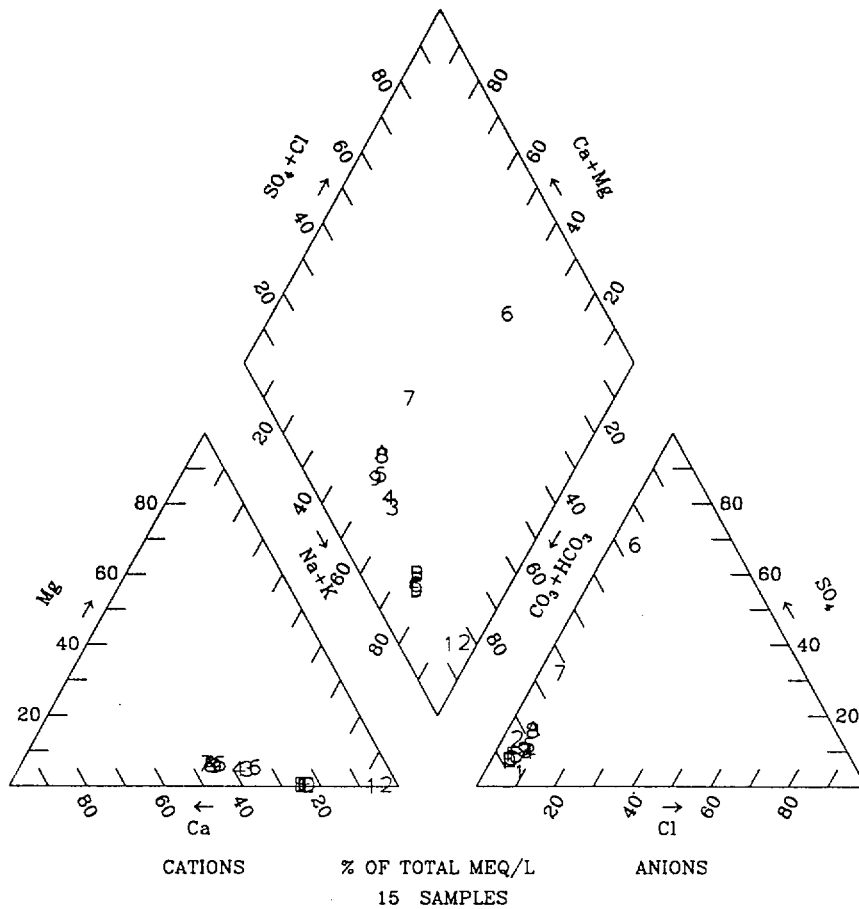
Legend								
List of Plotted Points, Borehole Identifiers, and Sampled Depths (feet)								
1	NRG7A	460.25	6	UZ14 C	390.75	B	SD7 (3/8/95)	479.76
2	SD9/TS	453.85	7	UZ14 PT1	390.75	C	SD7 (3/16/95)	488.29
3	UZ14 A	384.6	8	UZ14 PT2	390.75	D	SD7 (3/17/95)	488.29
4	UZ14 A2	384.6	9	UZ14 PT4	390.75	E	SD7 (3/20/95)	488.29
5	UZ14 B	387.68	A	UZ14 D	390.75	F	SD7 (3/21/95)	488.29

53-10.DOC.SITEDESC-R01

Source: CRWMS M&O (2000, Figure 17)

NOTE: Data are listed in Table 5.3-6. The intent of this plot is to show the extent to which different water samples are similar or dissimilar in composition. For those waters that are very similar (i.e., data symbols plot over each other), it is not important to be able to discern individual points.

Figure 5.3-10. Trilinear Diagram for Perched Water near Yucca Mountain
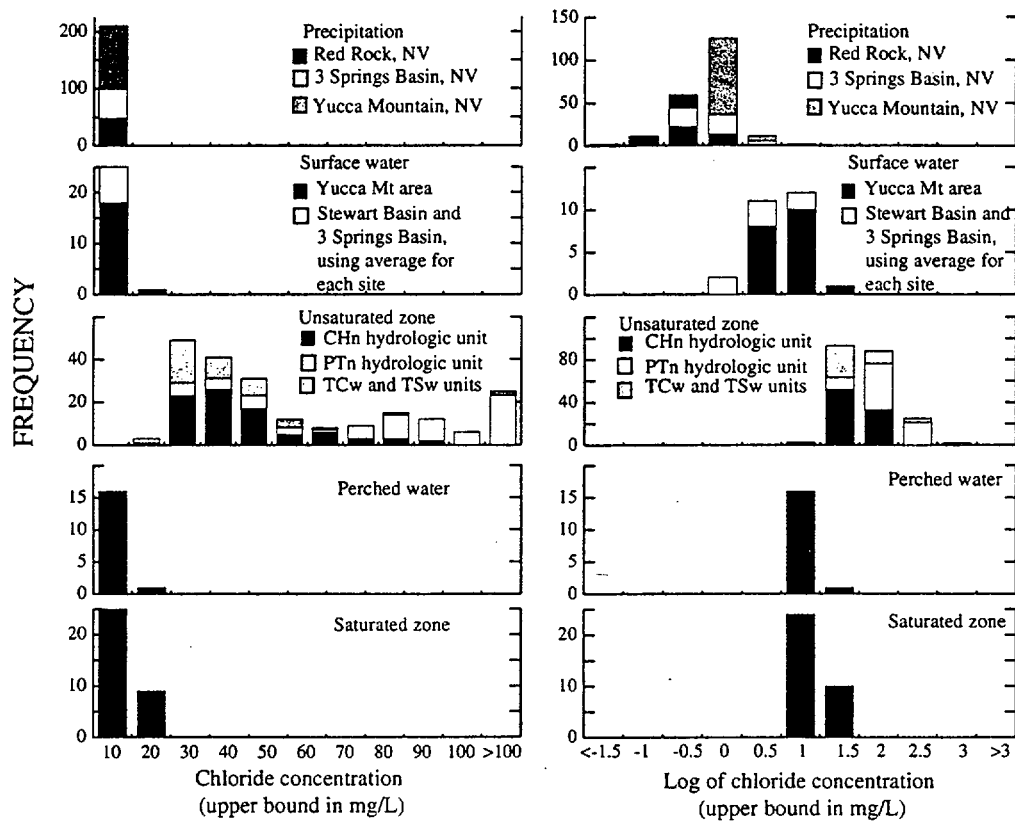
Source: CRWMS M&O (2000, Figure 18)

NOTE: Histograms are of chloride concentrations in precipitation, surface water, unsaturated zone pore water, perched water, and saturated zone groundwater. Part (a) shows chloride concentrations. Part (b) shows log of chloride concentrations.

Figure 5.3-11. Histograms of Chloride Concentrations
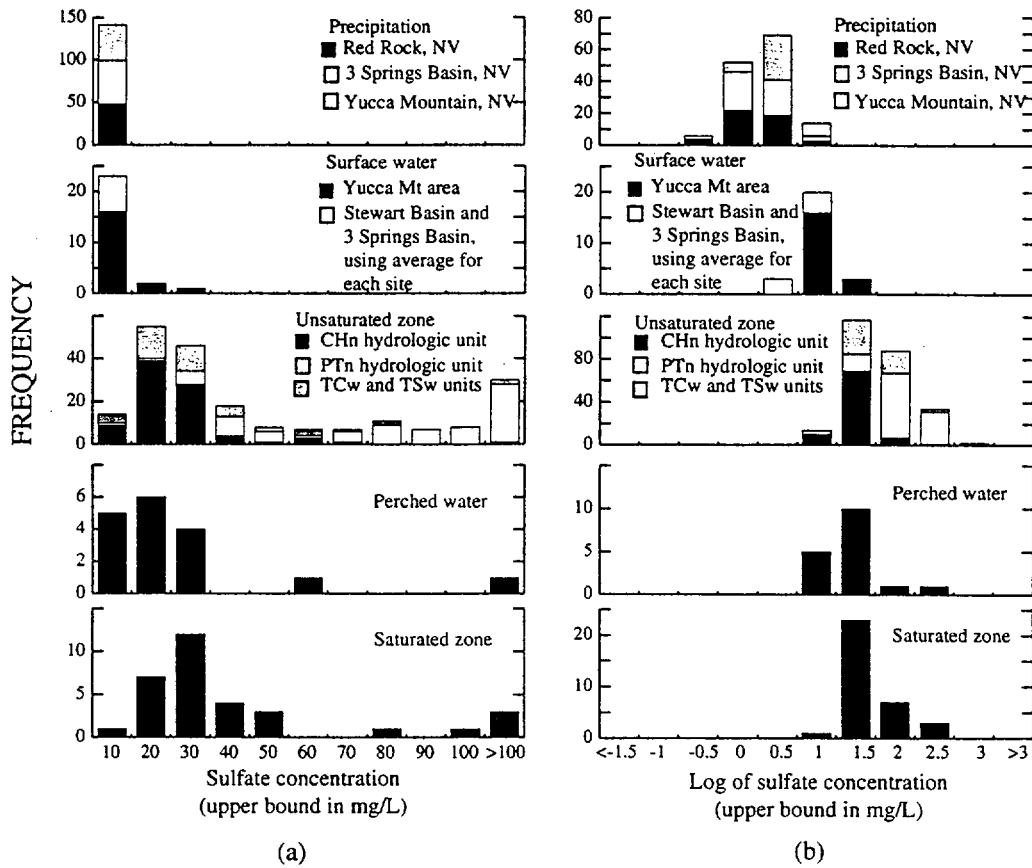
Source: CRWMS M&O (2000, Figure 19)

NOTE: Histograms are of sulfate concentrations in precipitation, surface water, unsaturated zone pore water, perched water, and saturated zone groundwater. Part (a) shows sulfate concentrations. Part (b) shows log of sulfate concentrations.

Figure 5.3-12. Histograms of Sulfate Concentrations

(a)

(b)
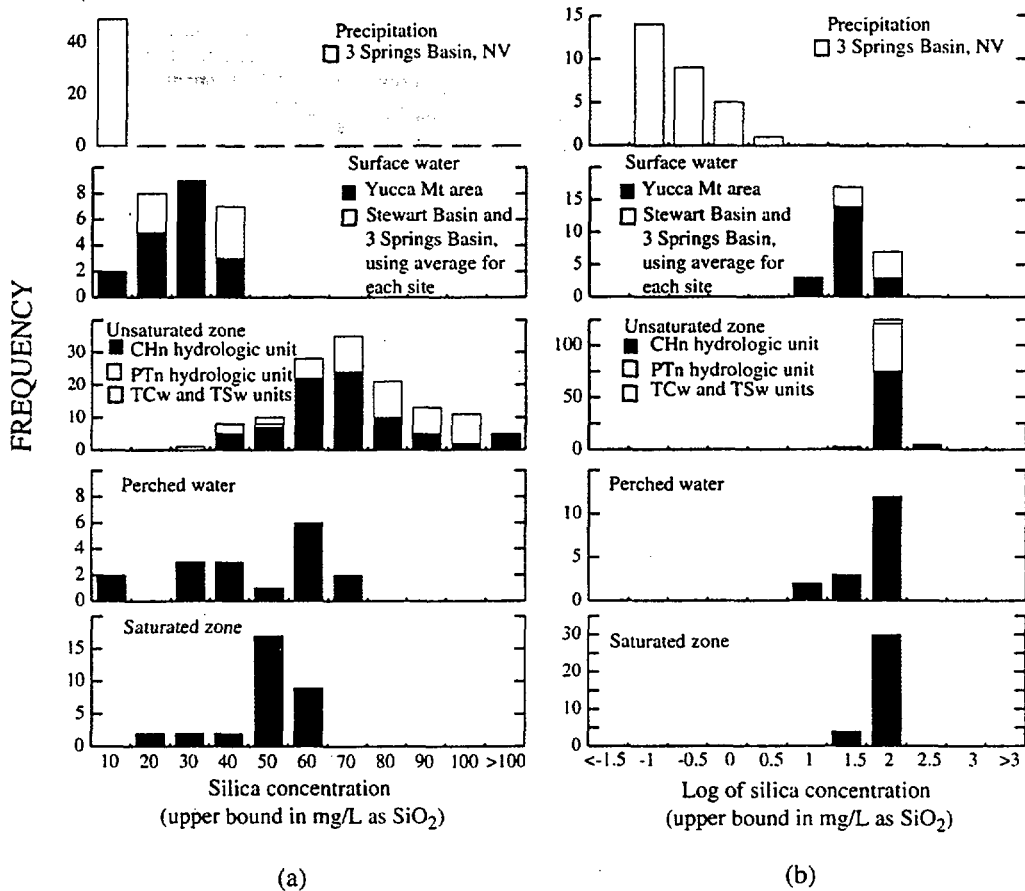
53-13.AI.SITEDESC-R01

Source: CRWMS M&O (2000, Figure 20)

NOTE: Histograms are of silica concentrations in precipitation, surface water, unsaturated zone pore water, perched water, and saturated zone groundwater. Part (a) shows silica concentrations. Part (b) shows log of silica concentrations.

Figure 5.3-13. Histograms of Silica Concentrations

(a)

(b)
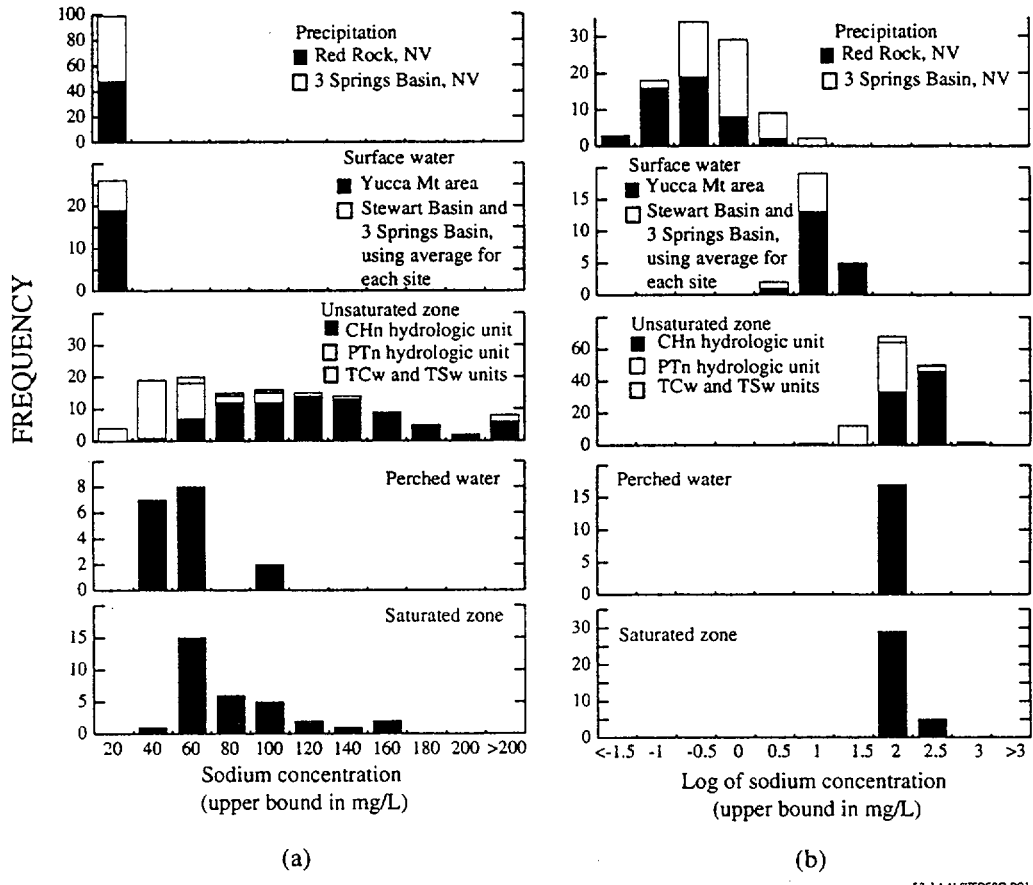
53-14.AI.SITEDESC-R01

Source: CRWMS M&O (2000, Figure 21)

NOTE: Histograms are of sodium concentrations in precipitation, surface water, unsaturated zone pore water, perched water, and saturated zone groundwater. Part (a) shows sodium concentrations. Part (b) shows log of sodium concentrations.

Figure 5.3-14. Histograms of Sodium Concentrations
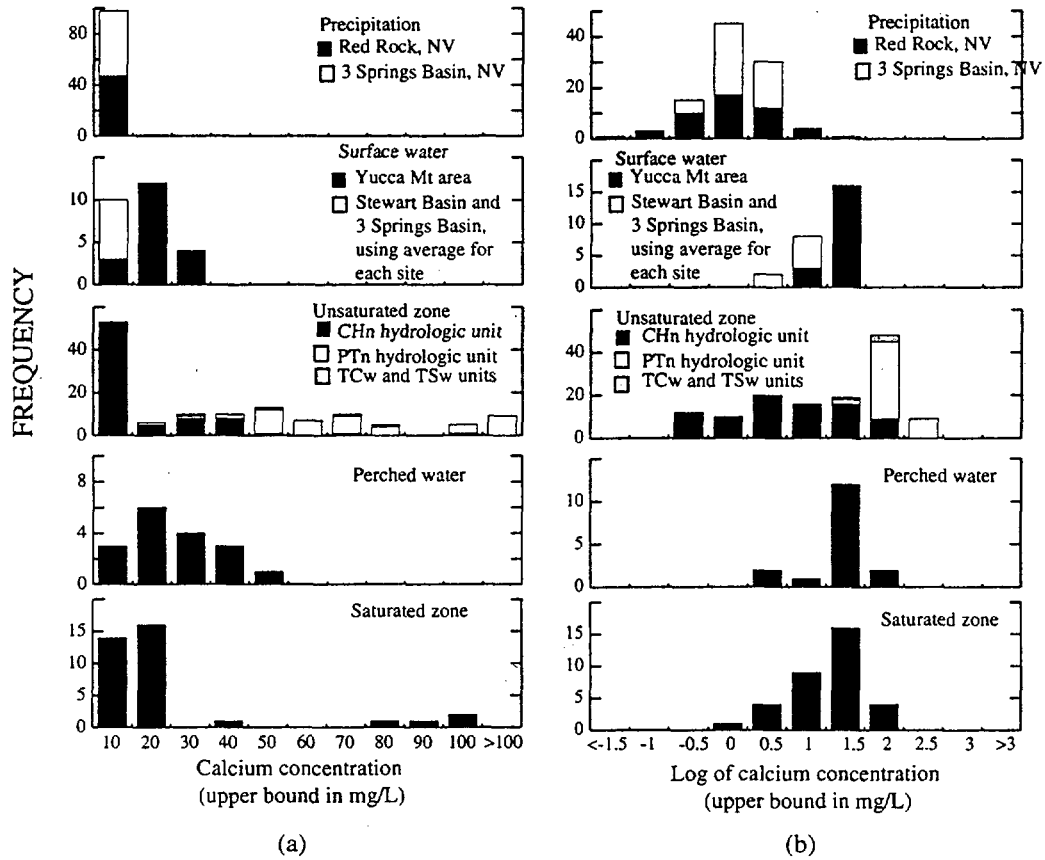
Source: CRWMS M&O (2000, Figure 22)

NOTE: Histograms are of calcium concentrations in precipitation, surface water, unsaturated zone pore water, perched water, and saturated zone groundwater. Part (a) shows calcium concentrations. Part (b) shows log of calcium concentrations.

Figure 5.3-15. Histograms of Calcium Concentrations
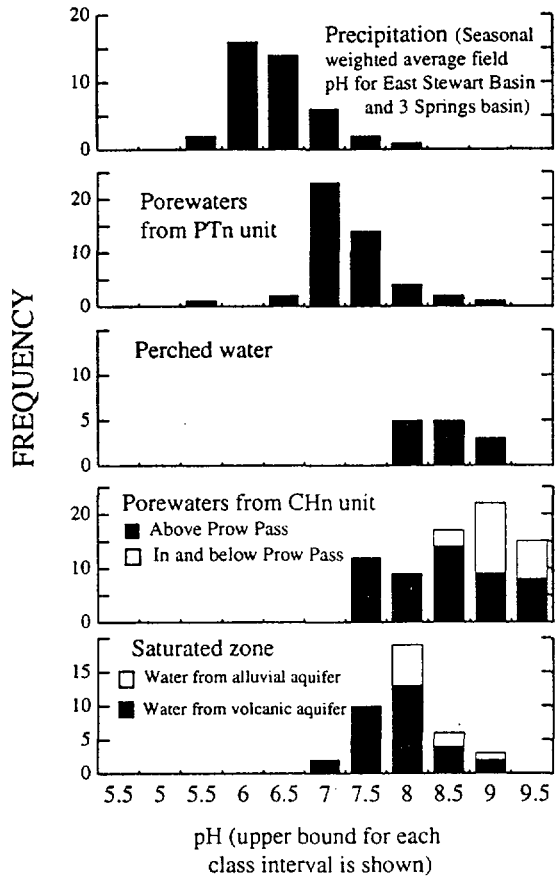
Source: CRWMS M&O (2000, Figure 23)

NOTE: Histograms are of pH values in precipitation, perched water, and saturated zone groundwater.

Figure 5.3-16. Histograms of pH Values
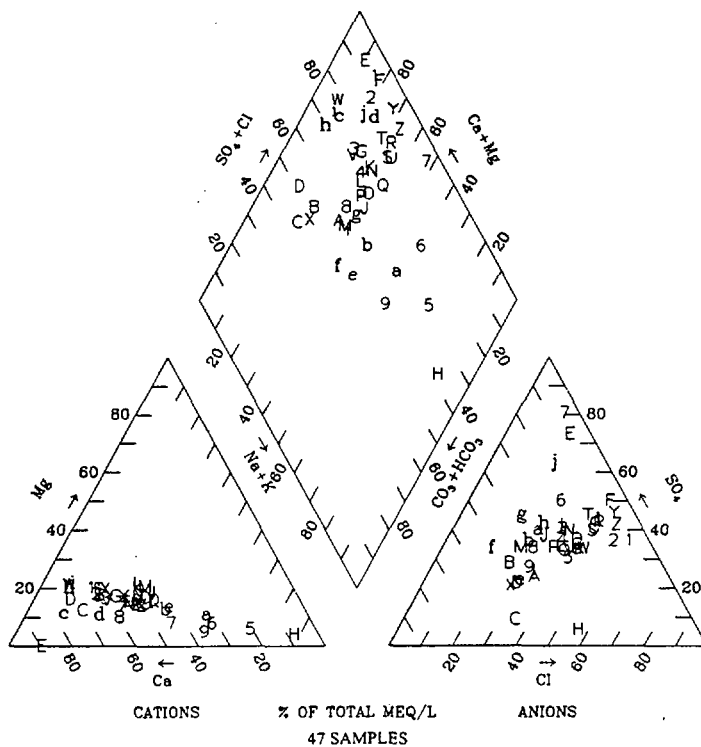
CATIONS   % OF TOTAL MEQ/L   ANIONS

47 SAMPLES

Legend
List of Plotted Points, Borehole Identifiers, and Tops of Sampled Intervals (feet)
1	NRG6-158.2	A	SD12-265.8	J	UZ14-91	S	UZ14-178.1	b	SD9-251.8
2	NRG6-160.8	B	SD12-278.6	K	UZ14-95.5	T	UZ14-215.7	c	UZN55-195.3
3	NRG6-171	C	SD12-296.1	L	UZ14-96.2	U	UZ14-225.9	d	UZN55-199.0
4	NRG6-175.6	D	SD7-339.7	M	UZ14-100.4	V	UZ14-235.1	e	SD6-430.3
5	NRG6-219.9	E	SD7-370.3	N	UZ14-114.8	W	UZ14-245.5	f	SD6-443.2
6	NRG6-244.6	F	SD9-94.2	O	UZ14-135.5	X	UZ#16-180.9	g	SD6-443.5
7	NRG6-255.9	G	SD9-154	P	UZ14-144.8	Y	SD9-114.1	h	UZ7a-203.3
8	NRG7A-165.8	H	UZ14-45	Q	UZ14-147.8	Z	SD9-135.1	i	UZ7a-220.2
9	NRG7A-258	I	UZ14-85.2	R	UZ14-177.6	a	SD9-176.2	j	UZ7a-241.4
								k	UZ14-240.8
								l	UZ#16-163.5

53-17.DOC.SITEDESC-R01

Source: CRWMS M&O (2000, Figure 12)

NOTE: The plotted data are listed in Table 5.3-4. The intent of this plot is to show the extent to which different water samples are similar or dissimilar in composition. For those waters that are very similar (i.e., data symbols plot over each other), it is not important to be able to discern individual points.

Figure 5.3-17. Trilinear Diagram for Pore Waters from the Nonwelded Paintbrush Tuff Hydrogeologic Unit

CATIONS   % OF TOTAL MEQ/L   ANIONS
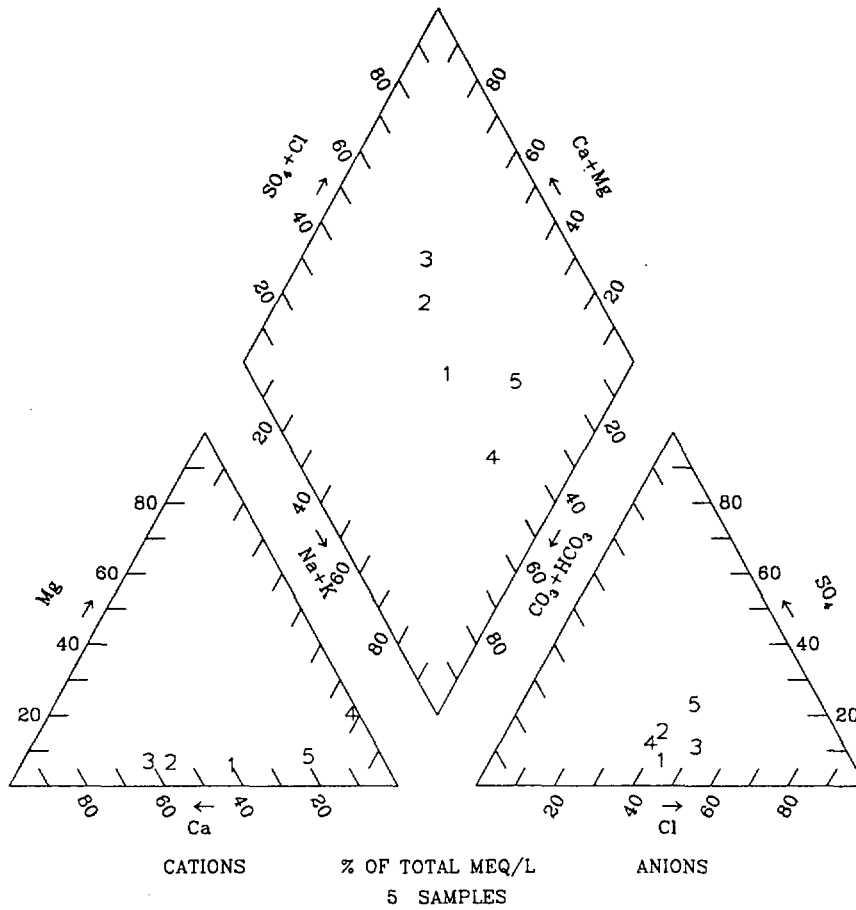
5 SAMPLES

Legend	
List of Plotted Points, Borehole Identifiers, and Tops of Sampled Intervals (feet)	
1 UZ-14 – 1258.5	4 UZ#16 – 952.6
2 UZ-14 – 1277.4	5 UZN55 – 166.1
3 UZ-14 – 1277.7	

Source: CRWMS M&O (2000, Figure 13)

NOTE: Sample UZN55–166.1 is from the Tiva Canyon welded unit; all other samples are from the Topopah Spring welded unit. The plotted data are listed in Table 5.3-4.

Figure 5.3-18.   Trilinear Diagram for Pore Waters from the Tiva Canyon Welded and Topopah Spring Welded Hydrogeologic Units
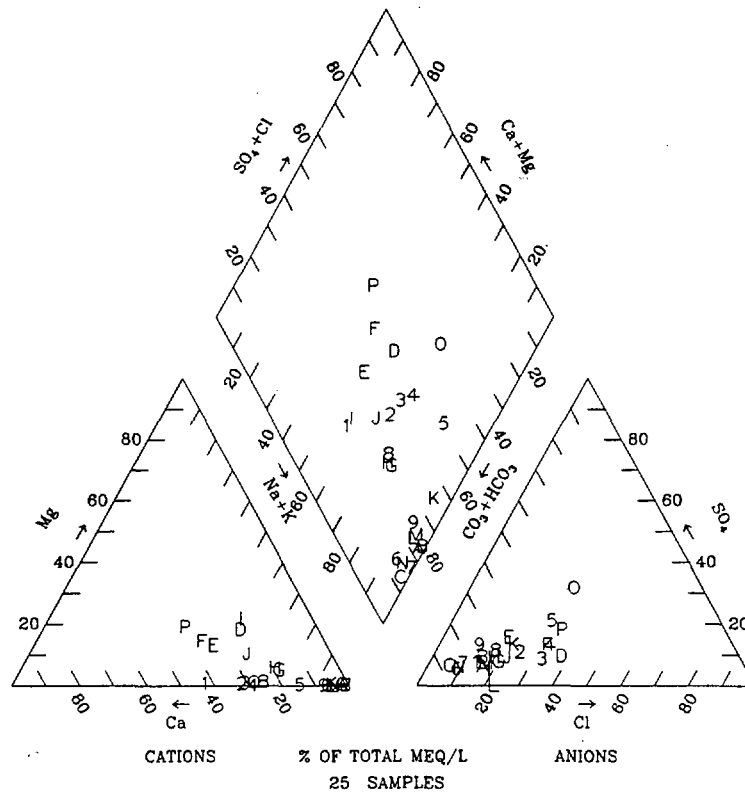
CATIONS   % OF TOTAL MEQ/L   ANIONS
                    25 SAMPLES

Legend							
List of Plotted Points, Borehole Identifiers, and Tops of Sampled Intervals (feet)							
1	NRG7A – 1483.5	7	SD9 – 1535.2	D	UZ#16 – 1166.2	J	UZ#16 – 1317.9
2	NRG7A – 1492.7	8	UZ14 – 1419.5	E	UZ#16 – 1227.4	K	UZ#16 – 1358.1
3	NRG7A – 1498.6	9	UZ14 – 1461.9	F	UZ#16 – 1235.1	L	WT24 – 1734.3
4	SD12 – 1460.7	A	UZ14 – 1495.8	G	UZ#16 – 1269.6	M	WT24 – 1744.2
5	SD12 – 1495.5	B	UZ14 – 1524.6	H	UZ#16 – 1280.4	N	WT24 – 1744.5
6	SD9 – 1452.6	C	UZ14 – 1542.3	I	UZ#16 – 1296.8	O	UZ14-1409.4
						P	UZ#16-1206.3

Source: CRWMS M&O (2000, Figure 14)

NOTE: The plotted data are listed in Table 5.3-4. The intent of this plot is to show the extent to which different water
         samples are similar or dissimilar in composition. For those waters that are very similar (i.e., data symbols
         plot over each other), it is not important to be able to discern individual points.

Figure 5.3-19.   Trilinear Diagram for Pore Waters from the Top 200 Feet of the Calico Hills Nonwelded
   Hydrogeologic Unit
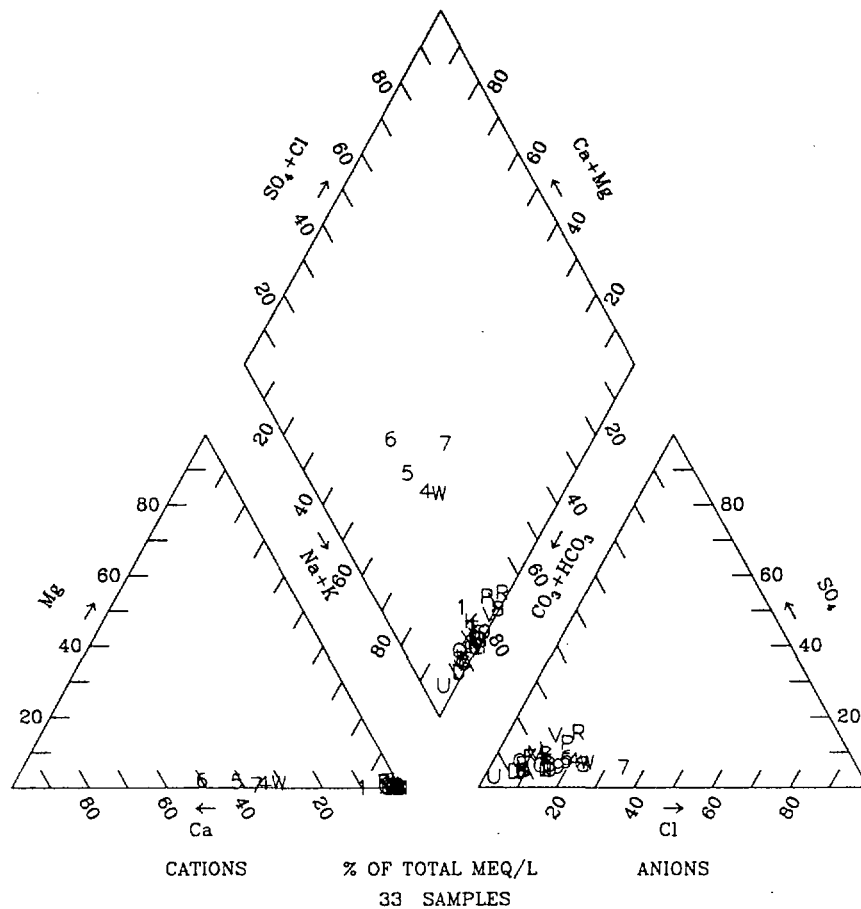
CATIONS   % OF TOTAL MEQ/L   ANIONS
                      33 SAMPLES

Legend						
List of Plotted Points, Borehole Identifiers, and Tops of Sampled Intervals (feet)						
1	SD12-1517	9	SD9-1661.1	H	UZ14-1585.3	P	UZ#16-1389.4
2	SD12-1600.6	A	SD9-1741	I	UZ14-1605.9	Q	UZ#16-1398.5
3	SD12-1636.8	B	SD9-1741.7	J	UZ14-1644.3	R	UZ#16-1412.9
4	SD7-1498.4	C	SD9-1800.7	K	UZ14-1674.8	S	UZ#16-1428.1
5	SD7-1524.6	D	UZ14-1563.6	L	UZ14-1695.4	T	UZ#16-1442.8
6	SD7-1558.4	E	UZ14-1564.6	M	UZ14-1715	U	SD12 – 1558.9
7	SD7-1617	F	UZ14-1564.9	N	UZ14-1734.5	V	SD12 – 1582.5
8	SD9-1619.9	G	UZ14-1585	O	UZ14-1735.3	W	SD7 – 1600.1
						X	UZ#16–1395.5

Source: CRWMS M&O (2000, Figure 15)

NOTE: The plotted data are listed in Table 5.3-4. The intent of this plot is to show the extent to which different water samples are similar or dissimilar in composition. For those waters that are very similar (i.e., data symbols plot over each other), it is not important to be able to discern individual points.

Figure 5.3-20.   Trilinear Diagram for Pore Waters below the Top 200 Feet of the Calico Hills Nonwelded Hydrogeologic Unit and above the Prow Pass Lithostratigraphic Unit
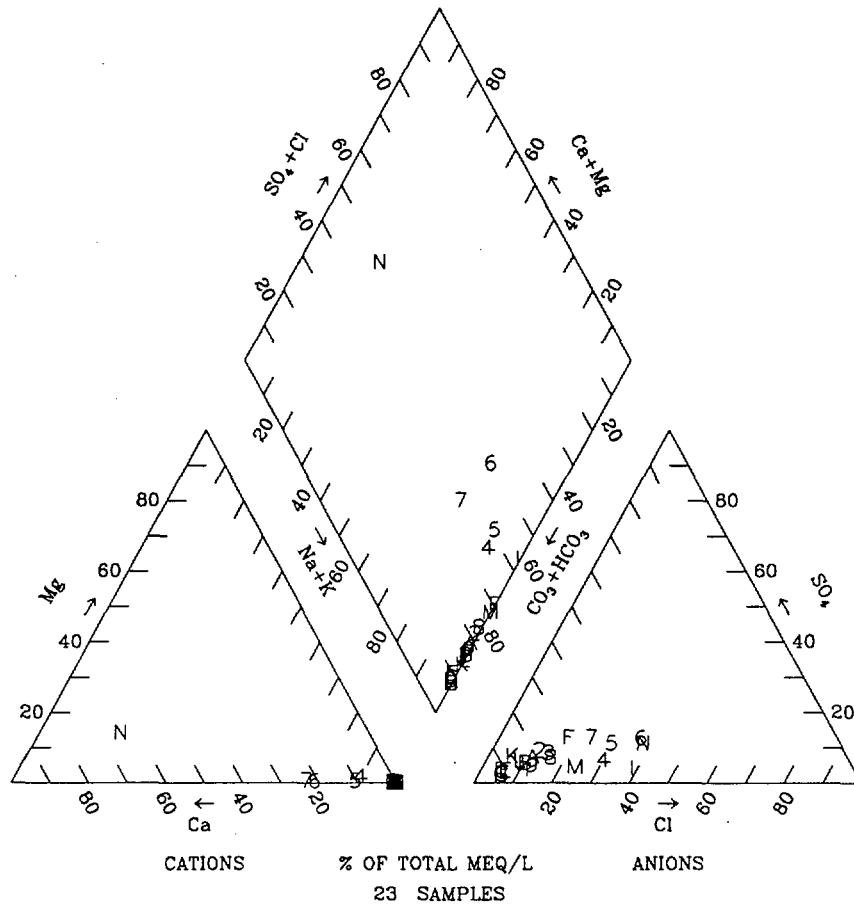
CATIONS   % OF TOTAL MEQ/L   ANIONS

23 SAMPLES

Legend			
List of Plotted Points, Borehole Identifiers, and Tops of Sampled Intervals (feet)			
1 SD12-1901.5	7 UZ#16-1651.6	D UZ14-2015.2	J SD7-2598.3
2 SD12-1942.4	8 UZ14-1804.5	E UZ14-2025.1	K SD7-2088.2
3 SD12-1938.8	9 UZ14-1825.8	F UZ14-2095.6	L SD7-2170.1
4 UZ#16-1486.9	A UZ14-1854.9	G SD7-1890.7	M SD7-2596.5
5 UZ#16-1601.1	B UZ14-1865.7	H SD7-1952.4	N UZ#16-1643.4
6 UZ#16-1607.7	C UZ14-2014.7	I SD7-2596.1	

53-21.DOC.SITEDESC-R01

Source: CRWMS M&O (2000, Figure 16)

NOTE: The plotted data are listed in Table 5.3-4. The intent of this plot is to show the extent to which different water samples are similar or dissimilar in composition. For those waters that are very similar (i.e., data symbols plot over each other), it is not important to be able to discern individual points.

Figure 5.3-21. Trilinear Diagram for Pore Waters from the Prow Pass, Bullfrog, and Tram Lithostratigraphic Units
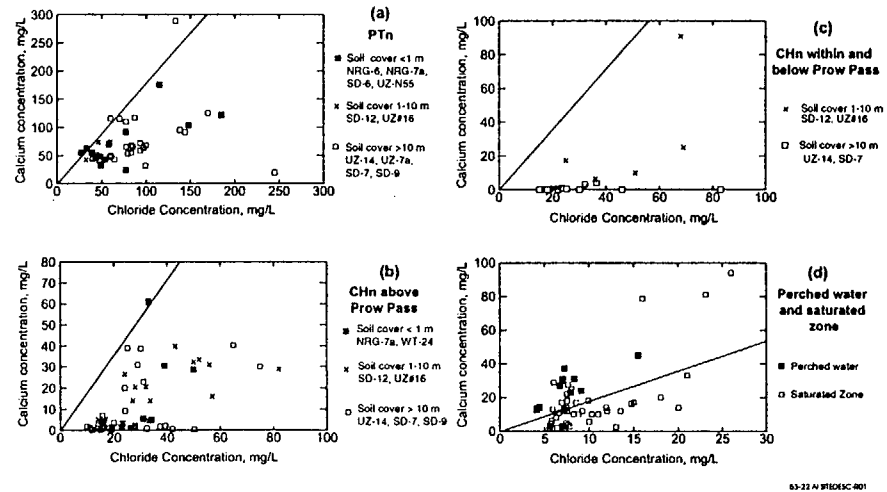
Source: CRWMS M&O (2000, Figure 24)

NOTE: Plots show calcium versus chloride in unsaturated zone pore waters (a) from the Paintbrush Tuff nonwelded hydrogeologic unit, (b) from the Calico Hills hydrogeologic unit above the lithostratigraphic Prow Pass unit, (c) from the Calico Hills hydrogeologic unit within and below the lithostratigraphic Prow Pass unit, and (d) in perched water and from the saturated zone. Pore water data are shown in Table 5.3-4, and perched water data are shown in Table 5.3-6. The solid line on each plot is the best-fit regression line for the precipitation data from Table 5.3-2.

Figure 5.3-22. Calcium versus Chloride Concentrations in Unsaturated Zone Pore Waters
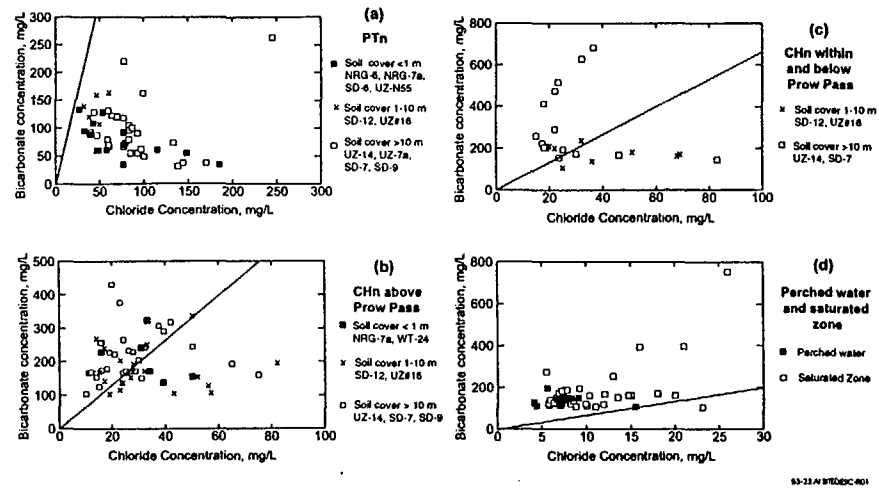
Source: CRWMS M&O (2000, Figure 25)

NOTE: Plots show bicarbonate versus chloride in unsaturated zone pore waters (a) from the Paintbrush Tuff nonwelded hydrogeologic unit, (b) from the Calico Hills hydrogeologic unit above the lithostratigraphic Prow Pass unit, (c) from the Calico Hills hydrogeologic unit within and below the lithostratigraphic Prow Pass unit, and (d) in perched water and from the saturated zone. Pore water data are shown in Table 5.3-4, and perched water data are shown in Table 5.3-6. The solid line on each plot is the best-fit regression line for the precipitation data from Table 5.3-2.

Figure 5.3-23. Bicarbonate versus Chloride Concentrations in Unsaturated Zone Pore Waters
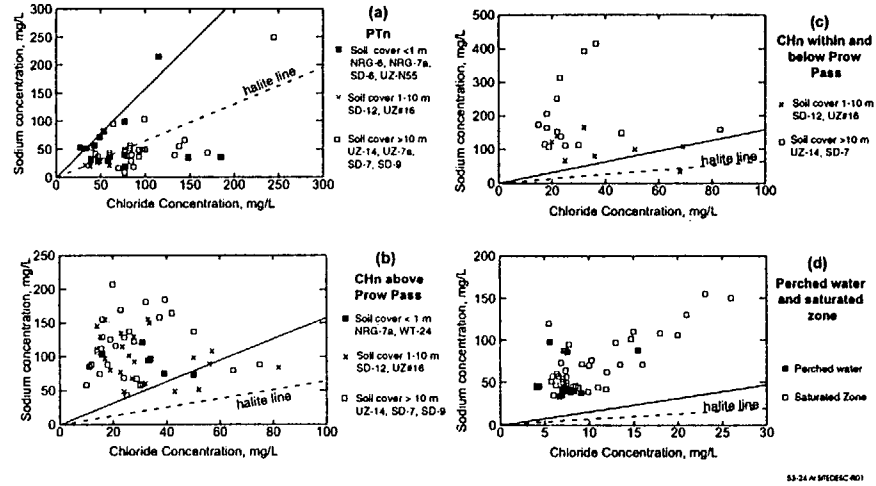
Source: CRWMS M&O (2000, Figure 26)

NOTE: Plots show sodium versus chloride in unsaturated zone pore waters (a) from the Paintbrush Tuff nonwelded hydrogeologic unit, (b) from the Calico Hills hydrogeologic unit above the lithostratigraphic Prow Pass unit, (c) from the Calico Hills hydrogeologic unit within and below the lithostratigraphic Prow Pass unit, and (d) in perched water and from the saturated zone. Pore water data are shown in Table 5.3-4, and perched water data are shown in Table 5.3-6. The solid line on each plot is the best-fit regression line for the precipitation data from Table 5.3-2. The halite line on these plots is based on a 1:1 molar ratio of sodium to chloride to show the trend for halite dissolution.

Figure 5.3-24. Sodium versus Chloride Concentrations in Unsaturated Zone Pore Waters
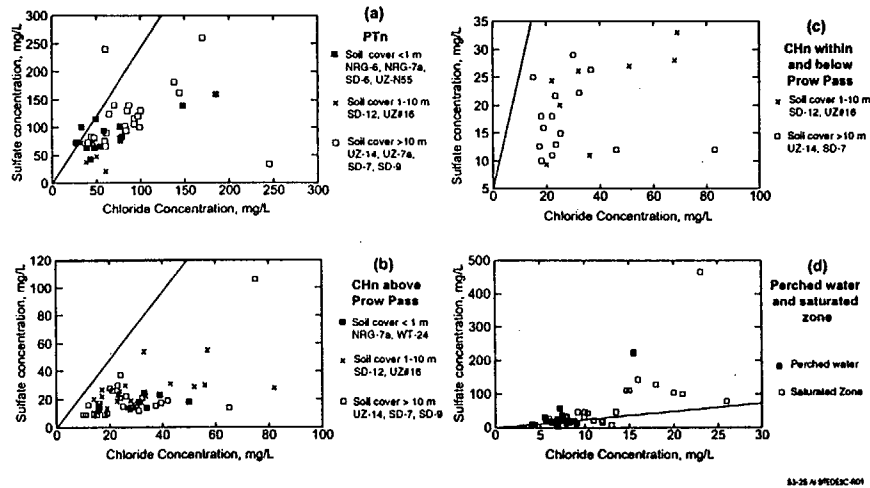
Source: CRWMS M&O (2000, Figure 27)

NOTE: Plots show sulfate versus chloride in unsaturated zone pore waters (a) from the Paintbrush Tuff nonwelded hydrogeologic unit, (b) from the Calico Hills hydrogeologic unit above the lithostratigraphic Prow Pass unit, (c) from the Calico Hills hydrogeologic unit within and below the lithostratigraphic Prow Pass unit, and (d) in perched water and from the saturated zone. Pore water data are shown in Table 5.3-4, and perched water data are shown in Table 5.3-6. The solid line on each plot is the best-fit regression line for the precipitation data from Table 5.3-2.

Figure 5.3-25. Sulfate versus Chloride Concentrations in Unsaturated Zone Pore Waters
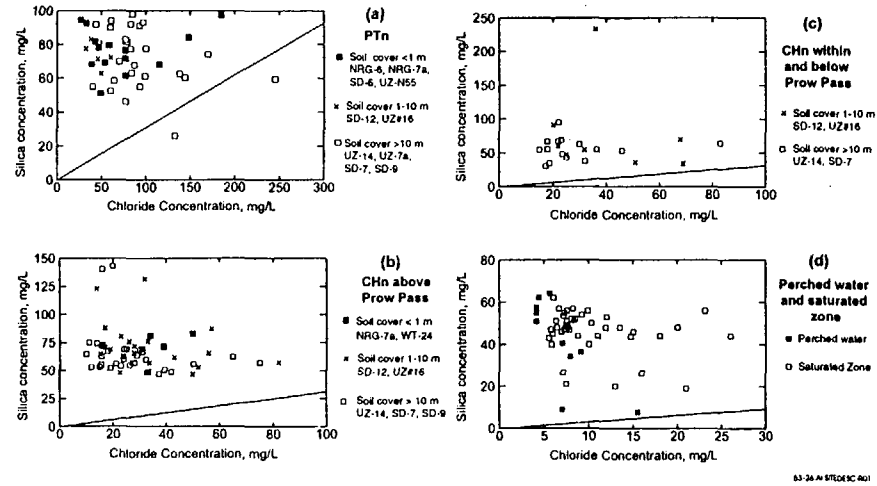
Source: CRWMS M&O (2000, Figure 28)

NOTE: Plots show silica versus chloride in unsaturated zone pore waters (a) from the Paintbrush Tuff nonwelded hydrogeologic unit, (b) from the Calico Hills hydrogeologic unit above the lithostratigraphic Prow Pass unit, (c) from the Calico Hills hydrogeologic unit within and below the lithostratigraphic Prow Pass unit, and (d) in perched water and from the saturated zone. Pore water data are shown in Table 5.3-4, and perched water data are shown in Table 5.3-6. The solid line on each plot is the best-fit regression line for the precipitation data from Table 5.3-2.

Figure 5.3-26. Silica versus Chloride Concentrations in Unsaturated Zone Pore Waters

CATIONS   % OF TOTAL MEQ/L   ANIONS

25 SAMPLES
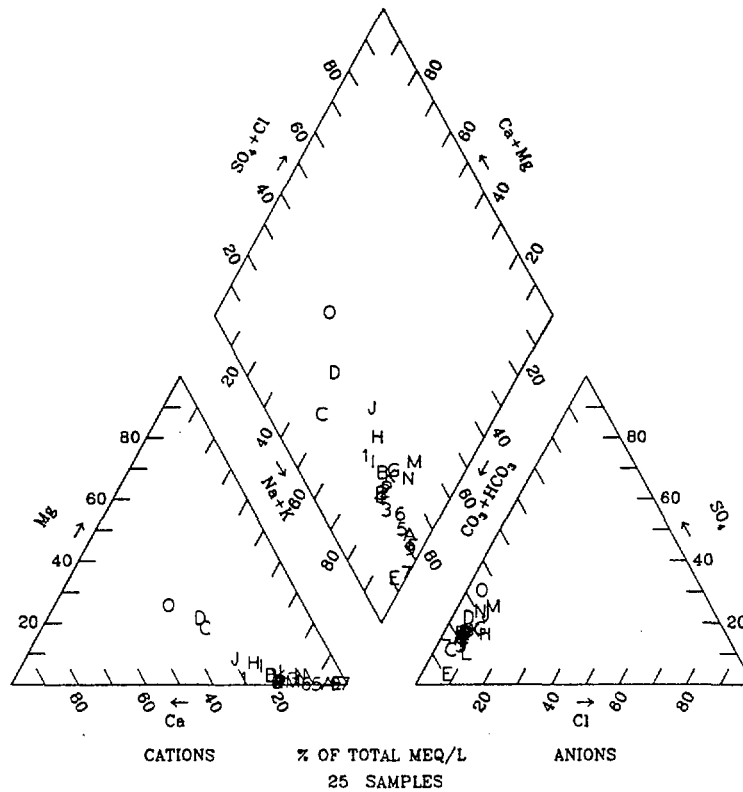
Legend
List of Plotted Points and Borehole Identifiers

	Yucca Mountain area				*40 Mile Wash*		*Other*
1	b#1	9	H-5	G	a#2 (87-213 m)	M	Gexa
2	c#2	A	H-6	H	J-12	N	VH-1
3	G-2	B	ONC#1	I	J-13	O	VH-2
4	G-4	C	p#1 (0-1200 m)	J	JF-3	P	WT#12
5	H-1 (572-6887 m)	D	p#1 (1300-1800 m)	K	WT#14		
6	H-1 (687-1829 m)	E	WT-7	L	WT#15		
7	H-3	F	WT-10				
8	H-4						

53-27.DOC.SITEDESC-R01

Source: Oliver and Root (1997).

NOTE: This trilinear diagram is for groundwaters from the vicinity of Yucca Mountain. Full identifiers for wells are given in Table 5.3-8. Well locations are shown in Figure 5.3-46. The intent of this plot is to show the extent to which different water samples are similar or dissimilar in composition. For those waters that are very similar (i.e., data symbols plot over each other), it is not important to be able to discern individual points.

Figure 5.3-27. Trilinear Diagram for Yucca Mountain Groundwaters
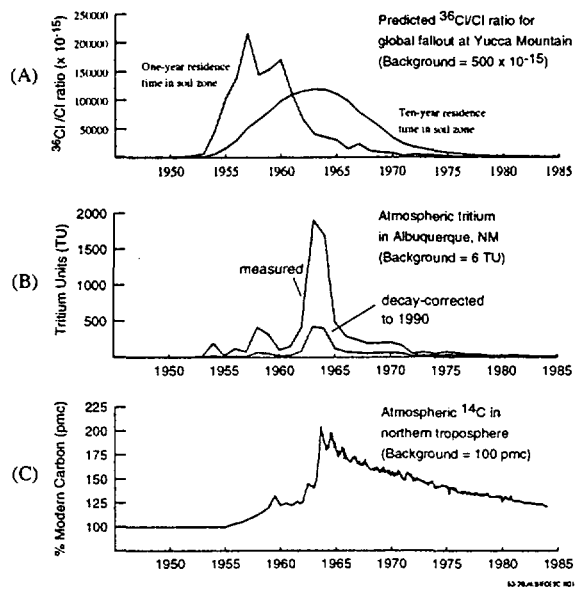
Source: CRWMS M&O (2000, Figure 29)

NOTE: Part (A) shows estimated chlorine-36/chlorine ratio for global fallout at Yucca Mountain as a function of average residence time in the soil zone, Part (B) shows tritium in atmospheric moisture in Albuquerque, New Mexico, and Part (C) shows atmospheric concentrations of bomb-pulse carbon-14 for the northern hemisphere.

Figure 5.3-28. Input Functions for Bomb-Pulse Nuclides
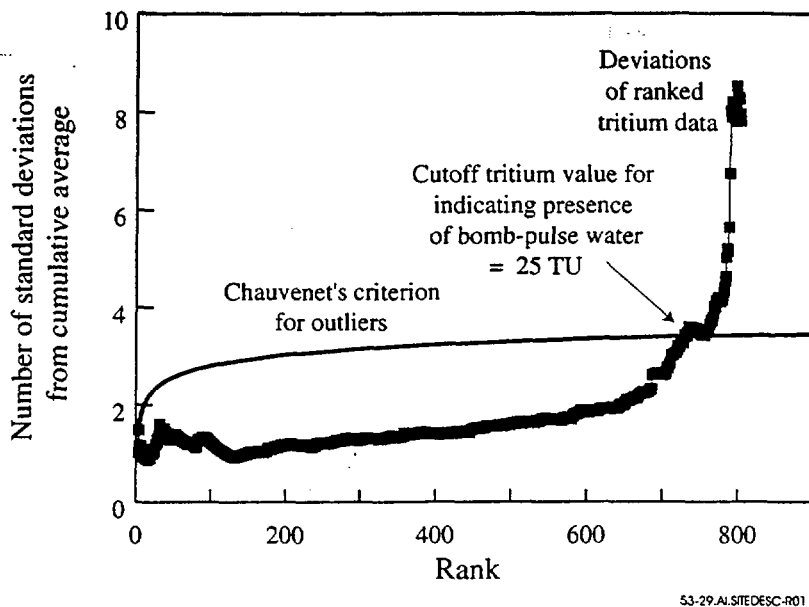
Source: CRWMS M&O (2000, Figure 30)

NOTE: The plot illustrates the statistical determination of the cutoff tritium value for the presence of bomb-pulse tritium in unsaturated zone fluid samples, using Chauvenet's criterion. Chauvenet's criterion is discussed in Bevington and Robinson (1992, p. 58).

Figure 5.3-29. Cutoff Tritium Value for the Presence of Bomb-Pulse Tritium
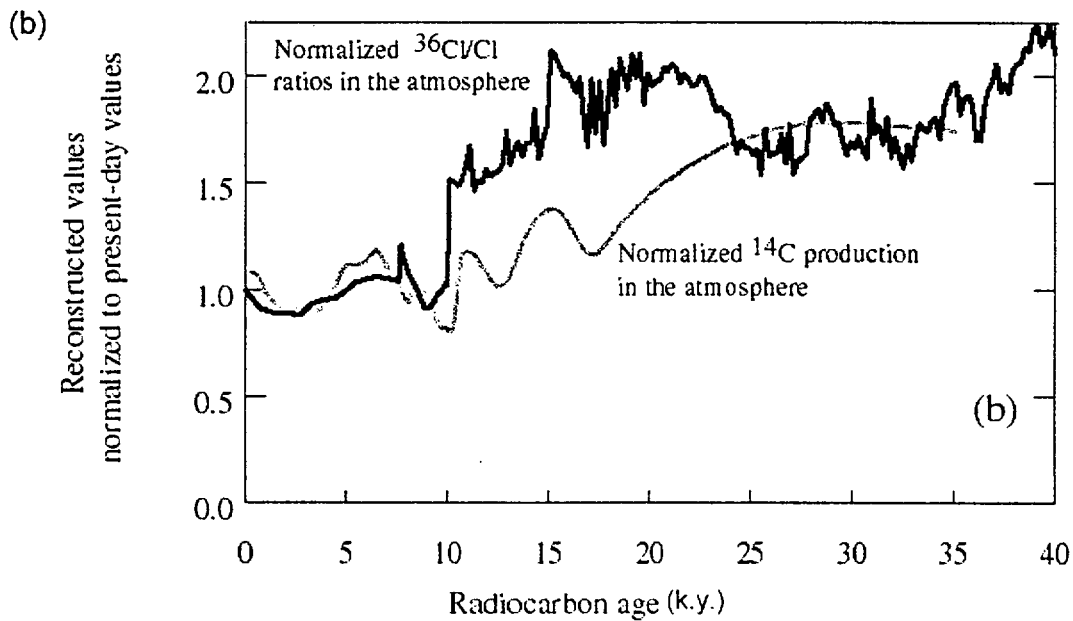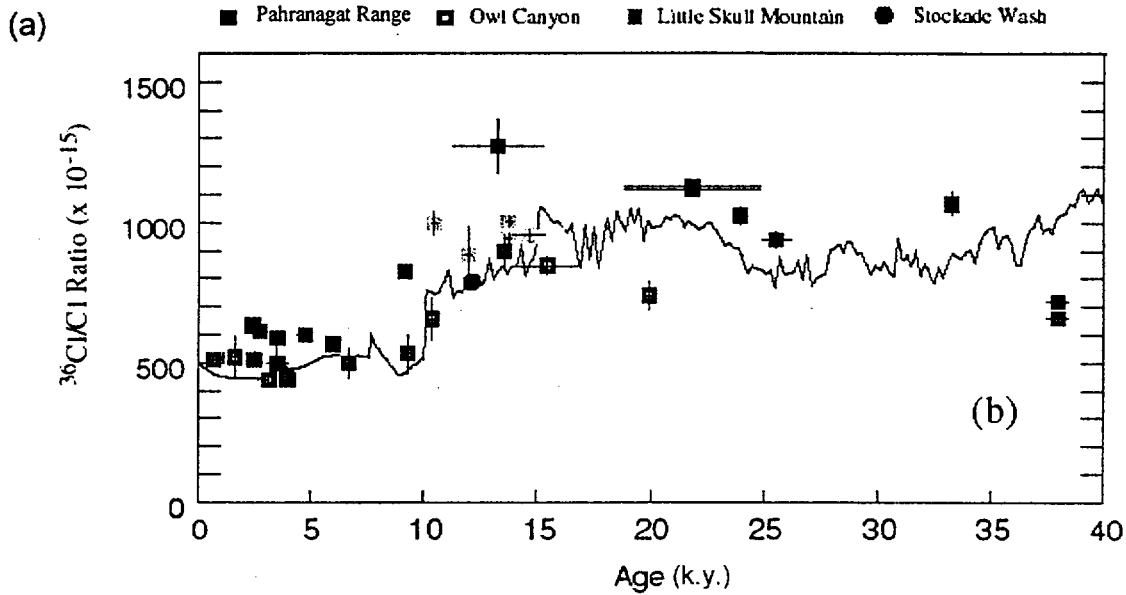
Source: CRWMS M&O (2000, Figure 31)

NOTE: The top plot compares the reconstructed chlorine-36/chlorine ratio to measured chlorine-36/chlorine ratios for fossilized pack-rat urine from southern Nevada (based on Plummer et al. 1997, Figure 2). The bottom plot compares the reconstructed chlorine-36/chlorine ratio (normalized to a present-day value of 500 x 10^{-15}) to the reconstructed carbon-14 activity of Plummer et al. (1997, Figure 3B).

Figure 5.3-30. Reconstructed Atmospheric Chlorine-36/Chlorine Ratio

North Ramp   Main Drift   South Ramp

Measured ^{36}Cl/Cl Ratio (x 10^{-15})

4000

3000

2000

1000

0

Estimated range
of meteoric signal
over past 50 k.y.

Present-day
meteoric
background

0   10   20   30   40   50   60   70   80

ESF Station

■ Systematic rock samples

□ Feature-based rock samples (e.g., fractures, faults, breccia, unit contacts)
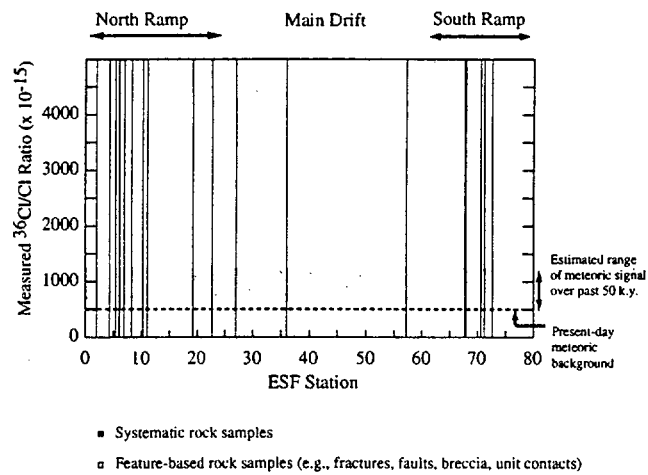
Source: CRWMS M&O (2000, Figure 32)

NOTE: This plot shows the distribution of chlorine-36/chlorine ratios measured for rock samples in the Exploratory Studies Facility. Faults in the Exploratory Studies Facility that correlate with mapped faults at the surface are shown. Exploratory Studies Facility stations are labeled in 100-m increments. Analytical uncertainties are less than 10 percent.

Figure 5.3-31. Distribution of Chlorine-36/Chlorine in the Exploratory Studies Facility
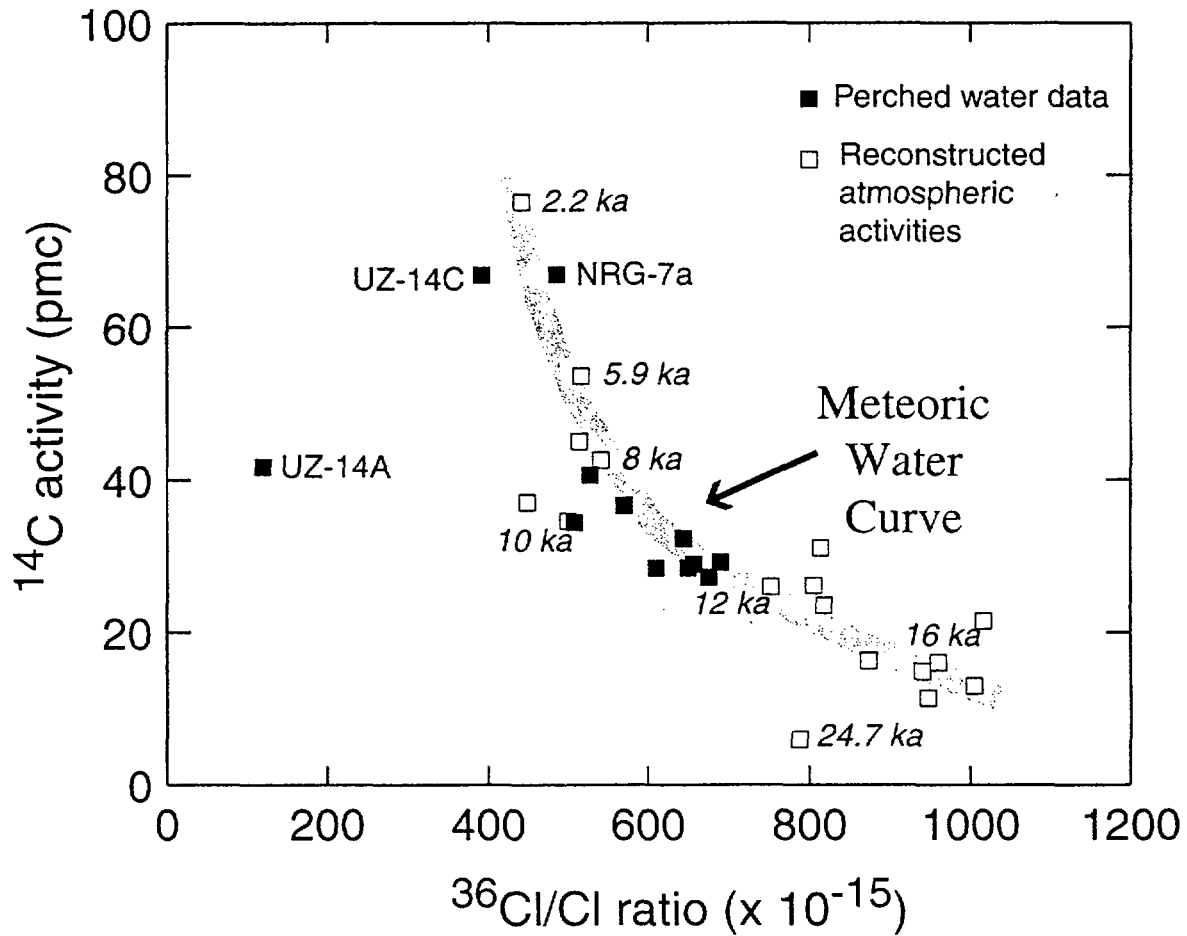
Source: CRWMS M&O (2000, Figure 33)

NOTE: Reconstructed carbon-14 and chlorine-36 activities in the atmosphere for the last 20 ka, compared with activities measured in perched water from UZ-14, SD-7, and NRG-7a. Perched water data are plotted with black squares, using carbon-14 and chlorine-36 data shown in Table 5.3-7. Reconstructed activities (gray squares) are plotted in the lower part of Figure 5.3-30. Key perched water data points are identified by borehole and sample identifier, and key reconstruction points are identified by age.

pmc = percent modern carbon.

Figure 5.3-32. Meteoric and Atmospheric Carbon-14 and Chlorine-36 Activities
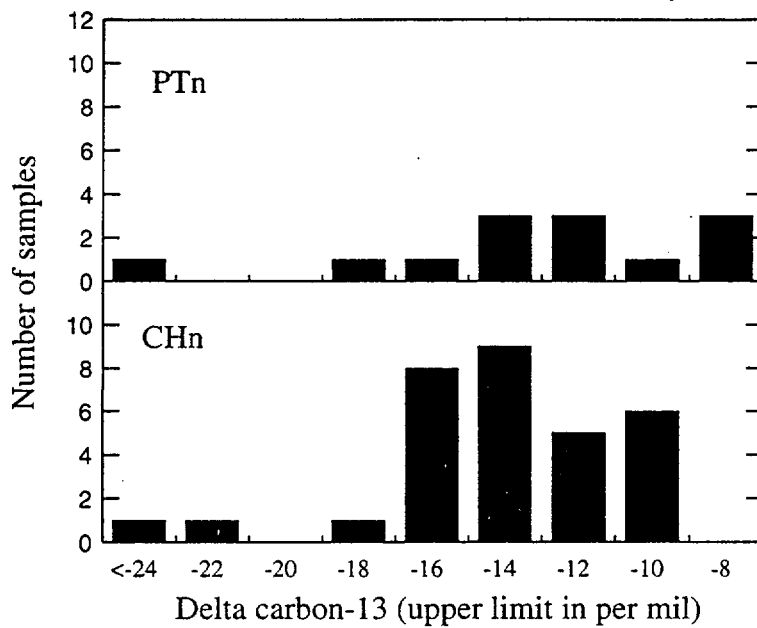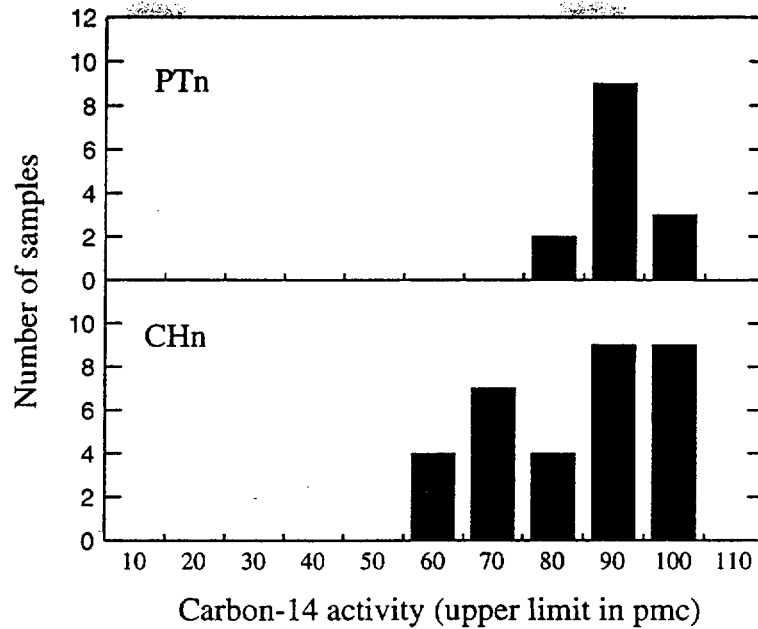
Source: CRWMS M&O (2000, Figure 34)

NOTE: Frequency histograms comparing the distribution of carbon-14 activities and stable carbon isotope ratios of unsaturated zone pore waters in the Paintbrush Tuff nonwelded and Calico Hills nonwelded hydrogeologic units of Yucca Mountain.

Figure 5.3-33. Histogram of Carbon Isotopes in Pore Waters

(a) Unsaturated zone porewaters

(c) Perched water

(b) Unsaturated zone gases

(d) Saturated zone groundwaters

Delta carbon-13 (per mil)

Carbon-14 activity (pmc)
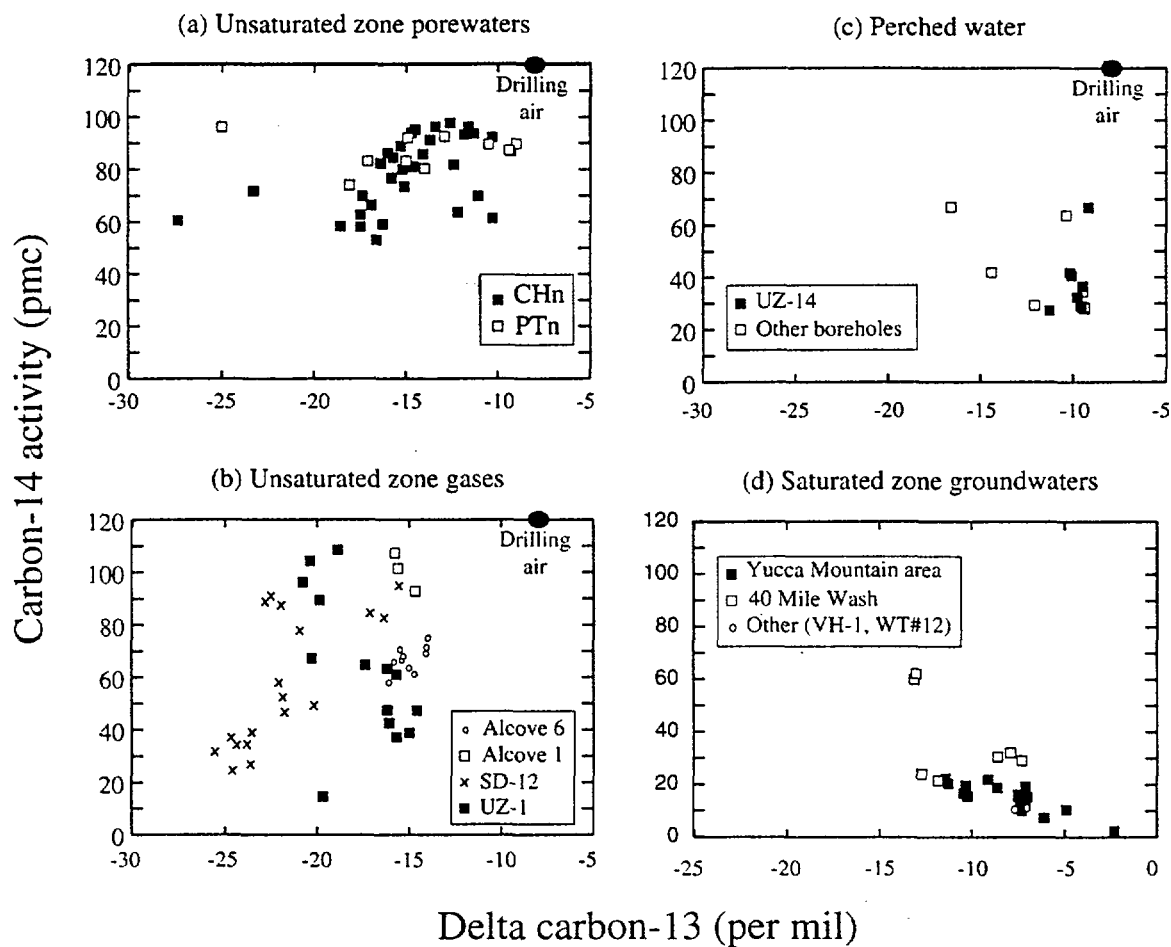
53-34.AI.SITEDESC-R01

Source: CRWMS M&O (2000, Figure 35)

NOTE: Plots show carbon-14 activity versus stable carbon isotopic ratio for (a) pore waters from the unsaturated zone, (b) gas from the unsaturated zone, (c) perched water, and (d) groundwaters. Delta carbon-13 is normalized to Peedee Belemnite Standard.

Figure 5.3-34. Carbon-14 versus Stable Carbon for Yucca Mountain Waters and Gases
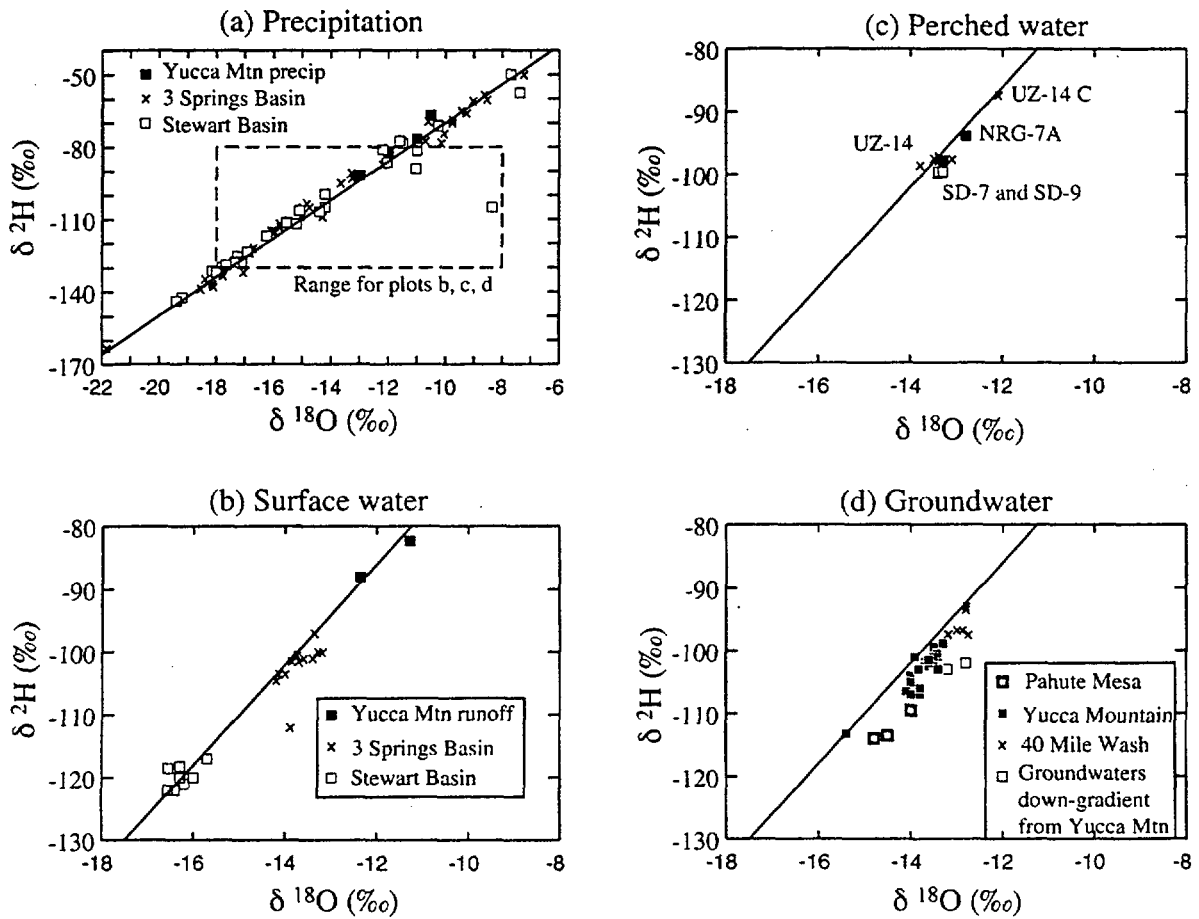
Source: CRWMS M&O (2000, Figure 36)

NOTE: This plot shows δ^2H and $\delta^{18}O$ compositions of (a) local precipitation, (b) local surface water, (c) perched water, and (d) Yucca Mountain groundwaters. Both $\delta^{18}O$ and δ^2H are normalized to standard mean ocean water (SMOW).

Figure 5.3-35. Delta Hydrogen-2 and Delta Oxygen-18 Compositions of Yucca Mountain Waters

(a) UZ-14 porewater, distilled

(b) UZ-14 porewater, squeezed
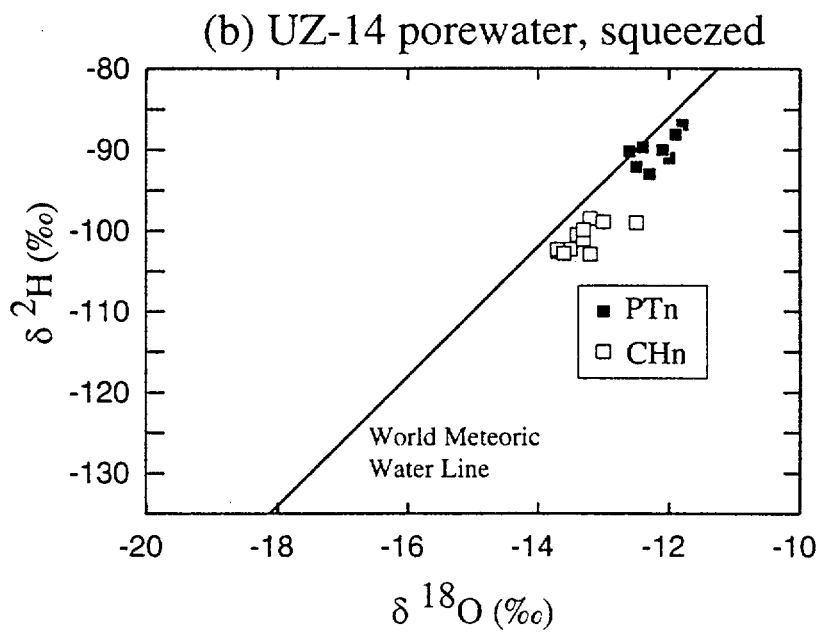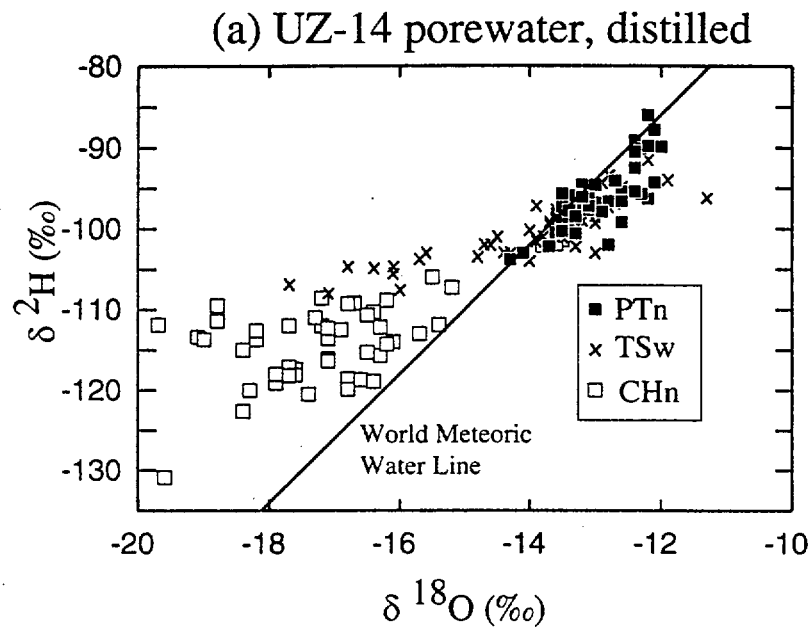
53-36.AI.SITEDESC-R01

Source: CRWMS M&O (2000, Figure 37)

NOTE: This plot contrasts the stable isotopic signatures obtained for pore waters extracted using two different methods of extraction: (a) pore water extracted by distillation and (b) pore water extracted by squeezing.

Figure 5.3-36.   Plot of Delta Hydrogen-2 versus Delta Oxygen-18 Showing Pore Water Compositions in UZ-14
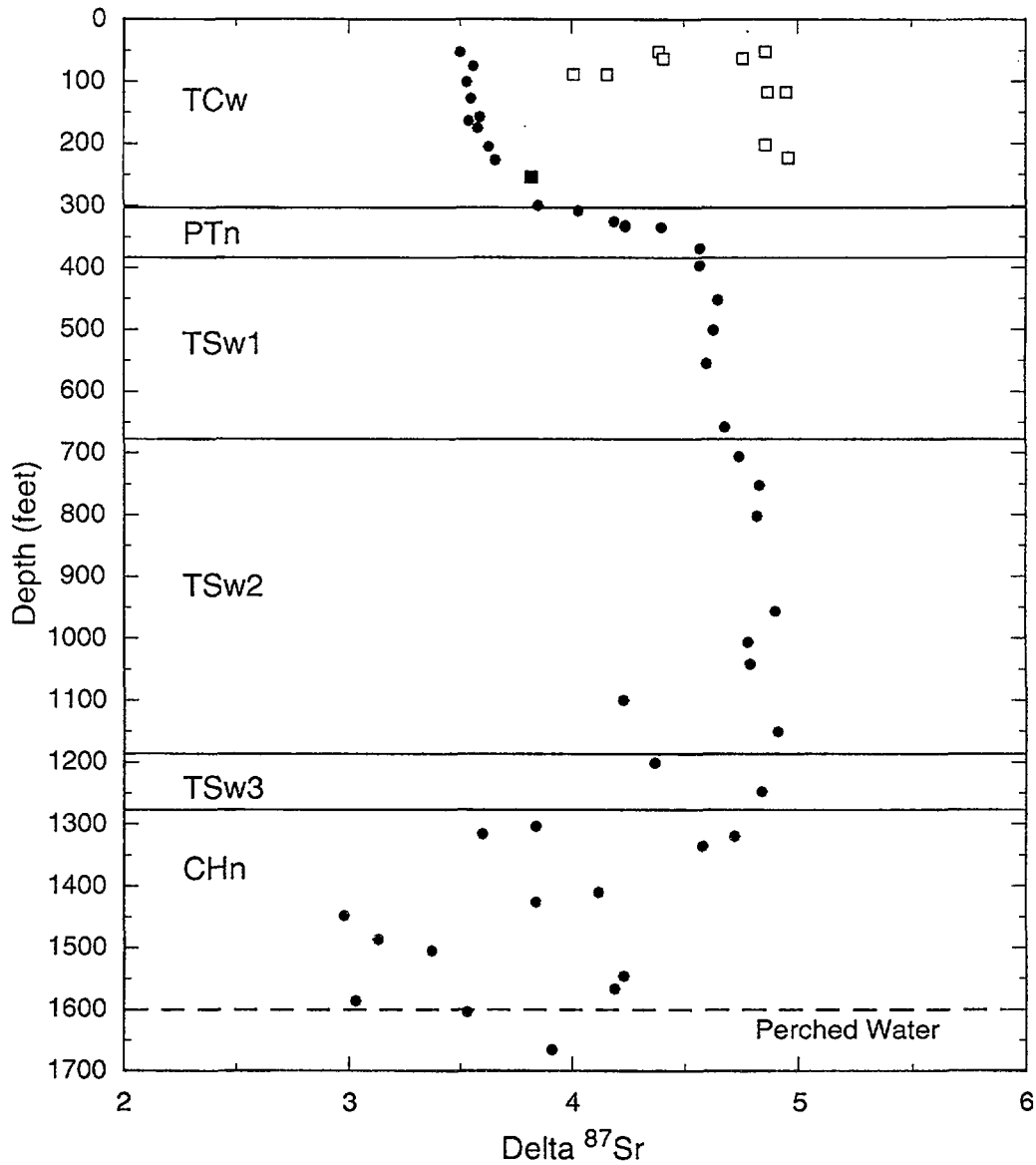
Source: CRWMS M&O (2000, Figure 38)

NOTE: Delta strontium-87 (per mil) of pore waters (black dots) and calcite fracture coatings (boxes) in SD-7 as a function of depth are shown. Pore water strontium isotope compositions in SD-7 vary as a function of depth due to water-rock interaction, especially within the Paintbrush Tuff nonwelded unit. The range of strontium isotope compositions of calcite collected from soils in the vicinity of the SD-7 drill pad are shown by the bar at top. Delta strontium-87 values are calculated from strontium isotopic ratios using Equation 5.3-7.

Figure 5.3-37. Delta Strontium-87 in SD-7 Pore Waters and Rocks

Uranium concentration and isotopic composition for water collected from the Single Heater Test.
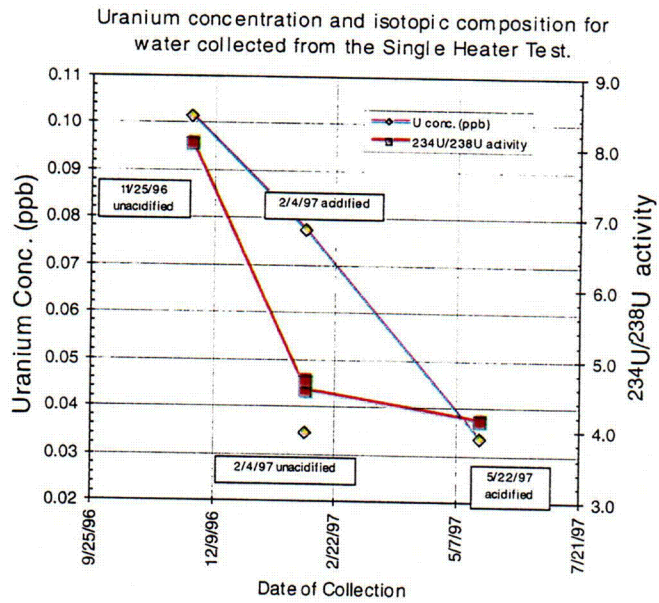
53-38.AI.SITEDESC-R01

Source: CRWMS M&O (2000, Figure 39)

NOTE: Plot shows uranium concentrations and ^{234}U/^{238}U activity ratios in water collected from borehole ESF-TMA-NEU2, zone 4, associated with the Single Heater Test, Exploratory Studies Facility Alcove 5.

Figure 5.3-38. Uranium Concentrations and Uranium-234/Uranium-238 Activity Ratios of Water from the Single Heater Test

C03
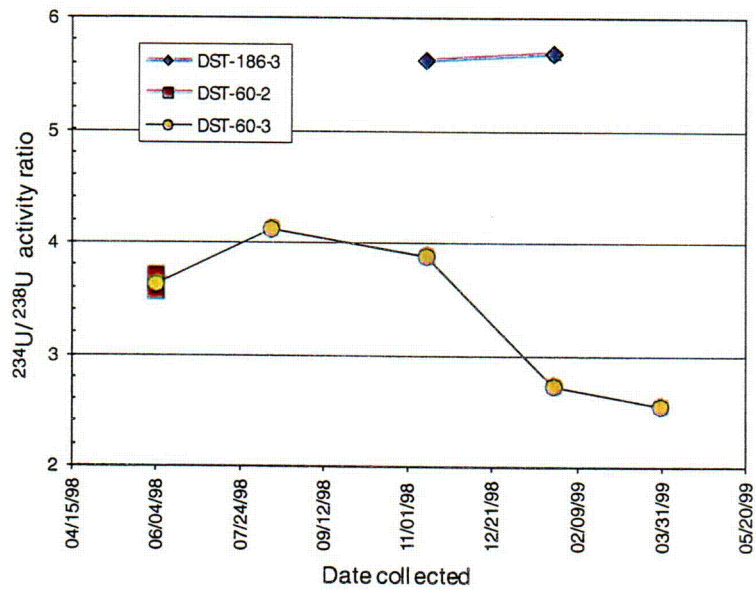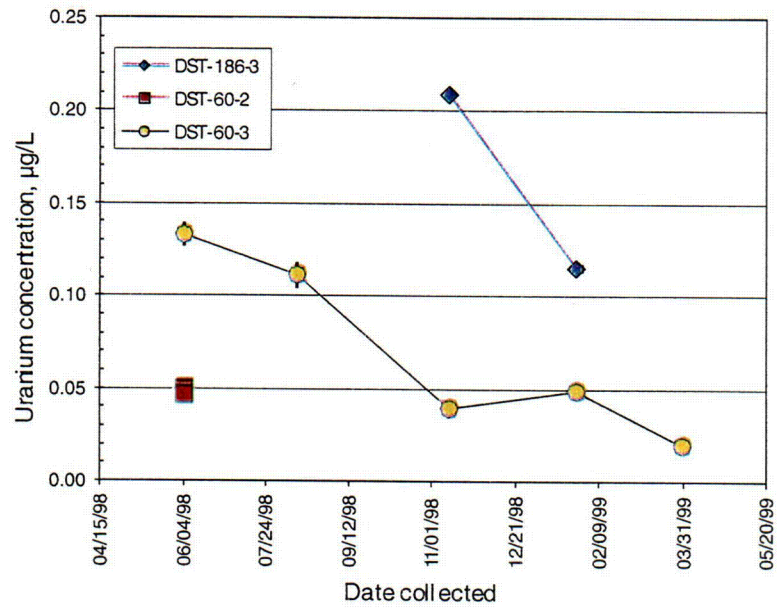
Source: CRWMS M&O (2000, Figure 40)

NOTE: Plots show uranium concentrations and uranium-234/uranium-238 activity ratios in water collected from boreholes associated with the Drift Scale Heater Test, Exploratory Studies Facility Alcove 5.

Figure 5.3-39. Uranium Concentrations and Uranium-234/Uranium-238 Activity Ratios in Water from the Drift Scale Heater Test

C o4

White Rock (1.92)
Captain Jack (2.19)
Comb Peak (2.23)
Water Pipe Butte (2.73)
Topopah (2.23)
Yucca Mtn
Cane (3.81)

UTM - y, in meters

4,140,000
4,120,000
4,100,000
4,080,000
4,060,000
4,040,000
4,020,000
4,000,000

500,000   520,000   540,000   560,000   580,000   600,000

UTM - x, in meters
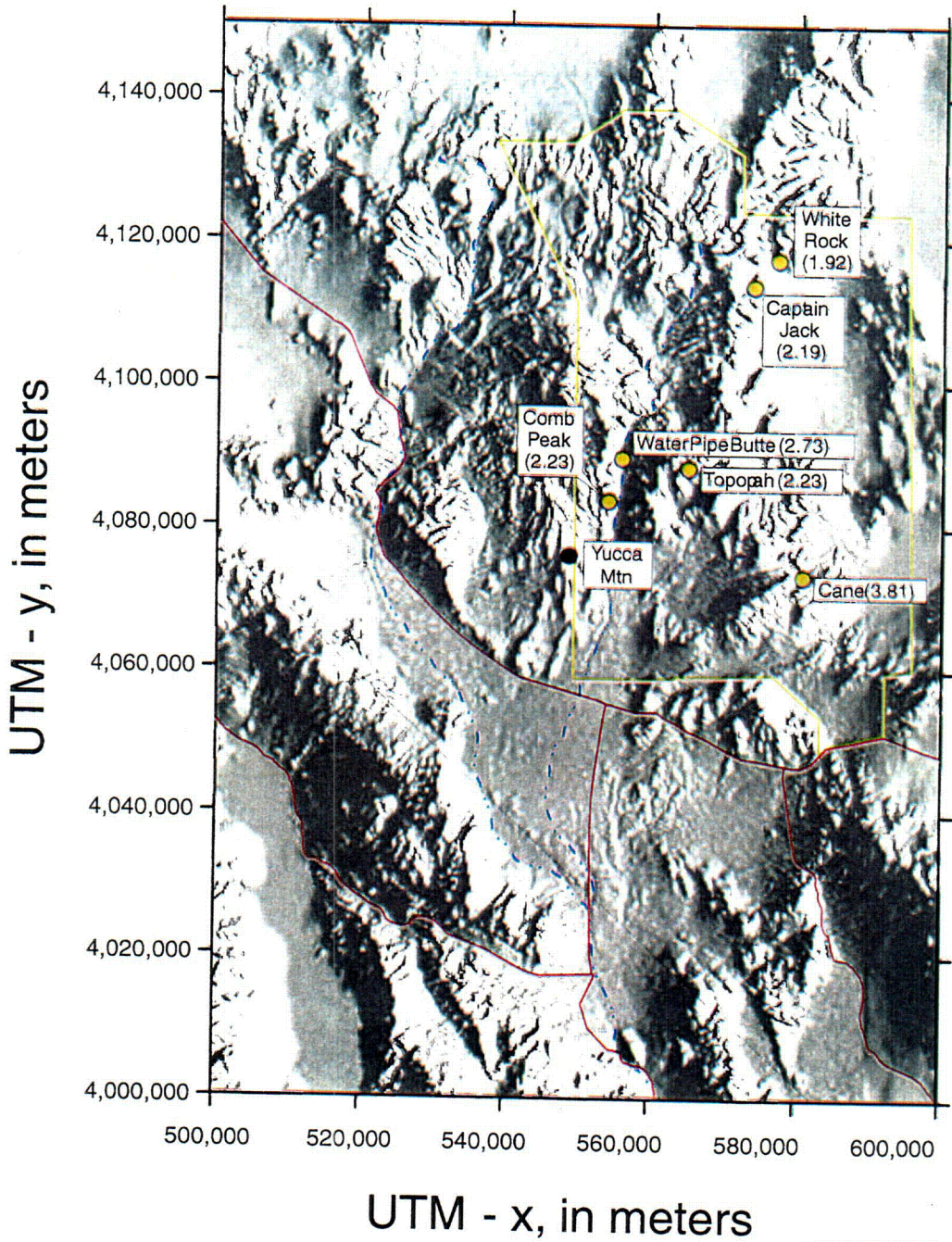
53-40.AI.SITEDESC-R01

Source: CRWMS M&O (2000, Figure 41)

NOTE: This map shows the locations of perched springs on the Nevada Test Site, as well as the uranium-234/uranium-238 activity ratios of the discharge. Yucca Mountain straddles the lower western boundary of the Nevada Test Site (boundary shown as yellow line).

Figure 5.3-40. Uranium-234/Uranium-238 Activity Ratios of Water from Perched Springs

C05
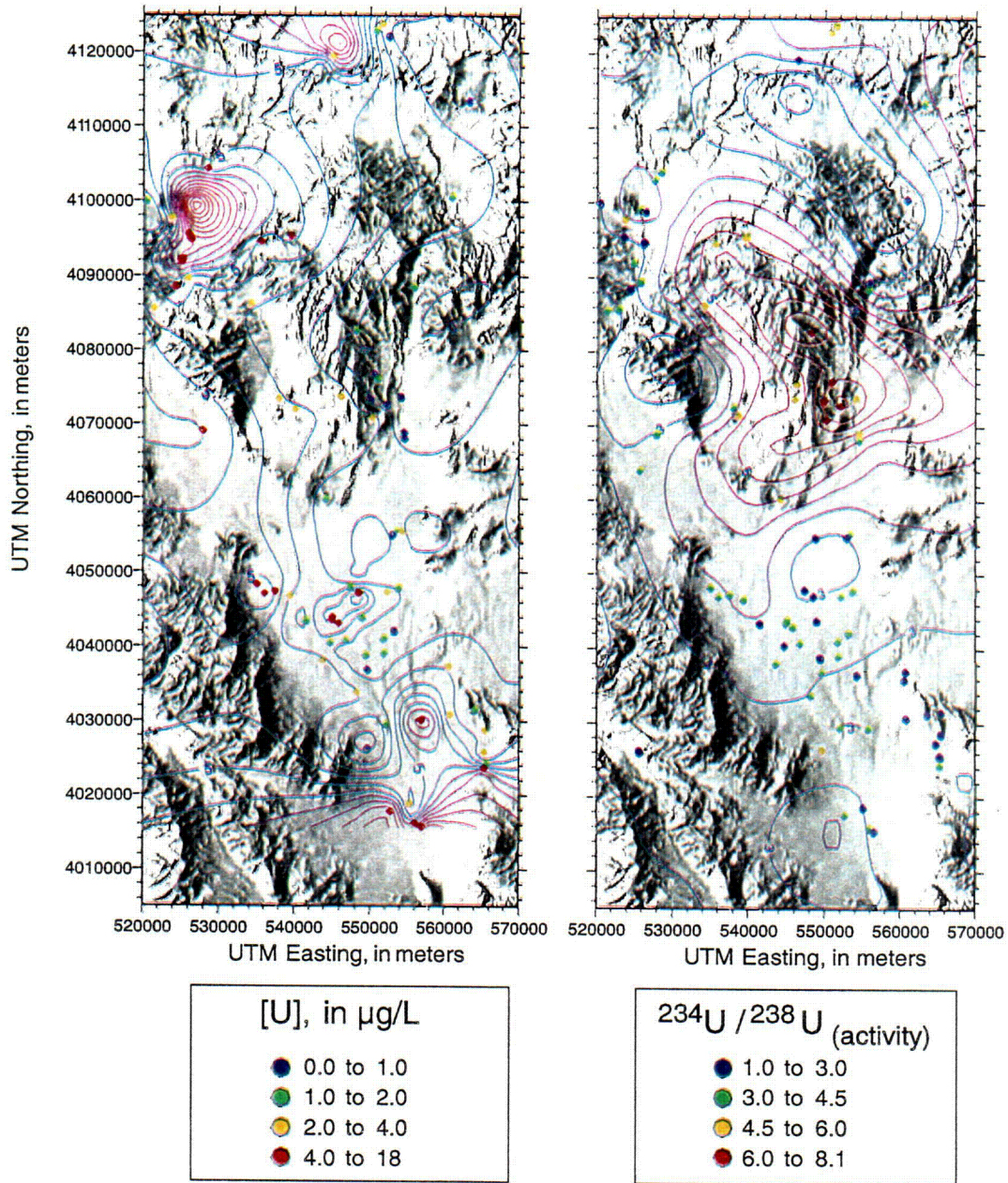
53-41.AI.SITEDESC-R01

Source: CRWMS M&O (2000, Figure 42)

NOTE: Uranium concentrations and $^{234}U/^{238}U$ activity ratios of saturated zone groundwater samples from the vicinity of the Nevada Test Site are shown. The highest activity ratios (right-hand figure) are beneath and slightly east of Yucca Mountain.

Figure 5.3-41. Uranium Concentrations and Uranium-234/Uranium-238 Activity Ratios in Regional Groundwater Samples

C06

53-42.AI.SITEDESC-R01
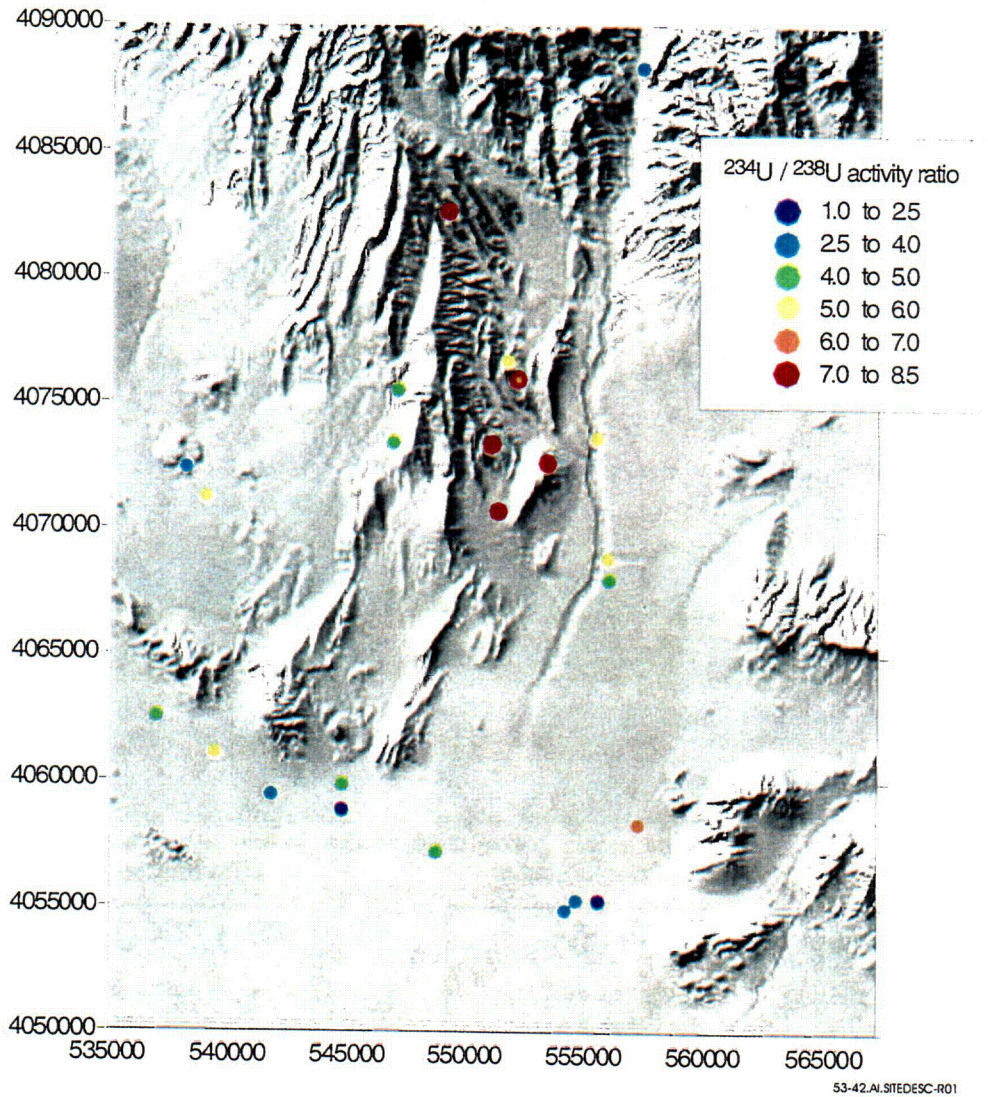
Source: CRWMS M&O (2000, Figure 43)

NOTE: Uranium isotopic compositions of regional saturated zone groundwater samples from the Yucca Mountain vicinity are shown. Yucca Mountain is the long ridge slightly west of the cluster of samples with the highest activity ratios on this map.

Figure 5.3-42. Uranium-234/Uranium-238 Activity Ratios of Groundwater in the Yucca Mountain Vicinity
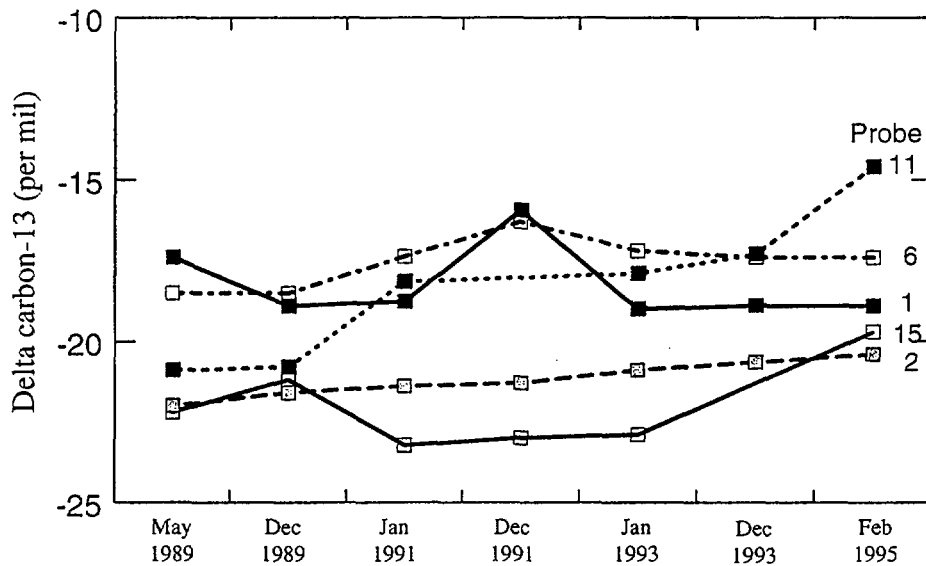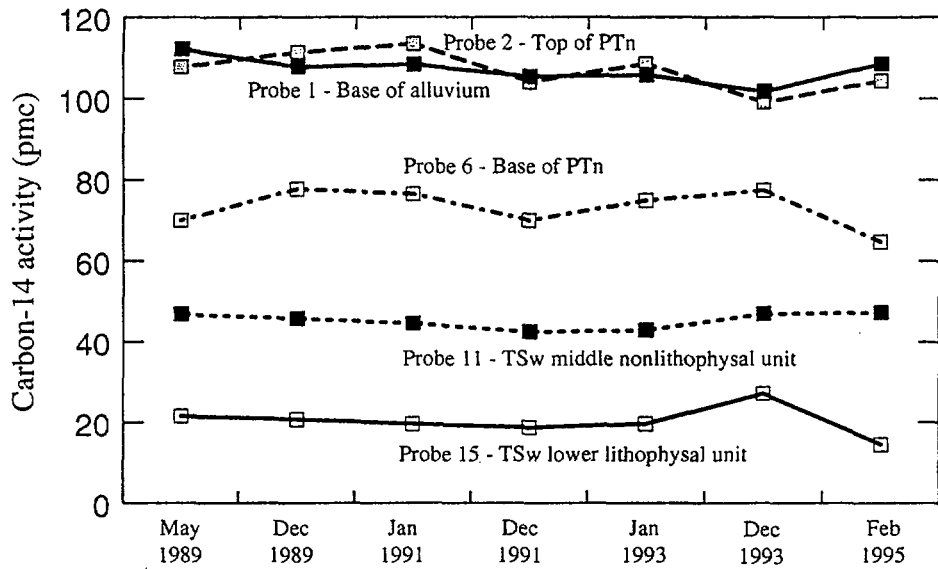
Source: CRWMS M&O (2000, Figure 44)

Figure 5.3-43. Carbon Isotopes in UZ-1 Gases

53-44.DOC.SITEDESC-R01
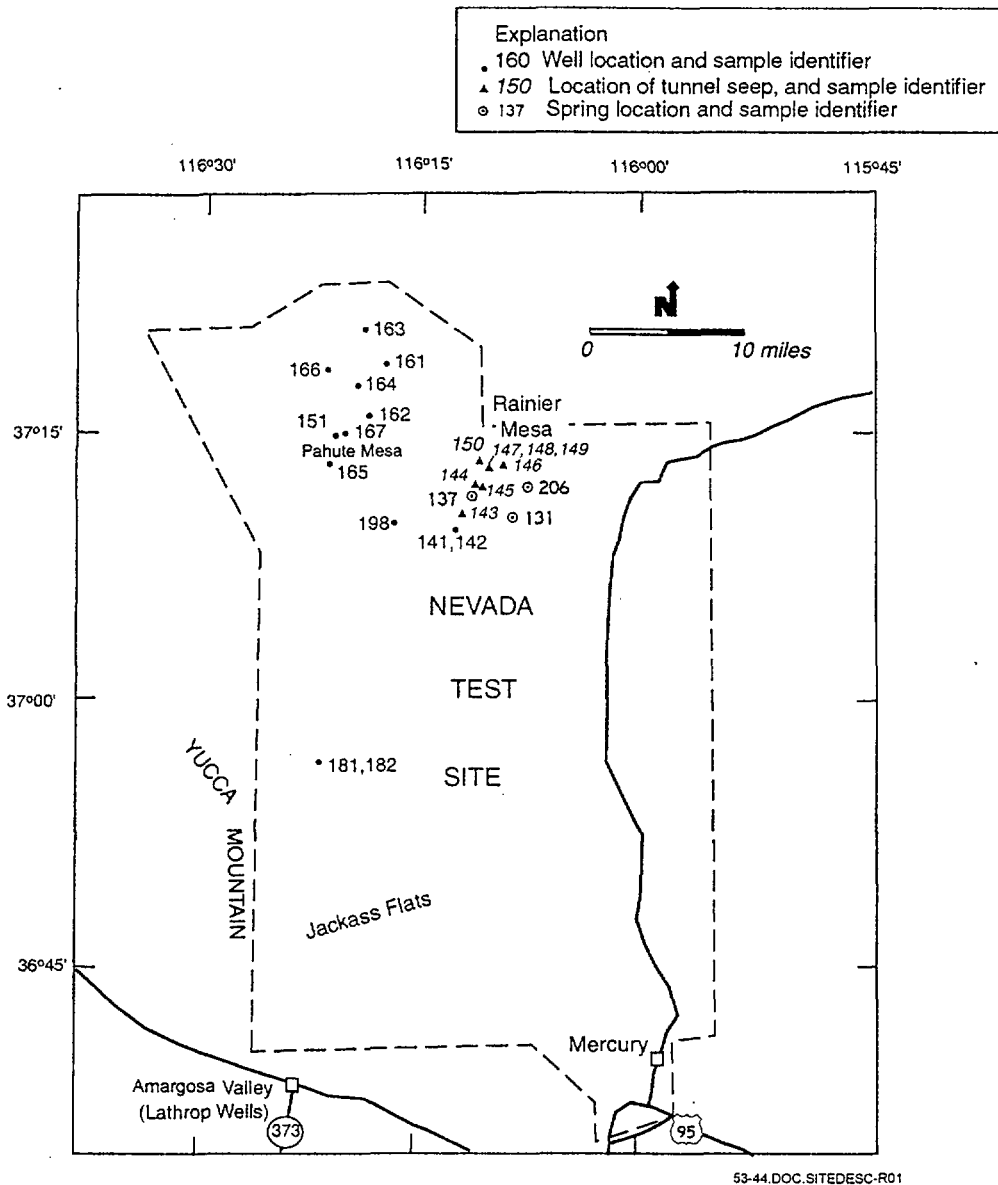
Source: CRWMS M&O (2000, Figure 45)

NOTE: This map shows locations of selected wells and springs in the Nevada Test Site area for which isotopic and geochemical data for water samples are available (McKinley et al. 1991, Figure 4, Table 5).

Figure 5.3-44. Nevada Test Site Wells and Springs

CATIONS   % OF TOTAL MEQ/L   ANIONS
                     13 SAMPLES
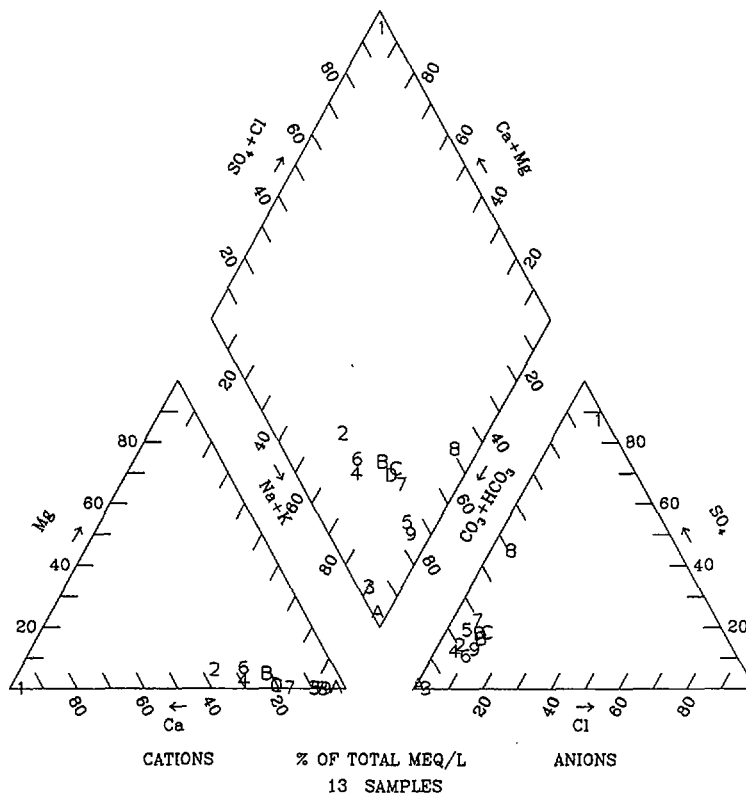
Legend				
List of Plotted Points, Site Numbers, and Borehole Identifiers				
1	152: U-20a#2	6	165: UE-19fs	B 198: Water Well 8
2	161: UE-19b#1	7	166: UE-19gs	C 181: UE-29 a#2 (250-355 m)
3	162: UE-19c	8	167: UE-19i	D 182: UE-29 a#2 (87-213 m)
4	163: UE-19d	9	141: TW-1 (0-171 m)	
5	164: UE-19e	A	142: TW-1 (0-1282 m)	

53-45.DOC.SITEDESC-R01

Source: CRWMS M&O (2000, Figure 47)

NOTES: This trilinear diagram is for groundwaters upgradient of Yucca Mountain, for Pahute Mesa and Rainier Mesa,
         Nevada. The intent of this plot is to show the extent to which different water samples are similar or dissimilar
         in composition. For those waters that are very similar (i.e., data symbols plot over each other), it is not
         important to be able to discern individual points.

Figure 5.3-45. Trilinear Diagram for Upgradient Groundwaters
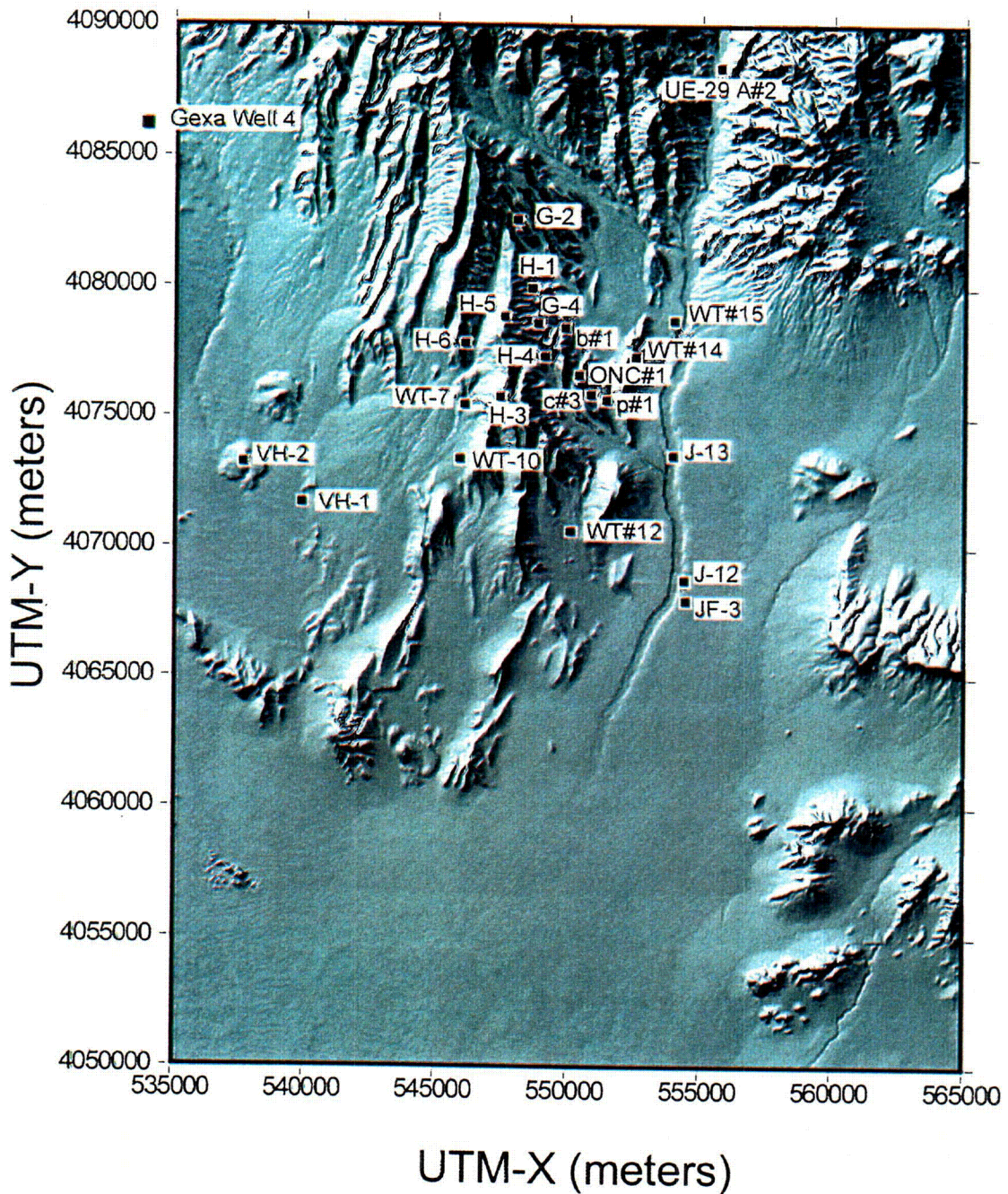
Source: CRWMS M&O (2000, Figure 46)

NOTE: This map shows the locations of selected wells in the vicinity of Yucca Mountain for which geochemical data for groundwater samples are available. Well coordinates are from Table 5.3-23. H-5 and H-3 mark the ridgeline of Yucca Mountain.

Figure 5.3-46. Location of Selected Wells in the Vicinity of Yucca Mountain

C08
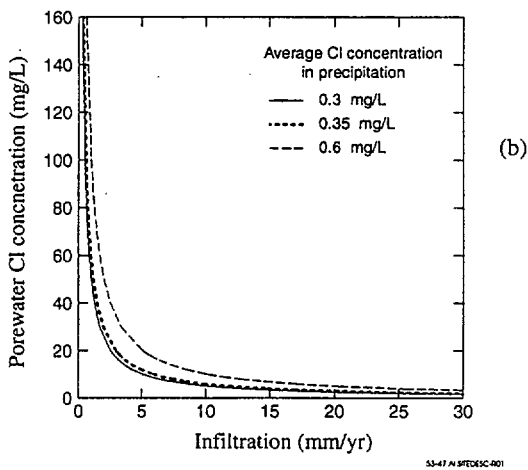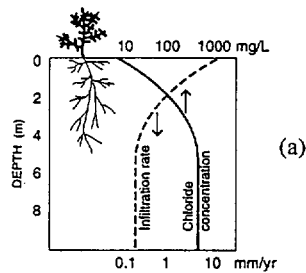
Source: CRWMS M&O (2000, Figure 49)

NOTE: Part (a) is a schematic diagram illustrating the underlying basis of the chloride mass balance method. Part (b) is a plot showing chloride concentrations as a function of infiltration, assuming a range of average chloride concentrations for local precipitation and an average annual precipitation rate of 170 mm. Section 5.3.10.2 contains a discussion of the model, its assumptions, and the basis for these parameter values.

Figure 5.3-47. Chloride Mass-Balance Method for Estimating Infiltration

INTENTIONALLY LEFT BLANK

Table 5.2-1. Chemical Variability in Drill Core Data for High-Silica Rhyolite, Topopah Spring Tuff, Core UE-25 UZ#16 (Normalized Anhydrous)

Compound	Concentration (%)		Average (1 std. dev.) (%)
	Minimum	Maximum	
SiO_2	76.37	77.40	76.92(31)
TiO_2	0.09	0.13	0.10(1)
Al_2O_3	12.43	13.01	12.74(17)
Fe_2O_3	0.97	1.07	1.00(2)
MnO	0.058	0.074	0.068(4)
MgO	0.00	0.24	0.12(8)
CaO	0.43	0.50	0.46(2)
K_2O	4.96	5.17	5.05(6)
Na_2O	3.42	3.68	3.54(6)
Trace Element	Concentration (ppm)		Average (1 std. dev.) (%)
	Minimum	Maximum	
Zn	44	62	50(5)
Rb	177	195	185(6)
Sr	13	44	29(8)
Y	11	49	29(9)
Zr	117	153	126(11)
Nb	0	31	20(8)

Source: Bish et al. (1996, Table 3.19)

NOTE: Values are for unaltered (stellerite-free) high-silica rhyolite; number of samples = 17.

Table 5.2-2. X-Ray Diffraction Mineralogy of Altered Topopah Spring Vitrophyre

			Concentration (wt. %)						
Sample	Depth (ft)	Depth (m)	Smectite	Heulandite	Quartz	Cristobalite	Alkali Feldspar	Opal-CT	Other
G-1	1286	392.0	33±7	10±1	3±1	16±1	38±5	ND	
GU-3	1195.7	364.5	ND	~1	8±2	22±3	70±5	ND	trace[a]
G-4	1299	395.9	2±1	5±2	8±2	23±4	62±10	ND	trace[a]
	1314	400.5	45±10	28±5	2±1	14±4	11±5	ND	
H-5	1666	507.8	37±16	20±5	3±1	ND	24±7	15±7	~0.6[b]

Source: Adapted from Bish and Chipera (1989, pp. 27, 36, 41) and Bish and Chipera (1991)

NOTES: [a] Mica

[b] Erionite–special techniques to detect erionite were used for this sample only.

ND = not detected

Table 5.3-1. Types of Isotopic and Geochemical Data Collected for Unsaturated Zone Fluids at Yucca Mountain

Borehole Shorthand Identifier	Official Borehole Identifier (Depth in Meters Shown for Surface-Based Holes)	Analyses of Pore Waters or Leached Salts						Gas and Water Vapor Analyses	Perched-Water Analyses
		Chem	^{3}H	^{13,14}C (Pore)	δ^2H, δ^{18}O	^{36}Cl	Other		
NRG#4	UE-25 NRG#4 (221)	–	–	–	–	•	–	–	–
NRG#5	UE-25 NRG#5 (411)	–	–	–	–	•	–	–	–
NRG-6	USW NRG-6 (335)	•	•	•	•	•	–	CO_2, CH_4, ^{13,14}C, ^{18}O	–
NRG-7a	USW NRG-7a (461)	•	•	•	•	•	^{234,238}U	CO_2, CH_4, ^{13,14}C	Chem, ^{3}H, ^{13,14}C, ^{2}H, ^{18}O, ^{36}Cl, ^{87}Sr, ^{234,238}U
ONC#1	UE-25 ONC#1 (469)	–	–	–	–	•	–	–	–
SD-12	USW SD-12 (660)	•	•	•	•	•	–	CO_2, CH_4, ^{13,14}C, ^{18}O	
SD-6	USW SD-6 (774)	•	•	•	•	–	^{87}Sr	–	–
SD-7	USW SD-7 (815)	•	•	•	•	–	^{87}Sr	^{13,14}C, CO_2, ^{18}O	Chem, ^{3}H, ^{13,14}C, ^{2}H, ^{18}O, ^{36}Cl, ^{234,238}U
SD-9	USW SD-9 (678)	•	•	•	•	–	^{234,238}U	CO_2, CH_4, ^{13,14}C, ^{18}O	Chem, ^{3}H, ^{13,14}C, ^{2}H, ^{18}O, ^{36}Cl, ^{87}Sr, ^{234,238}U
UZ#16	UE-25 UZ#16 (514)	•	?	•	•	•	–	^{13,14}C, CO_2, CH_4, ^{18}O	–
UZ#4	UE-25 UZ#4 (112)	•	•	•	•	–	–	–	–
UZ#5	UE-25 UZ#5 (111)	•	•	•	•	–	–	–	–
UZ-1	USW UZ-1 (387)	–	•	–	–	–	–	CO_2, atm gases, ^{13,14}C, ^{2}H, ^{18}O, ^{3}H	^{3}H, ^{13,14}C, ^{2}H, ^{18}O, ^{36}Cl
UZ-13	USW UZ-13 (18)	–	–	–	–	–	–	CO_2, CH_4, ^{13,14}C, ^{18}O	–

Table 5.3-1. Types of Isotopic and Geochemical Data Collected for Unsaturated Zone Fluids at Yucca Mountain (Continued)

Borehole Shorthand Identifier	Official Borehole Identifier (Depth in Meters Shown for Surface-Based Holes)	Analyses of Pore Waters or Leached Salts						Gas and Water Vapor Analyses	Perched-Water Analyses
		Chem	^{3}H	$^{13,\,14}$C (Pore)	δ^2H, δ^{18}O	^{36}Cl	Other		
UZ-14	USW UZ-14 (678)	•	•	•	•	•	^{234,238}U	^{13,14}C, CO_2	Chem, ^{3}H, ^{13,14}C, ^{2}H, ^{18}O, ^{36}Cl, ^{87}Sr, ^{234,238}U
UZ-6	USW UZ-6 (575)	–	–	–	–	–	–	CO_2, CH_4, ^{13,14}C, ^{18}O	–
UZ-6s	USW UZ-6s (158)	–	–	–	–	–	–	CO_2, ^{13,14}C, ^{18}O, atm gases	–
UZ-7a	USW UZ-7a (235)	•	•	–	–	–	–	CO_2, CH_4, ^{13}C, ^{18}O	–
UZN#1	UE-25 UZN#1 (15)	–	•	–	–	–	–	–	–
UZN#2	UE-25 UZN#2 (15)	–	–	–	–	–	–	–	Chem, ^{36}Cl
UZN#39	UE-25 UZN#39 (18)	–	–	–	–	•	–	–	–
UZN#8	UE-25 UZN#8 (14)	–	•	–	–	–	–	–	–
UZN#91	UE-29 UZN#91 (29)	–	–	–	–	–	–	–	^{36}Cl
UZ-N11	USW UZ-N11 (26)	–	–	–	–	•	–	–	–
UZ-N15	USW UZ-N15 (18)	–	–	–	–	•	–	–	–
UZ-N16	USW UZ-N16 (18)	–	–	–	–	•	–	–	–
UZ-N17	USW UZ-N17 (18)	–	–	–	–	•	–	–	–
UZ-N27	USW UZ-N27 (62)	–	–	–	–	•	–	^{13,14}C, ^{18}O	–
UZ-N36	USW UZ-N36 (18)	–	–	–	–	•	–	–	–
UZ-N37	USW UZ-N37 (83)	–	–	–	–	•	–	–	–
UZ-N38	USW UZ-N38 (27)	–	–	–	–	•	–	–	–
UZ-N43	USW UZ-N43 (14)	–	–	–	–	•	–	–	–
UZ-N46	USW UZ-N46 (30)	–	–	–	–	–	–	–	Chem
UZ-N53	USW UZ-N53 (72)	–	–	–	–	•	–	–	–

Table 5.3-1. Types of Isotopic and Geochemical Data Collected for Unsaturated Zone Fluids at Yucca Mountain (Continued)

Borehole Shorthand Identifier	Official Borehole Identifier (Depth in Meters Shown for Surface-Based Holes)	Analyses of Pore Waters or Leached Salts						Gas and Water Vapor Analyses	Perched-Water Analyses
		Chem	^{3}H	$^{13,\,14}$C (Pore)	δ^2H, δ^{18}O	^{36}Cl	Other		
UZ-N54	USW UZ-N54 (75)	–	–	–	–	•	–	–	–
UZ-N55	USW UZ-N55 (78)	•	–	–	–	•	–	–	–
UZ-N61	USW UZ-N61 (36)	–	–	–	–	•	–	–	–
UZ-N62	USW UZ-N62 (18)	–	–	–	–	•	–	^{13,14}C, ^{18}O	–
UZ-N64	USW UZ-N64 (18)	–	–	–	–	•	–	^{13,14}C, ^{18}O	–
UZ-N90	USW UZ-N90 (14)	–	•	–	–	–	–	–	–
UZ-N93	USW UZ-N93 (12)	–	–	–	–	–	–	CO_2, CH_4, ^{13,14}C, ^{18}O	–
UZ-N94	USW UZ-N94 (9)	–	–	–	–	–	–	CO_2, CH_4, ^{13,14}C, ^{18}O	–
UZ-N95	USW UZ-N95 (6)	–	–	–	–	–	–	CO_2, CH_4, ^{13,14}C, ^{18}O	–
WT#18	UE-25 WT#18 (623)	–	–	–	–	–	–	CO_2, CH_4, ^{13}C, ^{18}O	–
WT#4	UE-25 WT#4 (482)	–	–	–	–	–	–	CO_2, CH_4	–
WT-24	USW WT-24 (Not available)	•	•	–	–	–	–	–	Chem, ^{3}H, ^{13,14}C, ^{2}H, ^{18}O, ^{36}Cl, ^{87}Sr, ^{234,238}U
Busted Butte	UZTT-BB-PH1-2	•	–	–	–	•	–	–	–
Busted Butte	UZTT-BB-PH1-3	•	–	–	–	•	–	–	–
Busted Butte	UZTT-BB-PH1-4	•	–	–	–	•	–	–	–
Busted Butte	UZTT-BB-PH1-6	•	–	–	–	•	–	–	–
Busted Butte	UZTT-BB-PH1-7	•	–	–	–	–	–	–	–
Cross Drift	Cross Drift samples collected from walls (manually or with dry excavation method)	–	–	–	–	•	–	–	–
Cross Drift	ECRB-SYS-CSnnnn holes, where nnnn is distance in meters	Cl, Br, SO_4	–	–	–	–	–	–	–

Table 5.3-1. Types of Isotopic and Geochemical Data Collected for Unsaturated Zone Fluids at Yucca Mountain (Continued)

Borehole Shorthand Identifier	Official Borehole Identifier (Depth in Meters Shown for Surface-Based Holes)	Analyses of Pore Waters or Leached Salts						Gas and Water Vapor Analyses	Perched-Water Analyses
		Chem	^{3}H	$^{13,\,14}$C (Pore)	δ^2H, δ^{18}O	^{36}Cl	Other		
ESF	ESF samples collected from walls of Main Drift or alcoves (manually or with dry excavation method)	–	•	–	–	•	^{87}Sr	–	–
ESF Alcove #1	ESF-AL#1-RBT#1, #2, #3	–	–	–	–	–	–	^{13,14}C, ^{18}O	–
ESF Alcove #1	Seeps from infiltration test	Cl, Br, SO$_4$	–	–	–	•	–	–	–
ESF Alcove #2	ESF-AL#2-HPF#1	–	•	–	–	–	–	–	–
ESF Alcove #2	ESF-LPCA-MOISTSTDY#n	Cl, Br, SO$_4$	–	–	–	–	–	–	–
ESF Alcove #3	ESF-AL#3-RBT#1, #4	•	•	•	–	–	–	–	–
ESF Alcove #5	Single Heater Test (SHT) Hole 16	•	–	–	–	•	^{234,238}U	–	–
ESF Alcove #5	ESF-AL5	Sr	•	–	–	–	^{87}Sr	–	–
ESF Alcove #5	ESF-HD-PERM-1, -3	Cl, Br, SO$_4$	•	–	•	–	^{87}Sr, ^{234,238}U	–	–
ESF Alcove #5	ESF-TMA-NEU-2	–	•	–	–	–	–	–	–
ESF Alcove #5	Drift Scale Heater Test Holes, DST-60 and DST-186	–	–	–	–	–	^{234,238}U	–	–
ESF Alcove #6	ESF-NAD-GTB#1A	–	•	–	–	–	–	^{13,14}C, ^{18}O, CO$_2$	–
ESF Main Drift	ECRB-CWAT#1, #2, #3	Cl, Br, SO$_4$	•	–	•	–	^{87}Sr	–	–
ESF Main Drift	ESF-MD-WATMOV#nn	Cl, Br, SO$_4$	–	–	–	–	–	–	–
ESF Niche #1	ESF-MD-NICHE3566#1, #2, LT#1	Cl, Br, SO$_4$	–	–	–	•	–	–	–
ESF Niche #1	ESF-MD-NICHE3650#nn	Cl, Br, SO$_4$	–	–	–	–	–	–	–

Table 5.3-1. Types of Isotopic and Geochemical Data Collected for Unsaturated Zone Fluids at Yucca Mountain (Continued)

Borehole Shorthand Identifier	Official Borehole Identifier (Depth in Meters Shown for Surface-Based Holes)	Analyses of Pore Waters or Leached Salts						Gas and Water Vapor Analyses	Perched-Water Analyses
		Chem	^3H	$^{13,\,14}C$ (Pore)	$\delta^2H,\ \delta^{18}O$	^{36}Cl	Other		
ESF North Ramp	ESF-NR-MOISTSTDY#nn	Cl, Br, SO$_4$	–	•	–	•	–	–	–
ESF South Ramp	ESF-SR-MOISTSTDY#nn	Cl, Br, SO$_4$	–	–	•	–	–	–	–

Source: CRWMS M&O (2000, Table 3)

NOTES: Abbreviations for types of analyses: Chem = pore-water chemistry; ^3H = tritium; $^{13,\,14}C$ (pore) = carbon-13 and carbon-14 analyses for pore waters; $\delta^2H,\ \delta^{18}O$ = stable hydrogen (deuterium) and oxygen isotopes; ^{36}Cl = chlorine-36; – = no analyses conducted; • = analyses conducted

Table 5.3-2. Average Annual Weighted Concentrations for Precipitation, 3 Springs Basin, Nevada

Nominal Year	Start	End	Total Precipitation (cm)	Annual Weighted Concentration (mg/L)								
				Alkalinity as $CaCO_3$	Equivalent HCO_3	Ca	Mg	Na	K	SO_4	Cl	SiO_2
3 Springs Creek												
1986	850924	860930	13.93	2.67	3.26	0.61	0.06	0.40	0.15	0.73	0.34	0.13
1987	860930	880109	15.58	2.04	2.49	0.46	0.04	0.34	0.13	0.63	0.31	0.08
1988	880109	890223	14.24	2.93	3.57	0.98	0.09	0.78	0.28	1.12	0.47	0.13
1989	890223	891108	5.85	4.30	5.25	1.06	0.18	1.03	0.15	1.41	0.59	0.19
1990	891108	910130	12.62	1.40	1.70	0.81	0.08	0.79	0.20	1.12	0.56	N/C
1991	910130	910925	11.65	N/C	N/C	0.73	0.08	0.46	0.17	1.13	0.25	N/C
1992	910925	920917	13.94	N/C	N/C	0.49	0.05	0.23	0.15	0.81	0.17	N/C
Kawich Peak												
1989	881001	891108	13.44	3.23	3.94	0.97	0.16	0.97	0.16	1.27	0.64	0.20
1990	891108	910130	15.07	1.83	2.23	0.73	0.07	0.62	0.64	0.96	0.39	N/C
1991	910130	920218	17.77	N/C	N/C	0.68	0.07	0.95	0.15	0.95	0.31	N/C
1992	920218	920917	6.8	N/C	N/C	0.66	0.07	0.32	0.21	1.25	0.31	N/C
Results of linear regression for chlorine as the independent variable												
Y-intercept (assigned value of zero to force line through origin)				0	0	0	0	0	0	0	N/A	0
Standard error of y-intercept				0.91	1.11	0.15	0.03	0.18	0.16	0.30	N/A	0.02
R squared				0.13	0.13	0.38	0.65	0.63	-0.22	-0.49	N/A	0.88
Number of observations				7	7	11	11	11	11	11	N/A	5
X coefficient				5.433	6.628	1.787	0.220	1.578	0.489	2.431	N/A	0.313
Standard error of X coefficient				0.707	0.863	0.111	0.019	0.127	0.116	0.213	N/A	0.016

Sources: CRWMS M&O (2000, Table 5)

NOTES: The calculated regression lines are used solely to provide a way to graphically compare and contrast chemical compositions of the various sources of water at Yucca Mountain and to illustrate general trends of relative enrichment or depletion of one element compared to another. Precipitation data reported in the original source data tracking numbers in inches have been converted to centimeters in this table.

N/A = not applicable; N/C = not calculated

Table 5.3-3. Chemistry of Surface Waters in the Yucca Mountain Region

Location	Location on Figure 5.3-6	Sample Collection date	pH	Spec Cond µS/cm	Ca, mg/L	Mg, mg/L	Na, mg/L	K, mg/L	Cl, mg/L	SO$_4$, mg/L	F, mg/L	HCO$_3$, mg/L	SiO$_2$, mg/L	TDS, mg/L
Busted Butte Wash	60	8/14/84	8.3	120	12	1.8	7	8.1	1.7	7.9	0.3	57	23	100
Delerium Canyon @ mouth	55	2/9/93	7.8	118	12	2.4	7.6	–	3.2	7.8	0.3	48	33	–
Drill Hole Wash @ mouth	58	8/14/84	8.3	100	9.5	1.3	8.6	7.4	2.2	12	0.3	51	20	92
Fortymile Wash @ H Rd	59	8/15/84	8.0	170	21	2.9	8.2	9.1	1.4	10	0.2	91	24	122
Fortymile Wash @ J-12	61	8/14/84	8.2	59	6.7	0.7	2.4	6.3	2	6.3	<0.1	32	4.5	45
Fortymile Wash above Drill Hole	57	8/14/84	8.4	70	8.1	0.9	4.1	5.6	1.3	6.2	<0.1	44	8.7	–
Overland near Fortymile Canyon	56	1/24/95	8.1	164	20	2.9	8.4	4.5	2.6	8.5	0.2	72	23	–
Overland near Pah	52	1/6/95	7.8	134	15	2.8	4.9	3.7	3.4	7.8	0.1	34	18	–
Pagany Wash #1 near UZ-4	29	12/7/92	–	218	21	2.1	13	4.6	10	24	0.2	na	14	–
Pah Canyon	52	2/23/93	8.0	140	14	2.6	9.3	–	4.3	10	0.3	54	34	–
Pah Canyon	52	1/26/95	7.9	145	16	2.9	8.2	4.3	4	7.6	0.3	55	30	100
Split Wash below Quac Wash	33	1/25/95	8.2	199	24	3.4	9.3	8.8	3.7	8.7	0.2	88	19	–
Stockade Wash	23	2/10/93	–	122	15	3.1	6.4	4.3	3.1	6.5	<0.1	55	24	90
Unnamed Tributary	22	1/22/93	–	134	14	2.8	10	3.2	5.1	8.4	0.1	54	20	90
Unnamed Tributary	22	3/23/93	–	164	16	3.6	11	5.2	4.3	9	0.2	76	36	123
Wren Wash @ Yucca Mtn	31	1/25/95	8.2	258	28	3.9	16	11	5.8	16	0.2	109	21	–
Yucca Wash near mouth	26	1/18/93	–	133	15	2.3	11	4.1	4.4	6	0.2	55	24	94
Yucca Wash near mouth	26	1/26/95	8.1	117	15	2.1	5.8	4.1	2	4.1	0.2	53	22	–

Sources: Emett et al. (1994, p. 550); Perfect et al. (1995, attached file); Savard (1996, p. 28)

NOTES: TDS = total dissolved solids

– = not analyzed or not calculated

Table 5.3-4. Chemical Composition of Unsaturated Zone Pore-Water Samples from Surface-Based Boreholes at Yucca Mountain

Borehole	Depth Interval (ft)	Hydro-geologic Unit[b]	Litho-stratigraphic Unit[b]	Average Depth (m)	pH	Specific Conductivity (µS/cm)	Concentration (mg/L)										Charge Balance[a]
							Ca	Mg	Na	SiO_2	K	HCO_3	CO_3	Cl	NO_3	SO_4	
NRG-6	158.2–158.58	PTn	Tpbt4	48	6.4	1,070	122	23.3	35.6	97.4	–	34	0	185	32	159	-0.2
NRG-6	160.8–161.2	PTn	Tpbt4	49	7.0	860	104	18	35.0	84.0	–	55	0	148	35	139	-2.0
NRG-6	171.0–171.3	PTn	Tpbt3	52	7.0	620	70.5	11.5	29.2	79.4	–	48	13	58	43	94	2.1
NRG-6	175.6–175.95	PTn	Tpp	54	6.6	520	49.2	8.6	29.4	78.1	–	60	0	47	42	64	1.4
NRG-6	219.9–220.2	PTn	Tpp	67	7.0	660	24.3	4.2	99.3	61.4	–	92	0	77	47	77	-1.4
NRG-6	244.6–245.0	PTn	Tpbt2	75	6.6	630	33	4.9	72.0	51.0	–	61	0	49	40	115	-2.2
NRG-6	255.9–256.1	PTn	Tptrv3	78	6.7	1,910	176	19	215.0	68.0	–	61	0	115	35	840	-6.2
NRG-7A	165.75–166.0	PTn	Tpbt3	51	7.4	510	55.3	5.6	31.7	68.3	–	89	0	38.9	45.5	63.4	-0.1
NRG-7A	258.0–258.4	PTn	Tpp	79	8.2	600	43	3.7	82	68.9	–	128	0	53.6	43.7	65.5	2.9
NRG-7A	1,483.5–1,483.8	CHn	Tptpv1	452	7.9	580	61	0.6	94	48.6	–	323	0	33.1	16.7	24.4	1.3
NRG-7A	1,492.7–1,493.1	CHn	Tptpv1	455	7.9	580	30.6	0.3	74.7	71.5	–	104	34	39	18	23	1.0
NRG-7A	1,498.6–1,498.9	CHn	Tac	457	7.5	500	28.7	0.5	73.2	83.0	–	156	0	50	17	18	0.5
SD-6	430.3–430.6	PTn	Tpcpv1	131	7.4	430	46	9.4	56.8	81.7	2.8	109	0	43	69	43	5.7
SD-6	443.2–443.5	PTn	Tpbt4	135	7.3	580	55.2	11.2	53.2	94.8	1.4	134	0	27	64	73	4.5
SD-6	443.5–443.8	PTn	Tpbt4	135	7.2	630	62.4	12	51.6	92.8	1.8	95	0	33	57	101	7.4
SD-7	339.7–340.2	PTn	Tpbt3	104	7.4	690	110	15	20	82.8	–	220	0	77.2	1.5	76.7	1.3
SD-7	370.3–370.6	PTn	No core	113	6.7	1,420	289	0.2	39	25.9	–	73	0	133	0.6	650	-6.7
SD-7	1,498.4–1,498.6	CHn	Tac2	457	7.2	440	31	0.6	67	63.5	–	171	0	28.9	13.6	14.1	4.4
SD-7	1,524.6–1,525.7	CHn	Tac1	465	7.2	490	38.7	0.9	57.6	68.6	7	203	0	30.1	12.4	15.9	-0.2
SD-7	1,558.4–1,558.6	CHn	Tac1	475	7.2	390	39	0.9	43	69.3	–	171	0	25.1	9.0	14.9	-0.9
SD-7	1,600.1–1,600.33	CHn	Tacbt	488	7.6	380	23	0.6	59	66.7	–	150	0	31	5.7	12	1.2
SD-7	1,617.0–1,617.2	CHn	Tacbs	493	7.2	570	40.2	< 1	79	62.2	–	194	< 1	65	11.0	14	-0.3
SD-7	1,890.7–1,891.1	CHn	Tcp1	576	8.7	850	0	0.2	206	67	–	334	78	18	4.8	10	0.6
SD-7	1,952.4–1,952.7	CHn	Tcp1	595	8.8	980	0	0.3	251	67.4	–	353	120	22	6.7	11	0.9
SD-7	2,088.2–2,088.5	CHn	Tcp1	636	9.2	710	0	0	173	54.4	–	157	101	15	4.0	25	4.0
SD-7	2,170.1–2,170.5	CHn	Tcpbt	661	9.2	670	0	0	164	55.4	–	100	103	18	3.8	18	8.5
SD-7	2,596.1–2,596.3	CHn	Tcbts	791	9.0	670	< 1	< 1	158	64.3	–	79	65	83	3.2	12	5.9
SD-7	2,596.5–2,596.9	CHn	Tcbts	791	9.0	680	0	0	148	53.3	–	95	71	46	2.2	12	7.8
SD-7	2,598.3–2,598.5	CHn	Tct	792	8.7	630	< 1	< 1	152	94.8	–	231	59	22	4.0	18	-1.5
SD-9	94.2–94.4	PTn	Tpbt4	29	5.5	1,050	125	24	43	74	–	37	0	170	11	260	-4.3
SD-9	114.1–114.3	PTn	Tpy	35	6.8	920	95	18	55	62.3	–	31	0	138	10.9	181	1.6
SD-9	135.1–135.3	PTn	NR	41	8.5	890	91	15	66	60.1	–	37	0	144	12	162	2.5
SD-9	154.0–154.2	PTn	Tpbt3	47	6.8	650	72	13	36	55	–	90	0	93	4.7	106	-1.2
SD-9	176.2–176.4	PTn	Tpp	54	7.5	720	43	9.5	95	58.4	–	122	0	64	1.9	124	4.8
SD-9	251.8–252.0	PTn	Tpbt2	77	7.2	500	44	8	53	55.0	–	92	0	40	14.2	73	8.1

Table 5.3-4. Chemical Composition of Unsaturated Zone Pore-Water Samples from Surface-Based Boreholes at Yucca Mountain (Continued)

Borehole	Depth Interval (ft)	Hydro-geologic Unit[b]	Litho-stratigraphic Unit[b]	Average Depth (m)	pH	Specific Conductivity (μS/cm)	Ca	Mg	Na	SiO$_2$	K	HCO$_3$	CO$_3$	Cl	NO$_3$	SO$_4$	Charge Balance[a]
							Concentration (mg/L)										
SD-9	1,452.6–1,452.8	CHn	Tptpv1	443	7.3	530	6.9	0	112	62.5	–	256	0	15.7	10.6	62.5	1.4
SD-9	1,535.2–1,535.35	CHn	Tac3	468	7.4	530	0.8	0.1	112	54.9	7	226	0	15.6	10.6	15.5	4.7
SD-9	1,619.9–1,661.4	CHn	Tac2	500	8.3	610	0.4	0	136.6	55.6	4	232	12	50.2	9.0	18.3	-0.7
SD-9	1,661.1–1,661.3	CHn	Tac2	506	8.1	660	0.7	0	164	48.8	–	317	0	42.0	8.2	18.9	1.8
SD-9	1,741.0–1,741.2	CHn	Tac1	531	8.7	520	0.2	0	125	52	–	185	41	19	4.4	10	2.2
SD-9	1,741.7–1,741.9	CHn	Tac1	531	8.4	310	0.2	0	74	53	–	113	12	15	3.8	8.7	5.0
SD-9	1,800.7–1,800.9	CHn	Tacbt1	549	9.3	790	0.8	0	180.7	59.6	6	137	106	32.3	4.6	20.9	5.6
SD-12	265.8–266.1	PTn	Tpbt4	81	7.2	470	48.9	7.6	28.6	62.7	3	107	0	49.6	15.9	47.5	-0.1
SD-12	278.6–278.8	PTn	Tpp	85	7.3	580	74	12.7	27	71.2	–	159	0	46	16.0	75	1.7
SD-12	296.1–296.6	PTn	Tpbt2	90	6.9	490	75	8.0	21	72.2	–	163	< 1	60	18.0	21	2.2
SD-12	1,460.7–1,461.0	CHn	Tac4	445	8.5	490	31	0	89	65.5	–	98	30	55.9	7.3	30.1	4.8
SD-12	1,495.5–1,495.8	CHn	Tac3	456	8.5	550	16	0.2	108	87.3	–	49	57	57	8.1	55	-0.7
SD-12	1,517.0–1,517.4	CHn	Tac3	462	7.6	660	14	0	150	56.9	–	323	0	33.6	6.4	22.5	2.9
SD-12	1,558.9–1,559.5	CHn	Tac2	475	8.5	640	4.4	0.1	155	76.1	–	210	41	33	0.4	54	0.7
SD-12	1,582.5–1,582.7	CHn	Tac2	482	8.5	420	1.2	0.1	97	71.0	–	113	29	17	4.5	27	4.3
SD-12	1,600.6–1,603.0	CHn	Tac1	488	9.1	540	2.6	0	129	65.7	–	79	90	27.8	2.6	12.6	3.2
SD-12	1,636.8–1,637.0	CHn	Tacbt	499	9.1	520	3.8	0	129	64.6	–	67	102	15.2	1.7	11.2	5.6
SD-12	1,901.4–1,901.5	CHn	Tcp2	580	9.1	470	1.3	< 1	122	90.7	–	151	59	22	5.7	9.3	0.2
SD-12	1,938.5–1,939.0	CHn	Tcp2	591	8.7	650	1.4	0	165	55.0	–	171	66	34	1.0	26.1	5.2
SD-12	1,942.2–1,942.9	CHn	Tcp2	592	8.9	550	1.3	0	140	60.1	–	134	66	24	3.5	24.4	4.3
UZ-7a	203.3–203.7	PTn	Tpbt4	62	7.3	830	115	20.6	16.6	69.7	5.6	120	0	70	105	140	-1.4
UZ-7a	220.2–220.5	PTn	Tpbt2	67	7.3	820	117	23.1	18.3	67.6	5.5	100	0	87	112	140	-0.7
UZ-7a	241.4–241.7	PTn	Tpbt2	74	6.9	930	116	21.9	39	52.2	10	70	0	60	83	240	2.0
UZ-14	45.0–45.35	PTn	Tpy	14	8.6	1,340	19.6	6.1	249.3	59.5	6.1	245	18	245	35	33	-1.2
UZ-14	85.2–85.6	PTn	Tpbt3	26	6.9	630	49.9	13.2	43.5	89.8	–	131	0	60	22	66	-0.9
UZ-14	91.0–91.25	PTn	Tpbt3	28	7.6	530	40.7	10.1	37.1	80.6	–	87	0	47	26	81	-4.1
UZ-14	95.5–95.9	PTn	Tpbt3	29	7.2	600	53.3	13.2	38.1	81.5	–	73	0	79	29	83	-1.9
UZ-14	96.2–96.6	PTn	Tpbt3	29	6.9	550	46.9	12.7	33.6	79.6	–	79	0	59	26	75	-0.9
UZ-14	100.4–100.8	PTn	Tpbt3	31	7.0	600	51.1	13.8	41.3	91.8	–	128	0	44	23	83	0.4
UZ-14	114.75–115.0	PTn	Tpp	35	6.6	540	49.0	10.5	35.9	93.9	–	67	0	61	25	90	-2.2
UZ-14	135.5–135.8	PTn	Tpp	41	6.9	690	68.5	14.3	56.2	92.0	–	105	0	83	23	96	4.5
UZ-14	144.8–145.2	PTn	Tpp	44	7.7	650	65.5	12.0	48.2	81.5	–	118	0	77	22	102	-1.8
UZ-14	147.79–148.1	PTn	Tpp	45	6.9	640	54.8	11.5	51.6	77.3	–	79	0	83	22	102	-1.5
UZ-14	177.6–177.9	PTn	Tpp	54	6.5	730	67.8	11.3	48.7	77.5	–	49	0	100	23	130	-2.0
UZ-14	178.1–178.4	PTn	Tpp	54	6.8	740	64.0	10.6	49.1	93.1	–	62	0	97	21	120	-3.0
UZ-14	215.72–216.1	PTn	Tpp	66	6.8	670	65.5	10.7	39.4	97.8	–	55	0	85	14	130	-3.0

Table 5.3-4. Chemical Composition of Unsaturated Zone Pore-Water Samples from Surface-Based Boreholes at Yucca Mountain (Continued)

Borehole	Depth Interval (ft)	Hydro-geologic Unit[b]	Litho-stratigraphic Unit[b]	Average Depth (m)	pH	Specific Conductivity (μS/cm)	Ca	Mg	Na	SiO2	K	HCO3	CO3	Cl	NO3	SO4	Charge Balance[a]
UZ-14	225.9–226.2	PTn	Tpp	69	7.9	640	58.6	10.4	48.4	91.2	–	55	0	93	16	116	-2.5
UZ-14	235.1–235.4	PTn	Tpp	72	7.1	630	67	10.5	29	63	–	96	N/S	84	15	94	-5.7
UZ-14	240.8–241.12	PTn	Tpbt2	73	7.6	810	32	1	103	61	–	162	N/S	99	17	100	-11.8
UZ-14	245.5–245.8	PTn	Tpbt2	75	6.8	580	65	12	9	46	–	66	N/S	77	12	79	-4.8
UZ-14	1,258.5–1,258.8	TSw	Tptpln	384	–	–	43	3.7	67	35	–	170	N/S	88	16	19	-4.9
UZ-14	1,277.4–1,277.7	TSw	Tptpln	389	–	–	62	4.5	49	44	–	170	N/S	87	17	45	-7.1
UZ-14	1,277.7–1,278.0	TSw	Tptpln	389	–	–	74	5.1	45	38	–	170	N/S	130	15	38	-10.4
UZ-14	1,409.4–1,409.8	CHn	Tpbt1	430	8.0	720	30	0.7	88	57	–	160	0	75	5	106	-13.2
UZ-14	1,419.5–1,419.8	CHn	Tpbt1	433	8.6	410	20	0.6	68	60	–	166	0	24	6	21	0.9
UZ-14	1,461.9–1,462.1	CHn	Tac3	446	7.8	570	9.2	0.1	128	68.7	–	265	0	24.2	6.2	37.3	1.1
UZ-14	1,495.8–1,496.0	CHn	Tac2	456	8.6	500	2.1	0	122	56.7	–	228	0	28.0	10.8	14.3	3.9
UZ-14	1,524.55–1,524.75	CHn	Tac2	465	8.0	560	1.1	0.1	137	54.8	–	232	0	26.2	12.5	22.3	7.2
UZ-14	1,542.3–1,542.8	CHn	Tac2	470	–	–	3.6	0.5	207	143	–	384	46	20	4	28	1.0
UZ-14	1,563.6–1,563.8	CHn	Tac2	477	8.7	660	1.2	0.2	155	72.0	–	160	97	16	4	14	1.1
UZ-14	1,564.6–1,564.75	CHn	Tac2	477	–	–	1.3	0.2	129	140.4	–	61	113	16	4	17	0.5
UZ-14	1,564.9–1,565.0	CHn	Tac2	477	8.8	690	1.7	0.5	169	54.0	–	376	0	23	1	30	0.1
UZ-14	1,585.0–1,585.15	CHn	Tac2	483	9.7	560	0.9	0.3	106.8	74.5	–	98	67	14	7	10	1.7
UZ-14	1,585.3–1,585.6	CHn	Tac2	483	9.3	400	1.2	0.5	85	75.0	–	148	18	11	6	9	2.4
UZ-14	1,605.9–1,606.1	CHn	Tac2	490	–	–	1.0	0.3	87.8	67.2	–	178	0	18	6	9	2.4
UZ-14	1,644.3–1,644.5	CHn	Tac2	501	8.8	420	2.2	0.7	110	74.0	–	74	79	14	0	9	5.6
UZ-14	1,674.8–1,675.05	CHn	Tac1	511	–	–	1.8	0.6	58	64.6	–	104	0	10	4	9	8.6
UZ-14	1,695.4–1,695.6	CHn	Tabt1	517	–	–	1.4	1.1	115.8	55.9	–	203	18	21	5	26	0.5
UZ-14	1,715.0–1,715.3	CHn	Tabt1	523	7.3	390	0.2	0	88	52.9	–	168	0	11.9	3.1	16.0	5.0
UZ-14	1,734.5–1,734.7	CHn	Tabt1	529	9.1	750	2.0	0.3	184	50.7	–	211	79	39.4	5.6	17.5	3.0
UZ-14	1,735.3–1,735.53	CHn	Tabt1	529	9.0	700	1.7	0	158	46.9	–	288	18	37.4	3.4	15.4	1.5
UZ-14	1,804.5–1,804.8	CHn	Tcp4	550	8.0	480	0.5	0.2	111	43.0	–	181	12	25.1	15.3	14.9	2.5
UZ-14	1,825.8–1,826.0	CHn	Tcp3	557	9.4	590	0.6	0.1	138	47.9	–	42	112	23.5	11.8	12.9	4.3
UZ-14	1,854.9–1,855.1	CHn	Tcp3	565	8.0	460	0.5	0.2	107	34.5	–	181	23	18.8	13.7	15.9	-1.3
UZ-14	1,865.7–1,865.9	CHn	Tcp3	569	8.6	480	0.3	0	115	30.4	–	204	18	17.3	11.7	12.6	1.3
UZ-14	2,014.7–2,014.9	CHn	Tcp1	614	9.3	1,520	3.2	0.2	392	37.7	–	409	219	32.1	1.8	22.2	5.6
UZ-14	2,015.2–2,025.7	CHn	Tcp1	616	9.4	1,290	0.9	0	312.7	68.6	–	339	176	23.2	0.5	21.7	4.2
UZ-14	2,025.1–2,025.3	CHn	Tcp1	617	9.1	1,550	4.0	0.2	414	54.8	–	493	189	36.5	6.9	26.3	6.3
UZ-14	2,095.1–2,095.8	Cfu	Tcb	639	8.8	540	0	0	112.8	63.0	–	143	29	30	0.3	29	1.3
UZ#16	163.5–163.85	PTn	Tpbt4	50	6.8	420	42.5	13.4	21.5	77.5	–	94	45	32.4	23.1	72.3	-16.7
UZ#16	180.9–181.27	PTn	Tpbt3	55	7.3	450	55	11	20	83	3	120	0	38	33	38	2.7
UZ#16	952.6–952.9	TSw	Tptpln	290	8.2	–	2.2	13.7	99.5	31.7	–	179	–	81	30	34	-7.1

Table 5.3-4. Chemical Composition of Unsaturated Zone Pore-Water Samples from Surface-Based Boreholes at Yucca Mountain (Continued)

Borehole	Depth Interval (ft)	Hydro-geologic Unit[b]	Litho-stratigraphic Unit[b]	Average Depth (m)	pH	Specific Conductivity (μS/cm)	Concentration (mg/L)										Charge Balance[a]
							Ca	Mg	Na	SiO$_2$	K	HCO$_3$	CO$_3$	Cl	NO$_3$	SO$_4$	
UZ#16	1,166.19–1,166.47	CHn	Tptpv1	355	8.1	710	28.9	13.7	83.6	57.1	–	196	0	82	17	28	-1.4
UZ#16	1,206.33–1206.67	CHn	Tptpv1	368	7.2	540	39.8	11.7	48.5	61.6	–	105	–	43	28.4	31.1	11.2
UZ#16	1,227.35–1,227.7	CHn	Tac4	374	8.1	430	26.5	6.2	47.9	62.2	–	137	0	24	23	26	1.1
UZ#16	1,235.1–1,235.4	CHn	Tac4	377	7.7	480	33.5	7.9	51.3	52.9	–	154	0	52	26	29	-4.8
UZ#16	1,269.6–1,269.95	CHn	Tac3	387	8.5	430	14.1	2.4	67.5	57.1	–	139	13	27	18	14	-2.8
UZ#16	1,280.37–1,280.75	CHn	Tac3	390	8.3	530	20.5	3.7	92.0	71.8	–	192	0	28	19	19	6.9
UZ#16	1,296.8–1,297.06	CHn	Tac3	395	7.5	950	32.4	19.7	98.2	46.7	–	324	12	50	19	18	-1.9
UZ#16	1,317.86–1,318.24	CHn	Tac3	402	7.2	430	20.6	5.1	60.1	131.6	–	171	0	32	20	18	-4.0
UZ#16	1,358.05–1,358.4	CHn	Tac2	414	7.5	550	3.4	0.3	76.7	47.9	–	115	0	22.8	16.1	18.7	5.2
UZ#16	1,389.36–1,389.64	CHn	Tac2	424	9.4	480	3.6	0.9	114.6	62.5	–	100	36	23.5	18.5	23.8	9.9
UZ#16	1,395.5–1,395.7	CHn	Tac2	425	8.4	710	5.4	0.3	155	88.0	–	216	24	17	16	22	11.9
UZ#16	1,398.5–1,398.7	CHn	Tac2	427	–	–	5.0	0.4	145	123	–	237	31	14	16	20	4.8
UZ#16	1,412.9–1,413.2	CHn	Tac2	431	8.7	450	1.2	0.1	101	75.9	–	165	0	26	24	30	0.1
UZ#16	1,428.1–1,428.4	CHn	Tac2	435	8.8	570	1.9	0.1	134	80.5	–	160	43	23	19	23	3.8
UZ#16	1,442.89–1,443.22	CHn	Tac2	440	9.5	410	1.7	0.8	79.9	68.9	–	15	87.6	18.9	11.3	13.7	-7.0
UZ#16	1,486.9–1,487.3	CHn	Tcp4	453	8.9	370	6.3	0.8	79.5	233.3	–	137	0	38	6	11	2.6
UZ#16	1,601.1–1,601.5	CHn	Tcp3	488	9.0	580	10	0.3	100	36	–	181	0	53	13	27	-3.6
UZ#16	1,607.7–1,608.05	CHn	Tcp3	490	8.9	670	25	0.3	108	34	–	170	0	71	10	33	2.9
UZ#16	1,643.4–1,647.2	CHn	Tcp3	501	9.0	490	91	12	34	70	–	162	0	70	8	28	13.5
UZ#16	1,651.6–1,651.7	CHn	Tcp3	503	8.3	430	17.3	0.3	66	47.4	–	87	19	27	6	20	6.0
UZ-N55	166.1–166.42	TCw	Tpcplnc	51	7.8	845	28.7	7.6	126.9	47.7	–	136.6	–	106.8	97.7	74.9	-5.1
UZ-N55	195.27–195.47	PTn	Tpcpv1	60	6.7	630	91.8	8.6	18.4	71.5	–	69.5	–	77.1	93.3	80.7	-3.2
UZ-N55	198.97–199.45	PTn	Tpcpv1	61	6.7	765	91.2	9.5	39.9	76.4	–	35.4	–	76.6	101.7	101	4.4
WT#24	1,734.3–1,735.1	CHn	Tptpv1	529	8.2	420	4.9	0	96	81.1	8.4	172	0	34	1.7	14	6.1
WT#24	1,744.2–1,744.5	CHn	Tptpv1	532	7.9	500	5.5	0.1	121	69.5	9.5	242	0	31	2.3	18	4.8
WT#24	1,744.5–1,745.0	CHn	Tptpv1	532	8.3	440	4.2	0	103	72.7	7.7	210	19	16	2.7	14	0.2

Sources: CRWMS M&O (2000, Table 6).

NOTES: [a]Charge balance was calculated from data shown using the following formula: (meq cation - meq anion)/(meq cation + meq anion)*100.

– = data not available; 0 = values below detection limit; no core = no core available for stratigraphic examination; NR = not recorded

Table 5.3-5. Chemical Composition of Precipitation and Transient Shallow Perched Water at Yucca Mountain

Borehole[a]	Date	Concentration (mg/L)									Charge Balance[b]
		Ca	Mg	Na	SiO_2	HCO_3	CO_3	Cl	NO_3	SO_4	
Precipitation Samples											
NTS Area 25[c]	02-23-98	0.14	0.013	0.32	0.10	2.8	0	<0.1	–	0.41	–
UZN#2[d]	08-18-89	14	2.3	51	18	112	0	10	0	29	–
Shallow Transient Perched-Water Samples											
UZN#2	04-09-91	–	–	–	–	–	–	19.9	–	40.7	–
UZN#2	02-14-92	1.4	0.5	1.7	0	11.7	0	12	8.2	7.8	-63.4
UZN#2	03-16-92	14	3.9	25	5.8	58.2	0	10	27.3	21	-0.1
UZN#2	03-31-92	25	4.7	16	11.8	128	0	5.8	19.7	15.6	-10.9
UZN#91	03-05-92	–	–	–	–	–	–	19.5	–	17.8	–
UZ-N46	02-14-92	0.8	0.5	1.6	0.2	23.3	0	3.3	1.6	4.7	-59.8

Sources: CRWMS M&O (2000, Table 7)

NOTES: [a] Sampling depths for perched water: UZN#2, 15.8 m; UZ-N46, 30.1 m (Yang et al. 1996, Table 2)

[b] Charge balance calculated from data shown using the formula: (meq cation - meq anion)/(meq cation + meq anion)*100

[c] Sample from behind service station; pH 7.2, specific conductivity 4.5 μS/cm

[d] pH 7.7, specific conductivity 308 μS/cm

– = data not available; 0 = values below detection limit

Table 5.3-6. Chemical Composition of Deep Perched Water at Yucca Mountain

Borehole and Sample Identifier	Average Depth (m)	Date	Temperature (°C)	pH	Specific Conductivity (µS/cm)	Concentration (mg/L)											Charge Balance[a]
						Al	Ca	Mg	K	Na	SiO_2	HCO_3	CO_3	Cl	NO_3	SO_4	
NRG-7A	460.25	03-07-94	–	8.7	224	0.0	3	0	6.8	42	9	114	–	7	1	4	-0.4
SD-9/TS	453.85	07-17-94	27.0	8.6	445	2.1	2.9	0.2	9.8	98	64.2	197	10	5.6	3.3	27.6	7.6
UZ-14 A	384.60	08-02-93	27.1	7.6	312	0.7	23	1.8	5.6	39	34.2	150	0	7.9	8.6	14.3	0.3
UZ-14 A2	384.60	08-02-93	27.1	7.8	308	1.0	24	1.8	3.9	38	36.4	148.8	0	9.1	12.5	13.8	-1.4
UZ-14 B	387.68	08-03-93	23.8	8.1	335	6.1	31	2.7	4.4	40	51.4	147.6	0	8.3	16.9	16.3	5.2
UZ-14 C	390.75	08-05-93	24.2	8.3	518	0.0	45	4.1	5.8	88	7.7	106.1	0	15.5	0	223	-1.9
UZ-14 PT-1	390.75	08-17-93	–	–	–	0.0	37	3.1	6.3	40	21.4	144	0	7.2	12.7	57.3	0.5
UZ-14 PT-2	390.75	08-19-93	–	–	–	0.0	30	2.4	3.3	35	25.7	144	0	7.0	15.4	22.9	0.3
UZ-14 PT-4	390.75	08-27-93	–	–	–	0.0	27	2.1	1.8	34	32.1	141.5	0	6.7	14.5	14.1	0.2
UZ-14 D	390.75	08-31-93	–	7.8	–	0.0	31	2.5	4.1	35	40.7	146.4	0	7.0	17.1	24.2	0.1
SD-7(3/8)	479.76	03-08-95	–	–	–	0.28	14.2	0.13	5.3	45.5	62.3	112	0	4.4	33.8	9.1	2.5
SD-7(3/16)	488.29	03-16-95	21.8	8.1	239	0.44	13.3	0.13	5.3	45.3	57.4	128	0	4.1	33.8	9.1	-2.9
SD-7(3/17)	488.29	03-17-95	22.6	8.2	285	0	12.8	0.08	5.5	45.8	50.9	130	0	4.1	22.8	8.6	-0.3
SD-7(3/20)	488.29	03-20-95	23.3	8.0	265	0	12.9	0.07	5.4	45.5	55	127	0	4.1	13.4	8.5	3.3
SD-7(3/21)	488.29	03-21-95	23.2	8.2	259	0	13.5	0.08	5.5	44.6	55.9	128	0	4.1	13.2	10.3	2.2

Source: CRWMS M&O (2000, Table 8)

NOTES: [a]Charge balance calculated from data shown using the following formula: (meq cation – meq anion)/(meq cation + meq anion)*100.
          – = data not available; 0 = values below detection limit

Table 5.3-7. Isotopic Composition of Perched Water at Yucca Mountain

Borehole and Sample Identity	Depth (m)	Date	$\delta^{13}C$ (‰)	^{14}C (pmc)	^{14}C Age[a] (yr.)	^3H (TU)	δ^2H (‰)	$\delta^{18}O$ (‰)	$^{234}U/^{238}$ Uranium Activity Ratio	$\delta^{87}Sr$ (‰)	$^{36}Cl/Cl$ (x 10^{-15})
SD-7	479.76	03-08-95	-10.4	34.4	8,798	6.2	-99.8	-13.4	–	–	511
	488.29	03-16-95	-9.4	28.6	10,321	–	-99.7	-13.3	–	–	–
	488.29	03-17-95	-9.5	28.4	10,379	–	-99.6	-13.4	3.50	–	657
	488.29	03-20-95	-9.5	27.9	10,525	–	-99.6	-13.4	3.58	–	–
	488.29	03-21-95	-9.5	28.4	10,379	–	-99.6	-13.3	3.69	–	609 635
SD-9	–	03-07-94	-14.4	41.8	7,192	0	-97.8	-13.3	–	–	–
	–	07-07-94	–	–		–	–	–	2.42[b]	–	–
	453.85	07-17-94	-14.4	41.8	7,192	0	-97.8	-13.3	–	–	449
	–	09-12-94	–	–		–	–	–	2.42[b]	5.92	–
UZ-14 A	384.60	08-02-93	-10.2	41.7	7,212	0.3	-98.6	-13.8	–	4.51	559
UZ-14 A2	384.60	08-02-93	-10.1	40.6	7,432	3.1	-97.5	-13.5	–	4.47	538
UZ-14 B	387.68	08-03-93	-9.5	36.6	8,287	0	-97.1	-13.4	–	4.34	566
UZ-14 C	390.75	08-05-93	-9.2	66.8	3,327	0.4	-87.4	-12.1	–	4.37	389
UZ-14 PT-1	390.75	08-17-93	-9.8	32.3	9,318	1.8	-97.8	-13.3	–	3.91–4.30	644
UZ-14 PT-2	390.75	08-19-93	–	28.9	10,235	3.1	-97.9	-13.4	–	3.51–4.19	656
UZ-14 PT-4	390.75	08-27-93	-9.6	27.2	10,735	0	-97.3	-13.4	7.56	4.45–4.49	675
UZ-14 D	390.75	08-31-93	-11.3	29.2	10,150	0	-97.6	-13.1	–	–	690
WT-24	–	10-06-97	–	–	–	–	–	–	4.36[b]	4.08	–
		10-16-97	–	–	–	–	–	–	6.58[b]	2.61	–
		10-17-97		–	–	–	–	–	8.33	3.88	–
		10-22-97		–	–	–	–	–	8.37	4.00	586
NRG-7a	–	03-04-94	–	–	–	–	–	–	5.17[b]	4.94	518
	460.25	03-07-94	-16.6	66.9	3,314	10.4	-93.9	-12.8	–	2.54–2.91	474
	–	03-08-94	–	–	–	–	–	–	–	11.68	–
U2-1[c]	382	07-07-83 to 07-21-83	-12.1	64.0	3,680	1.0	-102	-13	–	–	999
UZN#91	28.7	03-05-92	–	–	–	–	–	–	–	–	880
UZN#2	15.2	04-09-91	–	–	–	–	–	–	–	–	2,012[c]
		02-22-95	–	–	–	–	–	–	–	–	3,150

Source: CRWMS M&O (2000, Table 9)

NOTES: [a] Uncorrected carbon-14 age calculated using the radioactive decay equation: $t = (t_{1/2} / \ln 2) \ln (A/A_0)$, where $t_{1/2}$ is the half-life for carbon-14 (5,715 yr.), A is the measured carbon-14 activity, and A_0 is the initial carbon-14 activity (100 pmc).

[b] This result is not representative of in situ conditions because of sample contamination.

[c] Data are unqualified because samples were collected prior to the establishment of a formal quality assurance program.

– = not available

Table 5.3-8. Summary of Tritium Analyses in Unsaturated Zone Pore Waters at Yucca Mountain

ESF or Borehole Location	Geomorphic Location	Collar Elevation (ft)	TCw and Above		PTn		TSw		CHn Above Tcp		TCp and Below		Total	
			Above 25 TU	Total	Above 25 TU	Total	Above 25 TU	Total	Above 25 TU	Total	Above 25 TU	Total	Above 25 TU	Total
ESF Alcove 2	Bow Ridge fault zone	–	8	9	–	–	–	–	–	–	–	–	8	9
ESF Alcove 3	–	–	–	–	–	3	–	7	–	–	–	–	–	10
ESF Alcove 5	–	–	–	–	–	–	–	7	–	–	–	–	–	7
ESF Alcove 6	Ghost Dance fault zone	–	–	–	–	–	–	7	–	–	–	–	–	.7
ESF North Ramp	–	–	–	3	–	–	–	2	–	–	–	–	–	5
ESF Main Drift	–	–	–	–	–	–	–	4	–	–	–	–	–	4
Subtotals, ESF			8	12	–	3	–	27	–	–	–	–	8	42
UZ#16	Terrace, large wash	4,000	1	5	–	3	11	51	2	27	–	13	14	99
NRG-6	Hillslope	4,092	–	–	6	13	–	–	–	–	–	–	6	13
NRG-7A	Hillslope	4,207	–	4	–	9	1	22	–	9	–	–	1	44
UZ-7a	Small wash bottom	4,228	–	–	–	1	–	13	–	–	–	–	–	14
SD-9	Small wash bottom	4,273	–	2	–	15	–	22	–	26	–	3	–	68
SD-12	Small wash bottom	4,343	–	13	–	10	–	27	–	18	1	7	1	75
UZ-1	Large channel (Drill Hole Wash)	4,425	–	1	–	5	1	9	–	–	–	–	1	15
UZ-14	Large channel (Drill Hole Wash)	4,425	–	–	1	35	–	53	–	35	–	14	1	137
SD-7	Ridgetop	4,472	–	10	–	7	–	15	–	18	–	–	–	50
WT-24	Ridgetop	4,900	–	–	–	–	7	10	–	–	5	58	12	68
SD-6	Small wash bottom	4,905	–	6	–	17	3	22	–	11	4	37	7	93
Subtotals, Boreholes			1	41	7	115	23	244	2	144	10	132	43	676
Total, All Samples			9	53	7	118	23	271	2	144	10	132	51	718

Sources: CRWMS M&O (2000, Table 10)

NOTES: Borehole elevations are listed to provide a rough surrogate for average annual precipitation, which typically increases as a function of elevation (Hevesi et al. 1992, Figure 7, p. 685).

The threshold for indicating the unambiguous presence of bomb-pulse or post-bomb tritium is 25 tritium units, based on the application of Chauvenet's criterion (Figure 5.3-29). This statistical test was applied to the 803 samples, including 75 duplicate analyses but excluding Exploratory Studies Facility data that were reported more than once. Where duplicate analyses exist, the sample results were only tallied once for this table.

The stratigraphic interval from which each sample was collected was determined using the appropriate references listed in Table 5.3-16.

Table 5.3-9. Tritium Levels above 25 Tritium Units in Unsaturated Zone Pore Waters at Yucca Mountain

Sampling Location[a]	Top of Sampled Interval (ft)	Hydrologic Unit[b]	Stratigraphic Unit[b]	Tritium (TU)
ESF-AL#2-HPF#1	34.3	TCw	Tpcpmn	28.8
	47.2	TCw	Tpcpll	30.9
	50.5	TCw	Tpcpll	118.3
	55.4	Bow Ridge fault zone	–	128.1
	58.9	TCw	Tmbt1	78.6
	61.2	TCw	Tmbt1	65.3
	68.6	TCw	Tmbt1	154.6
	83.6	TCw	Tmbt1	32.9
NRG-6	175.6	PTn	Tpp	30.9
	175.6	PTn	Tpp	39.1
	210.4	PTn	Tpp	117.3
	210.4	PTn	Tpp	139.9
	229.4	PTn	Tpbt2	(23.1)
	229.4	PTn	Tpbt2	30.2
NRG-7a	356.7	TSw	Tptrv1	46.8
UZ-1	621	TSw	Tptprl+Tptpul	28.0
UZ-14	135.5	PTn	Tpp	32.0
UZ#16	158.4	TCw	Tpcpv2	142.2
	158.4	TCw	Tpcpv2	148.5
	262.8	PTn	Tptrn	27.0
	262.8	PTn	Tptrn	31.2
	583.0	TSw	Tptpmn	95.8
	583.0	TSw	Tptpmn	105.9
	669.0	TSw	Tptpmn	(25.0)
	669.0	TSw	Tptpmn	28.7
	945.0	TSw	Tptpln	48.2
	945.0	TSw	Tptpln	59.1
	1,041.2	TSw	Tptpln	44.4
	1,041.2	TSw	Tptpln	56.1
	1,041.9	TSw	Tptpln	28.7
	1,090.6	TSw	Tptpln	(11.1)
	1,090.6	TSw	Tptpln	40.7
	1,110.6	TSw	Tptpln	(21.3)
	1,110.6	TSw	Tptpln	30.2
	1,113.2	TSw	Tptpv3	35.0
	1,113.2	TSw	Tptpv3	42.7
	1,113.2	TSw	Tptpv3	51.5
	1,113.6	TSw	Tptpv3	42.8
	1,122.2	TSw	Tptpv3	26.1
	1,122.2	TSw	Tptpv3	26.2
	1,122.2	TSw	Tptpv3	35.7
	1,129.5	TSw	Tptpv3	58.7
	1,397.7	CHn	Tac2	41.3
	1,397.7	CHn	Tac2	44.4
	1,434.3	CHn	Tac2	98.1
	1,434.3	CHn	Tac2	108.8

Table 5.3-9. Tritium Levels above 25 Tritium Units in Unsaturated Zone Pore Waters at Yucca Mountain (Continued)

Sampling Location[a]	Top of Sampled Interval (ft)	Hydrologic Unit[b]	Stratigraphic Unit[b]	Tritium (TU)
SD-6	1,437.5	TSw	Tptpln	26.7
	1,440.0	TSw	Tptpln	27.9
	1,440.7	TSw	Tptpln	29.7
	1,749.3	CHn	Tcpuc	29.7
	1,749.3	CHn	Tcpuc	29.9
	1,751.0	CHn	Tcpuc	43.2
	1,752.1	CHn	Tcpuc	32.7
	1,752.1	CHn	Tcpuc	41.6
	1,754.1	CHn	Tcpuc	36.6
SD-12	1,722.5	CHn	Tcp3	39.2
WT-24	1,688.8	TSw	Tptpv3	37.6
	1,689.3	TSw	Tptpv3	35.6
	1,690.5	TSw	Tptpv3	28.3
	1,690.5	TSw	Tptpv3	29.1
	1,694.4	TSw	Tptpv3	25.8
	1,694.4	TSw	Tptpv3	29.9
	1,697.6	TSw	Tptpv3	42.8
	1,697.6	TSw	Tptpv3	50.0
	1,699.7	TSw	Tptpv3	29.7
	1,699.7	TSw	Tptpv3	30.7
	1,702.9	TSw	Tptpv3	45.1
	2,515.9	CHn	Tac	28.3
	2,515.9	CHn	Tac	31.2
	2,515.9	CHn	Tac	34.3
	2,519.1	CHn	Tac	30.2
	2,522.2	CHn	Tac	25.7
	2,522.2	CHn	Tac	32.6
	2,525.3	CHn	Tac	29.0
	2,526.0	CHn	Tac	33.0

Sources: CRWMS M&O (2000, Table 11)

NOTES: [a] Data listed in parentheses lie below the threshold for indicating the unambiguous presence of bomb-pulse or post-bomb tritium, but are included in this table because they are duplicate analyses for samples with tritium concentrations above the threshold.

[b] The stratigraphic interval from which each sample was collected was determined using the appropriate references listed in CRWMS M&O (2000).

Table 5.3-10. Tritium Profiles in UZ#4 and UZ#5

Sampling Location	Depth (m)		Hydrologic Unit	Stratigraphic Unit	Tritium (TU)[a]
UZ#4	1.0	2.3	Alluvium	Alluvium	19
	2.5	4.5	Alluvium	Alluvium	22
	5.5	6.5	Alluvium	Alluvium	7
	8.8	10.3	Alluvium	Alluvium	2
	11.0	11.8	Alluvium	Alluvium	3
	24.7	24.8	TCw	TCw	28
	25.5	25.6	TCw	TCw	3
	33.5	33.6	PTn	Tpy	22
	41.8	41.9	PTn	Tpy	24
	44.8	44.9	PTn	Tpy	41
	44.9	45.0	PTn	Tpy	38
	46.3	47.9	PTn	Tpy/Tpbt3	45
	49.4	49.5	PTn	Tpbt3	45
	95.6	95.7	PTn	Tpbt2	0
UZ#5	28.3	28.4	TCw	TCw	60
	28.8	28.9	TCw	TCw	49
	29.8	30.0	TCw	TCw	65
	30.4	30.6	TCw	TCw	51
	31.4	31.5	TCw	TCw	11
	32.6	32.8	TCw	TCw	75
	33.6	33.7	TCw	TCw	39
	34.0	34.1	TCw	TCw	22
	34.8	34.9	TCw	TCw	42
	36.0	36.1	PTn	Tpbt4	66
	36.5	36.6	PTn	Tpbt4	15
	36.6	36.7	PTn	Tpbt4	36
	37.2	37.3	PTn	Tpy	4
	37.6	37.7	PTn	Tpy	13
	44.8	44.9	PTn	Tpy	6
	68.6	68.8	PTn	Tpp	10
	70.1	70.2	PTn	Tpp	1
	72.4	72.5	PTn	Tpp	0
	72.5	72.7	PTn	Tpp	7
	75.3	75.5	PTn	Tpp	0
	78.7	78.9	PTn	Tpp	0
	82.4	82.6	PTn	Tpp	4
	90.1	90.2	PTn	Tpp	1
	94.1	94.3	PTn	Tpp	6
	94.3	94.5	PTn	Tpp	0
	98.3	98.4	PTn	Tpbt2	1

Source: CRWMS M&O (2000,Table 12)

NOTES: [a] Typical uncertainties (one-sigma) for these sample data are ± 4 to ± 5 tritium units (Yang 1992, Table 1). These data are used to corroborate the limited penetration of infiltrating water into thick (13-m) alluvium (UZ#4), as contrasted with the deeper penetration of infiltrating water into a setting with negligible soil cover over densely welded fractured bedrock (UZ#5) (Yang 1992, p. 733). The data also support an interpretation of lateral flow at the bedrock/alluvial interface in order to account for bomb-pulse tritium underlying prebomb tritium in UZ#4.

Table 5.3-11. Background Chlorine-36/Chlorine in Precipitation at Yucca Mountain

Field Site	Sample Identifier	Depth or Age	$^{36}Cl/Cl \times 10^{15}$
Midway Valley soil pits		Depth (m)	
UE-25 MWV-P2	ST033	1.9	494 ± 16
	ST034	2.0	470 ± 16
	ST035	2.1	490 ± 10
UE-25 MWV-P6	ST078	3.1	458 ± 12
	ST079	2.75	462 ± 7
UE-25 MWV-P13	ST080	3.0	459 ± 15
	ST081	2.55	475 ± 14
UE-25 MWV-P23	ST084	2.6	483 ± 11
	ST085	2.3	459 ± 11
UE-25 MWV-P24	ST086	2.9	466 ± 11
	ST087	2.5	524 ± 10
UE-25 NRSF-TP-16	ST088	2.4	466 ± 9
	ST089	2.2	468 ± 13
Alluvium from boreholes		Depth (m)	
UZN#39	R502	12.5	515 ± 24
	R504	18.1	557 ± 29
UZ-N54	R006	4.9	526 ± 22
	R007	5.9	501 ± 21
	R008	7.3	507 ± 14
	R009	8.0	474 ± 13
UZ-14	R413	3.7	497 ± 16
	R414	4.2	526 ± 13
	R415	5.5	549 ± 18
	R417	7.6	429 ± 16
	R418	9.1	479 ± 11
UZ#16	R167	3.7	526 ± 16
	R168	4.2	500 ± 15
	R169	5.0	528 ± 24
	R170	5.5	750 ± 35
	R171	6.1	494 ± 21
	R172	6.6	538 ± 24
	R173	7.1	601 ± 26
	R174	7.7	507 ± 26
Fossil packrat urine		^{14}C age (ka)	
Little Skull Mountain	PM-002	1.09	516 ± 19
	PM-004	6.68	509 ± 16
Owl Canyon	PM-035	0.69	514 ± 16
	PM-039	1.65	518 ± 43
	PM-038	3.12	443 ± 21
	PM-034	3.96	442 ± 15
	PM-040	4.00	438 ± 15
	PM-036	6.70	505 ± 31
	PM-037	9.31	510 ± 48
Unweighted average, 41 samples			502 ± 53

Source: CRWMS M&O (2000, Table 25)

Table 5.3-12. Summary of the Distribution of Chlorine-36 in the Unsaturated Zone at Yucca Mountain

Location	Relevant Sample Sets	Observed Chlorine-Distribution
Soil	Surface soils[a] Surface runoff Soil profiles Alluvial profiles for UZ-N37, UZ-N39, UZ-N54, UZ-N61, UZ-14, UZ#16	In areas with sufficiently thick soil cover, bomb-pulse chlorine-36 is almost completely retained within the uppermost 2 to 3 m of soil. For thinner soils, some fraction of the bomb-pulse signal has moved down into the underlying bedrock. Elevated chlorine-36/chlorine ratios in shallow soils and surface runoff show that residual bomb-pulse chlorine-36 is still present on the surface.
TCw	Bomb-pulse in TCw: UZ-N11, UZ-N15, UZ-N16, UZ-N17, UZ-N27, UZ-N36, UZ-N38, UZ-N53, UZ-N55, UZ-N64; No bomb-pulse in TCw: UZ-N37, UZ-N54, UZ#16 ESF North Ramp ESF South Ramp	Based on borehole data, bomb-pulse chlorine-36 appears to be widely present in the fractured welded TCw unit where it is overlain by thin soil cover (ridgetops and sideslopes) and absent where the soil thickness is at least 3 m. Fracture transport is also indicated by UZ-N53 neutron logging data, which have shown changes in moisture content down to a depth of 12 m, well into the TCw (Flint and Flint 1995, p. 29). The North Ramp data provide evidence of transport of bomb-pulse chlorine-36 through the TCw.
PTn	Bomb-pulse in PTn: UZ-N11, UZ-N53, UZ-N55 ESF North Ramp[b] No bomb-pulse in PTn: most of PTn in UZ-N37, UZ-N53, UZ-N54, UZ#16, UZ-14 ESF North Ramp ESF South Ramp	Evidence for fast transport of water into the PTn is shown by elevated chlorine-36/chlorine ratios from this interval in boreholes with thin soil cover. Bomb-pulse chlorine-36 has also been measured in the PTn unit in several ESF samples from the North Ramp.[b] No unambiguous evidence of bomb-pulse chlorine-36 is seen in the South Ramp despite infiltration rates and soil thicknesses that are similar to those over the North Ramp.
TSw	ESF Main Drift, Alcove #6, ESF Niche#1 Cross Drift UE-25 NRG#4 UE-25 NRG#5 USW NRG-7a Perched water: UZ-14, NRG-7A, SD-7, SD-9	Bomb-pulse chlorine-36 has been observed at several locations in the ESF and Cross Drift and appears to be associated with faults.[b] No unambiguous levels of bomb-pulse chlorine-36 are observed in any of the perched-water bodies at the base of this unit or at the top of the CHn; values for these samples are at or slightly above present-day background. Borehole chlorine-36 data (from ream-bit cuttings) for this unit are usually too diluted by rock chlorine to provide a reliable indication of the presence or lack of bomb-pulse chlorine-36.
CHn	UZ-14 UZ#16 SD-12	No unambiguous levels of bomb-pulse chlorine-36 have been observed in the CHn in surface-based boreholes. Measured chlorine-36/chlorine ratios are generally at or somewhat above present-day background. The highest ratios have been measured in SD-12, to a maximum value of 843×10^{-15}.
Saturated Zone	C#3, G-2, SD-7, J-13, SD-9, WT-10, WT-12	The chlorine-36/chlorine ratio is uniformly at present-day background in the aquifer underlying the site, independent of location or depth.

Sources: CRWMS M&O (2000, Table 13)

NOTES: [a] Numerous analyses of chlorine-36 in surface soil samples from Yucca Mountain confirm the continued presence of the bomb-pulse signal.

[b] Numerous analyses of chlorine-36 in tunnel construction water confirm that this potential source of contamination cannot be the source of the elevated chlorine-36/chlorine used to identify the presence of bomb-pulse.

Table 5.3-13. Chlorine-36 in Faults and Fault Zones in the Cross Drift

Cross Drift Station (m)	Sampling Criterion	Description of Sampled Feature	^{36}Cl/Cl x 10^{-15} (a)		
CS1135.5	Systematic fault transect	Breccia from Sundance fault zone	347	±	16
CS1137	Systematic fault transect	Fractured wallrock adjacent to Sundance fault zone	1,206	±	98
CS1317	Systematic fault transect	Breccia	587	±	42
CS1318	Systematic fault transect	Breccia in fault zone	342	±	29
CS2154	Systematic fault transect	Breccia in fault zone	918	±	49
CS2154.5	Systematic fault transect	Breccia in fault zone	4,890	±	174
CS2238	Other through-going fault	Breccia in fault zone	2,361	±	106
CS2348	Other through-going fault	Fault with 3-m offset	1,052	±	38
CS2530.5	Systematic fault transect	Fractured rock between two faults	1,122	±	45
CS2545	Opportunistic	Highly fractured bedrock within Solitario Canyon fault zone	854	±	43
CS2550	Opportunistic	Fractured rock and gouge within Solitario Canyon fault zone	324	±	24
CS2570	Systematic fault transect	Solitario Canyon fault zone	2,158	±	87
CS2580	Systematic fault transect	Solitario Canyon fault zone	890	±	55
CS2585	Other through-going fault	Brecciated footwall of fault	2,460	±	103
CS2586.5	Other through-going fault	Brecciated hanging wall of fault	1,233	±	41
CS2590	Systematic fault transect	Solitario Canyon fault zone	1,379	±	58
CS2621	Other through-going fault	Solitario Canyon fault zone	974	±	50

Source: CRWMS M&O (2000, Table 14)

NOTES: [a] Measured chlorine-36/chlorine ratios have been adjusted to correct for the presence of construction water, as estimated from the measured bromine/chlorine ratio.

Table 5.3-14. Carbon Isotopes in Unsaturated Zone Pore Waters from Surface-Based Boreholes at Yucca Mountain

Drill Hole	Depth Interval (ft)	Processed Length of Core[a] (ft)	Hydrologic Unit	Litho-stratigraphic Unit	$\delta^{13}C$ (‰)	^{14}C (pmc)	Uncorrected ^{14}C Age (yr.)[b]
ESF-AL#3-RB T#4	72.0 to 74.2	2.2	TCw	Tpcplnc	-12.2	89	961
ESF rubble from CS07+57.3	–	–	TCw	–	-16.2	84.7	1,369
NRG-6	219.9 to 256.1	1.2	PTn	Tpbt2	-14.9	92.1	679
NRG-7a	166.2 to 167.0	0.8	PTn	Tpbt3	-12.9	92.6	634
	258.0 to 259.4	1.4	PTn	Tpp/Tpbt2	–	74.3	2,449
	1,492.7 to 1,498.9	6.2	CHn	Tpbt1	-18.6	58.4	4,435
SD-12	265.8 to 277.8	12.0	PTn	Tpbt4	-14	80.3	1,809
	1,517.0 to 1,517.9	0.9	CHn	Tac3	-17.4	69.9	2,953
	1,637.4 to 1,640.0	2.6	CHn	Tacbt	-16.9	66.5	3,364
	1,901.6 to 1,901.8	0.2	CHn	Tcp2	-12.2	63.7	3718
	1,940.0 to 1,942.6	2.6	CHn	Tcp2	-16.3	59.2	4,322
SD-7	338.3 to 340.8	2.5	PTn	Tpbt3	-18.1	74.1	2,471
	1,498.2 to 1,498.9	0.7	CHn	Tac2	-15.1	73.5	2,539
	1,524.6 to 1,525.0	0.4	CHn	Tac1	-17.5	62.8	3,836
	1,558.1 to 1,558.9	0.8	CHn	Tac1	-27.4	60.6	4,130
SD-9	1,452.6 to 1,453.0	0.4	CHn	Tptpv1	-14.1	85.9	1,253
	1,535.2 to 1,535.7	0.5	CHn	Tac3	-15.3	88.9	970
	1,619.7 to 1,661.4	41.7	CHn	Tac2	-14.5	95.3	397
	1,800.7 to 1,801.6	0.9	CHn	Tacbt	-16.4	82.3	1,606
UZ#16	158.1 to 158.4	0.3	PTn	Tpcpv1	-9.3	87	1,148
	180.9	–	PTn	Tpbt3	-9.0	89.8	887
	219.4 to 219.6	0.2	PTn	Tptrv3	-9.4	87.3	1,120
	1,344.1 to 1,344.3	0.2	CHn	Tac2	–	87	1,148
	1,343.7 to 1,379.9	0.6	CHn	Tac2	-17.5	58.2	4,463
	1,380.0 to 1,380.5	0.5	CHn	Tac2	-23.3	71.8	2,731
	1,395.5 to 1,398.7	0.6	CHn	Tac2	-12.6	97.7	192
	1,398.1 to 1,398.3	0.2	CHn	Tac2	–	88.3	1,026
	1,408.2 to 1,434.6	0.6	CHn	Tac2	-16.6	53.1	5,219
	1,442.8 to 1,443.2	0.4	CHn	Tac2	-10.3	61.5	4,008
UZ-14	85.2 to 86.1	0.7	PTn	Tpbt3	-17.1	83.2	1,516
	91.0 to 100.8	1.45	PTn	Tpbt3	-15.0	83.3	1,507
	114.7 to 115.5	0.8	PTn	Tpp	–	86.9	1,158
	144.8 to 148.1	1.2	PTn	Tpp	–	84.9	1,350
	148.2 to 148.5	0.3	PTn	Tpp	-13.0	–	–
	215.7 to 226.2	10.5	PTn	Tpp	-25.0	96.2	319
	235.1 to 246.4	6.9	PTn	Tpbt2	-10.5	89.6	905
	254.9 to 255.7	0.8	PTn	Tpbt2	-13.0	–	–
	1,409.35 to 1,420.9	1.0	CHn	Tpbt1	-12.4	81.8	1,656
	1,429.87 to 1,430.15	0.28	CHn	Tac3	-11.1	69.9	2,953
	1,460.8 to 1,462.1	0.6	CHn	Tac3	-13.4	96.3	311
	1,524.55 to 1,526.2	0.6	CHn	Tac2	-11.8	93.4	563
	1,563.6 to 1,564.3	0.7	CHn	Tac2	-15.8	76.8	2,176
	1,563.9 to 1,565.1	1.2	CHn	Tac2	-15.2	80	1,840
	1,585.0 to 1,585.8	0.8	CHn	Tac2	-11.3	93.7	537

Table 5.3-14. Carbon Isotopes in Unsaturated Zone Pore Waters from Surface-Based Boreholes at Yucca Mountain (Continued)

Drill Hole	Depth Interval (ft)	Processed Length of Core[a] (ft)	Hydrologic Unit	Litho-stratigraphic Unit	$\delta^{13}C$ (‰)	^{14}C (pmc)	Uncorrected ^{14}C Age (yr.)[b]
UZ-14 (Continued)	1,605.6 to 1,606.4	0.8	CHn	Tac2	-14.6	81.1	1,727
	1,644.3 to 1,645.2	0.8	CHn	Tac2	-16.0	86.3	1,215
	1,674.3 to 1,675.3	1.0	CHn	Tac1	-13.7	91.3	750
	1,694.9 to 1,696.0	1.1	CHn	Tacbt	-10.3	92.3	661
	1,714.5 to 1,715.8	1.4	CHn	Tacbt	-11.6	96.3	311
	2,014.5 to 2,025.7	11.2	CHn	Tcp1	-14.7	94.0	510
	2,095.1 to 2,096.0	0.9	CHn	Tcb	-15.7	84.6	1,379

Source: CRWMS M&O (2000, Table 15)

NOTES: [a] Total length of core processed is estimated from the lengths of individual core listed for each composite sample in the source data tracking numbers.

[b] Uncorrected carbon-14 age calculated using the radioactive decay equation: $t = (t_{1/2} / \ln 2) \ln (A/A_0)$, where $t_{1/2}$ is the half-life for carbon-14 (5,715 yr.), A is the measured carbon-14 activity, and A_0 is the initial carbon-14 activity (100 percent modern carbon).

Table 5.3-15. Carbon Isotopes in Unsaturated Zone Pore Waters from UZ#4 and UZ#5

Drill Hole	Hydrogeologic and Lithostratigraphic Unit[a]		Depth (m)	Processed Length of Core (m)	$\delta^{13}C$ (‰)	^{14}C (pmc)	Uncorrected ^{14}C Age (yr.)
UZ#4	PTn	Tpbt2	96.0–100.6	4.6	-20.0	88.6	998
UZ#5	PTn	Tpbt2	103.6–105.2	1.6	-26.7	55.1	4,914

Source: CRWMS M&O (2000, Table 16)

NOTES: [a] Uncorrected carbon-14 age calculated using the radioactive decay equation: $t = (t_{1/2} / \ln 2) \ln (A/A_0)$, where $t_{1/2}$ is the half-life for carbon-14 (5,715 yr.), A is the measured carbon-14 activity, and A_0 is the initial carbon-14 activity (100 percent modern carbon).

Table 5.3-16. Carbon Isotopes in Unsaturated Zone Gases from the Atmosphere and Shallow Boreholes at Yucca Mountain

Borehole	Location of Gas Collection	Collection Date	^{14}C (pmc)	δ^{13}C (‰)
UZ-1	Atmosphere	Apr-84	125.6	-8.9
UZ-1	Atmosphere	Apr/May-85	124.4	-8.6
UZ-13	Atmosphere	21-Mar-95	106.2	–
UZ-13	Atmosphere	26 & 29-Mar-95	115.4	-8.7
UZ-N75	Atmosphere	15-Mar-94	114.6	–
UZ-1	Surface	Apr-84	124.3	-16.6
UZ-1	Surface	Apr/May-85	123.4	-14.6
UZ-6	Annulus	15-Mar-94	90.4	–
UZ-6	Annulus	21-Mar-95	93.0	–
UZ-6	Annulus	26 & 29-Mar-95	94.2	-17.4
UZ-N93	Annulus	15-Mar-94	113.5	–
UZ-N93	Annulus	26 & 29-Mar-95	114.0	-17.4
UZ-N94	Annulus	15-Mar-94	114.0	–
UZ-N94	Annulus	26 & 29-Mar-95	109.8	-17.6
UZ-N95	Annulus	15-Mar-94	106.0	–
UZ-N95	Annulus	26 & 29-Mar-95	109.4	-17.2

Source: CRWMS M&O (2000, Table 17)

NOTES: These data are used to corroborate the present-day elevated carbon-14 activity in the atmosphere due to global fallout, and to corroborate that this activity is not greatly diluted by processes in shallow soil or bedrock, although the effects of microbial activity and plant respiration on surface and subsurface samples result in a shift in delta carbon-13 to more negative values.

Table 5.3-17. Carbon Isotopes in Unsaturated Zone Gases from Deep Open Surface-Based Boreholes at Yucca Mountain (NRG#5, NRG-6, NRG-7a, SD-7, SD-9, SD-12, UZ-14, and UZ#16)

Borehole	Depth	Hydrogeologic and Lithostratigraphic Unit[a]		Collection Date	CO_2 (vol. %)[b]	$\delta^{13}C$ (‰)[c]	^{14}C (pmc)[c]	Uncorrected ^{14}C Age (yr.)
NRG#5	133 ft	TCw	Tpcpln	14&15-Aug-96	–	-16.7	88.82	978
					–	-14.6	–	–
					–	-14.6	–	–
	243 ft	PTn	Tpp	14&15-Aug-96	–	-16.7	68.56	3,112
					–	-14.9	–	–
					–	-14.8	–	–
					–	-9.7	–	–
	298 ft	PTn	Tpbt2	14&15-Aug-96	–	-15.5	69.57	2,992
					–	-14.6	–	–
					–	-14.6	–	–
	354 ft	TSw	Tptrn	14&15-Aug-96	–	-15.3	54.19	5,051
					–	-14.4	–	–
					–	-14.4	–	–
	410 ft (Zone 5)	TSw	Tptrn	23-Aug-95	–	-14.9	–	–
				14&15-Aug-96	–	-15.7	65.77	3,455
					–	-14.6	–	–
					–	-14.4	–	–
					–	-13.1	–	–
					–	-12.1	–	–
	466 ft	TSw	Tptrn	14&15-Aug-96	–	-16.4	77.47	2,105
					–	-15.6	–	–
					–	-15.6	–	–
	475 ft	TSw	Tptrn	Mar-94	–	-16.1	51.3	5,503
	521 ft	TSw	Tptprl or Tptpul	14&15-Aug-96	–	-16.8	69.95	2,947
					–	-15.2	–	–
					–	-15.2	–	–
	572 ft (Zone 9)	TSw	Tptprl or Tptpul	23-Aug-95	–	-15.4	–	–
				14&15-Aug-96	–	-14.5	57.27	4,596
					–	-14.3	–	–
					–	-14.1	–	–
					–	-14.0	–	–
					–	-11.3	–	–
					–	-14.0	–	–
	633 ft	TSw	Tptprl or Tptpul	14&15-Aug-96	–	-14.3	–	–
					–	-14.4	–	–
					–	-15.7	61.31	4,034
	744 ft	TSw	Tptpul	14&15-Aug-96	–	-15.7	58.41	4,433
	799 ft	TSw	Tptpmn	14&15-Aug-96	–	-14.6	59.00	4,350
					–	-13.0	–	–
					–	-13.0	–	–
	1,225 ft (Zone 13)	TSw	Tptpln	Mar-94	–	-15.0	93.1	589
				23-Aug-95	–	-15.0	–	–

TDR-CRW-GS-000001 REV 01 ICN 01   T5.3-25   September 2000

Table 5.3-17. Carbon Isotopes in Unsaturated Zone Gases from Deep Open Surface-Based Boreholes at Yucca Mountain (NRG#5, NRG-6, NRG-7a, SD-7, SD-9, SD-12, UZ-14, and UZ#16) (Continued)

Borehole	Depth	Hydrogeologic and Lithostratigraphic Unit[a]		Collection Date	CO_2 (vol. %)[b]	$\delta^{13}C$ (‰)[c]	^{14}C (pmc)[c]	Uncorrected ^{14}C Age (yr.)
NRG-6	20 ft	TCw	Tpcpll	3-May-94	0.07	-15.2	–	–
	80 ft	TCw	Tpcpln	Mar-94	–	-15.2	92.1	679
				24-May-94	0.11	-14.3	–	–
	200 ft	PTn	Tpp	Mar-94	–	-14.9	91.0	778
				24-May-94	0.115	-14.3	–	–
	275 ft	TSw	Tptrn	3-May-94	0.06	–	–	–
				24-May-94	0.05	-15.1	–	–
	600 ft	TSw	Tptpul	Mar-94	0.10	-15.5	83.2	1,516
				24-May-94	0.115	-14.1	–	–
	725 ft	TSw	Tptpmn	3-May-94	0.06	–	–	–
				24-May-94	0.07	-14.8	–	–
	925 ft	TSw	Tptpll	Mar-94	0.11	-16.1	94.2	493
				24-May-94	0.11	-14.2	–	–
	1,000 ft	TSw	Tptpll	3-May-94	0.07	-14.5	–	–
NRG-7a	140 ft	PTn	Tpcpv2	Not specified	0.09	-17.35	–	–
				Mar-94	–	-16.8	108.0	Modern
				29-Jun-94	0.12	–	–	–
	490 ft	TSw	Tptrl	Mar-94	–	-18.2	111.7	Modern
				29-Jun-94	0.19	–	–	–
	890 ft	TSw	Tptpll	Mar-94	0.15	-19.0	111.0	Modern
				29-Jun-94	0.15	–	–	–
	1,215 ft	TSw	Tptpll	Mar-94	–	-18.0	–	–
				29-Jun-94	0.19	–	–	–
SD-7	300 ft	TCw	Tpcpv2	15-Aug-96	–	-17.6	100.27	Modern
					–	-16.4	–	–
					–	-16.3	–	–
	350 ft	PTn	Tpp	15-Aug-96	–	-16.4	91.38	743
					–	-15.1	–	–
					–	-14.1	–	–
	400 ft	TSw	Tptrn	15-Aug-96	–	-16.2	83.78	1,459
					–	-14.6	–	–
					–	-14.5	–	–
	500 ft	TSw	Tptpul	15-Aug-96	–	-16.9	72.18	2,688
					–	-13.0	–	–
					–	-13.0	–	–
	550 ft	TSw	Tptpul	15-Aug-96	–	-14.6	92.43	649
					–	-12.3	–	–
					–	-12.1	–	–
	600 ft	TSw	Tptpul	15-Aug-96	–	-14.6	79.40	1,902
					–	-12.7	–	–
					–	-12.6	–	–
	650 ft	TSw	Tptpul	15-Aug-96	–	-9.1	–	–
					–	-8.9	–	–

Borehole	Depth	Hydrogeologic and Lithostratigraphic Unit[a]		Collection Date	CO_2 (vol. %)[b]	$\delta^{13}C$ (‰)[c]	^{14}C (pmc)[c]	Uncorrected ^{14}C Age (yr.)
SD-7 (Continued)	700 ft	TSw	Tptpmn	15-Aug-96	–	-16.0	86.78	1,169
					–	-13.3	–	–
					–	-13.3	–	–
	800 ft	TSw	Tptpmn	15-Aug-96	–	-15.6	84.18	1,420
					–	-12.3	–	–
					–	-12.3	–	–
	508–633 m	TSw	Tptpul	Not specified	–	-25.0	41.52	7,247
SD-9	0–454 m (Zone 1)	TCw-CHn	Tpcplnc/Tac3	Not specified	–	-16.1	96.70	277
				2/01/95	0.27	-13.7	–	–
				8/23/95	–	-15.2	–	–
	454–560 m (Zone 2)	CHn	Tac3-Tcp4	Not specified	–	-19.1	51.04	5,545
				2/01/95	0.092	-19.6	–	–
				8/23/95	–	-19.8	–	–
SD-12	216–220 m	TSw	Tptpmn	Not specified		-11.6	74.33	2,446
	342–347 m	TSw	Tptpln	Not specified		-16.1	60.17	4,188
UZ-14	1,445 ft	CHn	Tac3	1997	0.05	-15.1	99.17	Modern
	1,490 ft	CHn	Tac3	1997	0.06	-19.4	50.42	5,646
	1,540 ft	CHn	Tac2	1997	1.0	-8.4	48.76	5,922
	1,590 ft	CHn	Tac2	1997	0.04	-9.3	99.2[d]	Modern
	1,640 ft	CHn	Tac2	1997	0.06	-9.2	100.9[d]	Modern
	1,690 ft	CHn	Tac1	1997	1.2	-20.9	67.8	3,204
	1,738 ft	CHn	Tacbs	1997	1.1	-20.0	80.1	1,830
UZ#16	45.7 m	TCw	Tpcplnc	–	–	-15.5	73.2	2,572
					–	-13.8	–	–
	14.3–74.1 m	TCw-TSw	Tpcpll-Tptrn	–	–	-14.0	72.7	2,629
					–	-12.3	–	–
	73.1 m	TSw	Tptrn	–	–	-13.2	–	–
	82.3 m	TSw	Tptrn	–	–	-13.0	–	–
	74.1–148 m	TSw	Tptrn-Tptpul	–	–	-16.5	87.0	1,148
					–	-20.2	–	–
	148–163 m	TSw	Tptpul	–	–	-14.7	81.6	1,677
					–	-18.3	–	–
	163–512 m	TSw-CHn	Tptpul-Tcp2	–	–	-17.0	89.2	942
					–	-15.6	–	–
	477–481 m	CHn	Tcp3	–	–	-18.4	25.8	11,170
					–	-16.4	–	–

Source: CRWMS M&O (2000, Table 18). Only the average CO_2 concentrations and carbon-13 values are reported in this table when replicate analyses are available. Data have been rounded to make it easier to compare them, although carbon-14 ages have been calculated from the unrounded values.

Table 5.3-17. Carbon Isotopes in Unsaturated Zone Gases from Deep Open Surface-Based Boreholes at Yucca Mountain (NRG#5, NRG-6, NRG-7a, SD-7, SD-9, SD-12, UZ-14, and UZ#16) (Continued)

NOTES: [a] In open boreholes, CO_2 gas concentrations are often quite variable from one collection time to another, even when the samples are collected from the same packed-off borehole interval within 24 hr. of one another. Thus, the CO_2 values reported in this table should be used only as an approximate indication of in situ conditions.

[b] Yang, Yu et al. (1998, p. 16) warn that samples collected for SD-7, SD-9, and SD-12 by the whole-gas balloon method varied from -10 to -25 percent for replicate samples (U.S. Geological Survey data), probably due to problems with the balloon nozzle; hence, these data are not reported here. The values reported above were obtained by the Desert Research Institute. These values were less variable than the U.S. Geological Survey data, although they also tend to be more negative by a few units per mil (‰) when collected with the molecular sieve.

[c] Contamination with atmospheric air is suspected, as indicated by carbon-14 data, although there were no known leaks present during sample collection.

– = data not available; no report = collection date not reported

Table 5.3-18. Carbon Isotopes in Unsaturated Zone Gases from Boreholes UZ-6 and UZ-6s

| Borehole | Depth (ft) | $\delta^{13}C$ (‰)[a] 26-Mar-95 WGM[b] | ^{14}C (pmc)[a] | | | Uncorrected ^{14}C Age (yr.)[b] 29-Mar-95 |
			15-Mar-94 WGM[b]	21-Mar-95 Molecular Sieve[b]	29-Mar-95 KOH[b]	
UZ-6	200	-17.40	–	88.47	88.15	1,040
	800	-17.14	–	83.27	84.91	1,349
	1,195	-17.18	–	84.74	86.09	1,235
	1,800	-16.62	–	50.36	40.98	7,355
UZ-6s	20	-16.68	107.90	90.67	106.81	Modern
	40	-16.59	107.33	100.93	106.75	Modern
	60	-16.90	106.09	96.17	105.24	Modern
	100	-16.45	107.90	109.53	105.62	Modern
	200	-16.42	109.07	102.03	107.82	Modern
	350	-16.34	107.79	107.61	107.32	Modern
	400	-15.16	100.73	101.90	99.45	Modern
	430	-16.42	–	95.00	94.72	447

Source: CRWMS M&O (2000, Table 19)

NOTES: [a] Gas collection methods: WGM = whole gas balloon method; Molecular Sieve = molecular-sieve method; KOH = gas bubbled through potassium hydroxide solution

[b] Uncorrected carbon-14 age calculated using the radioactive decay equation: $t = (t_{1/2} / \ln 2) \ln (A/A_0)$, where $t_{1/2}$ is the half-life for carbon-14 (5,715 yr.), A is the measured carbon-14 activity, and A_0 is the initial carbon-14 activity (100 percent modern carbon).

Table 5.3-19. Carbon Dioxide and Carbon Isotope Profiles in Unsaturated Zone Gases from Instrumented Boreholes UZ-1 and SD-12

Borehole	Depth	Probe or Station	Hydrogeologic and Lithostratigraphic Unit[a]		CO_2 (vol. %)[a]	$\delta^{13}C$ (‰)	^{14}C (pmc)	Uncorrected ^{14}C Age[a] (yr.)
UZ-1	42 ft	1	Qtac	UO	0.535	-18.9	108.5	Modern
	62 ft	2	PTn	Tpy	0.581	-20.4	104.3	Modern
	93 ft	3	PTn	Tpbt3	0.307	-20.8	96.2	319
	131 ft	4	PTn	Tpp	0.428	-19.9	89.4	924
	201 ft	5	PTn	Tpp	0.230	-20.3	67.2	3,277
	266 ft	6	PTn	Tptrv3	0.205	-17.4	64.7	3,590
	348 ft	7	TSw	Tptrn	0.104	-16.2	63.3	3,770
	421 ft	8	TSw	Tptrn	0.092	-15.7	61.1	4,062
	501 ft	9	TSw	Tptpul	0.082	-16.2	47.4	6,155
	621 ft	10	TSw	Tptpul	0.051	-16.1	42.6	7,036
	747 ft	11	TSw	Tptpmn	0.094	-14.6	47.2	6,190
	871 ft	12	TSw	Tptpll	0.121	-15.7	37.1	8,175
	998 ft	13	TSw	Tptpll	0.042	-16.9	–	–
	1,100 ft	14	TSw	Tptpll	0.091	-15.0	38.8	7,806
	1,207 ft	15	TSw	Tptpll	0.216	-19.7	14.5	15,921
SD-12	24.7 m	P	TCw	Tpcpmn/Tpcpll	–	-22.55	90.98	779
	43.9 m	O	TCw	Tpcplnh	–	-20.20	49.17	5,853
	65.2 m	N	TCw	Tpcplnc	–	-21.99	87.39	1,111
	91.7 m	L	PTn	Tptrv1	–	-16.41	82.71	1,565
	107.0 m	K	TSw	Tptrn	–	-20.98	77.75	2,075
					–	-15.58	94.91	431
	128.9 m	J	TSw	Tptrn	–	-22.11	57.95	4,498
	171.0 m	I	TSw	Tptpul	–	-23.57	38.95	7,774
	208.2 m	H	TSw	Tptpmn	–	-24.71	36.92	8,215
	236.8 m	G	TSw	Tptpmn	–	-25.57	31.57	9,506
	256.6 m	F	TSw	Tptpll	–	-24.40	34.13	8,863
	285.0 m	E	TSw	Tptpll	–	-21.89	52.41	5,327
	322.5 m	D	TSw	Tptpln	–	-21.79	46.65	6,287
					–	-23.83	34.43	8,791
	385.6 m	C	TSw	Tptpln	–	-22.86	88.69	990
	407.2 m	B	CHn	Tptpv2	–	-24.63	24.43	11,620
					–	-23.65	26.89	10,829
	435.9 m	A	CHn	Tac4	–	-17.17	84.47	1,392

Source: CRWMS M&O (2000, Table 20)

NOTES: [a]Uncorrected carbon-14 age calculated using the radioactive decay equation: $t = (t_{1/2} / \ln 2) \ln (A/A_0)$, where $t_{1/2}$ is the half-life for carbon-14 (5,715 yr.), A is the measured carbon-14 activity, and A_0 is the initial carbon-14 activity (100 percent modern carbon).

– = not available

Table 5.3-20. Carbon Isotopes in Unsaturated Zone Gases from Boreholes in Exploratory Studies Facility Alcoves

Borehole	Sampled Interval (m)	Hydrogeologic Unit	Lithostratigraphic Unit	^{14}C (pmc)	$\delta^{13}C$ (‰)
Alcove #1 air	NA	–	–	–	-9.13 -9.07
ESF-AL#1-RBT#1	30–32	TCw	Tpcpul	101.35	-15.61
	35–42.5	TCw	Tpcpul	–	-13.49
	44–48	TCw	Tpcpul	–	-16.40
	49–55	TCw	Tpcpul	–	-13.60
	55.75–59	TCw	Tpcpul	–	-14.49
	60–73	TCw	Tpcpul	–	-14.42
ESF-AL#1-RBT#2	6.5–9	TCw	Tpcpul	–	-18.35
	28–38	TCw	Tpcpul	–	-13.46
	62–65	TCw	Tpcpul	–	-16.20
	62–83	TCw	Tpcpul	92.76	-14.69
	86–105	TCw	Tpcpul	–	-16.23 -15.80
ESF-AL#1-RBT#3	50.75–62.5	TCw	Tpcpul	107.35	-15.79 -10.22
	64–66.5	TCw	Tpcpul	–	-17.86
	85.5–92.8	TCw	Tpcpul	–	-15.83
ESF-AL#6 ZONE 1 WGM	4.7	TSw	Tptpmn	69.24	-14.14
ESF-AL#6 ZONE 2 WGM	7.8	TSw	Tptpmn	75.09	-14.06
ESF-AL#6 ZONE 3 WGM	9.3	TSw	Tptpmn	71.58	-14.11
ESF-AL#6 ZONE 4 WGM	10.8	TSw	Tptpmn	63.74	-15.08
ESF-AL#6 ZONE 5 WGM	12.4	TSw	Tptpmn	66.77	-15.45
ESF-AL#6 ZONE 6 WGM	13.9	TSw	Tptpmn	68.23	-15.38
ESF-AL#6 ZONE 7 WGM	15.4	TSw	Tptpmn	70.76	-15.55
ESF-AL#6 ZONE 8 WGM	16.9	TSw	Tptpmn	61.37	-14.78
ESF-AL#6 ZONE 9 WGM	18.5	TSw	Tptpmn	58.14	-16.17
ESF-AL#6 ZONE 10 WGM	21.5	TSw	Tptpmn	66.01	-15.89

Source: CRWMS M&O (2000, Table 2).

NOTES: The delta carbon-13 values in this table are the averages of those reported for each zone in the Alcove 6 borehole.

Table 5.3-21. Uranium Isotopic Data for Ephemeral Streamflow in the Vicinity of Yucca Mountain

Location	Sample Name	Collection Date	Concentration		Activity Ratios	
			U (µg/L)	±2σ	$^{234}U/^{238}U$	±2 σ
Fortymile Wash runoff	CSS950106FMOV.4	01/06/95	0.0473	0.0002	3.670	0.081
Pah Canyon	SPC00009734 HOH	01/26/95	0.1111	0.0003	1.833	0.015
Fortymile Canyon	SPC00009805 HOH	01/25/95	0.2613	0.0007	1.497	0.015
Upper Split Wash	SPC00009732 HOH	01/25/95	0.3880	0.0010	1.501	0.009
Yucca Wash near mouth	SPC00009733 HOH	01/26/95	0.1086	0.0003	1.623	0.016
Upper reach, Wren Wash	SPC00009806 HOH	01/25/95	0.4868	0.0012	1.525	0.006
Wren Wash	SPC00529907-Wren Wash	02/20/98	0.2224	0.0007	1.543	0.005
Pagany Wash	SPC00529917-Pagany Wash	02/24/98	0.3766	0.0013	1.528	0.006
Yucca Wash	SPC00529927-Yucca Wash	02/24/98	0.1705	0.0005	1.721	0.01

Source: CRWMS M&O (2000, Table 23)

NOTE: Uranium isotopic data was obtained by mass spectrometry at the U.S. Geological Survey, Denver, Colorado. All errors are reported at the 95 percent confidence level.

Table 5.3-22. Comparison of Carbon Isotopes in Pore Water and Gas Samples Collected from Similar Borehole Intervals

Borehole	Pore-Water Results					Gas Results			
	Stratigraphic Unit		Depth (m)	$\delta^{13}C$ (‰)	^{14}C (pmc)	Stratigraphic Unit		Depth (m)	$\delta^{13}C$ (‰)	^{14}C (pmc)
NRG-6	PTn	Tpbt2	71.6	-14.9	92.1	PTn	Tpp	61	-14.1 to -14.9	91.0
SD-7	PTn	Tpbt3	103	-18.1	74.1	PTn	Tpp	107	-14.1 to -16.4	91.4
SD-9	CHn	Tac3	468	-15.3	88.9	CHn	Tac3	454	-19.1	51.0
	CHn	Tac2	494 to 506	-14.5	95.3		to	to	to	
	CHn	Tacbt	549	-16.4	82.3		Tcp4	560	-19.8	
SD-12	PTn	Tpbt4	82	-14	80.3	PTn	Tptrv1	92	-16.4	82.7
	CHn	Tac3	462	-17.4	69.9	CHn	Tac4	436	-17.2	84.5
UZ-14	CHn	Tac3	436	-11.1	69.9	CHn	Tac3	440	Variable	99.2
	CHn	Tac3	445	-13.4	96.3	CHn	Tac3	454	-19.45	50.4
	CHn	Tac2	465	-11.8	93.4	CHn	Tac2	469	-8.42	48.8
	CHn	Tac2	477	-15.8	76.8	–	–	–	–	–
	CHn	Tac2	477	-15.2	80.0	–	–	–	–	–
	CHn	Tac2	483	-11.3	93.7	CHn	Tac2	485	-9.3	99.2
	CHn	Tac2	490	-14.6	81.1	–	–	–	–	–
	CHn	Tac2	501	-16	86.3	CHn	Tac2	500	-9.24	100.9
	CHn	Tac1	510	-13.7	91.3	CHn	Tac1	515	-20.89	67.8
	CHn	Tacbt	517	-10.3	92.3	CHn	Tacbs	530	-20.05	80.1
	CHn	Tacbt	523	-11.6	96.3	–	–	–	–	–
UZ-14 pore water (compared with UZ-1 gas from similar depth)	PTn	Tpbt3	26	-17.1	83.2	PTn	Tpbt3	28	-20.8	96.2
	PTn	Tpbt3	29	-15.0	83.3	–	–	–	–	–
	PTn	Tpp	45	-13.0	84.9	PTn	Tpp	40	-19.9	89.4
	PTn	Tpp	67	-25.0	96.2	PTn	Tpp	61	-20.3	67.2

Source: CRWMS M&O (2000, Table 22)

Table 5.3-23. Locations and Other Physical Characteristics of Wells Sampled for Chemical and Isotopic Analyses of Groundwater in the Vicinity of Yucca Mountain

Site Name	UTM-x (m)	UTM-y (m)	Site Elevation (m)	Well Depth (m)	Water Table Depth (m)	Aquifer[a]
15S/49E-13dda	553312.5	4055302	796	174	90	Qal
15S/49E-22a1	550086.3	4054974	796	174	90	Qal
15S/49E-22dcc	549672.5	4053523	784	148	78	Qtal
15S/49E-27acc	549552.9	4052722	777	467	73	Qal
15S/50E-18ccc	553710.0	4055273	812	120	105	Qal
15S/50E-18cdc	553934.3	4055151	812	120	105	Qal
15S/50E-19b1	553862.5	4054720	–	110	103	Qal
16S/49E-05acc	546664.5	4049439	746	87	21	Qal
Airport Well	553289.0	4055086	804	229	76	Qal
BGMW-11	534410.9	4062631	786	–	72	Qal
Cind-R-Lite Well	544027.0	4059809	831	140	101	Tv
Cowboy Joe's	554132.4	4055245	–	–	–	Qal
Gexa Well 4	534068.9	4086110	1,198	488	188	Tv
JF-3	554498.3	4067974	944	347	216	Tv
NDOT well	554132.4	4055245	810	151	105	Qal
TW-5	562605.0	4054686	931	244	207	Qal
UE-25 b#1 (0-1220 m)	549954.5	4078422	1,201	1,220	470	Th/Tct
UE-25 b#1 (853-914 m)	549954.5	4078422	1,201	1,220	470	Tcb
UE-25 c#1	550957.7	4075943	1,131	914	401	Tcb/Tct
UE-25 c#2	550944.0	4075867	1,132	914	401	Tcb
UE-25 c#3	550919.8	4075886	1,132	914	402	Tcb/Tct
UE-25 J-11	563816.0	4071049	1,050	405	317	Tb
UE-25 J-12	554435.8	4068767	953	347	226	Tv
UE-25 J-13	554004.4	4073550	1,011	1,063	283	Tpt
UE-25 ONC-1	550479.9	4076608	1,163	469	433	Th/Tcp
UE-25 p#1 (0-1200 m)	551508.7	4075663	1,114	1,805	382	Tcp
UE-25 p#1 (1300-1800 m)	551508.7	4075663	1,114	1,805	382	Dslm
UE-25 WT#12	550162.9	4070647	1,075	399	345	Tpt/Th
UE-25 WT#14	552638.0	4077337	1,076	399	346	Th
UE-25 WT#15	554033.7	4078702	1,083	415	354	Tpt
UE-25 WT#4	550445.9	4079420	1,169	482	438	Th
UE-25 WT-7	546148.2	4075461	1,197	491	421	Tv
UE-29 a#2 (250-355 m)	555753.3	4088351	1,215	422	29	Th
UE-29 a#2 (87-213 m)	555753.3	4088351	1,215	422	28	Th
USW G-2	548138.6	4082554	1,554	1,831	534	Th/Tct
USW G-4	548938.0	4078590	1,270	915	541	Tct
USW H-1 (572-687 m)	548721.8	4079944	1,303	1,829	572	Tcp
USW H-1 (687-1829 m)	548721.8	4079944	1,303	1,829	572	Tcb
USW H-3	547537.0	4075762	1,483	1,219	751	Tct

Table 5.3-23. Locations and Other Physical Characteristics of Wells Sampled for Chemical and Isotopic Analyses of Groundwater in the Vicinity of Yucca Mountain (Continued)

Site Name	UTM-x (m)	UTM-y (m)	Site Elevation (m)	Well Depth (m)	Water Table Depth (m)	Aquifer[a]
USW H-4	549195.0	4077322	1,249	1,219	519	Tcb/Tct
USW H-5	547665.5	4078838	1,477	1,219	704	Tcb/Tct
USW H-6 (525-1220 m)	546196.1	4077816	1,302	1,220	526	Tcb/Tct
USW H-6 (600-650 m)	546196.1	4077816	1,302	1,220	526	Tcb/Tct
USW H-6 (753-835 m)	546196.1	4077816	1,302	1,220	526	Tcb/Tct
USW VH-1	539986.2	4071718	963	762	184	Tcb
USW VH-2	537737.6	4073222	974	1,219	164	Tv
USW WT-10	545976.0	4073389	1,123	431	347	Tpt

Source: CRWMS M&O (2000, Table 24)

NOTES: [a] Aquifer = geologic unit from which water was obtained (Oliver and Root 1997, p. 5)

Qal = Quaternary alluvium; Qtal = Quaternary-Tertiary alluvium; Tv = Tertiary volcanic rocks; Tpt = Tertiary Topopah Spring Member of Paintbrush Tuff; Tct = Tertiary Crater Flat Tuff; Th = TertiarytTuffaceous beds of Calico Hills; Tcb = Tertiary Bullfrog Member of Crater Flat Tuff; Dslm = Devonian and Silurian Lone Mountain dolomite.

Table 5.3-24. Chloride Concentrations and Infiltration Rates Calculated for Tunnel Pore Waters by the Chloride Mass-Balance Method

Borehole	Tunnel	Tunnel Distance (m)	Hydrologic Unit	Stratigraphic Unit	CI (mg/L)	Apparent Infiltration Rate[a] (mm/ yr.)	
						Rate 1	Rate 2
ECRB-SYS-CS150	Cross Drift	150	TSw	Tptpul	25.0	2.4	4.1
ECRB-SYS-CS200	Cross Drift	200	TSw	Tptpul	19.1	3.1	5.3
ECRB-SYS-CS200	Cross Drift	200	TSw	Tptpul	19.2	3.1	5.3
ECRB-SYS-CS400	Cross Drift	400	TSw	Tptpul	11.8	5.0	8.6
ECRB-SYS-CS450	Cross Drift	450	TSw	Tptpul	33.6	1.8	3.0
ECRB-SYS-CS550	Cross Drift	550	TSw	Tptpul	20.2	2.9	5.0
ECRB-SYS-CS600	Cross Drift	600	TSw	Tptpul	17.9	3.3	5.7
ECRB-SYS-CS650	Cross Drift	650	TSw	Tptpul	16.0	3.7	6.4
ECRB-SYS-CS750	Cross Drift	750	TSw	Tptpul	24.6	2.4	4.2
ECRB-SYS-CS800	Cross Drift	800	TSw	Tptpul	15.0	4.0	6.8
ECRB-SYS-CS850	Cross Drift	850	TSw	Tptpul	26.3	2.3	3.9
ECRB-SYS-CS900	Cross Drift	900	TSw	Tptpul	24.9	2.4	4.1
ECRB-SYS-CS950	Cross Drift	950	TSw	Tptpul	24.9	2.4	4.1
ECRB-SYS-CS1000	Cross Drift	1,000	TSw	Tptpul	36.6	1.6	2.8
ECRB-SYS-CS1050	Cross Drift	1,050	TSw	Tptpmn	16.6	3.6	6.1
ECRB-SYS-CS1550	Cross Drift	1,550	TSw	Tptpll	37.7	1.6	2.7
ECRB-SYS-CS1600	Cross Drift	1,600	TSw	Tptpll	31.3	1.9	3.3
ECRB-SYS-CS1650	Cross Drift	1,650	TSw	Tptpll	16.5	3.6	6.2
ECRB-SYS-CS1750	Cross Drift	1,750	TSw	Tptpll	12.9	4.6	7.9
ECRB-SYS-CS1950	Cross Drift	1,950	TSw	Tptpll	14.3	4.2	7.1
ECRB-SYS-CS2000	Cross Drift	2,000	TSw	Tptpll	22.4	2.7	4.6
ECRB-SYS-CS2100	Cross Drift	2,100	TSw	Tptpll	17.0	3.5	6.0
ECRB-SYS-CS2150	Cross Drift	2,150	TSw	Tptpll	16.4	3.6	6.2
ECRB-SYS-CS2300	Cross Drift	2,300	TSw	Tptpll	21.0	2.8	4.9
ESF-NR-MOISTSTDY#1a	ESF	727	TCw	Tpcplnc	19.7	3.0	5.2
ESF-NR-MOISTSTDY#2	ESF	750	TCw	Tpcplnc/mw	18.4	3.2	5.5
ESF/CS/07+57.53	ESF	758	PTn	Unknown	34.2	1.7	3.0
ESF-AL#3-RBT#1 32.1/UP	ESF Alcove 3	758	PTn	Unknown	40.9	1.5	2.5
ESF-NR-MOISTSTDY#3	ESF	770	TCw	Tpcplnc/mw	40.3	1.5	2.5
ESF-NR-MOISTSTDY#4	ESF	772	TCw	Tpcpv2	47.1	1.3	2.2
ESF-NR-MOISTSTDY#5	ESF	783	TCw	Tpcpv2	27.9	2.1	3.7
ESF-NR-MOISTSTDY#6	ESF	821	PTn	Tpcpv1	69.2	0.9	1.5
ESF-NR-MOISTSTDY#7	ESF	867	PTn	Tpbt4	15.1	3.9	6.8
ESF-NR-MOISTSTDY#8	ESF	870	PTn	Tpy	15.7	3.8	6.5
ESF-NR-MOISTSTDY#9	ESF	873	PTn	Tpbt3	5.7	10.4	17.9
ESF-NR-MOISTSTDY#10	ESF	880	PTn	Tpbt3	15.0	4.0	6.8
ESF-NR-MOISTSTDY#11	ESF	892	PTn	Tpp	6.7	8.9	15.2
ESF-NR-MOISTSTDY#13	ESF	1,008	PTn	Tpbt2	12.0	5.0	8.5
ESF-NR-MOISTSTDY#15	ESF	1,054	PTn	Tptrv3/rv2	20.8	2.9	4.9
ESF-NR-MOISTSTDY#16	ESF	1,069	TSw	Tptrv2	12.9	4.6	7.9
ESF-LPCA-MOISTSTDY#2	ESF Alcove 4	1,130	PTn	Tpbt2/argillic	17.7	3.4	5.8
ESF-LPCA-MOISTSTDY#3	ESF Alcove 4	1,130	PTn	Tpbt2	17.5	3.4	5.8

Table 5.3-24. Chloride Concentrations and Infiltration Rates Calculated for Tunnel Pore Waters by the Chloride Mass-Balance Method (Continued)

Borehole	Tunnel	Tunnel Distance (m)	Hydrologic Unit	Stratigraphic Unit	Cl (mg/L)	Apparent Infiltration Rate[a] (mm/ yr.)	
						Rate 1	Rate 2
ESF-HD-PERM-3	ESF Alcove 5	~2,800	TSw	Unknown	111.0	0.5	0.9
ESF-HD-PERM-3	ESF Alcove 5	~2,800	TSw	Unknown	133.0	0.4	0.8
ESF-MD-NICHE3566#1	ESF	3,566	TSw	Tptpmn	15.7	3.8	6.5
ESF-MD-NICHE3566LT#1	ESF	3,566	TSw	Tptpmn	27.5	2.2	3.7
ESF-MD-NICHE3650#6	ESF	3,650	TSw	Tptpmn	15.9	3.7	6.4
ESF-MD-NICHE3650#7	ESF	3,650	TSw	Tptpmn	32.3	1.8	3.2
ESF-SR-MOISTSTDY#10	ESF	6,648	TSw	Tptrv2	15.3	3.9	6.7
ESF-SR-MOISTSTDY#11	ESF	6,658	PTn	Tptrv3	26.5	2.2	3.8
ESF-SR-MOISTSTDY#12	ESF	6,668	PTn	Tpbt2	29.7	2.0	3.4
ESF-SR-MOISTSTDY#13	ESF	6,679	PTn	Tpbt2	32.2	1.8	3.2
ESF-SR-MOISTSTDY#14	ESF	6,696	PTn	Tpbt4	33.0	1.8	3.1
ESF-SR-MOISTSTDY#15	ESF	6,704	PTn	Tpcpv1	26.8	2.2	3.8
ESF-SR-MOISTSTDY#16	ESF	6,721	PTn	Tpcpv1	39.1	1.5	2.6
ESF-SR-MOISTSTDY#17	ESF	6,729	TCw	Tpcplnc/Tpcpv1	55.3	1.1	1.8
ESF-SR-MOISTSTDY#19	ESF	6,826	TSw	Tptpul	17.1	3.5	6.0
ESF-SR-MOISTSTDY#21	ESF	7,054	PTn	Tpbt2	80.9	0.7	1.3
ESF-SR-MOISTSTDY#22	ESF	7,056	PTn	Tpbt2	103.0	0.6	1.0
ESF-SR-MOISTSTDY#22r	ESF	7,056	PTn	Tpbt2	96.1	0.6	1.1
ESF-SR-MOISTSTDY#27	ESF	7,444	TSw	Tptrv1	38.9	1.5	2.6
ESF-SR-MOISTSTDY#28	ESF	7,446	TSw	Tptrv2	43.2	1.4	2.4
ESF-SR-MOISTSTDY#29	ESF	7,453	PTn	Tptrv3	63.2	0.9	1.6
ESF-SR-MOISTSTDY#30	ESF	7,460	PTn	Tpbt2	107.6	0.6	0.9
ESF-SR-MOISTSTDY#31	ESF	7,465	PTn	Tpbt2	97.6	0.6	1.0
ESF-SR-MOISTSTDY#32	ESF	7,472	PTn	Tpbt2	72.4	0.8	1.4
ESF-SR-MOISTSTDY#33	ESF	7,477	PTn	Tpbt2	87.3	0.7	1.2
ESF-SR-MOISTSTDY#34	ESF	7,481	PTn	Tpp	85.1	0.7	1.2
ESF-SR-MOISTSTDY#35	ESF	7,488	PTn	Tpbt3	72.2	0.8	1.4
ESF-SR-MOISTSTDY#36	ESF	7,490	PTn	Tpbt3	54.0	1.1	1.9
ESF-SR-MOISTSTDY#37	ESF	7,498	PTn	Tpbt4	83.4	0.7	1.2
ESF-SR-MOISTSTDY#38	ESF	7,503	PTn	Tpbt4	74.6	0.8	1.4
ESF-SR-MOISTSTDY#39	ESF	7,504	PTn	Tpcpv1	85.0	0.7	1.2
UZTT-BB-PH1-2	Busted Butte	NA	CHn	Below Tptpv1/Tac	70.6	0.8	1.4
UZTT-BB-PH1-3	Busted Butte	NA	CHn	Tptpv1	51.2	1.2	2.0
UZTT-BB-PH1-4	Busted Butte	NA	CHn	Tac	64.6	0.9	1.6
UZTT-BB-PH1-6	Busted Butte	NA	CHn	Tptpv2/pv1	36.7	1.6	2.8
UZTT-BB-PH1-7	Busted Butte	NA	CHn	Tptpv2	25.6	2.3	4.0

Source: CRWMS M&O (2000, Table 26)

NOTES: [a] The chloride mass balance method for estimating infiltration is discussed in Section 5.3.10.2. Rates 1 and 2 assume average annual precipitation of 170 mm, with average chloride concentrations of 0.35 mg/L and 0.6 mg/L, respectively.

Table 5.3-25. Apparent Infiltration Rates Calculated from Pore-Water Chloride Concentrations at Yucca Mountain

Borehole Location	Topographic Category[a]	Sample Stratigraphy	Average Chloride Concentration[b], (mg/L)	Apparent Infiltration Rate[c] (mm/yr.)	
				Rate 1	Rate 2
UZ-7a	A	PTn	70	0.7	1.5
UZ-N55	C	PTn	77	0.7	1.3
SD-6	C	PTn	43	1.2	2.4
UZ-N37	A	Alluvium	133	0.4	0.8
UZ-N54	A	Alluvium	7,400	0.01	0.01
UZ-14	A	Alluvium	520	0.1	0.2
UZ-14	A	PTn	245	0.2	0.4
UZ#16	A	Alluvium	3,700	0.01	0.03
UZ#16	A	PTn	32	1.6	3.1
NRG-6	A	PTn	185	0.3	0.6
SD-9	A	PTn	170	0.4	0.6
NRG-7a	B	PTn	39	1.3	2.6
SD-12	B	PTn	50	1.0	2.1
SD-7	C	PTn	77	0.7	1.3
ESF North Ramp (16 samples)	C	PTn	23	8	14
ESF South Ramp (31 samples)	C	PTn	64	1.2	2.1
ESF Main Drift (6 samples)	C	TSw	20	7	12
Cross Drift (24 samples)	C	TSw	22	5	9

Sources: LA0002JF831222.001 (alluvial samples), LA0002JF831222.002 (PTn samples), and Table 5.3-24 (Exploratory Studies Facility and Cross Drift samples)

NOTES: [a] Topographic categories for borehole locations—A = Beneath deep alluvium (center of large wash, soil greater than 3 m thick); B = Terrace (side of large wash or near base of sideslope, soil 0.5 to 3 m); C = Beneath thin alluvium (ridgetop or sideslope, soil less than 0.5 m thick)

[b] The average concentration for alluvial samples includes data only for samples below 5 m to ensure that the samples lie below the zone of evapotranspiration. Concentrations for PTn samples from surface-based boreholes are reported for the shallowmost PTn sample in each borehole because this sample is more likely to be representative of vertical infiltration at the borehole location than are deeper PTn samples, which are more likely to be affected by mixing with water transported laterally from adjacent zones.

[c] The chloride mass balance method for estimating infiltration is discussed in Section 5.3.10.1. Rates 1 and 2 assume average annual precipitation of 170 mm with average chloride concentrations of 0.3 mg/L and 0.6 mg/L, respectively.